TECHNISCHE UNIVERSITÄT DRESDEN

Fakultät Forst-, Geo- und Hydrowissenschaften

Stone pavements, vesicular structures and soil development – tackling evolution and dynamics of arid environments

Dissertation zur Erlangung des akademischen Grades

Doctor rerum naturalium (Dr. rer. nat.)

vorgelegt von

Dipl.- Geogr. Michael Dietze

Betreuer:

Herr Univ.-Prof. Dr. rer. nat. habil. Arno Kleber
Technische Universität Dresden/Institut für Geographie
Fakultät Forst-, Geo- und Hydrowissenschaften

Contents

Abstract

More than one third of the world is affected by semi-arid to hyper-arid conditions. Increasing land-use and demand for resources argue for an understanding of process interactions in arid environments, in the past, present and future. One of the spatially most extensive surface cover phenomena in arid environments may be stone pavements (desert pavements, Wüstenpflaster, gibber, reg): mono-layers of ideally tightly packed and desert varnish-covered clasts. These are typically associated with underlying fine aeolian sediments, which exhibit distinct foamy structures, composed of isolated spherical pores, the so called vesicular horizon (Schaumboden). Stone pavements and vesicular horizons provide crucial control functions for ecological characteristics, for dust, water and matter fluxes. Their morphological properties are supposed to change systematically with time and, thus, are frequently used as surface age indicators.

Stone pavements are regarded to form either by i) deflation or fluvial erosion of fines from an initially mixed sediment body, leaving behind a surface lag of coarse particles, ii) by exhumation of clasts through a sediment body due to swell-shrink processes, iii) by a bimodal weathering regime, i.e. predominantly physical weathering at the surface versus mainly chemical weathering below, iv) by trapping of aeolian material due to the rough clast-covered surface, fine material translocation below the surface and swell-shrink dynamics of soil aggregates, maintaining the clasts at the surface and leading to accretionary soil profile development, or v) by a combination of some of these processes. Vesicular structures are regarded to form either by air bubbles that ascend through a water-saturated, fine-grained soil matrix and eventually get stuck or by an increased soil air pressure within a surface-sealed matrix. Pressure increase is suggested to result from a variety of processes: i) gas production by algae photosynthesis, ii) hydrogen carbonate crystallisation, iii) solar heating of the matrix, iv) soil aggregate shrinking during drying or v) a prograding wetting front upon rainfall, which replaces soil air. These conceptual models of stone-pavement and vesicular-horizon formation are partly contradictory, inconsistent and not able to explain several properties of stone pavements, vesicular horizons and the soil profiles below.

Accepting the system of stone pavements and vesicular horizons as a collector of aeolian material allows interpreting the resulting accretionary soil-sediment successions as archives of environmental change, which record periods of dust activity, stone pavement formation, soil formation and weathering regimes. However, without a proper understanding of the processes that contribute to the formation and maintenance of the archive components, interpretation may be seriously biased. Accordingly, this dissertation depicts the ambiguities that arise when properties of stone pavement-covered soil-sediment successions are inappropriately used as relative-age indicators and suggests additional mechanisms that need to be considered. Among these mechanisms, unidirectional processes contribute to lateral clast transport and result in preferred alignment patterns of stone length axes. Unconcentrated overland flow as a key driver of clast transport is described

in a numerical model and is validated by physical experiments. Further experiments focus on environmental and sedimentologic control factors of vesicular structure formation and yield another essential process that is able to transport clasts downslope: degassing of fine-grained soil due to rapid wetting, resulting in clast lifting normal to the surface. With quantitative information about the processes that affect stone pavement and vesicular horizon formation it is possible to infer the evolutionary history of stone pavement-covered accretionary soil-sediment successions.

Stone pavements throughout all study areas, both in fossilised form and subaerially exposed, show preferred bimodal clast-length-axes orientation patterns (75 % of all investigated cases). In 50 % of all cases the clasts deviate from slope aspect with an angle of 40±14 °. This systematic property may be explained by lateral transport of clasts and rotation upon collision with other clasts downslope. The orientation patterns can be described by an angle-dependent equilibrium between water drag force and friction force. A numerical model of this equilibrium with measured physical parameters is able to consistently reproduce the orientation angle of 40±14 ° with an assumed overland flow depth of 1.7 cm. Flume experiments confirm both, the validity of the model and the formation of a bimodal clast orientation pattern by unconcentrated overland flow. An essential precondition for the described process is the presence of a fine-grained, runoff-supporting, even and firm surface, provided by the vesicular horizon. However, vesicle formation may also contribute to lateral clast transport by repeated surface-normal lifting of clasts due to air escaping from the soil upon water infiltration. This mechanism is essential to explain stone pavements with bimodal orientation patterns at sites which do not support sufficient overland flows.

Accordingly, the vesicular horizon is a key element for stone pavement formation and maintenance. Vesicular structure can form in a wide range of environmental (amounts of rainfall, drying temperatures) and sedimentologic (electric conductivities, sand and calcium-carbonate contents) properties. However, it is seriously affected by the root activity of vegetation and was not found at sites with mean annual precipitation above 350 mm. Therefore, vegetation cover appears to be the main limiting factor for vesicular horizon maintenance and, accordingly, stone pavement occurrence. It also is an agent which may take over the role as a trap for aeolian material and, thus, may lead to burial of stone pavements.

Surface and sub-surface do not act as coupled archives, as often assumed. The surface reflects alteration only since the last event of disturbance, whereas the underlying successions may comprise information about considerably longer periods. However, they may also show significant disparities in properties even within spatial distances of 10^1 metres which result in relative age index offsets as large as a temporal shift at the order of 10^5 a. In the case of the Cima volcanic field, eastern Mojave Desert, USA, the archive on a 540 ka old lava flow reveals an aeolian history presumably spanning the last 25 ka. There, three distinct units of aeolian sediments may be found. Each unit is covered by a stone pavement. Usually, aeolian activity phases are related to climatic changes, leading to system destabilisation. However, in the case of the Cima volcanic field only the

youngest aeolian unit may be unequivocally linked to a climatic trigger, whereas the other two may be a system response to geomorphologic triggers.

The relationships between stone pavements, vesicular horizons, vegetation and pedogenetic overprint of the accumulated aeolian sediments are manifold, but resolving them is essential to understand how stone pavement-covered landforms in arid environments evolved and which valuable information they comprise.

Kurzfassung

Mehr als ein Drittel der Erde sind von semiariden bis hyperariden Klimabedingungen betroffen. Steigender Landnutzungsdruck und die Ressourcennachfrage verlangen nach einem Verständnis der Prozessketten in ariden Gebieten; in Vergangenheit, Gegenwart und Zukunft. Eine der räumlich am weitesten verbreiteten Oberflächenbedeckungen in ariden Gebieten sind Wüstenpflaster (desert pavements, stone pavements, gibber, Reg): ein einlagiges Mosaik aus idealerweise dicht gepackten und mit Wüstenlack überzogenen Gesteinsfragmenten. Wüstenpflaster treten typischerweise zusammen mit unterlagernden feinkörnigen äolischen Sedimenten auf. Diese wiederum besitzen eine markante schaumartige Struktur, welche aus isolierten kugelförmigen Poren besteht; der sogenannte Vesikularhorizont (vesicular horizon, Schaumboden). Wüstenpflaster und Vesikularhorizonte üben wichtige ökologische Kontrollfunktionen, beispielsweise auf Staub-, Wasser, und Materialflüsse, aus. Es wird angenommen, dass sich ihre morphologischen Eigenschaften systematisch mit der Zeit ändern. Daher werden sie häufig als Indikatoren für Oberflächenalter genutzt.

Die Entstehung von Wüstenpflastern wird entweder erklärt i) durch Deflation oder fluviale Erosion von Feinmaterial aus einem ursprünglichen Mischsediment, was zu einer Residualanreicherung grober Komponenten führt, ii) durch die Exhumierung von Grobkomponenten aus einem Sedimentkörper infolge von Quell- und Schrumpfbewegungen der Matrix, iii) durch ein bimodale Verwitterungsregime, d.h. vorwiegend physikalische Verwitterung an der Oberfläche gegenüber hauptsächlich chemischer Verwitterung im Untergrund, iv) durch aufgrund der rauhen Oberfläche der Gesteinsfragmente eingefangenes äolisches Material, anschließende Verspülung des Feinmaterials unter die Steinoberfläche und schließlich Quell- und Schrumpfbewegungen der entstehenden Bodenaggregate, was die Steine an der Oberfläche hält und in Summe zu einem aufwachsenden, akkretionären Bodenprofil führt, oder v) durch eine Kombination einiger dieser Prozesse. Die Bildung von Vesikularstrukturen wird entweder erklärt durch Luftblasen, die in einer wasserübersättigten Bodenmatrix aufsteigen und irgendwann dort stecken bleiben, oder durch ansteigenden Gasdruck in einer oberflächlich abgedichteten Bodenmatrix. Die Druckerhöhung wird auf verschiedene Ursachen zurückgeführt: i) Gasproduktion durch Photosynthese von Algen, ii) kristallisierende Hydrogenkarbonate, iii) Erwärmung des Bodens durch Sonnenstrahlung, iv) schrumpfende Bodenaggregate während der Trocknung des Bodens und v) eine vorrückende Feuchtefront nach einem Regenereignis, welche die Bodenluft verdrängt. All diese konzeptionellen Modelle zur Entstehung von Wüstenpflastern und Vesikularhorizonten sind teilweise widersprüchlich, inkonsistent und nicht in der Lage, mehrere Eigenschaften von Wüstenpflastern, Vesikularhorizonten und den Bodenprofilen darunter zu erklären.

Akzeptiert man das System aus Wüstenpflaster und Vesikularhorizont als Senke für äolisches Material eröffnet sich die Möglichkeit, die resultierenden akkretionären Boden-Sediment-Abfolgen

als Archive des Umweltwandels zu interpretieren, die Phasen von Staubaktivität, Wüstenpflasterentstehung, Bodenbildung und verschiedene Verwitterungsregime aufgezeichnet haben. Ohne allerdings die Prozesse richtig zu verstehen, die zur Bildung und Aufrechterhaltung der Archivkomponenten beitragen, kann eine Interpretation stark verfälscht sein. Dementsprechend zeigt diese Dissertation die Schwierigkeiten auf, die entstehen wenn die Merkmale von wüstenpflasterbedeckten Boden-Sediment-Abfolgen in unangemessener Weise als relative Altersindikatoren genutzt werden, und schlägt weitere Mechanismen vor, die in die Betrachtung einbezogen werden müssen. Zu diesen Mechanismen gehören unidirektionale Prozesse, die Steine lateral transportieren und zu bevorzugten Einregelungsmustern der Steinlängsachsen führen. Unkonzentrierter Oberflächenabfluss als ein Schlüsselmechanismus für lateralen Steintransport ist in einem numerischen Modell beschrieben und durch physikalische Experimente validiert. Weitere Experimente dienen der Beschreibung von umweltbedingten und sedimentologischen Steuerfaktoren der Bildung von Vesikularstrukturen. Sie zeigen einen weiteren essentiellen Prozess auf, der in der Lage ist, Steine hangabwärts zu transportieren: Luft, die nach raschem Bewässern aus dem Boden entweicht und Steine anhebt. Mit quantitativen Informationen über jene Prozesse, die die Bildung und Aufrechterhaltung von Wüstenpflastern und Vesikularhorizonten kontrollieren, ist es möglich, die Entwicklungsgeschichte von wüstenpflasterbedeckten akkretionären Boden-Sediment-Abfolgen zu rekonstruieren.

In allen Arbeitsgebieten zeigen Wüstenpflaster, egal ob fossil oder an der Oberfläche vorkommend, bevorzugte Einregelungsmuster ihrer Steinlängsachsen (75 % aller untersuchten Fälle). In 50 % aller Fälle weichen die Längsachsen um 40±14 ° von der Hangexposition ab. Dieses systematische Merkmal kann erklärt werden durch den lateralen Transport der Steine und eine Rotation nach Kollision mit anderen Steinen hangabwärts. Die Einregelungsmuster können durch ein winkelabhängiges Gleichgewicht zwischen Wasserschubkraft und Reibungskraft beschrieben werden. Ein numerisches Modell dieses Gleichgewichts ist in der Lage, mit gemessenen physikalischen Parametern und einer angenommenen Tiefe des Oberflächenabflusses von 1,7 cm den Einregelungswinkel von 40±14 ° konsistent zu reproduzieren. Experimente in einem Abflusskanal bestätigen sowohl die Validität des numerischen Modells als auch die Bildung eines bimodalen Einregelungsmusters durch unkonzentrierten Oberflächenabfluss. Eine notwendige Bedingung für den beschriebenen Prozess ist das Vorhandensein einer feinkörnigen, abflussfördernden, ebenen und festen Oberfläche. Diese wird durch den Vesikularhorizont bereit gestellt. Die Bildung von Vesikeln kann jedoch auch zur lateralen Steinverlagerung beitragen, indem Steine durch entweichende Bodenluft wiederholt senkrecht zur Oberfläche angehoben und parallel zur Gravitationskraft abgesetzt werden. Dieser Mechanismus ist essentiell, um Wüstenpflaster mit bevorzugten Einregelungsmustern auch an solchen Standorten zu erklären, die die Bildung ausreichender Abflusshöhen nicht zulassen.

Dementsprechend ist der Vesikularhorizont ein Schlüsselelement für die Bildung und Aufrehterhaltung von Wüstenpflastern. Vesikularstruktur kann sich innerhalb großer

Spannweiten von Umweltmerkmalen (Regenfallmengen, Trocknungstemperaturen) und Sedimentparametern (elektrische Leitfähigkeiten, Sandgehalte, Kalziumkarbonatgehalte) bilden. Sie wird jedoch stark beeinträchtigt durch die Wurzelaktivität von Pflanzen und wurde an keinem Standort gefunden, der im Mittel mehr als 350 mm Niederschlag pro Jahr aufweist. Deshalb scheint Vegetationsbedeckung der Hauptlimitierungsfaktor für die Bildung und Aufrechterhaltung von Vesikularhorizonten zu sein, und damit auch für das Vorkommen von Wüstenpflastern. Vegetation kann auch die Rolle von Steinen in Bezug auf das „Einfangen" von äolischem Material übernehmen und dann zum Begraben von Wüstenpflastern führen.

Oberfläche und Untergrund sind nicht, wie oft angenommen, gekoppelte Archive. Die Oberfläche reflektiert nur Änderungen seit dem letzten Störungsereignis, wohingegen der Untergrund Informationen über weitaus größere Zeitspannen enthalten kann. Der Untergrund kann jedoch auch bemerkenswerte Unterschiede innerhalb räumlicher Distanzen von 10^1 m aufweisen, die dann in relativen Altersidex-Versätzen resultieren können, die in der Größenordnung von 10^5 Jahren liegen. Im Falle des Cima volcanic field, östliche Mojave Desert, USA, enthält ein solches Archiv auf einem 540 ka alten Basaltstrom eine äolische Geschichte von vermutlich nicht mehr als 25 ka. Innerhalb dieser lassen sich drei separate Einheiten äolischer Sedimente ausmachen. Jede Einheit ist von einem Wüstenpflaster bedeckt. Üblicherweise sind äolische Aktivitätsphasen mit Änderungen des Klimas verknüpft, die zur Destabilisierung des geomorphologischen Systems führen. Im Falle des Cima volcanic field jedoch kann nur die jüngste dieser drei Einheiten zweifelsfrei einer klimatischen Ursache zugeordnet werden, die anderen beiden können auch das Resultat einer Systemreaktion auf geomorphologische Impulse sein.

Die Beziehungen zwischen Wüstenpflaster, Vesikularhorizonten, Vegetation und pedogenetischer Überprägung der akkumulierten äolischen Sedimente sind vielfältig aber sie aufzulösen ist nötig um zu verstehen, wie sich wüstenpflasterbedeckte geomorphologische Formen in ariden Gebieten entwickeln und welche wertvollen Informationen sie enthalten.

Theses

1. Stone pavements (desert pavements, Wüstenpflaster, gibber, reg) may form by more than one geomorphologic process, but they are equifinal features. The present formation models cannot fully explain this surface cover type.
2. Stone pavements show indications of both, stability and lability of a geomorphologic surface. Their age indicator function is not a prior attribute. Established relative age indicators may not be appropriate for stone pavement-covered surfaces. The ambivalent nature of stone pavements needs to be explained by a further conceptual model of formation and maintenance.
3. Stone pavements typically show preferred alignment patterns of clast length axes as a result of unidirectional lateral transport. Stone pavements may heal from disturbance predominantly by one or more lateral processes without remarkable erosion of the surface. The lateral processes are tightly related to the vesicular horizon.
4. The present formation models of vesicular structure in fine-grained soils and sediments are partly inappropriate, contradictory and apply to special cases. They need to be tested and evaluated comprehensively.
5. Vesicular horizons may form and exist within broad, quantifiable environmental conditions and sedimentologic properties but are limited by root activity of vegetation. Vesicles form by surface sealing, water infiltration and soil air pressure increase upon rainfall. They are stable soil structure features. The mechanisms which contribute to vesicle formation in natural environments may play a fundamental role in the formation and maintenance of stone pavements. Vesicular horizons are unique and valuable proxies in sedimentologic archives.
6. Accretionary soil-sediment successions may be regarded as archive of palaeo-environmental information. Using a series of correlated profiles may allow deciphering a detailed history of environmental change that led to formation and fossilisation of separate geomorphologic surfaces formed by stone pavements and vesicular horizons.
7. In general, conceptual models should be independently tested and evaluated by numerical or physical models and experiments. Quantitative methods need to be utilised to deliver robust and least-biased information for further interpretations. In the case of the investigations presented in this dissertation, such models, experiments and quantitative methods were developed, first.

Thesen

1. Wüstenpflaster (desert pavements, stone pavements, gibber, Reg) können durch mehr als nur einen geomorphologischen Prozess gebildet werden. Sie sind Konvergenzformen. Die bisher bekannten Genesemodelle können diesen Oberflächentyp nicht in Gänze erklären.
2. Wüstenpflaster zeigen Anzeichen von Stabilität wie auch Labilität einer geomorphologischen Oberfläche. Ihre Altersindikatorfunktion ist kein a-priori-Merkmal. Etablierte relative Altersindizes können auf wüstenpflasterbedeckten Oberflächen versagen. Die ambivalente Natur von Wüstenpflastern muss durch ein weiteres konzeptionelles Modell für ihre Genese und Aufrechterhaltung erklärt werden.
3. Wüstenpflaster zeigen typischerweise bevorzugte Einregelungsmuster ihrer Steinlängsachsen als Resultat unidirektionaler lateraler Verlagerungsprozesse. Wüstenpflaster können sich von Störungen erholen. Dies erfolgt vorwiegend durch einen oder zwei laterale Verlagerungsprozesse, ohne dass dabei der Untergrund merklich erodiert wird. Die lateralen Verlagerungsprozesse sind eng mit dem Vesikularhorizont verbunden.
4. Die bekannten Genesemodelle für Vesikularstrukturen in feinknörnigen Böden und Sedimenten sind teilweise unzweckmäßig, widersprüchlich and nur für Spezialfälle zutreffend. Sie müssen umfassend überprüft und bewertet werden.
5. Vesikularhorizonte können sich innerhalb weiter und quantifizierbarer Spannen von Umweltbedingungen und Sedimenteigenschaften bilden und erhalten, sind aber limitiert durch die Wurzelaktivität von Pflanzen. Vesikel bilden sich durch Oberflächenversiegelung, Wasserinfiltration und die Erhöhung des Bodenluftdrucks infolge von Regenereignissen. Sie bilden stabile Bodenmakrogefügeformen. Die Mechanismen, die zur Vesikelbildung beitragen, können eine fundamentale Rolle bei der Entstehung und Aufrechterhaltung von Wüstenpflastern spielen. Vesikularhorizonte sind einzigartige und wertvolle Proxies in sedimentologischen Archiven.
6. Akkretionäre (aufwachsende) Boden-Sediment-Abfolgen können als Archiv für Paläoumweltinformationen genutzt werden. Die Auswertung von mehreren korrelierten Profilen kann es erlauben, eine detaillierte Geschichte des Umweltwandels zu entschlüsseln, die zur Bildung und Fossilisierung von separaten geomorphologischen Oberflächen – gebildet durch Wüstenpflaster und Vesikularhorizonte – geführt hat.
7. Generell sollten konzeptionelle Modelle durch numerische oder physikalische Modelle und Experimente unabhängig überprüft und bewertet werden. Quantitative Methoden müssen benutzt werden, um robuste und so gering wie möglich verfälschte Informationen für spätere Interpretationen zu liefern. Im Falle der Untersuchungen dieser Dissertation wurden solche Modelle, Experimente und quantitativen Methoden oftmals erst entwickelt.

List of figures

List of tables

1 Introduction

1.1 The geomorphologic realm of arid and semi-arid environments

More than one third of the world is currently affected by semi-arid to hyper-arid environmental conditions (Zomer, 2008) and deserts, especially desert margins, are neither stable in time nor stable in space. Arid environments receive rapidly increasing scientific attention. This is predominantly because of increasing land-use by humans and the demand of natural resources due to social and economic pressure. Accordingly, a broad body of scientific as well as political protagonists acknowledge the need to understand the arid environmental system with its processes, driving factors and potential impacts as well as connections between these.

From a geomorphologic point of view arid environments are valuable study areas for a series of reasons. The degree of palaeo-landform inheritance is high compared to environments in humid climates (Laity, 2008). These ancient landforms typically show a close spatial proximity to each other and interfinger with more recently modified landforms and sediments. Their relative barrenness allows more unobstructed observation of the direct relationships between geomorphologic processes, involved sediments and resulting landforms than any other environment may provide. Virtually all modern arid environments have experienced dramatic changes during the transition from the Pleistocene to the Holocene and throughout the Holocene (Parsons & Abrahams, 2009). This makes them a key object to study the impact of climate change on landscape evolution, dust flux dynamics, glacial, lacustrine, aeolian, alluvial and fluvial processes, vegetation patterns and soil development (e.g. Betancourt et al., 1990; Wells et al., 1985; McFadden et al., 1986; Oviatt, 1988; 1991; Quade, 2001; Tchakerian & Lancaster, 2002; Zech et al., 2007; Kröpelin et al., 2008; Spelz et al., 2008; Suchodoletz et al., 2009). Consequently, arid environments have received a broad and long history of scientific attention.

Semi-arid, arid and hyper-arid environments may be delimited according to a variety of criteria such as climatic, biologic and ecologic components (e.g. Laity, 2008). From a genetic point of view, aridity, i.e. dominance of mean annual potential evapotranspiration (MAE) over mean annual precipitation (MAP), appears to be the most robust parameter as base for a classification system. Aridity may be expressed by a variety of aridity indices (AI). In this dissertation, the latest definition of the United Nations Environment Programme is used. According to this scheme, hyper-arid ($AI < 0.05$), arid ($0.05 < AI < 0.20$) and semi-arid ($0.20 < AI < 0.50$) conditions are reached according to $AI = MAP/MAE$ (UNEP, 1997). Figure 1.1 illustrates the large areas that are affected by semi-arid to hyper-arid conditions. Aridity may be a characteristic feature in cold, temperate and hot climates (e.g. Schultz, 2008). In the following sections, the term arid integrates hyper-arid to semi-arid throughout cold and hot climatic conditions.

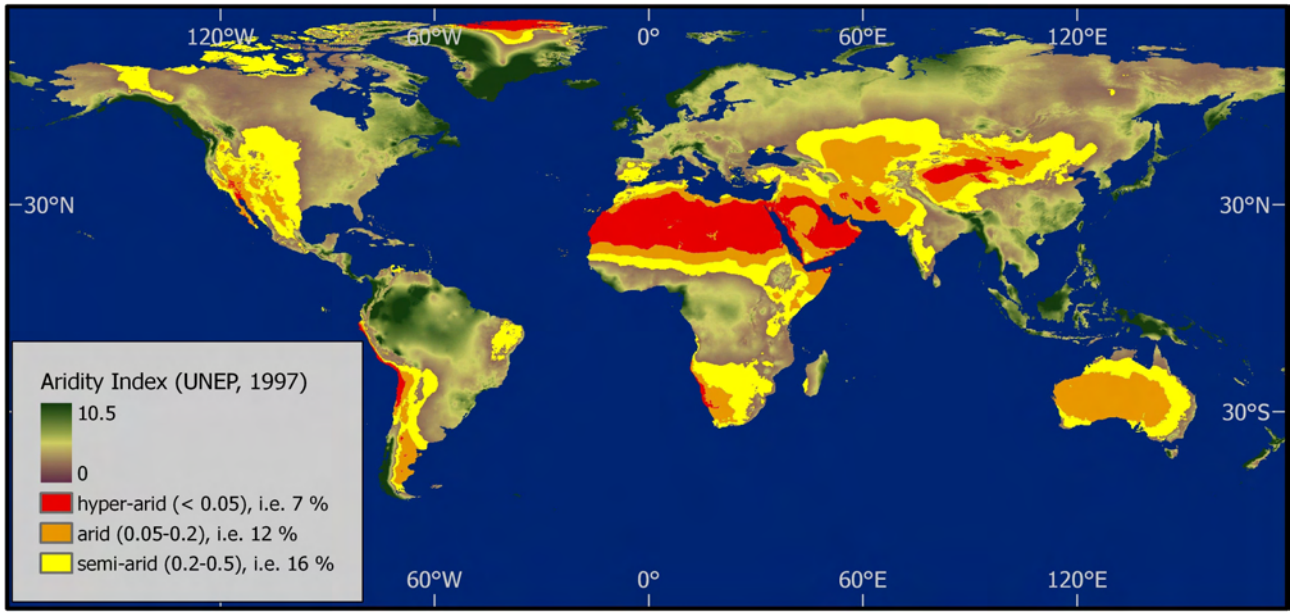

Figure 1.1. Global aridity index after UNEP (1997). The continuous aridity index values are overlain by classified areas of hyper-arid (red), arid (orange) and semi-arid (yellow) character. Percentages of the three aridity classes are given in the legend and refer to the total terrestrial surface. Data source: Zomer et al. (2008).

Arid environments foster a characteristic assemblage of landforms. Most prominent examples – especially with regard to the public – may be associated with aeolian processes. Although grand, solitaire dunes and other prominent accumulation forms of aeolian sand (e.g. sand fields or sand ramps) are most frequently associated with deserts, they cover only 20 % of the surface of arid environments. According to Walker (1986), more than 50 % of desert surfaces are covered by gravels. Further important landforms or surface covers are bedrock outcrops, fluvial structures and playas or lakes. The large spatial extent of gravelly surface covers in arid environments is also expressed by plenty of terms: reg, Hammada, Serir or Saih in North Africa, gobi in central Asia, stone pavements or desert pavements in North America and gibber surfaces or stony mantles in Australia (cf. Cooke, 1970). All these surface cover terms may actually relate to different landforms such as alluvial fans, pediments, fluvial or lacustrine terraces, degraded volcanic structures and further, gravel-hosting or gravel-producing landforms. In this dissertation gravel covers are referred to as stone pavements in the following scetions. Stone pavements are typically associated with a distinctive type of sub-surficial sediment (or rather soil) structure. Almost universally present is a usually some centimetres thick unit of fine, often allochthonous material with a foamy impression. It hosts many isolated, spherical to oval pores, up to some millimetres in diameter and is referred to as vesicular layer or vesicular horizon, Av (Springer, 1958). The stone pavement and the vesicular horizon are assumed to form a genetically coupled system (e.g. McFadden et al., 1986) based on their tight coexistence and interdependent evolution.

This dissertation examines stone pavements from four different study areas. These cover the range from hyper-aridity over aridity to semi-aridity. Two areas are hot deserts, one is a temperate and one is a cold desert. Climate charts in figure 1.2 provide further information about the climatic conditions of the studied areas. Many of the aforementioned landforms occur in each of the working areas. The study areas were chosen to cover the heterogeneity in landscape configuration and their influence on the nature of gravel-covered surfaces (or stone pavements) and the vesicular horizon. Nevertheless, the actual study sites in each area were chosen to be as similar as possible to ensure overlapping of as many geological and geomorphologic preconditions as possible. The four study areas are:

- Cima volcanic field, eastern Mojave Desert, USA. This hot and arid area has a long history of scientific research regarding landscape evolution, development of stone pavement formation models and studies about vesicular horizon interactions. It is therefore a key area for comparing new findings with a broad body of established knowledge.
- Black Rock Desert, southern Sevier Basin, USA. This temperate and semi-arid area appears to be the modern limit of both, stone pavement and vesicular horizon occurrence due to a prominent gradient of mean annual precipitation throughout the area.
- Laguna Salada, northern Baja California, Mexico. This hot area is an example of hyper-arid conditions.
- Nevado Tres Cruces, high Atacama Desert, Chile. This area is a hyper-arid and cold desert at elevations higher than 4000 m a.s.l.

Figure 1.2 shows the location and general features of the four study areas. Detailed study area descriptions can be found in chapters 2, 3 and 5. In general, investigations were restricted to abandoned landforms, such as dissected alluvial fan sections, isolated lava flows or palaeo-beach ridges, to minimise major geomorphologic modification of the studied sites. The investigated landforms were predominantly chosen to be of a material which allowed clear recognition of potential allochthonous sediment admixture, i.e. they consisted of quartz-free or at least quartz-poor crystalline rock types such as basalt and rhyolite.

All investigated sites share a further geomorphologic similarity: the abandoned, stone-pavement covered landforms have an active dust source in close to medial proximity. Cima volcanic field lies some 25 km downwind of the Soda Lake playa. Black Rock Desert was part of the Pleistocene Lake Bonneville and hosts several small modern playas (figure 1.2B). Laguna Salada has a 2 m high bar at its south-eastern margin which has been frequently overspilled by the Colorado River until massive dam constructions upstream greatly reduced its runoff. Today, only episodic rain events fill the area around the depot centre (figure 1.2C) and create a some decimetre deep intermittent lake. In the Nevado Tres Cruces area (figure 1.2D) both, the Valle de barrancas blancas and the Laguna Verde serve as sources of dust that is trapped by the extensive gravel-covered alluvial landforms.

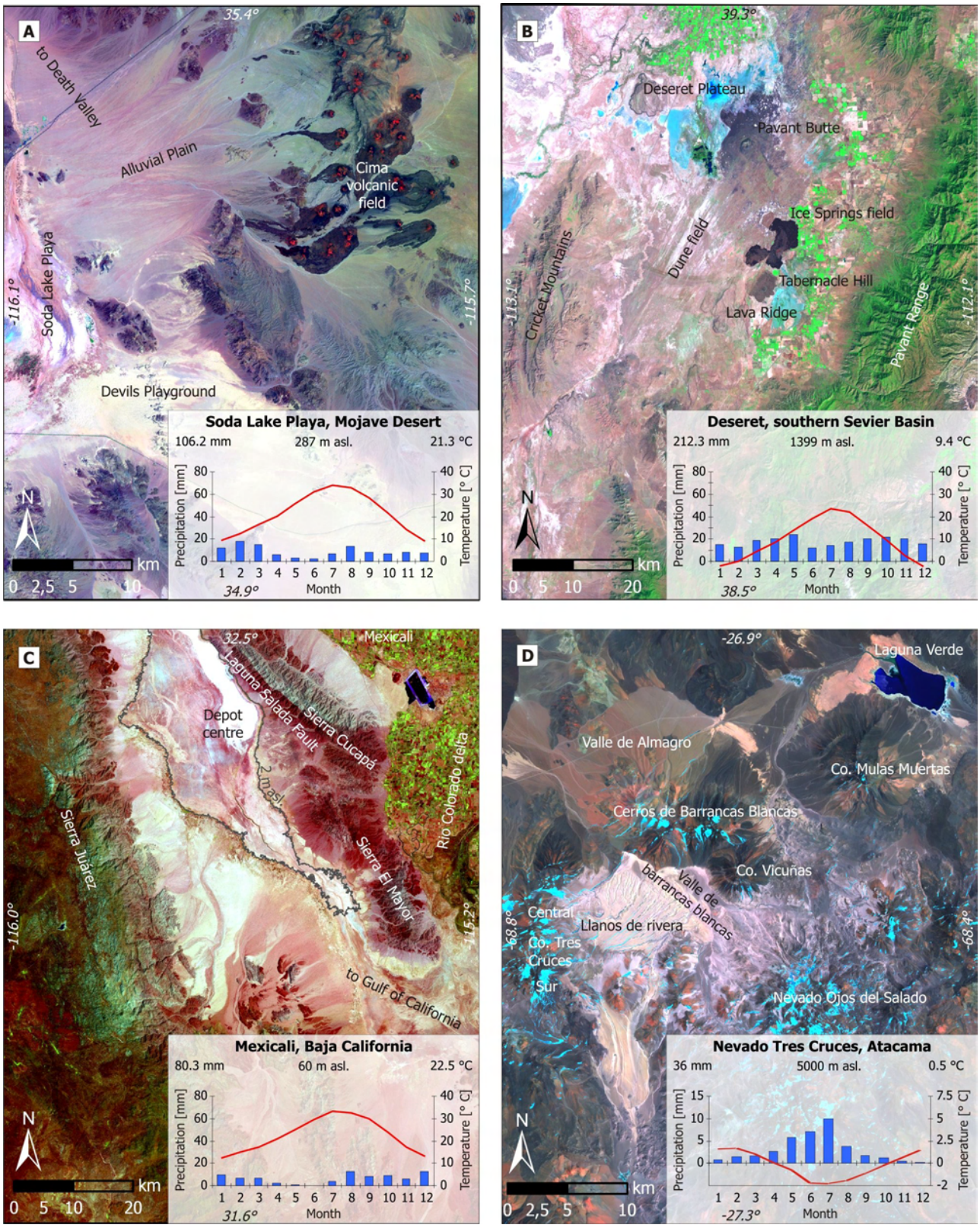

Figure 1.2. Satellite images and climate charts of the four study areas. A: Cima volcanic field, eastern Mojave Desert, USA. B: Black Rock Desert, southern Sevier Basin, USA. C: Laguna Salada, northern Baja California, Mexico. D: Nevado Tres Cruces, high Atacama Desert, Chile. The maps are of different scales and based on Landsat ETM+ scenes with the channel combination 7-4-2. Image data source: GLCF (2012). Major geomorphologic features are labelled. The climate chart of D has a different axes scaling than the other ones. Data sources: A to C NCDC (2012), D Legates & Willmott (1990).

1.2 Significance of stone pavements in arid environments

Stone pavements are peculiar surface features of arid environments. They ideally form a tightly packed mosaic of coarse particles that rest on or are partly embedded in finer sediment. Figure 1.3 shows some general impression of this surface type. The clast monolayer occurs as patches from some few square metres in size up to extensive areas, several hectares in extension (Cooke et al., 1993). The clasts are typically some centimetres in size. However, depending on lithological composition, previous transport processes and disaggregation processes, properties of stone pavements can vary greatly. The degree of sorting and rounding depends on the previous formation history of the landform, they cover: relatively well-sorted and rounded clasts are typical for alluvial fans whereas poorly-sorted and angular particles are common on e.g. abandoned and degraded lava flows (e.g. Wells et al., 1985; McFadden et al., 1989; Spelz et al., 2008). Mature stone pavements often exhibit strong coatings on the individual clasts. However, there are two distinct patina types: dark coatings, also referred to a desert varnish (cf. Dorn, 2009 for a summary), and orange to red coatings. Helms et al. (2003) describe these coatings as dorsal and ventral varnish, respectively. The dark coatings consist of around 100 µm thick laminae, made up of intercalations of iron oxides, manganese oxides and clay minerals (Liu & Broecker, 2007). Desert varnish is supposed to form under long-term subaerial (dorsal) exposure. In contrast, the orange coatings are assumed to form exclusively on the undersides of clasts, in contact with the subsurface (Helms et al., 2003).

Stone pavements have attracted scientists for centuries. Perhaps the first scientific description and concept of their formation dates back to 1858, when Blake speculated: "The fact that all the fine sand and dust is removed from between the pebbles near the surface, while it is abundant a few inches below, indicates the winds have gradually blown it away, leaving the heavy pebbles behind" (cited in Cooke, 1970: 561). *Deflation as the dominant process* of stone pavement formation was described by further researchers in different regions (e.g. Free, 1911; Walther, 1924) and remained a universal answer to explain this surface type even in recent text books (cf. Press & Siever, 2000 versus Press et al., 2003). In a similar manner, winnowing of fines through *water runoff* was discussed as likely explanation for surficial stone pavement properties (Lowdermilk & Sundling, 1950; Sharon, 1962; Wainwright et al., 1999). Figure 1.4A illustrates this concept. However, as Cooke (1970) or Cooke et al. (1993) point out, there is a clear need to consider that more than just one process is necessary to explain the aforementioned properties of stone pavements. Especially the inclusion of sub-surficial sediment and soil characteristics is crucial to deliver more sound formation and maintenance concepts for this surface type.

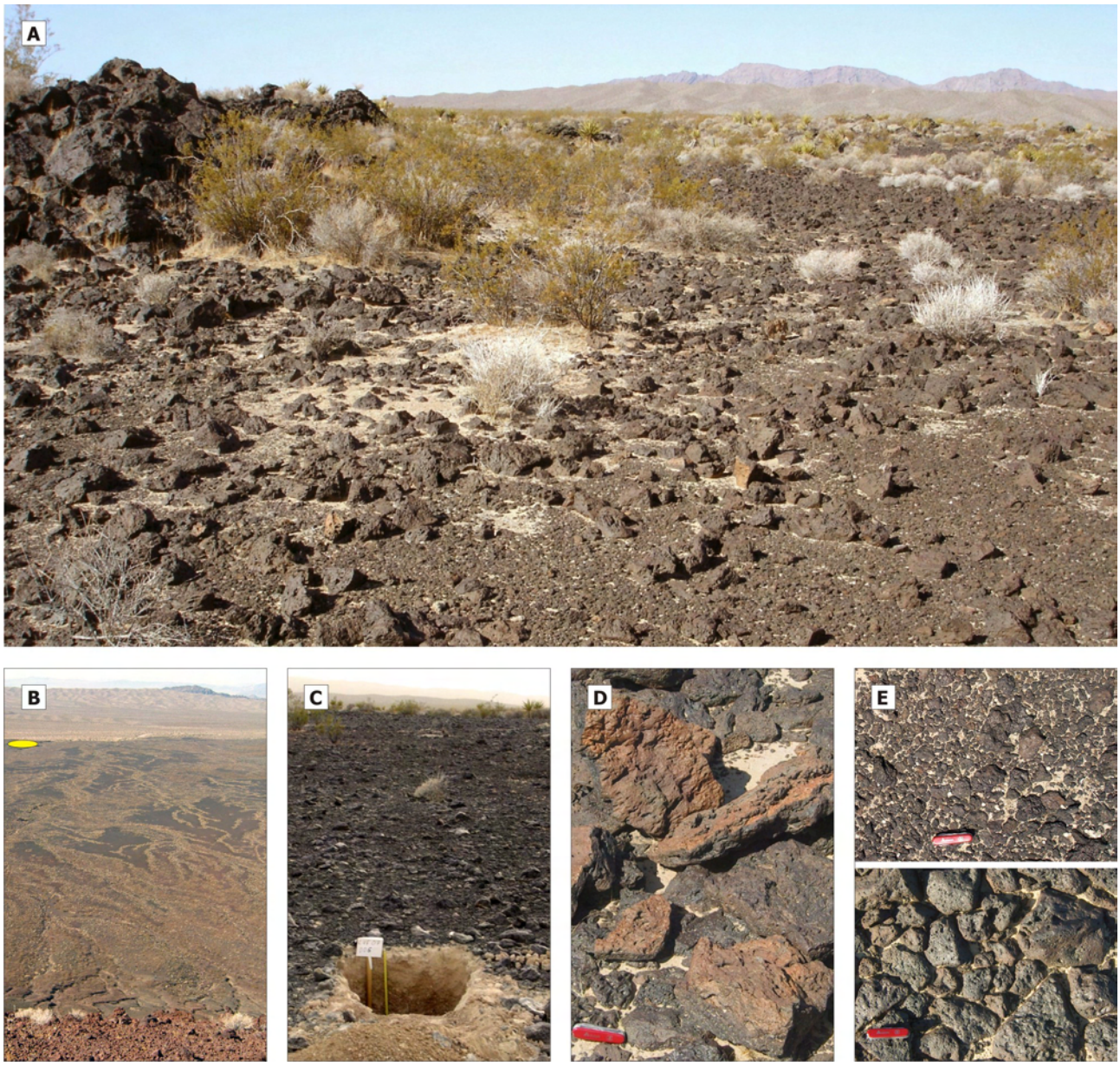

Figure 1.3. Images of stone pavements as surface cover type, examples from Cima volcanic field, USA. A: General appearance of stone pavement-covered lava flows. Clasts of different sizes and degrees of sorting achieve degrees of coverage up to 100 %. Bedrock outcrops of a few metres height serve as clast delivery centres. B: Oblique view from a cinder cone over a lava flow on an alluvial plain. The stone pavement-covered patches cover areas of several hectares and are bordered by vegetation-hosting drainage channels. Yellow ellipse indicates sites of images A and C to E. C: A barren stone pavement-covered area with two metres of almost stone-free aeolian material, revealed by the soil pit. D: Very coarse clasts that show the typical red colours, primarily formed on clast undersides. E: Two different clast sorting and clast size patterns of plots only 200 m apart from each other. Note the tightly packed clast fabric. Pocket knife length is 12 cm.

Considering frequent and prominent contrasts in textural, mineralogical and chemical characteristics, the deflation or erosion theories are no adequate explanations. Typically, the stone pavement is underlain by some decimetres of virtually stone-free fine sediment (e.g. Mabutt, 1977; Wells et al., 1985; Schmidt, 2008). Such a feature cannot be explained by assuming surficial remov-

al of specific grain size fractions alone. A possible way to create textural unmixing is *exhumation of clasts*, i.e. upward migration of coarse rock fragments through the soil or sediment matrix. Springer (1958), Jessup (1960) and Inglis (1965) present field descriptions and laboratory experiments that demonstrate how rock fragments may be exhumed by successive expansion and contraction of the fine-grained matrix. Cycles of freezing and thawing or wetting and drying are the suggested causes with the latter example probably the most common one in warm deserts (cf. figure 1.4B for a sketch).

Mabutt (1977), for Australia, and Bockheim (2010), for the Antarctic, suggest that *different types of weathering processes* may also lead to formation of a clast layer above finer material without any vertical process component. According to these concepts, surficial particles are predominantly suspect to physical weathering. This may result in cracked, chipped and flaked clast remnants. Below the surface atmospheric contrasts are less brutal and more abundant moisture may support predominantly chemical alteration and granular disintegration of particles (cf. figure 1.4C for a sketch).

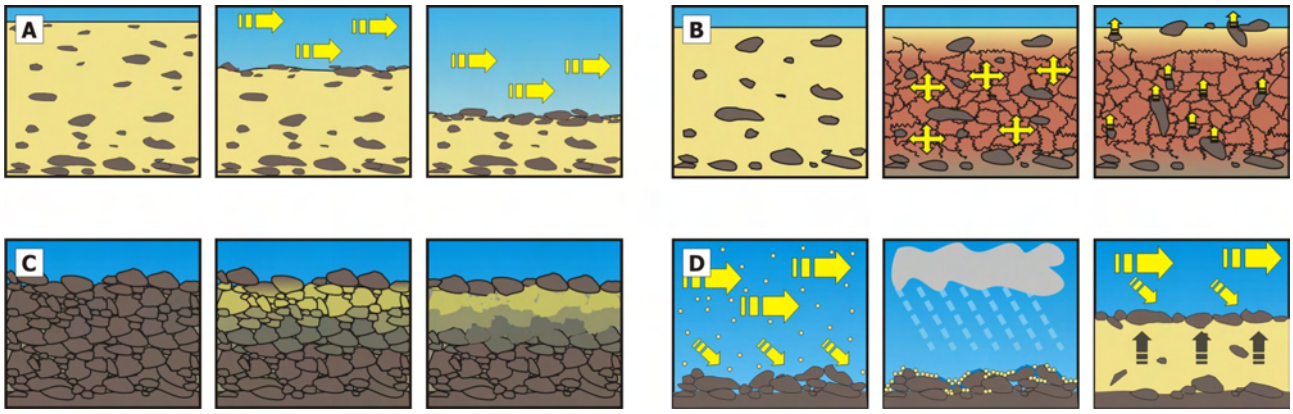

Figure 1.4. Sketches of stone pavement formation concepts. A: Deflation or fluvial erosion concept. The clast cover is suspected to represent a lag deposit of larger material due to winnowing of fines from a formerly mixed sediment column (after e.g. Blake, 1858). B: Clast exhumation by swell-shrink cycles of the matrix. In an initially mixed sediment column the coarse fragments rise upwards because they settle later than small particles (after e.g. Cooke, 1970). C: Different weathering regimes lead to different grain size classes on the surface (predominantly mechanical weathering) versus in the epipedon (predominantly chemical weathering). Stone pavements are autochthonous (after Mabutt, 1977). D: The rough surface of gravel-covered landforms trap aeolian material and episodic rainfall events flush the sediment below the coarse particles where it keeps the clast layer on the surface by swell-shrink dynamics and allows accretionary thickening of the aeolian mantle (after Mabutt, 1977; McFadden et al., 1986).

However, many soil or sediment profiles below stone pavements show abundant admixture of aeolian material (Fürst, 1965; Yaalon & Ganor, 1973; Wells et al., 1985; Amit & Gerson, 1986; Arnalds et al., 2001). This lead Mabutt (1977) and, later, Wells et al. (1985) and McFadden et al. (1986) to consider stone pavements as phenomenons of aeolian deposition (i.e. *dust accretion*) rather than deflation. According to this concept, a surface is initially covered by colluviation of rock fragments from topographic highs to local depressions or by alluvial cobbles on sedimentary landforms.

These clasts provide a rough surface, sufficient to reduce wind speed so that grains in suspension become deposited on the surface (Dong et al., 2002; Goossens, 2005). During subsequent rainfall events, the fine material becomes washed below the rocky cover and eventually gains in thickness to form the characteristic vesicular horizon (cf. chapter 5). Swell-shrink cycles of this horizon may lead to maintenance of the clasts on the surface. Accordingly, under moderate dust influx rates an accretionary system develops that results in time-transgressive thickening of the aeolian mantle and concurrent lifting of the stone pavement. Given that dust deposition (or availability) decreases exponentially with distance from source areas such as playas or ephemeral channels (Pelletier & Cook, 2005), the exceptionally thick aeolian deposits described by Wells et al. (1985) may be of limited spatial relevance. Nevertheless, the predominantly aeolian origin of vesicular horizon material (e.g. McFadden et al., 1998) argues for the efficiency of stone pavements as dust trap in general.

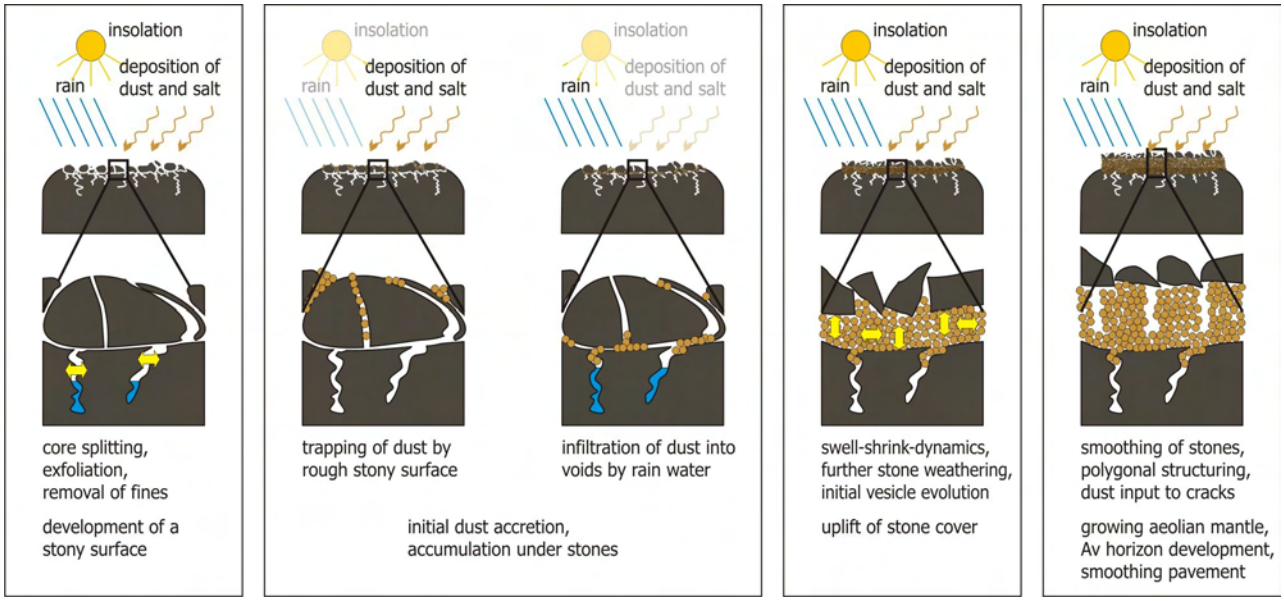

Figure 1.5. The concept of stone pavement formation by dust accretion after Mabutt (1977), McFadden et al. (1986) and Anderson et al. (2002). The sketches illustrate how bare bedrock is suspect to weathering processes that lead to a stony surface. This surface is able to trap aeolian dust due to its rough surface. With episodic rain events, the deposited dust is washed below the clasts. There it eventually forms an aeolian blanket (i.e. the vesicular horizon) that prevents burial of clasts by swell-shrink cycles and gradually lifts the clast layer to form a closed stone pavement.

There are further concepts that stress predominantly lateral processes during the initial stage of stone pavement formation or that contribute to maintenance of an established stone pavement. Clasts on bare bedrock may be entrained by colluviation (Wells et al., 1985) or unconcentrated overland flow (Williams & Zimbelman, 1994). Random lateral motion of clasts due to the contraction and expansion of vesicular horizon aggregates (McFadden et al., 1986; Pelletier et al., 2007) may strengthen the packed structure. Rain drops and wind may have some impact on small stones (Haff & Werner, 1996; Valentine & Harrington, 2006). Unsystematic dislodgement of clasts may be caused by animal activity (Haff & Werner, 1996).

There are attempts to integrate several geomorphologic processes and material fluxes into conceptional models of stone pavement evolution (Meckelein, 1959; Cooke, 1970; Amit & Gerson, 1986; Cooke et al., 1993). Although the equifinality character of stone pavements (Cooke, 1970) makes attribution as well as exclusion of single geomorphologic processes difficult, in many cases stone pavements show contribution of at least two of the aforementioned formation concepts.

Although stone pavements are often regarded as "hallmarks of stability" (Haff & Werner, 1996: 38) there are several independent arguments which contradict this assumption. There are indications of deviating cosmogenic nuclide-based ages of clasts lying at the surface and boulders which are partly embedded in it (Marchetti & Cerling, 2005). Stone pavements may become buried (Wells et al., 1985) which raises the question about how and from which material a new generation of this surface cover evolves. McFadden et al. (1998) mention evidence of tilted clasts and Haff (2001) reports frequently occurrence of stones that lie upside down in assumed mature formations (cf. figure 1.3D). Quade (2001) presents arguments for major disturbance of stone pavements by increased vegetation cover during moister climate and subsequent recovery. Pelletier et al. (2005) show by numeric modelling how stone pavements may recover from disturbance. McFadden et al. (1989) concluded that many relative age indicators fail on stone pavement-covered alluvial fan sections of different age.

Despite these ambiguities, stone pavements are still assumed to build up stable surfaces by predominantly vertical processes, continuously over time. Especially the accretionary type of stone pavements has attracted attention for its potentially valuable palaeo-environmental archive function (McFadden et al., 1986). Apart from the entire soil profile, the stone pavement itself is used for a variety of relative and absolute surface age estimations (Amit et al., 1993; Al-Farraj & Harvey, 2000; Liu & Broecker, 2007; Helms et al., 2003; Marchetti & Cerling, 2005; Matmon et al., 2009), all of them are based on the presumably fulfilled preconditions for chronofunctions. In consequence, stone pavements may be powerful tools of age-estimation, before and since the advent of cosmogenic radio nuclide-dating approaches. Their control function for geomorphologic processes (e.g. Wells et al., 1985) and ecological relationships (e.g. Wood et al., 2005) in arid environments as well as their immense value for scientific questions and land-use purpose highlights how crucial it is to understand their formation, stability, reaction to disturbance and interconnection with other elements of the arid earth system.

1.3 Significance of vesicular structure in arid environments

Vesicular structure in fine-grained soils and sediments (figure 1.6) is a typical feature of arid environments and is reported from hot to cold deserts of different continents but also from exceptional environmental settings such as takyr, playa and wadi floors, fillings of cracked rocks, irrigation furrows and flats in Antarctica (Paletskaya et al., 1958; Volk & Geyger, 1970; Miller, 1971;

Evenari et al., 1974; Figueira & Stoops, 1983; Bouza et al., 1993; Valentin, 1994; Brown & Dunkerley, 1996; McFadden et al., 1998; Ries & Hirt, 2008; Fox et al., 2009; Lebedeva et al., 2009; Bockheim, 2010). However, most times vesicular structure is mentioned in relation with stone pavements.

The key feature of soils and sediments with vesicular structure is the predominance of isolated, spheric to oval macropores, up to a few millimetres in diameter (figure 1.6E). These pores give the material a foamy or honeycomb-like appearance. The structure reaches a thickness between a few millimetres and several centimetres and is often overlain by a few millimetres of loose, slightly coarser sediment. It is referred to as pedogenetic feature: the vesicular horizon or Av (Springer, 1958). However, there are also descriptions of it as a sedimentary unit, a layer (e.g. McFadden et al., 1998). Anderson et al. (2002) highlight the ambiguities with designation and nomenclature as the vesicular horizon combines features of A, B and C horizons and often consists of allochthonous material. Mature vesicular horizons show a coarse prismatic to columnar and secondary platy structure (figure 1.6C). The aggregates form a polygonal surface with typical edge lengths of five to ten centimetres (McFadden et al., 1998; figure 1.6B). They are enriched in clay and calcium carbonate and may exhibit remarkable firmness despite that they consist of silt-dominated grain sizes (McFadden et al., 1998; Anderson et al., 2002).

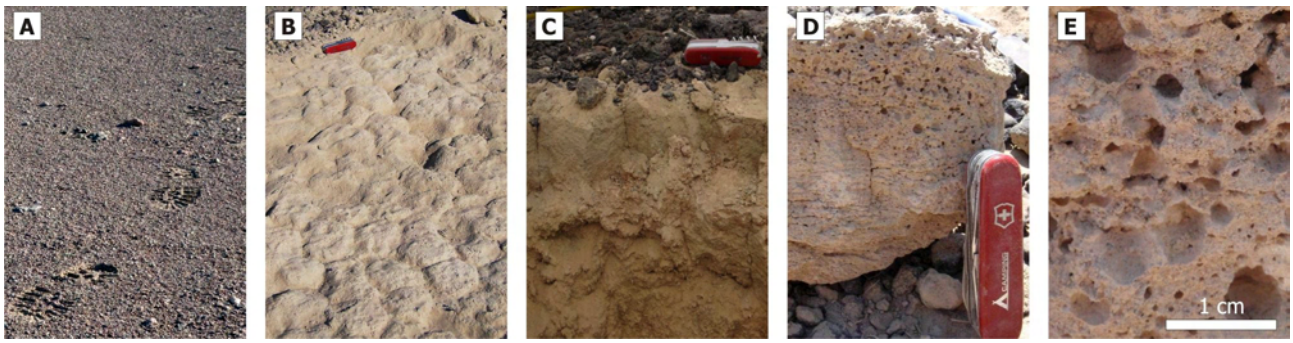

Figure 1.6. Vesicular structure in fine-grained sediment. A: Soft form of vesicular horizons that let one sink into the surface a few millimetres and leave ones foot steps behind. B: Surface cleared from the stone pavement and the loose material on top of the vesicular horizon. Note the polygonal pattern formed by the aggregate boundaries. C: Vertical section through a sediment column with stone pavement and vesicular horizon. The prismatic to columnar aggregates form clearly defined boundary faces. D: Vesicular voids up to a few millimetres in size. E: Close-up of vesicular voids from D.

Vesicular horizons play crucial roles in several environmental processes. Due to their isolated pore system they are very efficient in preventing rainfall infiltration. Young et al. (2004) show that hydraulic conductivity declines by two orders of magnitude if vesicular horizons can develop over a few thousand years. Hydraulic conductivity in turn controls infiltration rate and, hence, surface runoff. The latter is the trigger of one of the major geomorphologic processes in arid environments. There are further soil-chemical parameters, which are related to the infiltration rate or capacity of arid soils, such as element contents, element availability, depth of leaching and ascendence (e.g. McFadden & Tinsley, 1985). Hence, the vesicular horizon is of great significance for site ecological

characteristics and consequently for flora and fauna assemblages (Pierson et al., 1994; Wood et al., 2005). Due to its typical composition of allochthonous material the vesicular horizon may further decouple site characteristics from bedrock-determined constraints. Vesicular horizons are remarkable sinks of aeolian material as dust admixture or even dust mantles up to a few metres in thickness on isolated basalt flows or alluvial fan facets imply (Yaalon & Ganor, 1973; McFadden et al., 1986; Amundson et al., 1989). They are in combination with the overlying stone pavement essential agents that control the pathways of landscape evolution (Wells et al., 1985). However, although they are fragile formations they are under increasing influence of human pressure, mainly due to interests in land-use for military manoeuvres, facility building, over-grazing and off-road vehicle activities (Lovich & Bainbridge, 1999; Prose & Wilshire, 2000; Yonovitz & Drohan, 2009).

Despite their manifold and significant relevance for geomorphologic and ecological process systems, their actual formation has received only limited attention. The existing conceptual models or experiment-based suggestions are contradictory and were developed from site-specific sedimentologic and environmental properties. There are suggestions that vesicles form as a result of gas production by algae (Bazilevich et al., 1953) or the crystallisation of hydrogen carbonates (Paletskaya et al., 1958) within the surface-sealed soil. Gas pressure increase as main driving force of vesicle evolution is also explained by a downward migrating wetting front (Springer, 1958) and solar heating of the wetted soil (Evenari et al., 1974). Hugie & Passey (1964) explain vesicles by upward migrating air bubbles in a super-saturated soil matrix that eventually get stuck. Along with these multiple explanations of vesicle formation go interpretations of their stability and longevity, of vertical matter fluxes in the vesicular horizon and of the influence of environmental factors (Hugie & Passey, 1964; Miller, 1971; Evenari et al., 1974; Figueira & Stoops, 1983; Sullivan & Koppi, 1991; Brown & Dunkerley, 1996). Accordingly, there is only scarce and inconsistent knowledge about the relevance of formation processes and their control by sedimentologic and environmental boundary conditions. Furthermore, the spatial extent and distribution of soils with vesicular structure under the current climatic conditions is poorly discussed. Information about the conditions under which vesicular structure develops and can by maintained is however crucial to understand surface-related processes in arid landscapes, especially in their margin regions and with respect to climate change-related fluctuations of their spatial position.

1.4 Motivation, relevance and objectives

As briefly noted in chapter 1.1, aridity is neither a spatially nor a temporally fixed phenomenon and may cause great threats to human societies (e.g. Mächtle, 2007). As long as it is not clearly understood how a landscape reacts to shifts in external forcing parameters such as climate or tectonic pulses, strategies of adaptation or mitigation are of limited efficiency. To be of any worth, models and forecasts need a sound calibration based on sufficiently long and robust arrays of

measured or transferred data. Accordingly, the study of landscape archives that have recorded both, forcing parameters and system reactions is a key element to achieve this goal beyond the often short period of environmental data that are measured directly by man.

Palaeo-environmental studies typically evaluate archives that have recorded signals by a diversity of proxies. Ideally these signals are or can be made independent from each other and are recorded continuously as well as highly resolved over time. However, in arid environments such archives are very sparse and in general restricted to modern playas. These chatchment-wide depot centres typically hosted fresh water lakes during pluvial periods of the Pleistocene (e.g. Oviatt, 1988; 1991; Wells et al., 2003), but frequently suffered from temporal desiccation periods and thus from interrupted deposition, reworking or even erosion of deposited material.

Accordingly, there is a need to include other types of environmental archives, which are able to resolve such periods of missing lacustrine records. The majority of studies that concern landscape evolution in arid regions throughout and beyond the Holocene use sediment deposits that are affected by pedogenesis. Accretionary systems, i.e. soil-sediment complexes that thicken upwards with time, are of special interest for palaeo-environmental investigations (e.g. Kleber, 2000, McFadden et al., 1986, Suchodoletz et al., 2009; Meszner et al., 2011). Prior to the advent of numerical sediment dating techniques (e.g. luminescence and cosmogenic nuclide-based approaches), such soil-geomorphologic studies were the most promising approaches to infer landform age relations and environmental control factors of their alteration with time (McFadden & Kuepfer, 1990). A variety of morphological features were suggested as maturity proxies of the investigated formations: e.g. calcium carbonate morphology (Bachmann & Machette, 1977), gypsum morphology (Harden et al., 1991), colour changes (Shum & Lavkulich, 1999) or integrated indices (Harden & Taylor, 1983).

These approaches – including the more recent numerical dating techniques – rely on prior understanding of the processes that lead to the evolution of the sediment archive, i.e. geomorphogenesis of the investigated object must be known as precisely as possible. However, the aforementioned disagreements regarding formation and maintenance of two prominent and widespread features of arid environments (stone pavements and vesicular horizons) emphasise that there is a need for further work on these elements. This work may include conceptual, statistical, numerical and experimental considerations to contribute independent lines of argument. Inferring processes and boundary conditions beyond a conceptual and descriptive level is vital for delivering usable information for future studies.

This dissertation aims to improve the understanding of formation, maintenance and evolution of two key features of arid landscapes: stone pavements and vesicular horizons. Their genetic coupling, their relation to modern environmental conditions and their value as environmental

proxies in sedimentary archives will be focus of the dissertation. From the introducing remarks the following main objectives may be drawn:

1. The validity of stone pavements and associated soils as tools for age estimations need to be tested. Potential ambiguities need to be explained and solutions need to be discussed.
2. The known concepts of stone pavement formation need to be tested for their applicability throughout several study areas, from semi-arid to hyper-arid regions, from hot to cold desert environments.
3. The assumed contrasting mechanisms of vesicular structure formation need to be evaluated, using a broad data base of sedimentologic and environmental boundary conditions.
4. The proposed connections between stone pavements and soils with vesicular structure need to be tested for their ability to explain observed phenomena.
5. The values of fossilised stone pavements and vesicular horizons for palaeo-environmental reconstructions need to be evaluated.
6. If not already present, new statistical, numerical and experimental techniques need to be developed to provide quantitative descriptions of the properties and results of points 1 to 5.

Fundamental research typically runs into questions about the applicability of its results and its value for the society that supports it. Considering these reasonable questions may be sometimes difficult if one is cautioned to not fall back onto the argument that on the long time scale, the value will show up by itself. The public community may find in this dissertation some examples that elucidate the sensitivity of commonly occurring landforms which look “stable” but indeed are very sensitive to even comparably minor disturbance by e.g. man. Related to this topic, questions may be raised about whether the current tendencies of land-use management are appropriate or whether they may cause significant impact, on-site and off-site. Surface covers such as stone pavements may imply an initially very simple and reasonable formation process but turn out to be the result of a multitude of partly interconnected processes. And isn't it one duty of science to reveal to the public such examples of tight relationships in natural systems?

Besides these general arguments, this dissertation intents do contribute innovative issues to the scientific community, too. First of all, it is not the prime goal of the dissertation to present further regional examples of already existing knowledge. Rather, the four study areas serve as base for the integrated consideration of aridity and temperature regimes of arid environments. The work points to take care when applying established methods to different regions and different soils or sediments. A further main goal is to elucidate the tight connections between soil and sediment, between geomorphologic and pedogenetic processes together with the consequences for interpreting landform geomorphogenesis and environmental archives. The dissertation also

provides some examples that highlight the great benefit of quantitative instead of descriptive approaches. It highlights the readily applicability of experiment- and physically-based approaches to describe surface cover formation.

1.5 Document structure and formal conventions

This cumulative dissertation is the result of nearly six years of research. It comprises five scientific articles (chapters 2-4, 6-7), submitted to and partly already accepted by international, peer-reviewed journals. All five separate research topics are enclosed by an overarching introduction (chapter 1) and a synthesis (7). Each separate research topic is preceded by a covering page with information about title, authors, abstract, keywords, the journal it is submitted to and the submission history.

Language, especially the use of scientific terms (e.g. stone pavement versus desert pavement, vesicular layer versus vesicular horizon, Cima Volcanic Field versus Cima volcanic field), conventions of age expressions (years, a, ka, thousand years, 10^3 a, etc.), reference styles, both in the chapters and in the reference lists were copied from the original article manuscripts and not changed during the merging process for this dissertation. Accordingly, the chapters 2 to 6 may show formal inconsistencies among each other and should be treated as isolated articles, with formal constraints determined by editors and reviewers of the respective scientific journals. Headlines of each chapter were modified from their original, i.e. published or submitted version in order to establish a better context throughout this dissertation. Each specific research chapter has a separate list of references. The reference list at the end of chapter 7 includes only literature, referred to in chapters 1 and 7. Numbering of figures and tables is consecutively organised in chapters and the order therein with respective slight modifications of the original research articles. Position, size and rotation of figures and tables were changed only slightly to allow optimal text flow of the dissertation.

2. *Ambiguities of relative age indicators*

Chapter 2 is published in the peer-reviewed journal Zeitschrift für Geomorphologie/Annals of Geomorphology (ISSN 0372-8854) as:

Ambiguities of relative age indicators on abandoned surfaces of arid environments

Authors: Michael Dietze[1], Sebastian Muhs[1], Elisabeth Dietze[1]

[1] Institute of Geography, Technische Universität Dresden

Publication history: submitted: January 2009 , accepted: January 2010, published: April 2011.

Full reference: Dietze M, Muhs S, Dietze E. 2011. Ambiguities of relative age indicators on abandoned surfaces of arid environments. Zeitschrift für Geomorphologie 55, Supplementary Issue 3: 49-75.

Internet link: http://www.schweizerbart.de/papers/zfg_suppl/detail/55/76096/Ambiguities_of_relative_age_indicators_on_abandoned_surfaces_of_arid_environments

Abstract: Relative age indicators using geomorphologic and pedologic parameters are important tools for palaeoenvironmental reconstruction. Here we present results from two study areas in arid south-western North America (Mojave Desert, California, USA, and Laguna Salada, northern Baja California, Mexico), which advise using relative age indicators with care because we found no direct relationship between surface properties, soil development and age. On middle Pleistocene basalt flows with stone pavement cover in the Mojave Desert, soil properties vary largely within a small lateral distance without accompanying variation in surface properties. In Laguna Salada soils of similar maturity prevail on abandoned alluvial fan terraces of different surface characteristics. In both cases, chronosequence approaches via surficial relative age indicators explain variations in soil evolution insufficiently. Vice versa it is inappropriate to deduce surface ages from soil properties. Rather, we conclude soil and surface features represent proxies from uncoupled, independent archives. Geomorphologic processes, triggered by e.g. climatic change, have acted even on abandoned surfaces, leading to a small-scale variability of sediments and soils which do not necessarily have the same age throughout a single surface. Regarding stone pavements as dynamic surface constituents can explain diverging results of the two archives. However, a dynamic pavement has to be integrated in surface dating approaches. Using profile development indices for comparing soils from different regions has limitations stemming from inadequate standard soil profiles and regional specific climate history.

Keywords: Stone pavement; Arid environment; Aridic soil; Relative age indicator; Profile development index

Kurzfassung

Relative Altersindikatoren, die auf geomorphologischen und pedologischen Parametern basieren, sind wichtige methodische Hilfsmittel für Paläoumweltrekonstruktionen. Wir zeigen Ergebnisse aus zwei Arbeitsgebieten im ariden Südwesten Nordamerikas (Mojave Desert, California, USA, und Laguna Salada, Baja California, Mexico), die ein eingeschränktes Potential relativer Altersindikatoren zeigen. Wir fanden keine direkten Beziehungen zwischen dem Alter geomorphologisch entkoppelter Flächen, ihren Oberflächeneigenschaften und darin stattfindender Bodenentwicklung. Auf mittelpleistozänen Basaltströmen mit Wüstenpflasterbedeckung in der Mojave Desert ändern sich Bodeneigenschaften auf kurzer lateraler Distanz sehr stark, ohne dass sich dies in variierenden Oberflächeneigenschaften ausdrückt. Böden am Beckenrand der Laguna Salada zeigen trotz Entwicklung auf Segmenten alluvialer Schwemmfächer mit unterschiedlichen Oberflächeneigenschaften stets gleiche Merkmale und sind von schwachem, jungem Entwicklungsgrad. In beiden Fällen können Chronosequenzansätze, welche auf relativen, von Oberflächeneigenschaften abgeleiteten Altersindizes basieren, die Bodenentwicklung nur mangelhaft erklären. Ebenso wenig lassen Bodeneigenschaften gesicherte Schlussfolgerungen auf das Entkopplungsalter einer Oberfläche zu. Wir fassen deshalb Boden- und Oberflächeneigenschaften als Proxies unabhängiger Archive auf. Geomorphologische Prozesse, die z.B. von Klimaänderungen gesteuert werden, finden selbst auf entkoppelten Oberflächen statt und führen zu kleinräumiger Variabilität von Sedimenten und Böden, die nicht notwendigerweise gleichen Alters sein müssen. Die Auffassung von Wüstenpflastern als dynamische Elemente von Oberflächen kann die abweichenden Ergebnisse der beiden Archive erklären. Dynamische Wüstenpflaster müssen jedoch bei Ansätzen numerischer Oberflächendatierungen berücksichtigt werden. Die Eignung von Profilentwicklungsindizes zum Vergleich von Böden unterschiedlicher Regionen ist sehr begrenzt aufgrund unzureichender Standardbodenprofile und einer regional spezifischen klimatischen Vergangenheit.

2.1 Introduction

Relative age indicators are frequently utilised for unfolding the evolution of geomorphologic surfaces, where numerical dating is not available or interpolation of ages between dated archives is attempted. Vice versa, for receiving reliable numerical ages, knowledge of evolution, integrity and stratigraphy of sediment archives is crucial. Typically, relative age indicators use differences in topologic and topographic relationships, surficial properties as well as subsurficial parameters of respective sites to infer their relative temporal offset of geomorphologic decoupling, i.e. abandonment. Abandonment is referred to as isolation of a surface from upslope water runoff by channelisation and truncation or due to topographic configuration. Thus, abandoned surfaces such as dissected alluvial fans, fluvial terraces and lava flows are no more affected by the geomorphologic

processes that originally formed them. They should be therefore in general prevented from ongoing fluvio-geomorphological or other profile-disturbing processes.

Topography of abandoned surfaces in arid environments degrades with time. Primary morphology, i.e. bar-and-swale-topography on alluvial fans and constructional relief on volcanic landforms, becomes levelled and smoothened by small scale erosional and depositional processes. Bull (1996) and Wells et al. (1985) used this mechanism for relative age estimations. Very mature surfaces, however, may show increasing surface roughness as a result of fluvial dissection and vegetation evolution (Farr, 1992). Development of a drainage network on abandoned surfaces shows a consistent relationship to surface age as demonstrated by Wells et al. (1985). Relative height differences between alluvial fan sections and with respect to the modern stream channels are further important proxies for deciphering surfaces of different age (Bull, 1991; Spelz et al., 2008).

Site degradation is also expressed by surface constituent properties. Birkeland & Noller (2000) argue for the age-dependence of weathering features of surficial material on alluvial fans. Wherever a stone pavement develops on abandoned surfaces, it represents a powerful tool for relative age approximations, as shown by Wells et al. (1985). Given a primarily uniform distribution of stone dimensions and material properties, as may be the case on fluvial terraces, systematic changes in the percentage of pavement coverage, tightness of packing, particle size, particle sorting, clast angularity and degree of shattering may serve to establish relative stratigraphies, as demonstrated by Amit & Gerson (1986), Amit et al. (1993) and Al-Farraj & Harvey (2000). However, for sites with a primarily inhomogeneous composition and size distribution of pavement stones such correlations may be inappropriate (cf. discussion by McFadden et al. 1989). Pavement stones may carry a thin veneer of rock varnish. Dorn & Oberlander (1982) already discussed chances to use this feature for relative age estimations. More recent studies include the work by Liu & Broecker (2007) who use microlaminated generations of rock varnish developed on pavement clasts to establish a relative regional chronology. Samples from numerically dated sites may add fixed ages to such a chronology. Helms et al. (2003) present age indices from rubification intensities of pavement clasts on alluvial fans.

Subsurficial material alteration is primarily the result of pedogenesis. A broad number of single- and multi-proxy approaches aim at describing changes in substrate properties with time. Gile et al. (1966) and Bachmann & Machette(1977) define morphological stages of calcium carbonate development (e.g. changes from filaments, nodules and concretions towards calcretes) and use them to establish a time-dependant evolution history of sites in arid and semi-arid environments. Harden et al. (1991) present a comparable approach for pedogenetic gypsum morphology. Further studies compare down-profile changes in colour and relate them to iron mineral phases and soil maturity (cf. Shum & Lavkulich, 1999 for a summary). Harden (1982) and Harden & Taylor (1983) present a multi-proxy index which combines some of the above mentioned descriptions. They advanced an approach by Bilzi & Ciolcosz (1977) to derive quantitative horizon and soil profile de-

velopment indices (PDI) in order to describe pedologically distinct sites. This method became widely accepted and used until present, even in non-arid environments and under modified conditions (e.g. Tsai et al., 2007; Sauer et al., 2007; Haugland & Haugland, 2008; Zielhofer et al., 2009). Besides these index-focussed approaches soil may also be regarded as a complex, stratified, polygenetic system and the soil column as a whole may be used to infer surface maturity. Kleber (1994, 1999, 2000) showed the potential of stratified, intercalated soils to infer the evolutionary history of landscape in the arid southwestern United States.

The mentioned, soil-based, relative age approaches strongly rely on the concept of soil as a function of soil-forming factors (Dokuchaev, cit. after Jenny, 1941). Treating all factors but time as constant, a chronologically consistent increase in pedogenetic overprint of sediment may be used to infer the age of soil formation. Many North American studies utilise this strict chronostratigraphic approach. However, uncertainties, compromises and pitfalls regarding this perspective are discussed by many authors (e.g. Birkeland, 1985; Reheis et al., 1989; Ufnar, 2007). Further, topography-controlled, lateral soil or sediment displacement is often ignored. Also, climate did not evolve and change gradually during the past hundreds of millennia. Hence, interpolation between climatic boundaries neglects prominent changes, e.g. in the dynamics of vegetation and water flow patterns.

One general conceptional ambiguity is disjunctive timescales over which investigated parameters are sensitive. Formation of a stone pavement may happen within decades (Haff & Werner, 1996) but undergoes further alteration over much longer timescales (McFadden et al., 1986; McDonald et al., 1992). Liu & Broecker (2007) are able to cover at least Holocene timescales with rock varnish stratigraphies. Preservation of varnish on older, Pleistocene site depends on lithology and weathering characteristics of surface components. Weathering features of surficial clasts can be applied as relative age indicators on timescales of 10^5 to 10^6 years, as Spelz et al. (2008) demonstrated. Formation and increase of pedogenetic horizons may exhibit the most diverging temporal sensitivities. McFadden et al. (1986) present results from the Mojave Desert which show that vesicular horizons develop on Holocene surfaces and that with increasing surface age this horizon does not alter significantly. However, subsoil properties change in a systematic way and may provide information over hundreds of thousands of years. Calcium carbonate morphology studies (Bachmann & Machette, 1977) may be successfully applied to such long timescales. In general, relative age indicators need calibration sites. The question arises of how to define a representative site and soil profile.

Soils are the most complex archive for retrieving environmental proxy data. However, soil formation integrates and manifests a broad number of climatic, geomorphologic, biologic and further information (Birkeland, 1999). Hence, pedologically overprinted sediments are powerful archives to study landscape evolution. We discuss problems that arise when discrete parameters of sediments and soils are used as simplified, independent archives of environmental history. From

two study sites we show examples which underline uncertainties of relative age indicator application. The value of surface parameters like stone pavement formation, rock varnish cover and reduction of original topography is discussed. Additionally, ambiguities of two commonly applied PDI (Harden, 1982; Harden & Taylor, 1983) are presented.

2.2 Study sites

Terrestrial archives of landscape evolution and environmental change are best preserved on stable landforms, i.e. abandoned geomorphological surfaces. Such surfaces are common in arid to semi arid southwestern North America (cf. Kleber, 1994; Schmidt et al., 2008). Especially accretionary soils are valuable archives as McFadden et al. (1986) could show. They are often associated with abandoned surfaces which act as dust traps. Further, a close-by source of aeolian sediment (e.g. a playa) is required. Both preconditions are given at Cima Volcanic Field, eastern Mojave Desert, USA, and Laguna Salada, northern Baja California, Mexico. Our study compares two regions with similar modern environmental conditions and presents the significant differences expressed by relative age indicators.

2.2.1 Cima volcanic field

Cima volcanic field comprises cinder cones and associated lava flows, located in the eastern Mojave Desert, at the southwestern boundary of the Great Basin. It is situated on a slope gently inclined westward ranging from 2417 m high Cima Dome to Soda Lake Playa with an altitude of 284 m a.s.l. (cf. figure 2.1). Valley floors and depressions are covered by Holocene sediments, whereas slopes generally carry Quaternary alluvial material. Since the late Miocene (7.6 Ma BP, Turrin et al., 1985) periodic volcanic activity resulted in a set of 60 lava flows covering an area of approximately 150 km². Climate is arid and transient with 69 mm annual precipitation in Baker (320 m a.s.l.) and 160 mm/a at Yucca Grove (1204 m a.s.l.) in the northeastern part of the study area (WRCC, 2008). The gradient of mean annual temperature ranges from 21.0 °C in Baker to 14.7 °C at Yucca Grove (WRCC, 2008) and is mainly controlled by elevation. Central Mojave Desert climate is dominated by winter precipitation associated with southwestern storm fronts (Koehler et al., 2005).

Extensive geomorphologic and pedologic investigations were carried out in the area during the 1980s (e.g. Wells et al., 1985; McFadden et al., 1986). Research focused on surface alteration with time and deciphering stages of soil evolution under the influence of climate change. The history of sediments and soils on the lava flows stands in close relationship with the palaeohydrological evolution of the modern close-by playas. Detailed and overarching studies are presented in comprehensive publications edited by Enzel et al. (2003).

The investigated soil profiles CVF07-001 to CVF07-006 are situated on a lava flow with a constructional age of 560±80 ka BP (Turrin et al., 1985), profiles CVF07-008 and 009 upon a flow of approximately 16 ka (McFadden et al., 1986). The two flows are located upon an erosional landscape protecting morphological forms from burial and major fluvial modification. A 7-10 m high escarpment leads from the modern wash to the lava flow surfaces.

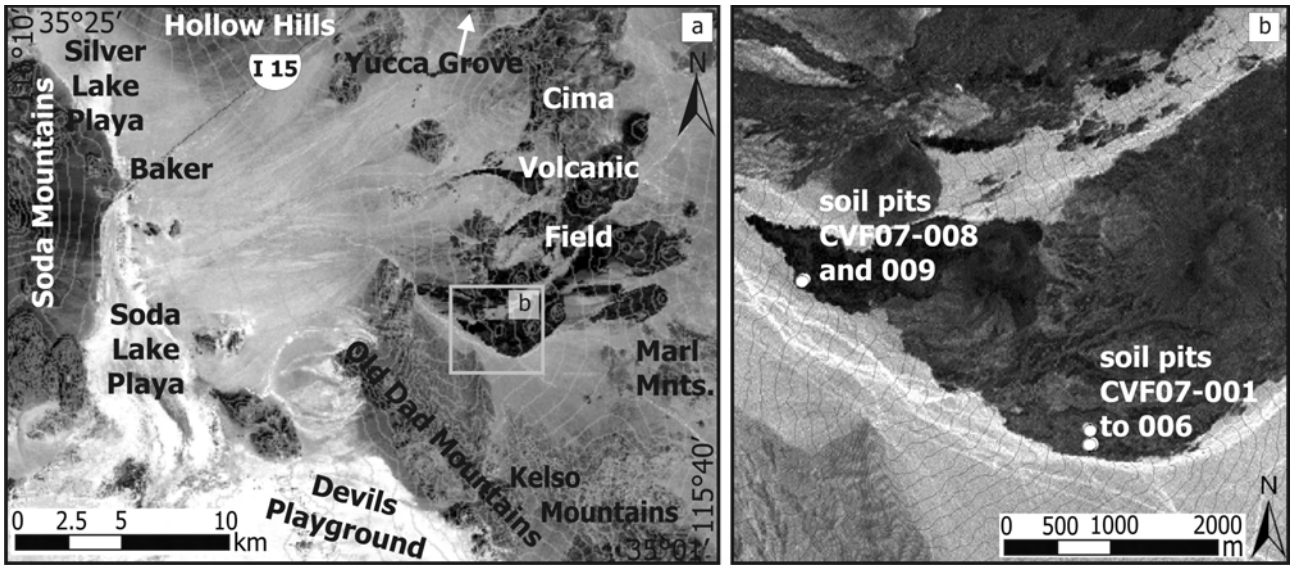

Figure 2.1. Study area Cima Volcanic Field. a) Satellite image (Landsat 7) of the severe cinder cones set on an alluvial grade that leads to Silver Lake Playa and Soda Lake Playa, surrounded by mountain ranges of heterogenic Precambric to Mesozoic rocks (data source: GLCF 2008, contour equidistance 50 m). b) Satellite image (Landsat 7) of the proximity of studied soil pits on basaltic lava flows (data source: GLCF (2008), contour equidistance 5 m).

2.2.2 Laguna Salada

Laguna Salada is an approximately 100 km long and 20 to 30 km wide, playa-type basin with southeast orientation covering the southwestern part of the Salton Trough (figure 2.2). It is a Cenozoic, detachment-related transtensional depression (Martín-Barajas et al., 2001). Its northern margin bounds the Mexican-US border whereas Sierra Pinta (max. 460 m a.s.l.) in the south, composed of colour rich, mostly rhyolithic rocks, adjoins the sedimentary margin of the Gulf of California. Laguna Salada is flanked by Sierra Juárez (max. 3500 m a.s.l.) to the west. Its mountain ranges are dominated by granite with small outcrops of basaltic cap rock in its northeastern part. The Sierras Cucapá (max. 1060 m a.s.l.) and El Mayor (max. 800 m a.s.l.) in the east are both composed of heterogenic, mainly granitic and complex metamorphic rocks (Spelz et al. ,2008).

Extensive alluvial fans reach towards the basin centre and delta floor (cf. figure 2.2 b). In the southeast a spillway (2 m a.s.l.) controls marine and fluvial incursions into the basin. Active dunes, sand ramps and sand sheets cover sporadically the western flanks of Sierra Pinta and Sierra Cucapá as well as steep eastern slopes of Sierra Juárez. Mean annual temperature in Mexicali, 30 km

east of the northern basin margin, is 22.5 °C (NCDC, 2008). It is comparable to low elevations in the eastern Mojave Desert. Seasonality patterns are similar as well. Precipitation (80 mm mean annual sum) is mainly of episodic, torrential nature and shows a bimodal distribution with maxima in December and January as well as in August.

Existing studies from this area focused on the tectonic evolution of the basin in relation to the San Andrews Fault system (cf. Spelz et al., 2008 for a review) as well as on sedimentologic characterisations (Martín-Barajas et al., 2001). Spelz et al. (2008) and Mueller & Rockwell (1995) use soils to characterise dissected alluvial fan surfaces but do not infer information about landscape evolution from these soils. However, Dietze et al. (2008) show the potential for tracing landscape change in this region. For the investigated sites there is, with one exception (site B1), no numeric age control. Hence, age relations between different abandoned surfaces cannot be stated, except when surfaces belong to the same alluvial fan system but to different levels (as is the case for sites F1 and F2). However, our study focuses on comparing surface characteristics with subsurficial properties in order to show discrepancies and not to establish a relative surface stratigraphy.

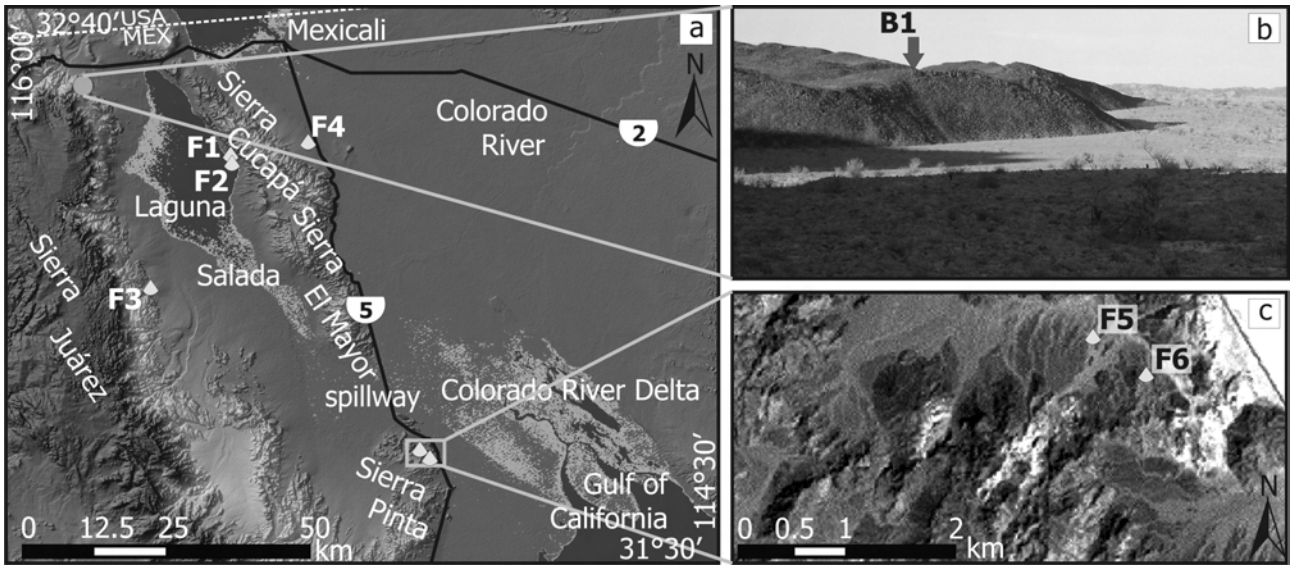

Figure 2.2. Study area Laguna Salada. a) Artificial hillshade and colour coded digital elevation model of the Laguna Salada Basin in the west and greater Colorado River delta system in the east (data source: GLCF, 2008). b) Oblique photo towards the north of a basaltic cap rock with soil profile. c) Alluvial fan systems in the northern Sierra Pinta with studied profiles (data source: GLCF (2008), Landsat 7, panchromatic channel).

Sites under study (cf. figure 2.2) are located on dissected and abandoned alluvial fan terraces (F#) throughout the basin and on top of a 12 Ma old (Martín-Barajas et al., 2001) basaltic cap rock (B1). Site F1 is located around 85 m above the present basin floor on a deeply dissected fan remnant, Q5 after Mueller & Rockwell (1995). On the same alluvial fan system site F2 is located on a different fan level, ca. 350 m downslope at an elevation of 40 m a.s.l., separated by dissection, Q4

after Mueller & Rockwell (1995). Profile F3 is located at the western margin of the basin at the uppermost level of the proximal to medial part of a granitic alluvial fan. Site F4 is situated at the eastern slopes of Sierra Cucapá on an alluvial fan surface presumably older than 125 ka, according to correlation with dated fan surfaces of Sierra El Mayor (Spelz et al., 2008; J. Fletcher pers. comm. 2008). Sites F5 and F6 are located in Sierra Pinta on alluvial fans of different catchment areas draining towards the northeastern Colorado River Delta. They are of identical relative surface height 2 to 3 m above the modern channels.

2.3 Materials and methods

2.3.1 Cima Volcanic Field

Parameters described for characterising the surface next to the excavated profiles included preservation of the primary relief, percentage of stone pavement cover, pavement texture (after Al-Farraj & Harvey, 2000), development of rock varnish (i.e. abundance and colour), weathering features and vegetation dispersion. Due to the primarily high variance in particle size and morphology of cinder, basalt and tuff clasts we omitted recording mean particle size, particle sorting and clast angularity.

For pedologic investigations eight soil pits were dug by hand until bedrock was reached or a massive calcium carbonate-dominated horizon prevented further deepening. Profiles were described in the field according to Soil Survey Division Staff (1993) and Birkeland (1999). Vesicular soil structure was indicated by the horizon modifier "v" (cf. McFadden et al., 1986). The modifier "t" for clay accumulation was used only if morphological features, i.e. at least clay cutans on ped faces, were visible. Calcium carbonate and gypsum morphology were estimated following Birkeland (1999) and Harden et al. (1991), respectively. Sampling was carried out following field profile descriptions. Whenever possible, three samples were taken from each designated horizon or stratigraphical unit in order to resolve internal variations. Loose, fine material between desert pavement clasts, some mm thick, atop the vesicular horizon was also sampled. Laboratory analyses involved grain size measurements (sieve-pipette method), determination of calcium carbonate content, electric conductivity (10 g sample and 50 ml deionised water) and pH value (in KCl solution) as described in Schlichting et al. (1995). Soil colour was determined in the laboratory under natural light with air dried and artificially wetted samples using a standard Munsell soil colour chart.

PDI were calculated based on field descriptions and laboratory results according to Harden (1982) and Harden & Taylor (1983). However, as the accretionary soils at the investigated sites in Cima Volcanic Field are nearly entirely composed of aeolian fines (cf. McFadden et al., 1986) basaltic bedrock was not regarded as parent material in the sense of Harden (1982). Potential sources of the trapped dust may be Silver Lake or Soda Lake playa. However, sediment composition there (cf. table 2.3) resulted from processes other than aeolian transport. Therefore, this sedi-

ment could not be regarded as representative parent material for soil development on basalt flows in Cima Volcanic Field. Hence, we used the fresh aeolian dust from the surface between pavement clasts and around plants close by, treating this dust as potential parent material and least altered by pedogenesis.

2.3.2 Laguna Salada

Surface properties and soil morphology were recorded as described for Cima Volcanic Field. Laboratory pedological data was not evaluated because field data suggested overall similar, weakly developed soils close to the surface. We dug 2 to 4 soil pits at each site to check for heterogeneity, which was never the case. Therefore, we present only one profile for each site. Whereas soils in Cima Volcanic Field consist primarily of aeolian fines with few basaltic components, for profiles in Laguna Salada the origin of sediment constituents remain uncertain. Birkeland (1985) and Harden et al. (1991) discuss problems arising from such profiles when applying PDI. Therefore, we did not calculate PDI.

2.4 Results

2.4.1 Surface and soil properties

Descriptions of surface properties for all investigated sites are summarised in table 2.1. For Cima Volcanic Field results are grouped for both lava flows because surface properties around the closely spaced profiles do not change significantly. In tables 2.2 and 2.3 evaluated field and laboratory properties for all profiles from Cima Volcanic Field are presented.

2.4.1.1 Cima Volcanic Field

Surface properties of the 560±80 ka old lava flow in Cima Volcanic Field show a systematic pattern. Patches of denser vegetation alternate with virtually bare ground. Typical species are Creosote bush (*Larrea tridentata*), Burrobush (*Ambrosia dumosa*) and Mojave Yucca (*Yucca schidigera*). The flow is dissected by small valleys and forms stepped plateaus. These plateaus are structured by shallow drainage networks and local outcrops of parent rock. The investigated profiles are located on a barren part of the basalt flow, approximately 300 m long and 80 m wide. Inclination is 3 to 5 degree.

Below the well-varnished and tightly interlocking desert pavement a well developed vesicular structure is always present. Mean ped thickness is 7 cm and edge length is between 3 and 6 cm. Peds are split into an upper part with vesicles some mm in diameter and a medium hard to hard consistence. Towards the lower horizon boundary vesicles become smaller and ovoid. Structure is predominantly platy and consistence is even harder. Clay films become the most characteristic

Table 2.1. Results of surface characterisation at Cima Volcanic Field (CVF) and Laguna Salada (LS). Parameter descriptions after Birkeland (1999), Al-Farraj & Harvey (2000) and Spelz et al. (2008).

Site (rock type)	***Topography***	***Pavement cover [%]***	***Pavement texture***	***Rock varnish***	***Rock weathering***	***Vegetation***
CVF 16 ka flow (basaltoid)	rough morphology, sharp escarpments, pressure ridges, unconnected drainage network, pavement patches < 100 m²	80-90 %	packed, interlocking stones, almost no vertical a b planes	all clasts varnished, dark grey colours	clast surfaces mostly rugged, smooth forms also present, few fractured clasts	very restricted, disperse
CVF 560 ka flow (basaltoid)	smooth morphology, widely dispersed small bedrock outcrops, no sharp vertical forms present, shallow interconnected drainage network, pavement patches > 10000 m²	90-100 %	tightly packed, interlocking stones, no vertical a b planes	all clasts varnished, dark grey colours	clast surfaces rugged to smooth , few fractured clasts	no vegetation on patches, concentrated in drainage lines
LS B1 (basaltoid)	dominated by basaltic boulders, no drainage network developed (subsurficial flow), pavement patches 20 to 200 m²	90-100 %	tightly packed, interlocking stones, no vertical ab planes	most clasts varnished, dark grey to dark brown colours	smooth clast surfaces, very few fractured clasts	virtually free of vegetation, very few xerophytes
LS F1 (tonalite, quartzite)	smooth morphology, bar-and-swale topography virtually eliminated, surface dissected by deeply incised channels	90-100 %	tightly packed, interlocking stones, no vertical ab planes	ca. 20 % varnished, brown colours, tonalitic rocks free of varnish	rocks often disintegrated and shattered, original clast surfaces not preserved	no vegetation on patches, concentrated in drainage lines
LS F2 (tonalite, quartzite)	initial bar-and-swale topography dominating, dissected by shallow channels	70-80 %	unordered, loosely dispersed	almost no varnish present	initial disintegration	no vegetation on patches, concentrated in drainage lines
LS F3 (granite)	very rough morphology due to up to 4 m large boulders, bar-and-swale topography moderately preserved, dissected by shallow channels	60-80 %	partly interlocking stones with sandy intercalations, no vertical ab planes	ca. 20 % varnished, brown colours	rocks disintegrated or flaked, few stones with initial surfaces	very restricted, disperse
LS F4 (granite)	smooth morphology, gently undulating surface, bar-and-swale topography virtually eliminated, dissected by shallow channels	60-70 %	very sandy with small stones, clasts are interlocking	almost no varnish present	not resolvable if sandy material is of primary origin or results from weathering	restricted to drainage channels
LS F5 and F6 (diverse types of rhyolite)	smooth morphology, gently undulating surface, bar-and-swale topography virtually eliminated, dissected by shallow to deep channels	90-100 %	tightly packed, interlocking stones, no vertical ab planes	depending on rhyolite type partly to completely varnished	sharp rock fragments, partly shattered	restricted to drainage channels

feature. As a result, the diagnostic property for assigning a vesicular horizon becomes less prominent in some profiles as clay morphological features emerge. In such cases we designated the horizon as AvBt horizon to express compound properties. Furthermore, there are buried Av horizons. Since Av horizons are commonly regarded to form on the surface only (e.g. McFadden et al., 1986), buried ones are certainly fossil and, thus, designated Avb. In case they have been overprinted by argillic properties, AvbBt was assigned.

Field and laboratory results imply significant pedogenetic alteration of subsurficial sediments but also show large differences in parameters of soils even within small spatial distance. For two

profiles, CVF07-001 and CVF07-004 (cf. figure 2.3), less than 20 m apart from each other and typical for the range in soil properties found in all eight investigated profiles, these differences will be discussed in detail. Both outcrops did not show any differences in surface topography, diameter of rock fragments, desert varnish or any other surface property (cf. table 2.1) which would suggest subsurface heterogeneity. However, despite of similar Av and AvbBt horizons, soil and sediment properties of the outcrops vary remarkably.

CVF07-001 exhibits a complex stratigraphic and pedologic succession in accordance with descriptions by McFadden et al. (1986). Below the desert pavement two vesicular horizons are separated by nearly unaltered aeolian dust with single grain structure. The buried AvbBt with weakly developed subangular blocky structure is followed by several decimetre thick, argillic horizons with prominent angular blocky structure which end up in the chemically weathered basaltic rubble zone at a depth of approximately 115 cm. Gypsum and calcium carbonate enrichment is frequent throughout the entire profile, but most prominent within the argillic lower part. The sediment column exhibits two zones of stone enrichment. Between 7 and 15 cm as well as between 40 and 70 cm below the surface, buried basaltic rock fragments are concentrated, whereas being nearly absent in the rest of the profile. Such stone lines were detected in profiles CVF07-002, CVF07-003 and CVF07-006, as well. Wells et al. (1985) describe only one stone enrichment zone in 50 cm depth from some surfaces in Cima Volcanic Field.

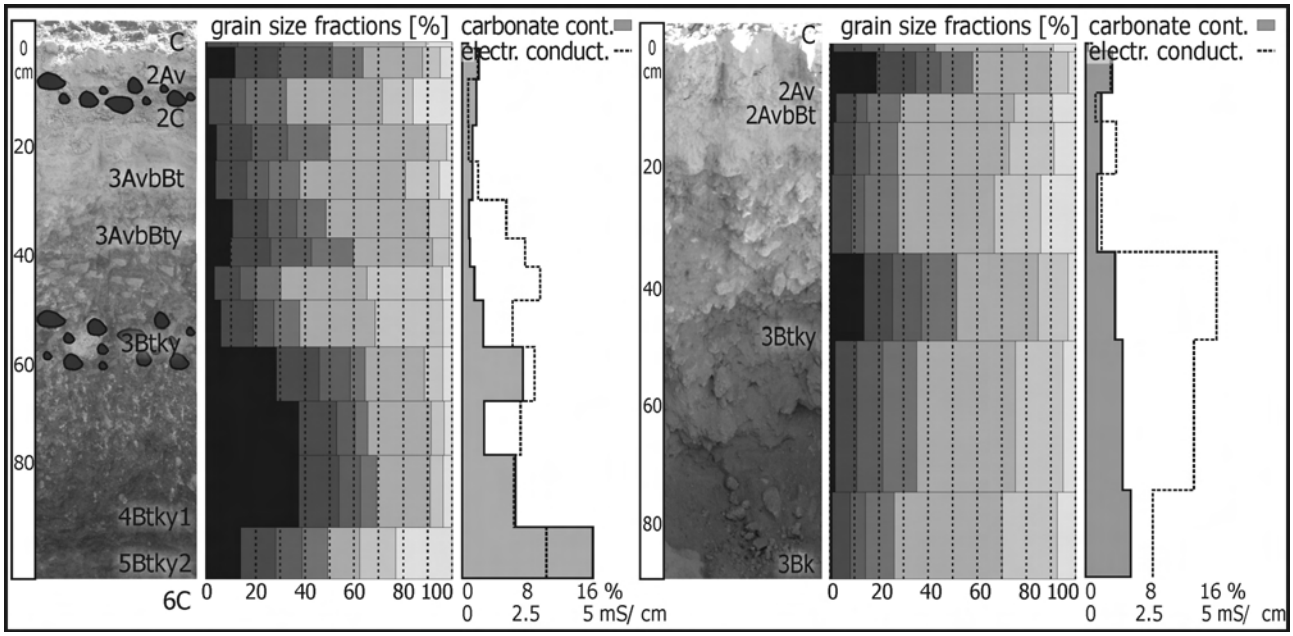

Figure 2.3. Soil profiles with laboratory results. For two typical soil profiles on a 560 ka old lava flow surface in Cima Volcanic Field laboratory data underline distinct differences in complexity and morphology. Left: profile CVF07-001, right: profile CVF07-004. Grain size class limits: 2, 6.3, 20, 63, 200, 630, 2000 µm. Stone lines are sketched, calcium carbonate content in percent is illustrated as grey area and electric conductivity in mS/ cm as dashed line.

Table 2.2. Results of soil field description in Cima Volcanic Field (CVF) and Laguna Salada (LS).

Soil profile	*Horizon*	*Depth [cm]*	*Boundary*	*Stones*	*Colour dry*	*Colour wet*	*Structure*	*Consistence*
CVF07-001	C	1	a, s	50	9.5YR 6/ 2	9.5YR 4/ 2.5	sg	lo/ ss/ sp
608609	2AvBt	8	a, s	0	9YR 6/ 2.5	9YR 4.5/ 3	3 c pri, pla	mh/ ms/ vp
3891967	2C	16	a, s	25	8.75YR 6/ 3	9YR 4.5/ 3	sg	so/ ms/ np
	3AvbBt	25	c, s	0	9YR 6.5/ 2	9.5YR 5/ 3.5	3 vf sbk	sh/ vs/ mp
	3AvbBty	38	c, s	2	8YR 5.5/ 3	9YR 4.5/ 3	3 m sbk, pla	h/ ms/ sp
	3Btky	60	c, s	2	7.5YR 5/ 3	8YR 4.5/ 3.5	3 vc abk, pla	h/ ms/ sp
	4Btky1	94	g, s	2	7YR 5/ 3	7.5YR 4.5/ 3.5	3 vc abk	mh/ vs/ vp
	5Btky2	106	a, s	2	8.5YR 5.5/ 3	8YR 5/ 3.5	3 vc abk	mh/ vs/ vp
	6C	115+	n.d.	100	n.d.	n.d.	n.d.	n.d.
CVF07-002	C	2	a, s	90	9YR 6.5/ 2.5	9.5YR 4.5/ 2.5	sg	lo/ ns/ np
608576	2AvBt	9	a, s	0	9YR 6.5/ 2.5	9YR 5/ 3	3 c pri, pla	mh/ ss/ np
3891964	3Btk1	23	g, w	5	7.75YR 6/ 3	7.5YR 5/ 3.5	2 m sbk	vh/ ss/ np
	3Btk2	51	g, w	5	7.5YR 6/ 3	8YR 4.5/ 3	3 vc sbk	h/ ss/ sp
	3Btky	95	c, w	2	8YR 6/ 3	8.5YR 4.5/ 3.5	3 vc sbk	h/ ss/ sp
	4C1	115	a, s	2	7.5YR 6/ 3	9.5YR 4.5/ 3	1 c sbk	so/ ns/ np
	5C2	140+	n. d.	50	7.5YR 5.5/ 3	8.5YR 4/ 2.5	sg	lo/ ns/ np
CVF07-003	C	1	a, s	90	5.5YR6.5/ 3	8.5YR5/ 3.5	sg	lo/ ss/ sp
608563	2AvbBt	8	a, w	5	8.5YR5/ 3	8.5YR4.5/ 3	3 c pri, pla	h/ ms/ vp
3891954	3C	18	c, s	10	8YR5.5/ 3.5	8.5YR4.5/ 3.5	sg	lo/ ss/ sp
	4Btky	40	c, w	5	8YR5.5/ 3.5	7.5YR4.5/ 3.5	3 f sbk	sh/ ss/ mp
	5Btk	80+	n.d.	90	7.5YR6/ 3.5	7.5YR5/ 3.5	2 vc abk	h/ ms/ vp
CVF07-004	C	1	a, s	100	9.5YR 6.5/ 2.5	9YR 4.5/ 2.5	sg	lo/ ss/ np
608601	2Av	7-10	g, w	2	9YR 6.5/ 2.5	9.5YR 5/ 3	3 c pri, pla	mh/ vs/ vp
3891986	2AvbBt	12	a, s	10	8.5YR 6.5/ 2.8	8.5YR 5/ 3.5	2 f pla	h/ ms/ vp
	3Btky	50	c, w	90	8.5YR 6/ 3	8.5YR 4.5/ 3.5	2 vf sbk	h/ ss/ mp
	3Bk	100+	n.d.	100	9YR 6.5/ 2.5	9.5YR 5/ 3	sg	lo/ ns/ np
CVF07-005	C	1	a, s	90	n.d.	n.d.	sg	lo/ ss/ np
608574	2Av	4-7	a, w	2	n.d.	n.d.	3 c pri, pla	mh/ vs/ vp
3892127	2BAvbBt	8	c, s	5	n.d.	n.d.	2 f pla	mh/ ms/ sp
	2Bky	80	a, w	50	n.d.	n.d.	sg	lo,so/ ss/ np
	3C	85+	n.d.	100	n.d.	n.d.	n.d.	n.d.
CVF07-006	C	2	a, s	100	n.d.	n.d.	sg	lo/ ss/ sp
608589	2Av	8	c, w	0	n.d.	n.d.	3 c pri, pla	mh/ ss/ sp
3892125	2AvbBt	12	a, i	2	n.d.	n.d.	2 f pla, sbk	so/ ss/ sp
	3Btky1	25	c, s	3	n.d.	n.d.	1 vf abk, sbk	so/ ss/ np
	3Btky2	50	c, s	5	n.d.	n.d.	3 vc abk	mh/ ss/ sp
	4Btky3	65	c, s	2	n.d.	n.d.	3 vc abk	mh/ ms/ vp
	5Btk	90+	n.d.	2	n.d.	n.d.	3 vc abk	h/ ms/ mp
CVF07-008	Av	5-7	a, w	2	10YR 7/ 2	10YR 3/ 4	2 c pri, pla	sh/ vs/ mp
605756	AvbBt	14	a, s	50	7.5YR 7/ 2	10YR 3/ 6	2 vf pla, sbk	mh/ ms/ mp
3893603	C1	30	c, i	90	10YR 6/ 3	10YR 3.5/ 4	sg	lo/ ss/ np
	2C2	30+	n.d.	100	n.d.	n.d.	n.d	n.d.
CVF07-009	Av	3-10	c, w	5	10YR 6/ 4	10YR 3.5/ 3	2 f pri, pla	so/ ms/ sp
605731	AvbBt	16	c, s	50	2.5Y/ 7/ 4	10YR 4.5/ 4	2 f pla, sbk	sh/ ss/ sp
3893579	C1	30+	c, i	90	10YR 6/ 3	10YR 3.5/ 4	sg	lo/ ss/ sp
	2C2	30+	n.d.	100	n.d.	n.d.	n.d	n.d.
LS-B1	Av	4	a, s	0	n.d.	n.d.	2 c pri, pla	so/ ss/ sp
610773	Bw	40	c, s	5	n.d.	n.d.	1 vf sbk	lo/ ss/ np
3591029	2C	40+	n.d.	90	n.d.	n.d.	n.d.	n.d.
LS-F1	AvBt	3	c, s	5	n.d.	n.d.	2 m pri, pla	h/ ss/ sp
635231	By	30	c, s	50	n.d.	n.d.	1 vf sbk	so/ ms/ mp
3586111	Cc	35+	n.d.	75	n.d.	n.d.	3 vc coh	r/ n.d./ n.d.
LS-F2	AvBt	3	c, s	5	n.d.	n.d.	2 m pri, pla	so/ ss/ sp
635045	Bw	65+	n.d.	75	n.d.	n.d.	1 vf sbk	lo/ ns/ np
3585804								
LS-F3	AvBt	2	a, s	2	n.d.	n.d.	3 m pri, pla	so/ ss/ np
611476	Bw	55+	n.d.	75	n.d.	n.d.	1 vf sbk	lo/ ns/ np
3578900								
LS-F4	AvBt	2	a, s	2	n.d.	n.d.	2 m pri, pla	so/ ss/ sp
653139	By	14	c, s	5	n.d.	n.d.	1 vf sbk	lo/ ns/ np
3587972	Bky	65+	n.d.	5	n.d.	n.d.	1 vf sbk	so/ ns/ np

Table 2.2. continued.

Soil profile	*Horizon*	*Clay*	*Carbonate/ Gypsum*	*Carbonate/Gypsum stage*
CVF07-001	C	0	fd/ 0	0/ 0
PDI* 56.9	2AvBt	1 f cfpf	0/ 0	0/ 0
PDI** 44.2	2C	0	fd/ 0	0/ 0
	3AvbBt	1 d cfpf, cfpo	fd/ 0	0/ 0
	3AvbBty	2 p cfpf, cfpo, br	fd/ co, cr	0/ II
	3Btky	3 p cfpf, cfpo, br	m/ cr	0/ II
	4Btky1	3 p cfpf, cfpo, br	m/ cr	I-/ II
	5Btky2	3 p cfpf, cfpo, br	0/ cr	0/ II
	6C	0	0/ 0	0/ 0/ 0
CVF07-002	C	0	0/ 0	0/ 0
PDI* 60.9	2AvBt	0	fd/ 0	0/ 0
PDI** 47.4	3Btk1	1 f cfpo	m/ 0	I/ 0
	3Btk2	v1 f cfpf, cfpo	m/ 0	I/ 0
	3Btky	v1 f cfpf	m/ cr	I-/ II
	4C1	0	fd/ 0	0/ 0
	5C2	0	fd/ 0	0/ 0
CVF07-003	C	0	fd/ 0	0/ 0
PDI* 44.3	2AvbBt	1 d cfpf, cfpo	fd/ 0	0/ 0
PDI** 36.1	3C	0	fd/ 0	0/ 0
	4Btky	1 d cfpf	m, fi/ m	I/ I
	5Btk	2 p cfpf, cfpo, br	m, fi, co/ 0	II/ 0
CVF07-004	C	0	0/ 0	0/ 0
PDI* 25.2	2Av	1 f cfpf	fd/ 0	0/ 0
PDI** 19.6	2AvbBt	2 d cfpf, cfpo	fd/ 0	0/ 0
	3Btky	2 d cfpf	fd/ n, cr	II+/ II
	3Bk	0	fd/ 0	II+/ 0
CVF07-005	C	0	fd/ 0	0/ 0
PDI* 17.5	2Av	0	fd/ 0	0/ 0
PDI** 14.6	2BAvbBt	1 f cfpf	m/ 0	0/ 0
	2Bky	0	fd/ m, n	I/ I
	3C	n.d.	n.d./ n.d./ n.d.	n.d./ n.d.
CVF07-006	C	0	fd/ 0	0/ 0
PDI* 50.0	2Av	0	fd/ 0	0/ 0
PDI** 41.6	2AvbBt	1 d cfpf, cfpo	m/ 0	0/ 0
	3Btky1	v1 d cfpf	fd/ m	0/ I
	3Btky2	2 p cfpf	m, fi/ m, fi	I+/ I
	4Btky3	3 p cfpf, hc	m, fi/ m, cr	I+/ II
	5Btk	3 p cfpf, hc	m, co/ 0	I+/ 0
CVF07-008	Av	v1 f cfpf	fd, m/ 0	0/ 0
PDI* 11.9	AvbBt	2 d cfpf, cfpo	fd/ 0	0/ 0
PDI** 9.9	C1	0	fd/ 0	0/ 0
	2C2	0	0/ 0	0/ 0
CVF07-009	Av	0	fd/ 0	0/ 0
PDI* 15.3	AvbBt	2 d cfpf, cfpo	m/ 0	0/ 0
PDI** 12.7	C1	0	fd/ 0	0/ 0
	2C2	0	0/ 0	0/ 0
LS-B1	Av	v1 f cfpf	fd/ 0	0/ 0
	Bw	0	fd/ 0	0/ 0
	2C	0	0/ 0	0/ 0
LS-F1	AvBt	1 f cfpf, cfpo	fd/ 0	0/ 0
	By	0	fd/ m, fi	0/ 0
	Cc	0	co/ 0	II/ 0
LS-F2	AvBt	1 f cfpf	fd/ 0	0/ 0
	Bw	0	fd/ 0	0/ 0
LS-F3	AvBt	1 f cfpf	fd/ 0	0/ 0
	Bw	0	fd/ 0	0/ 0
LS-F4	AvBt	1 f cfpf	fd/ 0	0/ 0
	By	0	fd/ n	0/ 0
	Bky	0	n/ m	I/ 0

Locations of the profiles are given in fig. 1 and fig. 2. Descriptions according to Gile et al. (1966), Bachmann & Machette (1977), HARDEN et al. (1991), Soil Survey Division Staff (1993) and Birkeland (1999). Coordinates under Profile ID in UTM system, zone 11 N. * Profile Development Index after Harden (1982). ** Profile Development Index after Harden & Taylor (1983).

Abbreviations: Depth: basal horizon depth in cm, Boundary: distinctness (a-abrupt c-clear g-gradual d-diffuse)/ topography (s-smooth w-wavy i-irregular b-broken), Stones: maximum percentage of material > 2 cm, Colour: Munsell colour code, data for colour was summarised to horizon resolution though originally determined for each sample, cf. laboratory data sheet. For samples, where no colour was determined, these parameters were omitted in PDI calculation, according to Harden & Taylor (1983), Structure: grade (1-weak 2-medium 3-strong 4-very strong)/ size (vf-very fine f-fine m-medium c-coarse vc-very coarse)/ type (sg-singe grain pri-prismatic pla-platy sbk-subangular blocky abk-angular blocky coh-coherent), Consistence: firmness (lo-loose so-soft sh-slightly hard mh-medium hard h-hard vh-very hard r-rigid)/ stickiness (ns-nonsticky ss-slightly sticky ms-medium sticky vs-very sticky)/ plasticity (np-nonplastic sp-slightly plastic mp-medium plastic vp-very plastic). Clay: frequency (0-no v1-very few 1-few 2-common 3-many)/ distinctness (f-faint d-distinct p-prominent)/ morphology (cfpf-clay films on ped faces cfpo-clay films on pores co-coatings br-bridges), Carbonate/ Gypsum: 0-not present fd-finey disseminated m-masses fi-filaments n-nodules co-concretions cr-crystals, Carbonate Stage after Birkeland (1999) and gypsum stage after Harden et al. (1991). Substages of soil morphology from field work were generalised here.

In contrast, profile CVF07-004 appears only weakly developed with an overall high stone content. Beneath the pavement-covered, stone free vesicular horizon, the soil column consists of up to 90 % coarse basalt fragments always coated by calcium carbonate rinds. Fine material shows weak subangular structure in the upper 50 cm and is loose in the basal part. Gypsum nodules and small crystals are found in the upper part. Grain size distribution is more homogeneous except for the vesicular horizon and a clay rich zone around 40 to 50 cm. Hence, this profile stands in prominent contrast to CVF07-001.

Surfaces on the 16 ka old basalt flow expose a rough morphology dominated by sharp escarpments of basaltic lava, pressure ridges, spines and local depressions filled with colluvial boulders, rocks and fine material. Drainage network development is of initial stage (Wells et al. 1985). Vegetation is restricted to widely dispersed Creosote bush. Patches with varnished, interlocking desert pavement are restricted to some tens of meters in size, disrupted by outcropping bedrock. Soil profiles were dug on a culmination spot and a depression. In contrast to the older lava flow, these soils (CVF07-008, CVF07-009) do not show major differences in any investigated subsurface feature. They have a vesicular horizon with coarse prismatic and columnar structure beneath the desert pavement. A subsequent shallow AvbBt horizon with weak subangular blocky structure is followed by a matrix of unconsolidated dust and almost unweathered volcanic rock. This C1 horizon consists to 90 % of clasts larger than 2 cm whereas in the upper horizons only few stones with calcium carbonate coatings are found. Calcium carbonate is finely disseminated throughout the profile but occurs as masses in the vesicle bearing horizons. At a depth of 30 cm massive volcanic bedrock forms the 2C2 horizon.

2.4.1.2 Laguna Salada

Abandoned surfaces around Laguna Salada vary considerably in surface morphology, stone pavement coverage and texture, desert varnish intensity and relative height (cf. table 2.1). At the eastern basin margin, sites F1 and F2 show prominent differences in topography and surface parameters, underlining their deviating relative ages. Desert pavement begins to establish at site F2 (loosely, unordered, not varnished) whereas it shows a higher stage of maturity on site F1 (tightly packed and interlocking, varnish present on favourable quartzitic lithology). Site F3 at the western basin margin is covered by 50 to 400 cm large, rounded, granitic boulders with intensive desert varnish but also flaked surfaces and grainy disintegration. Shrubs of up to 2 m height occur sporadically. Desert pavement is of intermediate stage compared to the former two sites. Stones within a sandy matrix carry moderate varnish and show interlocking arrangement. Site F4 displays a granitic desert pavement consisting of sand and small stones without desert varnish. The surface is levelled to a smooth topography with slight bar and swale relief dissected by shallow channels which host small shrubs.

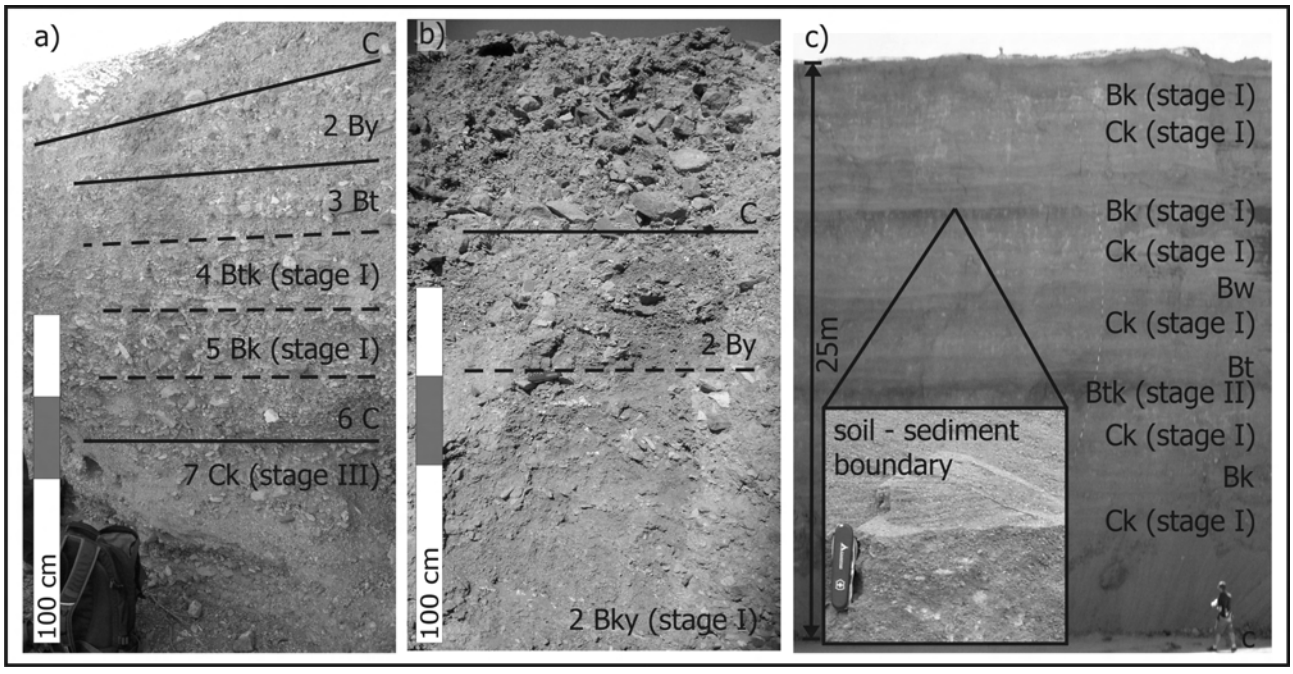

Figure 2.4. Palaeosol sequences of different habit. Surficial soils are not included in nomenclature for these three examples. Stages denote nomenclature of calcium carbonate morphology in soils after Gile et al. (1966), Bachmann & Machette (1977) and Birkeland (1999). For profile in 4c) no complete layer designation is possible and, hence, nomenclature does not include leading numbers. Inset in c) shows a typical erosional boundary between alluvial sediment covering mature soil with carbonate concretions.

Table 2.3. Results of laboratory analyses in Cima Volcanic Field (CVF).

Profile data		***Grain size distribution [%], class limits in µm***							***chemical data***		
Soil profile	Depth [cm]	< 2	2-6.3	6.3-20	20-63	63-200	200-630	630-2000	CC [%]	EC [mS/ cm]	pH in KCl
Silver Lake Playa*	0-5	9.57	9.57	6.14	31.62	42.45	0.64	0.02	n.d.	n.d.	10.09
CVF07-001	0-1	0.79	12.61	18.61	19.50	28.80	9.04	10.65	0.10	0.15	7.42
	4-7	12.02	17.49	21.82	12.59	24.09	7.16	4.82	1.40	0.54	7.31
	13-15	1.37	9.30	5.58	16.65	38.72	12.62	15.76	1.10	0.18	7.57
	17-20	4.55	14.04	14.61	17.27	39.92	7.43	2.18	0.70	0.21	7.46
	26-29	4.21	12.53	8.91	12.53	42.92	13.64	5.26	0.70	0.56	7.58
	32-34	11.09	14.25	11.68	11.88	41.67	8.38	1.05	0.30	1.62	7.26
	41-43	10.22	16.24	17.34	16.34	31.90	7.28	0.68	0.40	2.32	7.37
	46-48	3.65	10.25	6.51	10.25	34.75	30.63	3.96	0.90	2.88	7.62
	52-54	6.20	13.24	8.30	10.40	30.64	27.58	3.64	1.90	1.86	7.93
	64-66	28.86	17.27	12.60	6.00	24.02	6.66	4.60	6.40	2.68	7.99
	73-75	37.83	15.44	7.26	5.29	25.67	5.33	3.18	2.00	2.15	7.89
	85-87	37.86	16.36	8.64	6.69	21.57	5.26	3.62	5.60	1.90	7.90
	101-104	14.37	14.17	10.65	10.35	13.10	14.58	22.77	14.40	3.12	7.98
CVF07-002	0-1	5.71	13.49	12.60	20.18	34.31	10.35	3.34	1.00	0.26	7.83
	2-9	12.22	34.00	11.94	10.79	23.73	5.71	1.61	3.10	0.37	7.68
	13-15	1.70	18.34	7.09	14.56	37.79	15.08	5.44	5.90	0.1	8.04
	26-28	12.30	11.82	6.00	14.24	36.51	15.47	3.67	7.20	3.94	7.89
	33-35	16.17	12.05	7.46	12.63	39.36	9.25	3.07	7.00	3.01	7.9
	43-45	29.26	15.47	9.16	9.85	29.97	4.40	1.89	8.90	3.42	7.88
	58-60	19.43	18.45	9.37	11.54	29.54	7.74	3.93	7.40	2.96	7.94
	69-72	17.64	15.80	9.30	9.89	36.84	6.74	3.80	4.80	2.79	7.96
	78-80	n.d.	n.d.	n.d.	n.d.	n.d.	n.d.	n.d.	10.20	4.32	7.74
	87-90	15.33	12.29	6.00	16.71	25.67	16.21	7.80	8.20	4.32	7.77
	99-101	2.82	10.99	6.23	14.59	19.85	20.53	24.99	4.40	4.31	7.89
	109-111	1.88	8.13	3.17	15.17	16.56	20.27	34.81	1.80	3.46	8.2
	125-132	1.45	9.09	2.81	8.03	10.65	30.31	37.66	1.20	1.32	8.35
CVF07-003	1-8	16.62	15.56	11.14	16.04	32.14	6.40	2.09	4.20	0.73	7.84
	13-16	1.76	10.24	7.12	17.16	34.66	16.68	12.38	2.20	0.91	7.83
	20-22	4.93	12.67	13.77	16.79	33.30	11.97	6.57	0.40	2.2	7.73
	30-33	5.83	15.13	12.46	13.65	37.81	10.82	4.30	6.30	4.8	7.77
	45-49	18.20	17.91	9.39	10.65	32.95	7.51	3.38	16.10	5.57	7.98
CVF07-004	0-1	1.52	11.39	9.21	20.79	35.95	12.10	9.05	0.20	0.22	7.87
	2-7	19.08	15.95	10.08	13.11	31.45	7.39	2.94	3.40	0.95	7.5
	10-12	2.61	7.92	4.73	13.42	46.28	15.65	9.38	2.00	0.39	7.71
	15-17	1.48	8.85	5.90	11.31	45.52	18.26	8.68	2.00	1.16	7.85
	28-32	0.77	8.03	5.32	13.74	39.15	18.81	14.17	1.40	0.61	7.65
	40-42	14.04	11.49	11.69	14.44	33.19	12.18	2.97	3.80	4.93	7.71
	60-68	2.19	8.78	10.67	13.67	40.29	19.36	5.03	4.70	4.08	7.58
	86-92	0.99	7.39	6.11	11.83	43.65	22.52	7.52	5.80	2.52	7.85
CVF07-005	0-1	2.17	10.29	10.95	24.64	40.19	6.74	5.02	n.d.	n.d.	7.73
	3-7	12.52	15.85	14.09	20.58	25.17	6.43	5.36	12.40	2.05	7.85
	7-8	17.44	17.44	15.90	17.72	19.53	6.23	5.74	n.d.	n.d.	7.94
	12-16	4.78	12.35	9.26	20.62	32.87	10.92	9.19	n.d.	n.d.	7.66
	30-33	2.30	10.42	7.01	19.33	32.34	16.21	12.39	n.d.	n.d.	7.69
	70-75	2.30	11.11	10.15	29.98	28.15	7.96	10.35	n.d.	n.d.	7.78
CVF07-006	0-1	2.71	11.90	15.19	23.99	33.64	6.70	5.88	1.20	0.35	8.02
	2-8	22.17	17.62	13.83	18.10	22.69	4.46	1.13	9.80	0.36	7.77
	10-11	3.14	11.29	10.60	30.72	27.28	7.90	9.06	6.50	0.47	7.84
	15-17	4.87	11.63	11.93	18.69	28.90	15.71	8.26	7.00	1.64	8.04
	28-30	3.76	12.23	7.88	17.17	35.22	16.83	6.92	n.d.	n.d.	7.78
	36-38	5.28	14.30	11.11	23.32	33.19	8.86	3.94	n.d.	n.d.	7.87
	44-46	6.65	13.50	13.10	19.56	34.35	8.96	3.88	8.80	5.34	7.88
	55-57	13.54	17.09	13.76	26.85	19.19	7.70	1.87	6.00	4.98	8
	70-72	6.06	12.72	10.83	19.57	28.55	16.47	5.81	n.d.	n.d.	7.69
	81-83	10.22	14.80	13.63	23.65	30.74	5.85	1.11	9.20	3.71	7.89
CVF07-008	1-5	n.d.	n.d.	n.d.	n.d.	n.d.	n.d.	n.d.	n.d.	n.d.	7.65
	6-8	7.03	16.01	15.25	30.50	13.74	9.19	8.27	n.d.	n.d.	7.97
CVF07-009	2-7	2.29	13.12	12.80	34.97	32.59	2.93	1.30	n.d.	n.d.	7.69
	11-14	10.55	17.84	16.31	27.34	21.97	3.44	2.56	n.d.	n.d.	7.7
	19-21	8.15	11.37	10.43	18.01	35.61	11.95	4.48	3.70	0.18	7.8
	28-35	1.74	9.66	9.18	30.44	29.79	8.77	10.42	n.d.	n.d.	7.87

* Sediment sample from Silver Lake Playa as potential source of dust, CC-carbonate content, EC-electric conductivity.

Superficial soils on alluvial fans in Laguna Salada show overall similar properties, regardless of the deviating properties of the surface they are developed on (cf. table 2.2). A thin, 2 to 4 cm thick vesicular horizon is always present beneath the stone pavement layer and is followed by a generally weakly developed sub-horizon composed of local material with weathering features and a loose, sometimes weak to medium subangular blocky soil structure (cf. table 2.2). Fine material is not dominated by any grain size fraction. Aeolian dust as primary sediment component like in soils from Cima Volcanic Field has not been identified in Laguna Salada. Pedogenetic clay enrichment indicated by clay coatings of different morphology was not observed anywhere within the soil column. Calcium carbonate and gypsum occurs finely disseminated or forms filaments. In some profiles the basal part is impregnated with calcium carbonate concretions or salt crystallisations.

On the 12 Ma old basaltic cap rock (profile B1) barren patches of varnished and interlocking desert pavement stones form flat and homogeneous surfaces some hundred m² in size which are bounded by fields of boulders. The described soil profile has developed in a setting obviously sheltered from erosion, but with topographic features allowing deposition of dust. Hence, this site should have faced a sufficiently long sedimentologic and pedogenetic history to develop a mature soil. However, below the tightly packed and well-varnished pavement and 4 cm thick Av horizon a silt-rich, stone bearing Bw horizon of few dm thickness with loose structure and only finely disseminated calcium carbonate directly overlays bedrock (cf. table 2.2).

We also examined outcrops of 2 to 3 m depth on steep entrenched walls of alluvial fan sequences in Sierra Pinta (F5 and F6, cf. figure 2.4a and b). Their dissected, broadly undulating, barren surfaces are covered by tightly interlocking, angular, rhyolitic fragments with varying varnish cover intensity. Top soils of the two adjacent outcrops are similar in morphological properties and weakly developed as described above.

In contrast, deeper parts of the profile walls show remarkable differences in pedological and sedimentological features. Profile F5 (figure 2.4a) displays a complex sequence of sediment boundaries and sections of partially strong soil development. Horizon nomenclature is simplified by neglecting surface soil and regarding burying surficial material as C horizon. Pedogenesis involved calcium carbonate precipitation and weathering within the upper- and lowermost parts of the trench. Furthermore, indications for pedogenetic clay illuviation were found between 130 and 180 cm depth. In contrast, the sediment column of profile F6 (figure 2.4b) is monotonous and weakly overprinted by pedogenesis. A weathered and gypsum-enriched B horizon is buried by fresh C-material in which the surface soil develops.

A sequence comprising 25 m of alluvial sediments, palaeosols and reworked soil material (figure 2.4c) was accessible in a sand pit in the distal part of the granitic alluvial piedmont spanning the eastern slope of Sierra Cucapá (cf. figure 2.2, profile F4). From correlations of dipping stratae

along the large outcrop 2 km in circumference at least three zones of soil formation could be identified by weathering features and calcium carbonate nodules and concretions. In situ soils could be deciphered from frequently occurring reworked soil material by sharp upper boundaries and downward decreasing pedogenetic features (cf. figure 2.4c inset). The lowermost palaeosol at around 14 m depth is most strongly developed. It exhibits clay cutanes as well as calcium carbonate nodules and concretions resulting from clay translocation and subsequent carbonatisation. Discrete sedimentologic boundaries were not designated and included in horizon nomenclature. The surface soil on the flat and apparently inactive, sparsely vegetated site around this outcrop (cf. table 2.2) is monotonous and weakly developed, similar to all investigated soils close to the surface as described above.

2.4.2 Profile development indices

Calculation of the PDI requires ascertainment of parent material properties, least influenced by pedogenetic alteration. Table 2.4 summarises properties of aeolian fine sediment between desert pavement clasts and around plants. Average values were used as reference data for PDI calculations. The aeolian material of six samples typically shows similar properties. It consists of sandy loam with slight stickiness, no plasticity and loose dry consistence. Secondary argillic features are totally absent as well as pedogenetic structure formation.

Table 2.4. Reference data for PDI calculations. Mean properties of five aeolian dust samples, collected between pavement stones.

Hue dry	*Value dry*	*Chroma dry*	*Hue wet*	*Value wet*	*Chroma wet*	*pH*	*Texture class*	*Stickiness*	*Plasticity*	*Clay abundance*	*Clay thickness*	*Clay location*	*Structure grade*	*Structure type*	*Dry consistence*
9.25	6.41	2.31	9.25	4.44	2.41	7.77	sandy loam	ss	np	no	no	no	no	no	lo

Field descriptions of soil features serve as input data for the calculation of PDI. Table 2.2 shows these features as well as the calculation results. In general, values calculated after Harden (1982) are 22-17 % higher than values calculated after Harden & Taylor (1983). PDI for the four proximate soil profiles on the 560±80 ka old surface range from 61 to 25 (47 to 20) after Harden (1982) (after Harden & Taylor, 1983). The two additional soil profiles (CVF07-005 and CVF07-006) on this lava flow also show this large range by even lowering the minimum value of profile development to 18 (15). PDI values for the 16 ka surface are 15 and 12 (13 and 10). Figure 2.5 summarises the results and shows a comparison with results by McFadden et al. (1986) who also investigated soil profiles in Cima Volcanic Field. Further, comprehensive results by Harden & Taylor (1983) are given to show the overall range and scatter in PDI distribution. These authors derived indices from

abandoned surfaces of fluvial, alluvial, glacial and aeolian origin in modern aridic (xeric) moisture regimes around southwest North America. A grey bar in figure 2.5 illustrates the range of index values for the 560±80 ka old basalt flow.

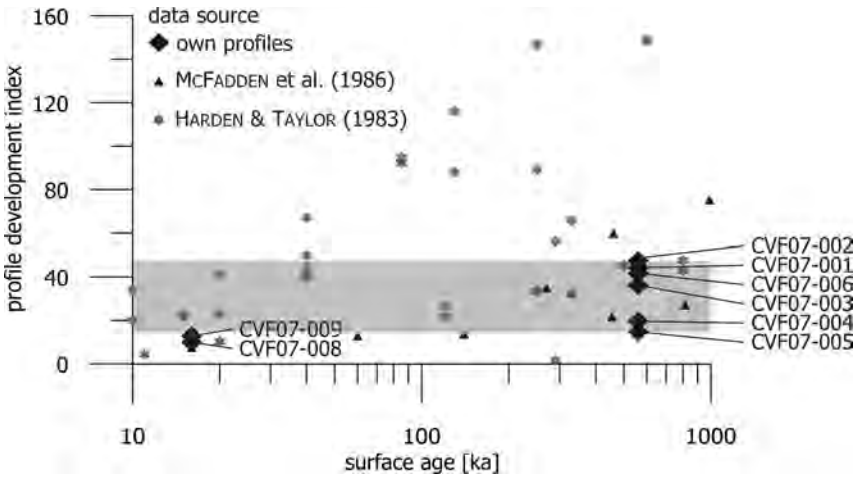

Figure 2.5. Profile development indices. Results from the own investigated profiles (diamonds, after Harden & Taylor, 1983) in comparison with results from further profiles at Cima Volcanic Field (triangles, McFadden et al., 1986, after Harden, 1982) and general values of soils from study areas in the arid southwestern US (stars, after Harden & Taylor, 1983). The grey bar illustrates the value range for the 560±80 ka old surface.

2.5 Discussion

2.5.1 Surface characteristics as relative age indicators

Results from Cima Volcanic Field show the general potential of surface parameters to distinguish different maturity stages. Wells et al. (1985) already characterised several basalt flows of specific age for this study area. The change from rough, bedrock-dominated topography with a juvenile drainage network and colluviation-dominated material dislocation on the 16 ka flow to a smooth surface with barren patches of desert pavement that is levelled by aeolian sediment accretion with intercalated soil formations and dissected by an intact drainage network on the 560 ka basalt flow is obvious and covers an enormous age offset. On such long timescales surface degradation by relief levelling, drainage network development and surface dissection apparently shows sensitivity as relative age indicator. The properties of stone pavements on the two investigated basalt flows, however, are not as varying as other surface properties (cf. table 2.1). They show similar characteristics, independent of flow age and even topography. Considering ancient, buried stone pavements on the 560 ka lava flow, a stone pavement does not necessarily carry information about the entire time period since lava flow formation. Consequently, a stone pavement appears to be sensitive to surface alteration over much smaller timescales. In Cima Volcanic Field, it further cannot trace obvious differences in subsurface, i.e. soil properties.

In Laguna Salada there is no direct numeric age control for the investigated sites. Consequently, we cannot establish and discuss a relationship between surface properties and time period since abandonment. However, sites show distinct differences in topographic as well as in stone pavement properties. For the two sites of the same alluvial fan system (F1 and F2) surface degradation is reflected by a clear change from dominating primary topography and initial dissection (F2) towards surface smoothening and deeply incised channels (F1). Alteration in stone pavement properties includes increased interlocking, desert varnish cover and stone disintegration on the older F1 site. Comparison with the results of Spelz et al. (2008) would suggest a Q5 to Q6 stage for site F1 and a Q3 stage for site F2. As all surface features show consistent change, designation of relative ages by classical approaches (cf. table 2.1) is allowed. We conclude that the period of abandonment which separates the two sites is too short to reach maturity stages of the investigated surface parameters. The surface of the 12 Ma old basaltic cap rock site clearly represents smoothening of topography by accretion of aeolian material and development of a mature stone pavement (tightly interlocking, varnished clasts). However, it only takes an intermediate stage of degradation (when expressed by stone pavement patch size, surface levelling and drainage network formation) in comparison to the 16 and 560 ka old sites in Cima Volcanic Field. Therefore, site B1 illustrates inadequacy of comparing surface features to infer relative ages in different regions, even if these regions would have a similar modern geomorphologic and climatic setting.

More general uncertainties in comparing surfaces of different alluvial fan systems arise from several sources, e.g. differing lithology of adjacent fan systems or even intra-fan changes of material properties. Desert varnish intensity and rock weathering grade vary with rock type. Granular disintegration and flaking as it is typical for granitic rock prevents using rock varnish as reliable age indicator because stepwise rejuvenation of the rock surface successively removes already formed coatings. Further, alluvial fan sections change surface habit and topography with increasing distance from their apex. Strongly dissected surfaces of the same age show significant differences in bar and swale topography, with proximal parts tending to conserve initial rough topography due to greater clast sizes. It is improper to use similar surface features when comparing proximal to medial parts of one fan with medial to distal parts of another fan. Therefore, we suggest considering longitudinal section dependency when using surface properties to estimate relative ages.

2.5.2 Soil formation on the 560 ka basalt flow in Cima volcanic field

Besides similar properties of vesicular horizons, profiles on the 560 ka basalt flow exhibit strong heterogeneities in accretionary soils until bedrock is reached, even though the pavement surfaces show overall similarities. Bedrock inhomogeneity appears not to play a significant role for explaining heterogeneity in the accretionary mantle. The similarly developed surface may be the

result of dust accretion and subsequent uplift of stones as suggested by McFadden et al. (1986). However, stone contents in the soils of up to 90 % vs. less than 5 % need to be explained by a geomorphologic mechanism which is able to dislocate this coarse material within small-scale patterns and which further may not be traced by surficial features. We suggest fluvial processes to be responsible for spatially restricted accumulation of rock fragments. Accretion of aeolian material fills the voids and leads to subsequent uplift of the surficial stones in order to establish the present stone pavement surface. A temporal fixation of these processes, however, remains uncertain. These findings imply that stone-rich soil profiles (i.e. CVF07-004 and CVF07-005) as well as surface properties in general do not represent the time period since the formation of this 560 ka old volcanic landform. McFadden et al. (1986) conclude that accretion of aeolian material occurred during phases of enhanced dust activity. Surface modification may thus be the result of discrete episodes rather than continuous evolution. Buried stone lines in accretionary profiles may be interpreted as fossil desert pavements (Wells et al. 1985). They also document switches in geomorphologic process systems as aeolian sediment input alternates with concentration of stones and leads to their subsequent burial.

An explanation for the decoupled evolution of soils and surfaces would be to regard stone pavements as a systematic, non-stable surface feature, able to reseal gaps or disruptions. Our suggestion is supported by experiments from Panamint Valley on the reformation of patches cleared from desert pavement (Haff & Werner, 1996) and studies from ancient plant scar features, also recovered by an interlocking stone pavement (McAuliffe & McDonald, 2006). However, if a stone pavement can reform, if stones can become turned upside down as reddish colours on clast faces suggest (Haff, 2001), the quality of such a dynamic surface for estimating ages has to be called into question.

2.5.3 Soil formation on the 16 ka basalt flow in Cima volcanic field

Localisation of a soil profile either in a depression or at a local culmination position, wind-exposition, surface roughness, potential water budget and further factors presumably do not have the potential to cause differences in pedogenetic sediment alteration on this 16 ka old lava flow. Development depth of the dust-bearing vesicular horizon and pedogenetic features such as matrix structure, consistence, clay and calcium carbonate morphology is alike at both investigated sites. Either soil alteration is not primarily influenced by topography in general or a surface age of 16 ka is not sufficient to allow topographically induced soil differentiation. Our study cannot resolve this question. Further, the amount of accumulated dust is also independent from topographical position which might be explained by supply limitation rather than differing dust trapping efficiency due to relief properties. Redistribution of deposited dust by fluvial activity is also unlikely as it would result in different thickness values.

A hiatus between lava flow age and the age of the soil developed on it appears to exist in this case, too. Soil morphological features lack properties for soil formation under a moister climate than at present, though 16 ka ago moisture should have been sufficient (Van Devender & Spaulding, 1979) to be traced by soil structure or even clay morphology (Birkeland, 1999). An incipient period of dust mobilisation only after the switch to arid climate as proposed by McFadden et al. (1986) would explain these findings.

2.5.4 Soil formation in Laguna Salada

In the Laguna Salada area soil development throughout the first 5 to 8 decimetres is weak and homogenous at all investigated sites, independent of parent material and surface properties. Consequently, a clear relationship of soil formation with relative surface maturity cannot be stated from field descriptions.

Surficial soils, apart from the vesicular horizon, are not primarily composed of aeolian dust and there is no substantial change in stone content throughout the soil column. Except for site B1, soils are not lithologically decoupled from parent material properties by aeolian components. Therefore, soils in Laguna Salada are not comparable to those in Cima Volcanic Field, though modern climate and geomorphologic setting (abandoned surfaces with stone cover and a close-by dust source) is comparable. This discrepancy underlines uncertainties resulting from transferring concepts of soil and surface evolution from one landscape to another. Profile B1 on the 12 Ma old surface possesses an aeolian mantle, similar in material properties and thickness to profiles on the 16 ka old lava flow in Cima Volcanic Field. This means, soil displays similar properties on landforms which are abandoned for time periods three orders of magnitude apart.

In agreement with the results from Spelz et al. (2008) our investigations could not state any argillic features. Even soils on fan surfaces as old as 204 ka (Spelz et al., 2008) do not exhibit clay cutanes. This lack may be explained by a moisture deficit since abandonment that was efficient enough to prevent decalcification and subsequent clay translocation. Hence, even during the Pleistocene climate was not wet enough to favour argillic horizons. However, as soils from outcrops east of Laguna Salada and in Sierra Pinta (cf. figure 2.4b and 2.4c) imply, there has been a time period with a climate sufficiently wet to allow soil formation with distinct clay cutans. These soils are now buried by alluvial sediment and overprinted by calcium carbonate formation. However, due to missing numerical age determination the timing of this period remains speculative so far.

Fossil palaeosol sequences from both outcrops in Sierra Pinta (figure 2.4a and 2.4b) are as varying as soils on the 560 ka basalt flow from Cima Volcanic Field, regarding stratification and complex vs. monotonous pedogenesis. Surface features do not trace these differences here, too. This suggests similar ambiguities in soil formation and surface degradation, apparently resulting from different geomorphologic and pedogenetic processes.

2.5.5 Profile development indices

As expected, the investigated soils developed on younger surfaces exhibit lower PDI values than soils on older surfaces. However, a clear age relationship cannot be stated. Some soils on the 560 ka surface yield development indices as they are characteristic for 16 ka surfaces. Four soil profiles, located less than 50 m apart, (CVF07-001 to CVF07-004) expose value deviations of 240 % even though no indication of differing site properties is present from surface observation.

Index value range is primarily controlled by the strongly deviating pedogenetic properties of the investigated soils which are the result of deviating sediment formation and rework by small-scale differentiated geomorphologic processes as well as subsequent soil formation. Our results from Cima Volcanic Field imply that there is no representative profile for the entire 560 ka surface at all. Rather, a mosaic of clast rich, weakly pedogenetically overprinted soils alternates with almost clast free, strongly overprinted aeolian sediments which form successions of accretionary soils. We therefore suggest PDI should be used with care. Their adequacy as proxy for evaluating chronofunctions is not always given but may be impaired by non-systematic differences in soil morphological features.

Comparison of our own results with other published data from Cima Volcanic Field gave similar values for the 16 ka old basalt flow, only. A weak time-dependence of PDI may be observed for flows younger than 200 ka (triangles in figure 2.5). However, PDI fluctuated broadly between values of 21 and 75 (McFadden et al., 1986; calculated after Harden, 1982) for older basalt flows without any relation to age. The own results of closely spaced profiles mimic this scatter. Considering the generally 22 to 17 % lower values when using calculation directives from Harden & Taylor (1983) even the range is resembled. As McFadden et al. (1986) emphasise there may be pedogenetic processes in mature aridic soils that result in a lowering of PDI due to masking effects.

Hence, PDI do not explain chronologically consistent overprinting of sediments by pedogenesis. Their value for quantifying soil maturity is questionable if not supported by expert information in the field that can resolve and omit unsuitable input data for calculation. Correlation of PDI from different regions to designate surface ages (Mueller & Rockwell, 1995) appears even more improper.

2.6 Conclusions

Studies of surface and soil features on abandoned surfaces in two areas with comparable modern arid climate suggest that a soil and its associated surface do not act as congeneric archives. They do not record the same signals of palaeoclimatic, palaeo-geomorphologic and palaeo-environmental conditions. Rather, the both archives appear to be separate, decoupled from each other. It is, thus, not possible to deduce soil properties from surface features and vice versa.

Desert pavements appear to be a dynamic feature on abandoned surfaces in arid environments. This would have consequences for their usability to retrieve maturity proxies (e.g. stratigraphy of desert varnish microlaminations or dating of varnish constituents). It should be considered that surface exposure dating of a mobile stone pavement may lead to age underestimations, as well.

Soils at one site of supposed uniform evolution show prominent maturity differences, when expressed by PDI. At Cima Volcanic Field even within a few metres discrepancies are nearly as distinctive as maturity differences caused by a time offset of approximately 540000 years. On the investigated 560 ka basalt flow there is no standard soil profile representative for the lava bed. Rather, there is a profile-fabric, resulting from spatially different pedogenesis and geomorphodynamics. Spatial variation on small scales can thus be much higher than temporal variation on large scales. Consequently, it is not possible to use single soil profiles as archives for chronosequences without clarifying their relationship to the geomorphologic setting. To reconstruct palaeo-landscapes it is necessary to focus on both, soil properties in a spatial context, and the geomorphologic process environment co-affecting soil formation. A linked network of outcrops has to be investigated and interpreted both, as soils and sediments.

Results from Laguna Salada and Cima Volcanic Field show that landscape history, if only expressed by soil formation, may differ remarkably when comparing regions that are alike today. In Laguna Salada soils on 12 Ma old sites are of comparably weak and uniform development as soils on 16 ka old sites in Cima Volcanic Field. Using PDI from modern arid to hyperarid sites as time markers and transferring them to other regions with a varying petrographic, tectonic, geomorphologic and presumably palaeo-climatologic framework appears to be inadequate considering the described uniformity of soil maturity even on sites temporally separated by three orders of magnitude.

Acknowledgements

Valuable contribution regarding financing, infrastructure, field work, thought-provoking and interpretation was generously provided by Arno Kleber, Dominik Faust and Carsten Lorz ,TU Dresden, Juan Carlos Herguera, John Fletcher, Arturo Martin-Barajas, CICESE Ensenada as well as Denisse, Horacio and the student group who joined the Ambas Californias Field Trip 2008. We would like to thank Adrian Harvey for his helpful comments on the manuscript. Our paper greatly improved from this review.

References

AL-FARRAJ, A. & A. M. Harvey (2000): Desert pavement characteristics on wadi terrace and alluvial fan surfaces: Wadi Al-Bih, U.A.E. and Oman. – Geomorphology **35**: 279-297.

AMIT, R. & R. Gerson (1986): The evolution of Holocene Reg (gravely) soils in deserts – An example from the Dead Sea region. – Catena **13**: 59-79.

AMIT, R., R. Gerson & D.H. Yaalon (1993): Stages and rate of the gravel shattering process by salts in desert Reg soils. – Geoderma **57**: 295-324.

BACHMANN, G.O. & M.N. Machette (1977): Calcic soils and calcretes in the southwestern United States. – US Geological Survey Open-File Report **77-794**: 1–163.

BILZI, A. & E. Ciolkosz (1977): A field morphology rating scale for evaluating pedological development. – Soil Science **124**: 45–48.

BIRKELAND, P.W. (1985): Quaternary soils of the western United States. In: Boardman, J. (Ed.): Soils and Quaternary Landscape Evolution: 303-324; Whiley, Chichester etc.

- (1999): Soils and geomorphology. – 3rd edition, Oxford University Press, New York, Oxford: 430 pp.

BIRKELAND, P.W. & J.S. Noller (2000): Rock and mineral weathering. In Noller, J.S., J.M. Sowers & W.R. Lettis (Eds.): Quaternary Geochronology: Methods and Applications. – American Geophysical Union, Washington, D. C., pp 293-312.

BULL, W.B (1991): Geomorphic response to climatic change. - Oxford University Press, New York, 326 pp.

- (1996): Global climate change and active tectonics: effective tools for teaching and research. – Geomorphology **16**: 217–232.

DIETZE, M., A. Kleber & J.-U. Schmidt (2008): Desert pavements with stratified soils as indicators of Quaternary landscape development. – Geological Society of America Abstracts with Programme **40/ 6**: 58-4.

DORN, R.I. & T.M. Oberlander (1982): Rock varnish. – Progress in Physical Geography **6**: 317-367.

ENZEL, Y., S.G., Wells & N. Lancaster (Eds., 2003): Paleoenvironments and paleohydrology of the Mojave and Southern Great Basin Deserts. – Geological Society of America Special Paper **368**: 249 pp.

FARR, T.G. (1992): Microtopographic evolution of lava flows at Cima volcanic field, Mojave Desert, California. – Journal of Geophysical Research **97**: 15171–15179.

GILE, L.H., F.F. Peterson & R.B. Grossman (1966): Morphological and genetic sequences of carbonate accumulation in desert soils. – Soil Science **101**: 347–360.

HAFF, P.K. (2001): Desert Pavement: An Environmental Canary? – The Journal of Geology **109**: 661–668.

HAFF, P.K. & B.T. Werner (1996): Dynamical Processes on Desert Pavements and the Healing of Surficial Disturbances. – Quaternary Research **45**: 38–46.

HARDEN, J.W (1982): A quantitative index of soil development from field descriptions: examples from a chronosequence in central California. – Geoderma **28**: 1–28.

HARDEN, J.W. & E.M Taylor (1983): A quantitative comparison of soil development in four climatic regimes. – Quaternary Research **20**: 342–359.

HARDEN, J.W., E.M. Taylor, C. Hill, R.K. Mark, L.D. McFadden, M.C. Reheis, J.M. Sowers & S.G. Wells (1991): Rates of soil development from four soil chronosequences in the Southern Great Basin. – Quaternary Research **35**: 383–399.

HAUGLAND, J.E. & B.S.O. Haugland (2008): Cryogenic disturbance and pedogenetic lag effects as determined by the profile developmental index: The styggedalsbreen glacier chronosequence, Norway. – Geomorphology **96**: 212–220.

HELMS, J.G., S.F. McGill & T.K Rockwell (2003): Calibrated, late Quaternary age indices using clast rubification and soil development on alluvial surfaces in Pilot Knob Valley, Mojave Desert, southeastern California. – Quaternary Research **60**: 377–393.

JENNY, H. (1941): Factors of Soil Formation. – McGraw-Hill, New York, 281 pp.

KLEBER, A. (1994): On the paleoecology of the northern Great Basin and adjacent Rocky Mountains. – Zeitschrift für Geomorphologie N. F. **38**: 421-434.

- (1999): Cover-beds as relative-dating tools - examples from the western U.S.A. – Zeitschrift für Geomorphologie N. F. **43**: 51-59.

- (2000): Compound soil horizons with mixed calcic and argillic properties - examples from the northern Great Basin, USA. – Catena **41**: 111-131.

KOEHLER, P.A., R.S. Anderson & W.G. Spaulding (2005): Development of vegetation in the Central Mojave Desert of California during the late Quaternary. – Palaeogeography, Palaeoclimatology, Palaeoecology **215**: 297–311.

LIU, T. & W.S Broecker (2007): Holocene rock varnish microstratigraphy and its chronometric application in the drylands of western USA. – Geomorphology **84**: 1–21.

MARTÍN-BARAJAS, A., S. Vásquez-Hernández, A. Carreno, J. Helenes, F. Suárez-Vidal & J. Alvarez-Rosales (2001): Late Neogene stratigraphy and tectonic control on facies evolution in the Laguna Salada Basin, northern Baja California, Mexico. – Sedimentary Geology **144**: 5–35.

MCAULIFFE, J.R. & E.V. McDonald (2006): Holocene environmental change and vegetation contraction in the Sonoran Desert. – Quaternary Research **65**: 204–215.

MCDONALD, E.V., L.D. McFadden & S.G. Wells (1992): The influence of dust, lithology, and microtopography on the formation of desert pavement. – Technical Reports 10, Proceedings of the east Mojave Desert Symposium 7-8 November1992, University of California, Los Angeles: 85-86.

MCFADDEN, L.D., S.G. Wells & J.C. Dohrenwend (1986): Influences of quaternary climatic changes on processes of soil development on desert loess deposits of the Cima volcanic field, California. – Catena **13**: 361–389.

MCFADDEN, L.D., J.B. Ritter & S.G. Wells (1989): Use of multi-parameter relative-age methods for age estimation and correlation on alluvial fan surfaces on a desert piedmont, eastern Mojave Desert, California. – Quaternary Research **32**: 276-290.

MUELLER, K.J. & T. K. Rockwell (1995): Late Quaternary activity of the Laguna Salada fault in northern Baja California, Mexico. – Geological Society of America Bulletin **107**: 8–18.

REHEIS, M.C., J.W. Harden, L.D. McFadden & R.R. Shroba (1989): Development rates of late Quaternary soils, Silver Lake Playa, California. – Soil Science Society of America Journal **53**: 1127–1140.

SAUER, D., G. Schellmann & K. Stahr (2007): A soil chronosequence in the semi-arid environment of Patagonia (Argentina). – Catena **71**: 382–393.

SCHMIDT, J.-U., A. Kleber & M. Dietze (2008): Soil evolution during the past 30,000 years in the Black Rock Desert, Utah, SW USA. – Geological Society of America Abstracts with Programme **40/ 6**: 532

SCHLICHTING, E., H.-P. Blume & K. Stahr (1995): Bodenkundliches Praktikum. – 2nd Edition, Blackwell Verlag, Berlin, Oxford, 295 pp.

SHUM, M. & L.M. LAVKULICH (1999): Use of sample color to estimate oxidized Fe content in mine waste rock. – Environmental Geology **37**: 281-289.

SOIL SURVEY DIVISION STAFF (1993): Soil Survey Manual. – Soil Conservation Service. U.S. Department of Agriculture Handbook **18**, 315 pp.

SPELZ, R., J. Fletcher, L. Owen & M. Caffee (2008): Quaternary alluvial-fan development, climate and morphologic dating of fault scarps in Laguna Salada, Baja California, Mexico. – Geomorphology **102**: 578-594.

TSAI, H.,W.-S. Huang & Z.-Y. Hseu (2007): Pedogenic correlation of lateritic river terraces in central Taiwan. – Geomorphology **88**: 201–213.

TURRIN, B.D., J.C. Dohrenwend, R.E. Drake & G.H. Curtis (1985): K-Ar ages from Cima volcanic field, eastern Mojave Desert, California. – Isochron/ West **44**: 9–16.

UFNAR, D.F. (2007): Clay coatings from a modern soil chronosequence: A tool for estimating the relative age of well-drained paleosols. – Geoderma **141**: 181–200.

VAN DEVENDER, T.R. & W.G. Spaulding (1979): Development of Vegetation and Climate in the Southwestern United States. – Science **204**: 701-710.

WELLS, S.G., J.C. Dohrenwendt, L.D. McFadden, B.D. Turrin & K.D. Mahrer (1985): Late Cenozoic landscape evolution on lava flow surfaces of the Cima Volcanic field, Mojave Desert, California. – Geological Society of America Bulletin **96**: 1518-1529.

ZIELHOFER, C., Recio Espejo, J.M., Nunez Granadoz, M.A. & Faust, D., in press: Durations of soil formation and soil development indices in a Holocene Mediterranean floodplain. – Quaternary International.

GLCF (2008): Global Landcover Facility. – http://glcf.umiacs.umd.edu/ index.shtml [10.12.2008]

NCDC (2008): National Climatic Data Center, Global Historical Climatology Network. – http://www.worldclimate.com/cgi-bin/data.pl?ref= N32W115+2100+7605018G1 [10.12.2008]

WRCC (2008): Western Regional Climate Centre at Desert Research Institute. – www.wrcc.dri.edu/summary/ Climsmsca.html [10.12.2008]

3 Contribution of lateral processes to stone pavement formation

Chapter 3 is published in the peer-reviewed journal Geomorphology (ISSN 0169-555X) as:

Contribution of lateral processes to stone pavement formation in deserts inferred from clast orientation patterns

Authors: Michael Dietze[1], Arno Kleber[1]

[1] Institute of Geography, Technische Universität Dresden

Publication history: submitted: February 2001, accepted: October 2011, published: February 2012.

Full reference: Dietze M, Kleber A. 2012. Contribution of lateral processes to stone pavement formation in deserts inferred from clast orientation patterns. Geomorphology 139-140: 172-187.

Internet link: http://www.sciencedirect.com/science/article/pii/S0169555X11005319

Abstract: Stone pavements are widespread landforms of arid environments. They typically develop by accretionary rise above a thickening aeolian mantle which usually contains a surficial vesicular unit. Hence, stone pavements are regarded as stable landforms and, thus, are often used as surface-age indicators. We studied orientation patterns of pavement clasts and depict their geometrical properties. We introduce a new statistical approach for quantitative description of circular data. From four study regions in a wide variety of environmental settings we show that preferred, non-random orientation of clast length axes is a recurrent feature of modern stone pavements. Orientation is primarily determined by no other relief parameter than slope aspect. In 40 out of 52 measured plots an angle of 72 ± 9° separates two angle maxima. The same patterns are present in stone lines buried under a cover of aeolian dust. We interpret these features as fossil stone pavements, accordingly. Furthermore, on artificially cleared plots disturbed stone pavements begin to recover within few months by a process which creates essentially the same orientation pattern.

We suggest that lateral surficial processes such as unconcentrated overland flow and creep contribute to the formation and maintenance of stone pavements as well as to this preferred clast orientation. They arrange clasts symmetrical to slope aspect with an angle determined by the axes ratio of the transported object. This results in the frequent bimodal pattern of stone length axes. This special type of transport requires previous accumulation of aeolian material forming a fine grained, even vesicular layer. Thus, there is close relationship between stone pavement and vesicular layer.

We conclude that lateral processes take part in stone pavement formation. The commonly accepted model of dust accretion, which is not rendered obsolete by our findings, has to be complemented by this lateral component. This has implications for the stability of stone pavement-covered surfaces and for their applicability as age indicators. Quickly resealing disturbances as well as fossilised stone pavements imply this prominent desert surface feature may become fragile and transient.

Keywords: Stone pavement; Fabric analysis; Circular data; Arid geomorphology; Stone orientation pattern

3.1 Introduction

Stone pavements are distinct surface features in arid environments. Their formation is interpreted by several, partly contradicting models: lag deposits due to aeolian/ fluvial erosion (e.g. Blake, 1858; Sharon, 1962), exhumation of clasts (e.g. Cooke, 1970), differential weathering (Mabbutt, 1977). Cooke et al. (1993) give a review of these models. McFadden et al. (1986) propose a model based on Mabbutt (1977) which is now widely accepted. According to this, the rough stony surface acts as a trap for aeolian material and accounts for accretionary profile development. As a consequence, the aeolian mantle thickens with time and the pavement always remains at the surface. In present models stone pavement development is restricted to vertical processes whereas lateral processes are virtually neglected. Williams & Zimbelman (1994) explain clast concentration on bare bedrock by sheetfloods but these phenomena do not comply with the commonly accepted stone pavement definition as a tightly interlocking monolayer mosaic of coarse particles resting upon or being partly embedded in fine sediment, which often exhibits a prominent foamy structure (the vesicular layer, cf. McFadden et al., 1998 for a review).The above models regard stone pavement covers as mature surfaces and, thus, as representing a chronofunction, with properties changing gradually with time. Many studies rely on this perception and utilise stone pavements as well as associated features as relative age indicators (Wells et al., 1985; McFadden et al., 1989; Al-Farraj & Harvey, 2000; Helms et al., 2003; Liu & Broecker, 2007). Crack measurements on clasts by Eppes et al. (2010) also imply surface stability. Arguments for long-term surface exposure (up to 10^6 years) of clasts as well as concordance with bedrock age come from cosmogenic nuclide studies (e.g. Wells et al., 1995; Fujioka et al., 2005; Nichols et al., 2007; Matmon et al., 2009).

However, there are also several arguments against stability. Marchetti & Cerling (2005) show distinct age differences between stone pavement clasts and embedded boulders. Wells et al. (1985) and Higgitt & Allison (1999) describe buried pavement clasts within accretionary aeolian mantles. This implies that stone pavements may become buried and the modern surficial stone cover does not necessarily represent the time span since initial stone pavement formation. Fossilising a stone pavement requires a lateral source of new coarse covering material. McFadden et al. (1998) mention studies about tilted carbonate collars around pavement clasts and suggest non-random geomorphologic processes such as soil creep to account for this. Haff & Werner (1996) report oriented-stone migration into disturbed plots but do not suggest processes to account for this. Quade (2001) concludes that stone pavements may be seriously disrupted by immigrating vegetation under moister climatic conditions and are able to re-establish on time-scales of 10^2 to 10^5 years. Pelletier et al. (2007) show by numeric modelling that distorted stone pavements recover on even shorter time-scales (10^1 to 10^2 years). Dietze et al. (2011) raise doubt about the relationship of stone pavement properties and surface age based on the remarkable variability of soil maturity and profile stratification within small distances, although stone pavement characteristics do not change. This implies an age hiatus of this feature, its instability and ability to re-establish rapidly. Frequent oc-

currence of clasts with reddish colours on their upper sides argues for up-turned stones and thus surface instability, since these colours develop only on under sides of clasts (Helms et al., 2003).

The term mosaic in the above definition of stone pavements suggests random to normal distribution of azimuthal stone length axes angles (Pelletier et al., 2007; Moores et al., 2008). Few studies have focused on orientation patterns of stone pavement surfaces. Abrahams et al. (1990) present fabric analyses from debris-covered hill slopes in the arid southwestern United States, suggesting hydraulic processes as the most reasonable cause of preferred orientation generation. Adelsberger & Smith (2009) show preferred orientation directions for a few stone pavement plots (but also many unoriented ones) from the hyper-arid Libyan Plateau, Egypt, but do not link them to geomorphologic processes. During five field campaigns in several hyper-arid to semi-arid areas we observed stone pavement surfaces to commonly exhibit preferred orientation patterns (i.e. stone length-axes orientation), whereas uniform or random distributions are much less frequent. Identification and quantitative description of orientation patterns provide insight into controlling factors and processes of stone pavement formation.

One objective of this study is to assess the control of stone pavement orientation patterns by environmental and clast parameters. According to McFadden et al. (1986), stone pavements result from initial colluvial displacement of bedrock material from local source areas and subsequent accretionary profile development by dust trapping. In this case, distance from local bedrock outcrops may be a controlling factor of pattern development. If lateral geomorphologic processes during the process of accretion play a major role they will be related to relief parameters such as slope gradient, slope length or slope aspect (Higgitt & Allison, 1999). Geometric properties of surficial clasts themselves may contribute to preferred orientation patterns as well. Principal parameters used in many standard analyses are stone size, often expressed as a and b axis length, anisotropy (i.e. ratio of a and b axis), perimeter and clast surface area (Abrahams et al., 1990; Poesen et al., 1998). Further, weighted parameters (e.g. surface weighted-mean diameter), parameters including the c axis of clasts (e.g. Corey shape factor) as well as averages and parameters of sorting for respective plots have been quoted (Abrahams et al., 1990; Dunkerley, 1995; Higgitt & Allison, 1999).

For studying pattern-forming processes, sedimentology relies on the classic methods of fabric analyses (Pettijohn, 1975; Leeder, 1982; Collinson & Thompson, 1989; Bridge & Demicco 2008). Most information on fabrics exists for aeolian, solifluctional and fluvial processes. However, much less is known regarding other types of sediment displacement, especially unconcentrated overland flow (Abrahams et al., 1990). There appears to be uncertainty as to whether a axes in fluvial sediments become oriented parallel or perpendicular to slope aspect (Pettijohn, 1975; Major, 1998). Commonly, flowing water creates long-axes orientations perpendicular to flow direction, i.e. to slope aspect (e.g. Collinson & Thompson, 1989; Bridge & Demicco, 2008). However, Parsons et al. (2009) show that obstacles may override this initial tendency of object orientation. They further state that field experiments with overland-flow-transported objects are poorly published, as yet

there is no consistent model for the special case of coarse clasts resting on and transported over fine-grained, accretionary aeolian material.

Another objective of this study is to evaluate the stability of stone pavements. According to McFadden et al. (1986) swelling and shrinking of vesicular layer aggregates (i.e. ped doming) would result in maintenance of an intact stone pavement. Furthermore, vesicular layer structure triggers water infiltration capacity and flow paths (Meadows et al., 2008) and may thus be an important controlling factor for stone pavement surfaces. Recovery rates for disturbed sites may differ, depending on the ability of the vesicular layer to control water infiltration and clast mobilisation by swell-shrink processes. Stone pavement recovery experiments have been carried out (Sharon, 1962; Wainwright et al., 1999) but these relied on stone pavements as lag deposits and, therefore did not focus on re-migration of clasts into plots. If sites with a distorted pavement surface are able to recover (Haff & Werner, 1996; Pelletier et al., 2007), orientation patterns of migrated stones may allow deduction of responsible formation processes.

As mentioned by Wells et al. (1985), Higgitt & Allison (1999) and Dietze et al. (2011), pavement clasts can become buried. The orientation pattern of such fossilised formations should also provide insight into their formation processes given that no subsequent dislocation has taken place.

Description of clast orientation characteristics rests on viable statistical procedures. Circular data (i.e. orientation data) are common in earth science. Most approaches rely on unidirectional data or on prior separation of multi-directional data (e.g. strike directions of aeolian deposits by their stratigraphic position or by temporal brackets). Mardia & Jupp (2000) give some approaches to deal with bimodal distributions, but these also rely on prior knowledge of the angle which separates the two distributions. Typical circular data descriptors are *resultant vector length R*, *mean orientation* $\bar{\theta}$, *circular variance* V_c, *circular dispersion* D_c and the *concentration parameter* κ (Mardia & Jupp, 2000; Rao, 2001; Borradaile, 2003). Adelsberger & Smith (2009) used κ based on von Mises-Fisher distributions to describe the variance in stone pavement clast orientation. This is appropriate for unimodal data. However, κ evolves from the scatter of data around the mean orientation $\bar{\theta}$. Thus, strongly bimodal orientations result in low κ and consequently in misinterpretation of the distribution. This effect is illustrated in fig. 3.1: uniform and strongly bimodal patterns yield similar values for R, V_c and κ. Therefore, an approach should be used which avoids these ambiguities. Accordingly, a third aim of this study is developing a statistical procedure to retrieve quantitative measures of type and clearness of clast orientation and to use relationships of these parameters with clast and relief properties to better understand processes of both, orientation and stone pavement formation.

Altogether this study aims at improved understanding of stone pavement formation utilising orientation measurements on intact, recovering and buried stone pavements from four study areas with different environmental conditions.

3.2 Study areas

Warm to cold deserts we studied with moisture gradients from less than 80 to more than 400 mm mean annual precipitation (table 1). We focused on locations on basaltic and rhyolitic lava flows close to local (quartz-rich) dust sources to ensure proper identification of allochthonous material. All studied landforms exhibit geomorphologically abandoned or isolated topographies to rule out fluvial disturbances from outside the closer process catchment (Dietze et al., 2011). The formation or abandonment ages given in table 3.1 may serve as upper age limits for the surfaces under study. Stone pavements are generally underlain by a virtually stone-free vesicular layer of differing properties (cf. table 3.1, also for subsoil descriptions). Some stones, especially larger ones, are partly embedded in the aeolian unit.

In particular we examined the key site for the development of the current model of stone pavement formation: Cima Volcanic Field, California, USA (McFadden et al., 1986). On an alluvial plain stretching 30 to 40 km west towards Silver Lake and Soda Lake playa 40 basaltic cinder cones and associated lava flows (Turrin et al., 1985) are covered by stone pavements of different maturity depending on flow age (McFadden et al., 1986). We focused on a 560 ka-old flow with patches of densely packed, smooth and strongly varnished stone mosaics, free of vegetation.

With the Laguna Salada area, Baja California, Mexico, we present an extreme example of aridity. The area receives presumably less than 80 mm mean annual precipitation. The basin is the result of detachment-related transtensional movements associated with the San Andreas fault system (Martín Barajas et al., 2001). Alluvial fan systems reach into the basin centre which was occasionally flooded by the Colorado River until water reservoirs were built on US territory. Along the western margin, cap rock basalts form the foot of the Sierra El Mayor. The Sierra Pinta forms the southern margin of the basin. Study sites are located on dissected alluvial fan sections and the cap rock basalts. They are virtually free of any vegetation and often show thick desert varnish coatings on clasts.

Black Rock Desert, Utah, USA, appears to be the modern distribution limit of stone pavements. It is characterised by a sharp moisture gradient crossing the basin (fig. 3.2c). Study sites are situated on isolated lava beds of Tertiary to modern age. During the Pleistocene this basin was part of ancient Lake Bonneville, presently it is a considerable dust source (Oviatt, 1991).

The Nevado Tres Cruces area, Atacama Desert, Chile, is located at 4400 m asl. This cold desert region probably receives negligible liquid precipitation. During austral summer only 29±14 mm of precipitation occurs (table 1), with night temperature typically below 0 °C. Therefore, liquid precipitation is mainly restricted to the day time. Due to intense sublimation, surface runoff is negligible (Garreaud et al., 2003). Consequently, vegetation is virtually absent there. We have studied stone pavements on a steep alluvial landform with varnished volcanic gravel.

Table 3.1. Geographic properties of the study areas.

Study area	***Cima volcanic field***	***Laguna Salada***	***Black Rock Desert***	***Nevado Tres Cruces***
Geographic location				
Administrative location	California, USA	Baja California, Mexico	Utah, USA	Copiapó, Chile
Latitude/ longitude	35°25' N/116°10' W to 35°01' N/115°40' W	32° 40' N/116° 00' W to 31° 30' N/114°30' W	39° 16' N/113° 02' W to 38° 37' N/112° 15' W	26° 52' S/68° 50' W to 27° 06' S/ 68°27' W
Mean elevation [m asl.]	850 to 950	2 to 200	1400 to 1500	4200 to 5100
Geologic/ geomorphologic setting				
Structural type	Cinder cones with lava flows upon alluvial plain	Alluvial fan systems with enclosed playa, cap rock basalt	Volcanic ridges with interfingering palaeolake features	Isolated volcanoes with debris cones and lava flows
(Bed-) rock type	Basaltic lava	Granitoid, rhyolitic and basaltic gravel	Basaltic and rhyolitic lava	Basaltoid and rhyolitic lava
Landform age	580 ka (Turrin et al. 1985)	mostly undated, modern to 300 ka (Spelz et al. 2008)	modern to Tertiary (Oviatt 1991, Schmidt 2008)	undated, no references available
General soil characteristics, after Soil Survey Division Staff (1993), Birkeland (1999)	Av (strongly developed, coarse-sized, prismatic and platy structure, medium hard to hard consistence) over bBt (weakly developed, medium-sized, subangular blocky structure, loose to medium hard consistence), Dietze et al. (in press)	Av (medium developed, coarse-sized, prismatic and platy structure, soft to hard consistence) over bBw or bBy (weakly developed, very fine-sized, subangular blocky structure, loose to soft consistence), Dietze et al. (in press)	Av (weakly to strongly developed, medium to coarse-sized, prismatic and platy structure, soft to very hard consistence) over bBw or bBt (subangular blocky structure, soft to hard consistence), Schmidt (2008)	Av (strongly developed, coarse-sized, prismatic and platy structure, hard consistence) over bBw (weakly developed, fine-sized, subangular blocky structure, soft consistence), own data.
Dust source	Playas, ca. 30 km upwind	Playa, surrounded by alluvial fans	Playa surrounding volcanoes and lava flows	undulating lake, < 5 km upwind
Climate				
Data source	NCDC (2010), 5 stations, interpolation ± residuals	NCDC (2010), station Mexicali	NCDC (2010), 6 stations, average ±2σ	Legates & Willmott (1990), 4 cells, average ±2σ
Mean annual temperature [° C]	18±3	23	10±1	-2±4
Annual precipitation sum [mm]	161±62	81	292±183	62±36
Precipitation boreal summer [mm]	60±43	35	139±58	53±48
Precipitation boreal winter [mm]	101±35	45	152±127	29±14
Relief, general properties				
Slope [°]	0.9 - 5.5	0.2 - 4.4	0.1 - 3	2 - 21
Type of isolation	Abandonment and isolation by constructional volcanic relief	Abandonement by fluvial dissection	Abandonment and isolation by constructional volcanic relief	Isolation by local topography
Further properties				
Vegetation	barren with patches of shrubs	barren, very sparse grasses	barren to grassland cover	barren
Landuse	virtually unused	virtually unused	extensive cattle farming	unused
Magnetic declination, source: NGDC (2010)	12° 31'	11° 42'	12° 18'	-2° 35'

3.3 Materials and methods

3.3.1 Field methods

Relief characteristics were measured at each plot. Distance to the nearest upslope bedrock outcrop and the closest downslope drainage channel were determined via measuring tape or Garmin gpsmap 60CSx. Coordinates of each plot were also recorded with this GPS device, often with stated uncertainties of±2 m. Clast lithology was noted according to macroscopic properties. Stone pavement coverage was estimated by comparison with calibration charts.

For retrieving orientation data of surficial stones, a square template with 1 m edge length was placed on the ground and the corners were marked with cross stickers. After removal of the template, a GPS position and orientation reference were placed along one edge of the remaining square and digital nadir images were taken.

For assessing changes with time at disturbed sites, we prepared 11 special plots at Cima Volcanic Field in June 2007 and March 2008. These followed a toposequence from a local culmination point towards a depression. We cleared square plots (1 m edge length) from the covering stone pavement by hand. Clasts were not deposited in the vicinity of the plots. All clasts > 5 mm were carefully removed to not disturb the vesicular voids in the underlying aeolian material. This resulted in a sixfold larger cleared area compared to previous experiments (Haff & Werner, 1996) to reduce boundary effects. We took photographs of the crack patterns of the exposed fine material. Subsequently, at half of the plots the entire vesicular layer was destroyed mechanically. This was done to elucidate the influence of soil structure on stone pavement re-establishment. Clast exhumation may be a recovering process. We accounted for this by determining the stone content of 10 dm^3 aeolian sediment below the stone pavement at several nearby locations. All plots and a surrounding 40 cm-wide belt were photographed with orientation and position references. Revisions to document changes of surface features took place in March 2008, October 2008 and July 2009.

Several profiles at Cima Volcanic Field exhibit buried, fossilised stone pavements (cf. Dietze et al. (2011) for detailed profile descriptions). From four such soil profiles properties of buried stones were evaluated. Therefore, the profile wall was cleared and sediment was scraped off carefully. Once a stone was located, its burial depth was noted. Thereafter, it was dissected out of the wall to exclude those tilted against the horizontal line for more than 30 °. From the remaining clasts a axes orientation was determined with a situmetry disk (the stone is placed on a semicircle chart, fixed at the profile wall, with imprinted reference angles) within uncertainties of±5 °. Finally, the length of a and b axes of the stone were measured. Every detected stone was examined, until at least 60 specimens were recorded.

3.3.2 Digital data retrieval and preparation

For the Black Rock Desert we used data from 11 weather stations (NCDC, 2010) throughout the wider study area. By ordinary kriging we approximated mean annual precipitation at the respective plot locations.

For orientation data processing the nadir images were imported into ArcGIS 9.3 software and geometrically corrected based on the aforementioned cross stickers. Axes of at least 100 objects were digitised. Digitising started in the upper left corner and every stone from which axes could be retrieved was edited. This approach was chosen to minimise biases towards large stones. Further, subjective implications according to preferred orientations were ruled out by this technique

(cf. Adelsberger & Smith (2009) on random selection of pavement clasts and resulting biases). Finally, the orientation reference was digitised for correction of angles towards magnetic North. Magnetic deviation at each location (table 1; NGDC, 2010) was subsequently taken into account. The resulting data sets were imported into the statistical software R and a axes angles against magnetic North were calculated. These operations yielded data sets for each 1 m by 1 m plot with typically 90 to 105 orientation angles. For one data set (LS-03, on an alluvial fan in the Laguna Salada), 465 angles were evaluated. Based on this data set the influence of object numbers on the results was examined. We further plotted development of arithmetic mean ($\bar{x}$) and standard deviation (σ) of the resulting a axes orientation angles to check for representative results.

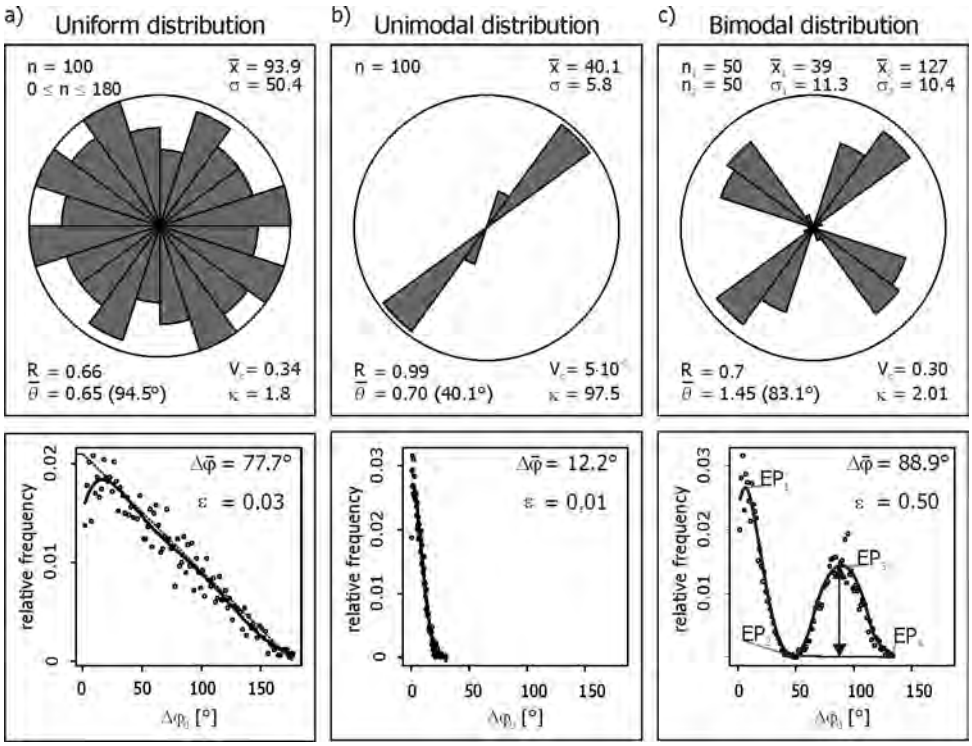

Figure 3.1. Rose plots and derived relative frequency distributions of $\Delta\varphi_{ij}$ for uniform, unimodal and bimodal angle distributions. Rose plots are created bidirectional (i.e. angles ϕ and ϕ + 180 °) and with linear scale for a better illustration of the modality type. Typical orientation descriptors are given below the rose plots. Their definitions and ambiguities are discussed in the methodology section. The lower part of the figure shows relative frequency distributions and calculated measures of topological properties from fitted polynomials (solid lines).

We kept only digitised stones which passed the following geometric preconditions: ratio of a and b axis greater than 1.3 (Major, 1998) and a axis length within the interval of 20-200 mm. Particles below the centimetre-scale have a large influence on digitising uncertainty. They are also prone to remobilisation by rain splash and strong winds (Wainwright et al., 1999; Valentine & Harrington, 2006; Pelletier et al., 2007). Further, they are often constrained to occupy spacings of coarse particles (Major, 1998). This excludes linking their orientation to stone pavement patterns. Particles

coarser than 20 cm were overall very rare. They may only be transported by extreme events, thus being uncharacteristic of orientation of the main assemblage of stones.

3.3.3 Statistical analyses of orientation angles

As outlined in the introduction, typical approaches to quantitatively assess orientation patterns of circular data are ambiguous. Fig. 3.1 (upper part) shows rose diagrams for three different distribution types and respective classic measures of modality (R, $\bar{\theta}$, V_c and κ). For each distribution 100 random numbers (*raw angles* φ) were generated to fill a matrix Φ. Each sequence had the following properties:

- Uniform, values range between 0 and 180 ° with a mean of 93.9 ° and σ of 50.4 °.
- Unimodal, values are normally distributed with a mean of 40.1 ° and a low σ of 5.8 °.
- Bimodal, values consist of 50 normally distributed numbers with a mean of 39 ° (σ 11.3 °) and 50 normally distributed numbers centred at 127 ° (σ 10.4 °).

Bimodal patterns (fig. 3.1c) yield similar statistical measures as uniform ones (fig. 3.1a), but in fact result from contrasting angles. Further, $\bar{\theta}$ indicates a completely wrong direction for bimodal patterns (83.1 instead of 39 and 127 °). To overcome such pitfalls, our new approach is based on relative angle differences (topologic domain) rather than absolute description of directions (topographic domain), e.g. deviations of single data from calculated mean orientations. We calculate the absolute deviation among Φ using equation 1:

$$\Delta\Phi = \Delta\varphi_{ij} = \sqrt{(\varphi_i - \varphi_j)^2}\,,\ \forall\, i\,,\ j = [1,\ldots,n]\,,\ i \neq j \qquad (1)$$

$\Delta\Phi$ is a matrix with the *overall angle deviation* throughout the data set. It comprises the absolute differences between two angles φ_i and φ_j for all n elements i, j of the data set. Its relative frequency distribution (fig. 3.1 lower part) provides characteristic properties for respective orientation distributions. For uniform values a negative linear trend appears, spanning the whole data range (0 to 180 °). Unimodal values result in a narrow data range of approximately 4σ (standard deviation of the initial random values). Bimodal values produce two clear peaks separated by a mean angle (i.e. difference between the two arithmetic means of the initial random values).

Description and classification of modality type based on rose diagrams is problematic (Wells, 2000). This is mainly due to the strong influence of class width and starting angle on the appearance of the plot. Eppes et al. (2010) suggest Rao's Spacing Test as an appropriate tool for deciphering multimodal from uniform distributions. There is a range of further statistical tests to check for

uniformity in circular data within arbitrary confidence intervals (cf. Mardia & Jupp, 2000; Rao, 2001). However, for discriminating the three possibilities depicted in fig. 3.1 from one another these are not applicable. Therefore, we fit the relative frequency distribution of $\Delta\Phi$ with a seventh degree polynomial. This results in optimal residuals for all types of data. Theoretically, by increasing the polynomial degree detection of trimodal orientation distributions and even higher maxima counts is possible. However, given a reasonable standard deviation for each local maximum, the overall distribution then gets too blurred for recognising clear signals. Therefore, our quantitative description does not take into account higher degrees of clustering.

Parameters of the polynomials allow quantitative description of the initial distribution pattern. The roots of the first derivative yield *extreme points (EP)*. Respective *x* and *y coordinates* may be interpreted as data distribution quantifiers. In general, the relative frequency of angle differences decreases with angle range. We refer to this as background. Bimodality causes elevation of a peak above background (double arrow in fig. 3.1c). The difference between peak height (i.e. *y* value at *EP3*) and the mean background (i.e. arithmetic mean of *y* values at *EP2* and *EP4*) at this location gives an *index for the strength of bimodality* (*Ibm*, equation 2). Normalisation to one is achieved by multiplication by two.

$$Ibm = 2 \cdot \left(y_{EP3} - \frac{y_{EP2} - y_{EP4}}{2} \right) \quad (2)$$

Completely uniformly distributed data would result in a straight line through the relative frequency distribution plot with negative slope (dashed line in fig. 3.1a). The slope of this line is described by the term (180 – x_i) / 180 in equation 3. Multiplication by y_{max} scales it according to the relative frequencies of *y*. The index *i* accounts for respective *x* and *y* values of the frequency distribution. Cumulic deviation of data from this line accounts for non-uniformity, i.e. unimodality. An *index of unimodality* (*Ium*) may therefore be defined as follows:

$$Ium = \sum_{1}^{180} \sqrt{\left(y_i - y_{max} \cdot \frac{180 - x_i}{180} \right)^2} \qquad (3)$$

Vice versa, uniform data distribution is best fitted by the straight line with negative slope. Hence, the *index of uniformity* (*Iuf*) is given as the inversion of *Ium* (equation 4).

$$Iuf = 1 - Ium \quad (4)$$

All indices were scaled to sum up to one for each data set. Classification may subsequently be based on the highest value. Bimodal distributions may be further characterised by the following two parameters:

- $\Delta\bar{\varphi}=x_{EP3}$, *mean angle* between the (first) two orientation maxima. There are two values: original mean angle $\Delta\bar{\varphi}$ and complementary mean angle $\Delta\bar{\varphi}'=180-\Delta\bar{\varphi}$. These values may be used to check for perpendicular versus oblique orientation maxima in multimodal distributions. Deciphering extreme points from noise (significance estimation) may be a serious issue when dealing with empirical data. However, as already noted it is only useful to calculate $\Delta\bar{\varphi}$ for data which are already designated bimodal, i.e. its *Ibm* is higher than any other modality index. This implies dominance of two clear peaks over continuous decrease of relative frequency with larger angle differences.

- $\varepsilon=\frac{y_{EP3}}{y_{EP1}}$, *degree of equilibrium* between the first two maxima. Equilibrium is expressed in terms of data amounts and scatter between the two maxima. For uniform and unimodal distributions, this value is irrelevant as there is no distinct (second) maximum.

Having the mean angle $\Delta\bar{\varphi}$ in the topologic domain we are able to go back to the topographic domain and deliver absolute values for the orientation maxima. Again, this is only meaningful for bimodal distributions. Uniform and unimodal data have no modes with a separating angle. To calculate these absolute values we put our data (φ) into classes of 5 ° size in order to get a sufficient number of counts for each interval. Then each class median is calculated and its deviation from φ it is derived. From the lowest 10 values of all these deviation data the arithmetic mean is calculated, representing the *absolute mean direction* of the first orientation maximum φ_1 of a data set. To retrieve this value also for the second orientation maximum (φ_2), the mean angle $\Delta\bar{\varphi}$ is added to φ_1 in both directions. The class which includes a greater number of values is chosen to calculate φ_2 as the arithmetic mean of all class elements.

For evaluating the relationship between measured stone and relief parameters and the presented orientation descriptors, Pearson's coefficient of correlation (r) and explained variance (R^2) were calculated. Correlation results are discussed as R^2 and negative signs of r are indicated. Scatter is generally given as 1σ.

3.4 Results

3.4.1 Properties of natural surficial stone pavements

Tests for sufficient data amount showed that from 40 to 60 samples per plot onward, there is no improvement of information by including more samples. Development of $\bar{x}$ and σ reach stable

values with total scatter below 10 °. Results of site properties, clast axes measurements along with derived ratios and orientation measures are given for all investigated plots in tables 3.A.1 and 3.A.2. All study regions yielded overall similar results and are therefore presented together. Only unique features of particular sites are mentioned separately.

Generally 93 % of the digitised objects fulfilled the necessary geometric preconditions and could be used for orientation analysis. Mean a axes sizes range broadly between 25 and 117 mm, i.e. 52±18 mm mean size, and mean b axes sizes between 14 and 70 mm, i.e. 30±11 mm mean size, resulting in mean anisotropy of 1.9±0.1. Scatter among the plots is smaller on alluvial fan sites than on isolated lava flows. Correlations of stone dimension parameters with distance to drainage channel and bedrock outcrop yielded R^2 values less than 0.09 and 0.21, respectively. Even on the alluvial landform in the Nevado Tres Cruces area stones do not clearly coarsen towards the upslope source area. This is expressed by an R^2 below 0.23 for mean stone size and specific catchment. There is a close relationship between stone pavement coverage and slope gradient, specific catchment and distance to bedrock outcrop, expressed by R^2 values of 0.91, 0.55 and 0.71, respectively. For Black Rock Desert R^2 values of approximated precipitation sum with diverse parameters remain below 0.17 except for stone pavement coverage for which it yields 0.48.

According to the calculated indices of modality type, bimodal orientation is dominant in most data (40 out of 52 plots). Preferred unimodal patterns are rare (2 plots). Preferred uniform clast orientation is present at 10 plots. Mean indices of modality are as follows: *Iuf* 0.52±0.07, *Ium* 0.42±0.01, *Ibm* 0.61±0.06. Bimodal orientations are generally separated by oblique angles. Very few stone pavement plots show perpendicular modes (CVF-12, BRD-06, LSM-05). At plots LSM-04 a clear and at LSM-07a an incipient, trimodal pattern with separating angles around 60 ° is visible in the rose plots (fig. 3.2b). However, due to high noise within angle distributions these trimodal patterns are not well resembled in the relative frequency distributions and the fitted polynomial. At all plots mixtures of all three modality types are present. This is expressed by both the three indices and rose diagrams (fig. 3.2). Average degree of equilibrium ε for bimodal orientation patterns is 0.53±0.11. However, at Cima Volcanic Field it is lower (0.42±0.05) than elsewhere, e.g. than at Laguna Salada (0.53±0.07) and Black Rock Desert (0.62±0.11). Correlation of ε with relief parameters yielded an R^2 of 0.28 for both, distance to outcrop and pavement coverage but was less than 0.1 for all other parameters. Averaged over all study sites, bimodal distributions exhibit a mean $\Delta\,\overline{\varphi}$ of 72±9 °. The narrow scatter is a systematic feature at all study sites. Correlations of this angle with any relief and stone geometry parameter yield R^2 values lower than 0.11. However, ε is negatively correlated with $\Delta\,\overline{\varphi}$ (R^2 = 0.48).

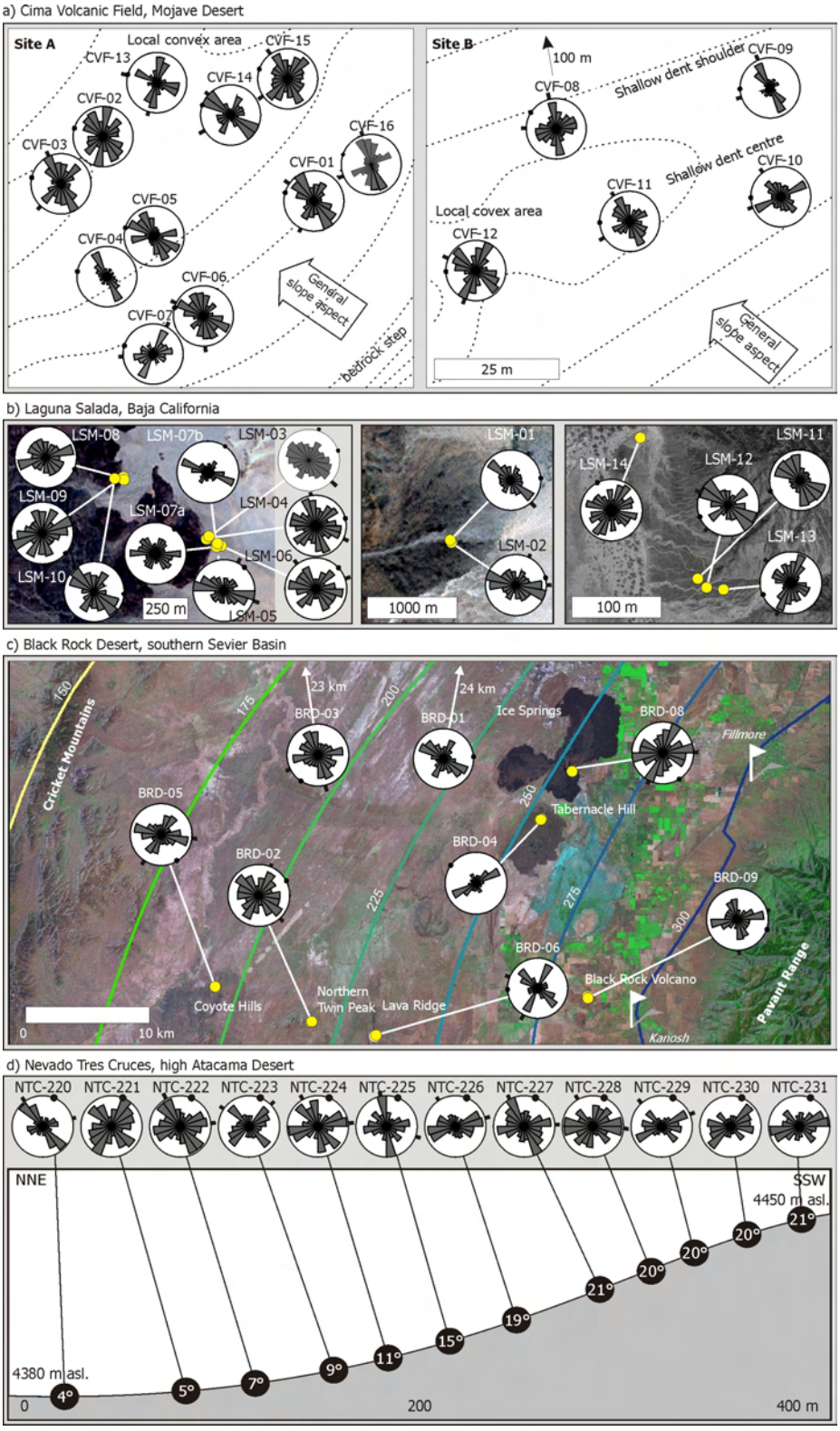

Figure 3.2. Results of orientation measurements from four study areas. All sketches are referenced towards geographic North. Black dots on angle axis of rose plots indicate slope aspect. Black bars illustrate mean angles for bimodal patterns. a) Cima Volcanic Field, contours are sketched from DEM. b) Laguna Salada, Landsat ETM+ image. c) Black Rock Desert, Landsat ETM+ image. Contours show interpolated annual precipitation sum (mm). White flags illustrate weather stations. d) Nevado Tres Cruces, numbers in black circles indicate slope inclination.

A closer look at bimodal orientation data with respect to slope aspect reveals two regimes. An *asymmetric regime* may be observed at plots CVF-01, CVF-05, LS-01, LS-10, NTC-221 and NTC-230. There, one of the two orientation modes is strongly aligned towards slope aspect but always deviates by a given angle. A common *symmetric regime* is characterised by symmetric deviation of both modes from slope aspect, e.g. CVF-03, CVF-08, BRD-06, BRD-08, LS-03, LS-09, NTC-222 and NTC-224. To quantify these two regimes we calculated the arithmetic mean of $\overline{\varphi}_1$ and $\overline{\varphi}_2$, i.e. the *symmetry angle* or angle bisector. Its deviation from slope aspect (*symmetry deviation*) is 17±17 ° for all bimodal data. The respective frequency distribution is highly skewed with a sharp drop in abundance for values higher than 17 °. Therefore, we classified all plots with symmetry deviation lower than 17 ° as symmetric and the remaining ones as asymmetric. This way, the symmetric regime (25 plots) has a mean symmetry deviation of 6±4 °. Further, we isolated the mean angle $\overline{\varphi}_1$ or $\overline{\varphi}_2$ which yielded the smallest deviation from slope aspect (*angle deviation*). For all symmetric regimes angle deviation is 40±14 °. This is somewhat higher than half of $\Delta\,\overline{\varphi}$ for all bimodal patterns but well within the 1σ scatter. Correlation analyses of slope aspect and symmetry angle for the symmetric regime yield an R^2 of 0.87. Besides this strong relationship all further relief and stone dimension parameter relationships are negligible, with R^2 values below 0.02. For asymmetric regimes (15 plots) symmetry deviation reaches 37±16 °, whereas angle deviation is 21±10 °. Correlation of angle deviation with slope aspect gives an R^2 of 0.69. A further important R^2 occurs for angle deviation and distance to outcrop (0.50). All other parameters yielded R^2 values of less than 0.2. Regime types do not show any spatial pattern among the plots.

3.4.2 Recovery features of cleared plots

Fig. 3.3 shows two adjacent plots (A1a and M2a, respectively) cleared from their stone cover in June 2007. These are representative for the other plots. Table 3.A.3 provides statistical data for these and the other prepared plots. We did not find remarkable erosion or denudation of aeolian dust from the plots at any time slice. The migrated stones do not show any clear spatial gradient, e.g. from the margins towards the centre of the plot. Clasts appeared not to be embedded in the underlying fine material but rested upon it. However, we did not lift them to fully check this impression as this would have harmed the experiment.

Visual inspection of the images suggests a clear difference between the two settings. Plots with a preserved vesicular layer show better stone recovery. Taking into account the absolute numbers of re-migrated stones > 5 mm, plots with a preserved vesicular layer show a higher degree of stone cover within the first period of 11 months compared to the ones with a destroyed vesicular layer. However, this rate declined remarkably for the following two time slices.

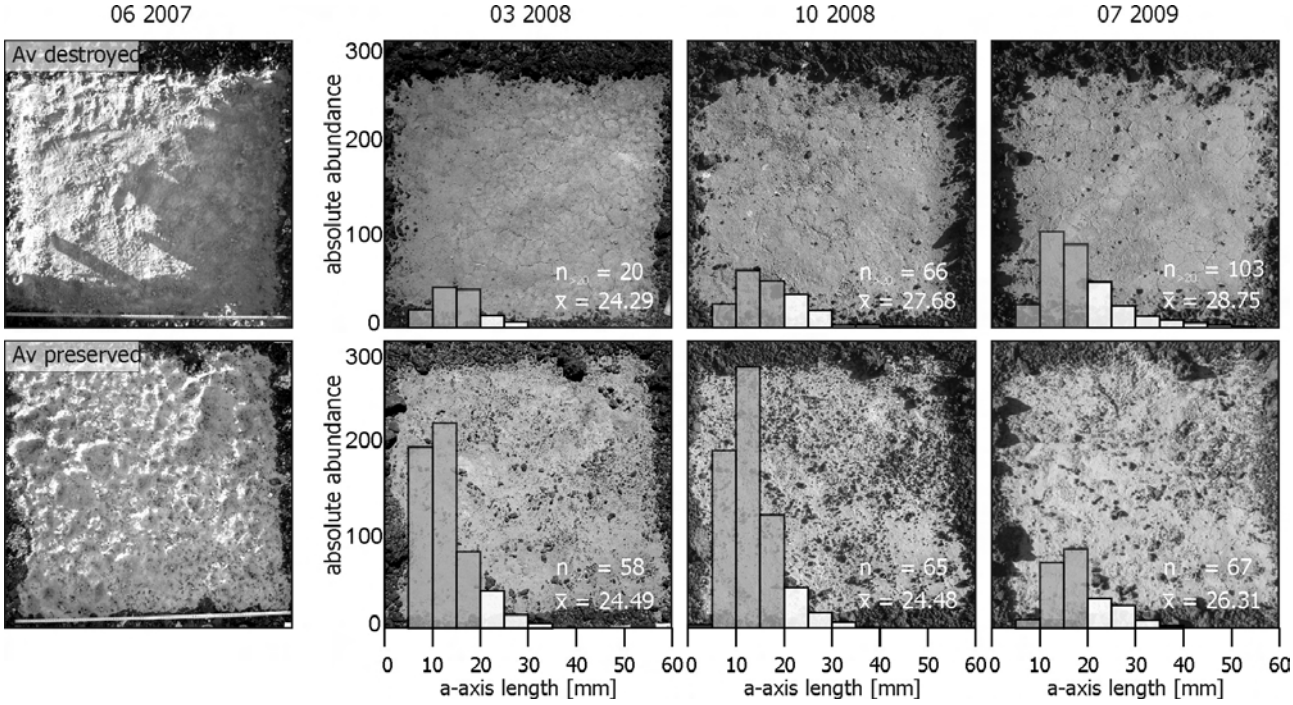

Figure 3.3. Time slices of 1 m by 1 m plots, cleared from their covering stone pavement at Cima Volcanic Field. The upper series shows minor changes at the plot with a mechanically destroyed vesicular layer, whereas at the lower series with preserved vesicular soil structure lateral migration of stones is obvious. Histograms provide a closer description of the migrated stones with white bars indicating a axes lengths larger than 20 mm. Numbers and means are given for stones with a axes longer than 20 mm.

The histograms in fig. 3.3 show an increase in both, total number of migrated stones and their a axes lengths. Further, the histograms illustrate that a stable recovery rate of stones larger than 20 mm is apparent for the plot with destroyed vesicular layer structure, only. Stone dimensions show a general increase in mean a axes length and anisotropy with time. Compared to the digitised stones from all plot surroundings migrated clasts are smaller and better sorted. No stones larger than 55 mm were transported into the plots. There are no differences between the plot locations from the local culmination point towards the local depression. Measurements of particle content coarser than 2 mm within the first 8 cm of sediment below the stone pavement gave overall values of less than 3 % with virtually no material reaching lengths of 2 cm. After ten months the destroyed polygonal pattern in the aeolian material is re-established at the surface. However, compared to the original structure it is still weak and shallow. There is no clay enrichment in the central ped interiors (Anderson et al., 2002).

To get an explanation for the decreased number of stones on some plots in 2009 vs. 2008 further surface features were observed (fig. 3.4). Visual inspection showed that in July 2009 most plot areas were covered by fresh fine material which exhibited desiccation cracks and fine laminations as well as clasts which are homogeneously coated by the fine material. At some plots tiny incised channels were visible. Excavated soil pits have been repeatedly filled and their scarps were incised several decimetres deep. On several stone pavement patches shallow depressions showed a systematic radial increase of stone sizes from their centres.

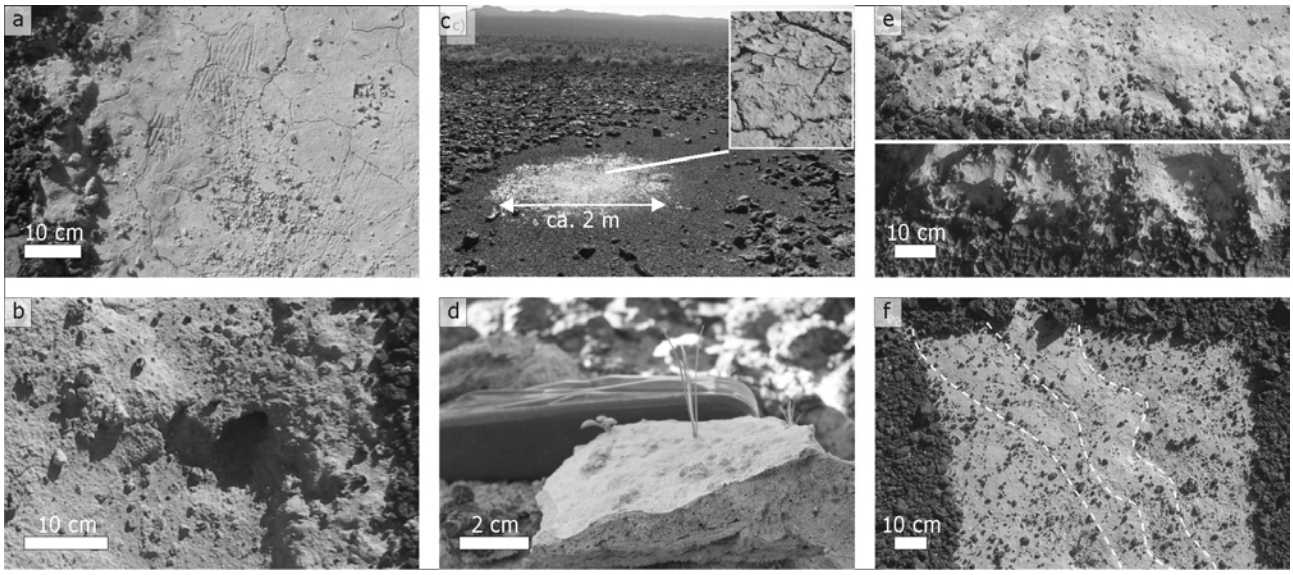

Figure 3.4. Surficial features of disturbed stone pavement surfaces at Cima Volcanic Field. a) and b): traces of animals, c) shallow depressions with a radial gradient of increasing stone size from the alluvium-filled centre, diameter of the inner circle approximately 2 m, d) recently formed vesicular structure from aeolian material, which became washed into a soil pit (formation within less than six months), e) the same cleared plot in October 2008 (upper part) and July 2009 (lower part) with clear incision traces, filled with stones from the surrounding stone pavement, f) shallow fluvial channels crossing a cleared plot from the upper left to the lower right (dashed white lines).

3.4.3 Orientation patterns of recovery plots

Retrieval of adequate stones with sufficient size and geometry was sparse for most of the recovery plots. Therefore, we could not calculate orientation parameters for all plots. Fig. 3.5 and table 3.A.3 illustrate the measurement results. Bimodality is the most common type of orientation again. $\Delta\,\overline{\varphi}$ (82±9 °) is close to the values of undisturbed plots. Again, symmetric and asymmetric regimes are apparent. Mean angle deviation is 42±7 ° and 21±7 °, respectively. There is a weak tendency of preferred bimodal arrangement at plots with a preserved vesicular layer (mean *Ium* is 0.20±0.07, mean *Ibm* is 0.56±0.05). Preferred unimodal stone a axes orientation may be found in destroyed-Av plots (mean *Ium* is 0.29±0.12, mean *Ibm* is 0.43±0.22). This tendency is also represented by the different mean degrees of equilibrium (preserved-structure ε is 0.55±0.01, destroyed-structure ε is 0.42±0.10).

As expected, the edges of the polygonal vesicular layer yielded trimodal orientation patterns with angle maxima separated by approximately 60 °. Orientations of the polygonal crack patterns of the vesicular layer do not show any relationship to the re-migrated stones, regardless of the condition of vesicular layer.

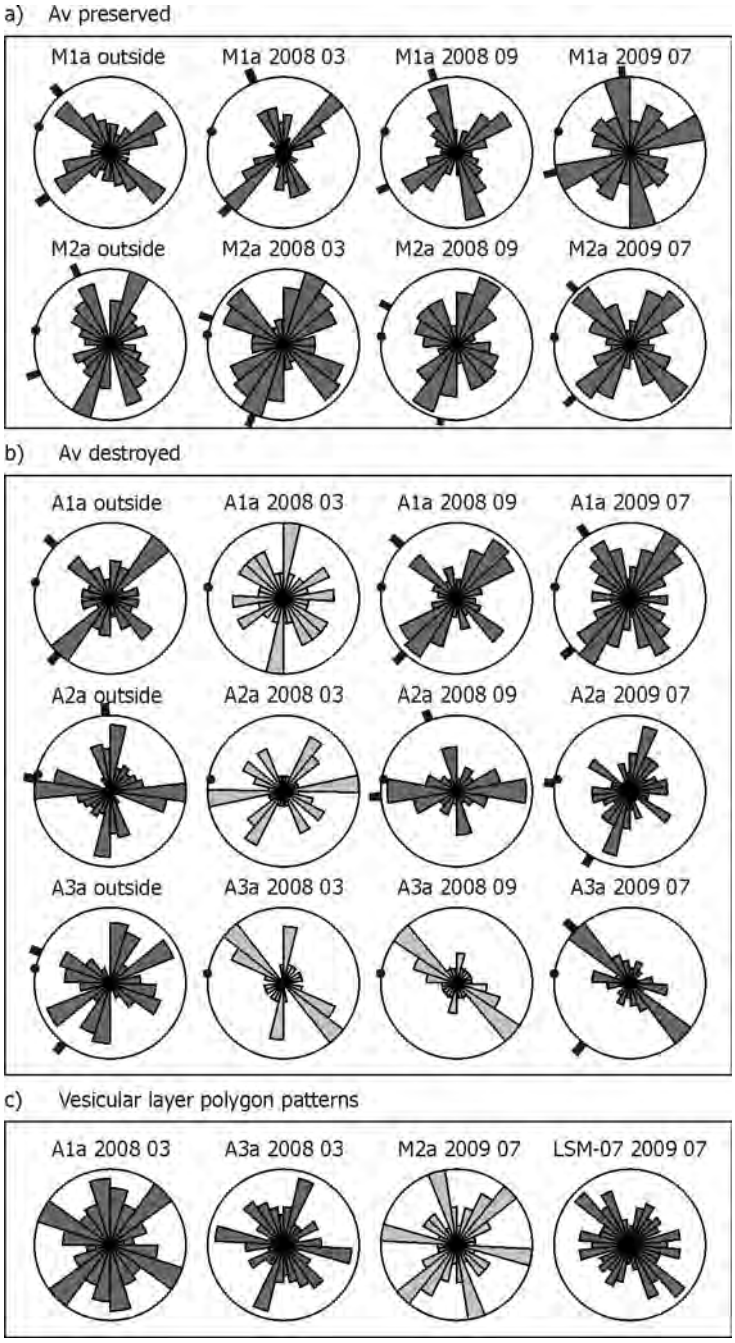

Figure 3.5. Orientation patterns of 1 m by 1 m plots cleared from stone cover. a) Orientation patterns of plots with intact vesicular structure for several time slices and plots. b) Orientation patterns of plots with destroyed vesicular structure for several time slices. c) Orientations of edges of vesicular layer polygons from different plots (destroyed structure at A1a and A3a, intact structure at M2a and LSM-07). Light grey colours indicate insufficient data amounts for angle calculations.

3.4.4 Buried stone strata

CVF-101 and CVF-102 represent two well developed, mature soils (fig. 3.6a). The solum is composed of nearly stone-free aeolian material with prominent features of pedogenetic clay, calcium carbonate and gypsum enrichment. Stones do occur at discrete depth intervals (fig. 3.6b): 12±2

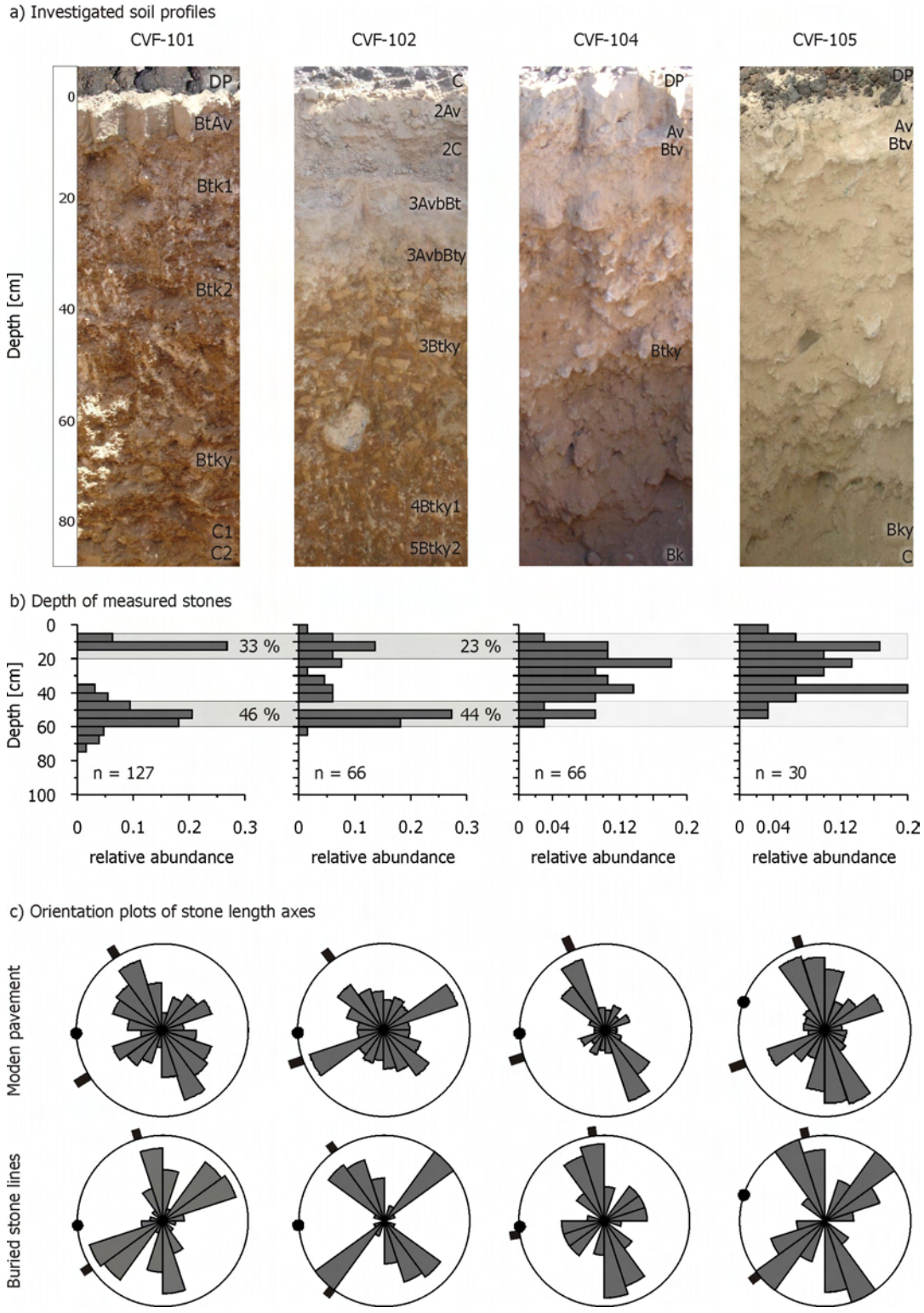

Figure 3.6. Depth distribution and orientation patterns of modern and fossil stone pavements from Cima Volcanic Field soil profiles. a) Images of the investigated soil profiles. Horizon nomenclature after Soil Survey Staff (1993) and Birkeland (1999). b) Histograms of burial depth of all investigated stones with two marked intervals of stone enrichment for profiles CVF-101 and CVF-102 (grey horizontal bars, 5-20 and 45-60 cm). c) Orientation plots of the modern stone pavement and buried stones. Black dots on angle axis of rose plots indicate slope aspect. Black bars illustrate mean angles for bimodal patterns.

cm (12±5 cm) and 54±8 cm (55±3 cm) in profile CVF-101 (CVF-102). In contrast, CVF-104 and CVF-105 show only weak pedogenetic overprint of the stone-rich matrix with aeolian material. Stone content ranges between 50 and 90 %. Measurements were conducted between 5 and 60 cm depth only, because no more changes in sediment texture and structure were apparent beneath. Dimensions of fossil stones (table A.3) are systematically smaller compared to those of the modern pavement. Mean anisotropy is also weaker for buried stones.

Fig. 3.6c shows orientation patterns of buried stones versus those of the associated modern stone pavement. The general similarity of stone a axes orientation is obvious even from the rose diagrams. $\overline{\varphi}_1$ or $\overline{\varphi}_2$ from buried stones deviate by less than 12 ° from those of surficial clasts on average. Only profile CVF07-101 shows a remarkable deviation of one orientation maximum. Bimodality is present in all four profiles with $\Delta\,\overline{\varphi}$ of 71±14 °. Degrees of equilibrium ε are systematically higher (0.57±0.05) compared to those of associated surficial stones.

3.5 Discussion

3.5.1 Orientation descriptors of circular data

Tests for appropriateness of digitised axes suggest sufficient data (50 to 60 samples) in all cases. This is in agreement with reported results from other authors (e.g. Kohlbeck et al., 1994; Major, 1998). With our approach we present a comprehensive method for assessing quantitative characterisation of circular data. For 79 data sets clear characterisation of dominant orientation type as well as the modality strength is possible. However, our proposed algorithm is not always able to highlight trimodal patterns because the polynomial fit is often blurred too much by the scatter in angle data. From visual inspections of rose diagrams, strength of uniformity appears to be somewhat overestimated whereas strength of unimodality shows slight underestimation. Further independent indicators of orientation type might be needed to address this topic.

3.5.2 Orientation patterns of modern stone pavements

Preferred orientation is a robust feature under all studied climatic conditions. Results from Black Rock Desert show that at locations with more than 300 mm mean annual precipitation and stone coverage of less than 50 %, replaced by dense grassy vegetation, clear bimodal or unimodal stone orientation still exists. Similarly, preferred orientation of stones also dominates in the hyperarid cold desert region of Nevado Tres Cruces.

Having stated ubiquitous unimodality and bimodality, questions arise about controlling factors of pattern generation. At all investigated sites stone geometry does not explain any aspect of orientation pattern. Hence, processes which cause orientation patterns are not specific to stone dimensions. The importance of relief parameters such as slope gradient, specific catchment, dis-

tance to drainage channel and distance to bedrock outcrop on orientation patterns is also negligible. Slope aspect alone explains almost all variance (87 %) of this feature for the symmetrical bimodal regime. Stone orientations at plots with an asymmetrical regime are generally controlled by slope aspect but also by distance to bedrock outcrop. Therefore, we suggest processes responsible for orientation-pattern formation to be primarily controlled by slope aspect. Further, but not necessarily ubiquitously, these processes may be sensitive to the distance from potential source areas for clasts (bedrock outcrops). Moisture provides a boundary condition for formation and maintenance of stone pavement surfaces. However, preferred orientation is still present, even where stone coverage is as low as 40 %. Stone orientation patterns at these sites appear to represent relics of drier and thus more barren periods, as a modern formation is unlikely.

Consequently, after having identified controlling factors, causal processes may be inferred. We suggest unconcentrated overland flow and surficial creep as the most likely causes to generate the dominating orientation angles in symmetrical bimodal regimes. Field evidence of modern fluvial activity (fig. 3.4) and reports of tilted carbonate collars (cf. McFadden et al., 1998) underline the presence of these processes. Removal of aeolian material, which forms the vesicular layer, may be significantly limited due to the typical medium-hard to hard consistence of its aggregates (cf. Dietze et al., 2011) and reduced flow velocity in the basal flow section due to surface roughness. Remarkable influence of surface runoff in the Nevado Tres Cruces area is unlikely. Therefore, creep may be the dominant process there.

Allen (1982) discusses processes which take place during deposition of non-spherical objects moved by flowing water. He shows that orientation of a axes perpendicular to flow direction is the only stable position if the ground is (unnaturally) homogeneous and flat or if the ground consists of material of the same size as the moved objects (i.e. bedload transport over river beds). However, obstacles such as already resting stones and spatially differing ground roughness cause rotation of objects during lodgement. An obstacle introduces a torque to a moving object, given that the contact point is not in line with the moving object's mass centre. Consequently, the object is forced to align its a axis towards flow direction. For natural axes ratios the following equation is given after Allen (1982) to describe the final orientation of a cylindrical object:

$$\tan \alpha = -2\frac{r}{l} \qquad (5)$$

There, l is the cylinder length (i.e. a axis length), r the radius (i.e. half of the b axis length) and α is the object's rotation angle out of flow direction. The equation assumes zero bed friction. Otherwise the angle would be larger. Considering mean anisotropy values of our investigated plots, equation 5 gives a mean angle α of 26±1 °. This minimum, frictionless angle is well below mean angle deviation of symmetric regimes (40±14 °). Statistical evidence of impure orientation is reported from Buchalter & Bradley (1992). They deduce from Monte Carlo simulations that straight ori-

entation of elliptic objects relative to a force field (e.g. gravity) occurs only for axes ratios larger than 3, a value not observed in pavement clast data.

Hydraulic processes may also explain the typical bimodal orientation pattern in general. A stone may be deposited with a given angle α clockwise against slope aspect and become an obstacle for following stones. These may be aligned with the same (clockwise) α, resulting in deposition parallel to the former stone. But also, they may be aligned counter-clockwise with α against slope aspect which results in a total angle difference of 2α. Consequently, a bimodal pattern, symmetrical to slope aspect and with a mean separation angle $\Delta\overline{\varphi}$ of 2α is formed. Our mean angle deviation (40±14 °) would explain mean separating angles $\Delta\overline{\varphi}$ between 62 and 106 °. This covers the 72±9 ° observed in bimodal plots. The positive relation of ε and stone pavement coverage provides another argument: the better the stones are aligned parallel to each other, the tighter the stony surface becomes.

Clasts may be deposited on a fine-grained surface intermittently (without collision with other objects) due to decreasing drag force at the end of a runoff event. But with the next strong event they will be reactivated and transported further downslope until they collide with one or more fixed obstacles to reach a stable position from which even strong runoff events cannot remobilise them. Such iterative collision events result in upslope propagating cones of tightly packed clasts which may coalesce to form broad fronts. The cones grow from initially fixed obstacles by repetitive "catching" of dragged stones which do only partly overlap with the downslope obstacle's a axes and thus broaden the entire obstacle front. Therefore, unconcentrated overland flow is very effective in creating tightly-packed stone pavements. It creates clustered and propagating clast distributions and not dispersed ones which would require increasingly hindered filling of gaps by stone dragging through the already resting objects.

We further emphasise that although unconcentrated overland flow is a very plausible agent of orientation pattern formation, the presence of obstacles may also introduce a torque to clasts which are transported by a lateral gravitational process such as creep. This process may become the dominating one for further tight closing of the stone pavement. Creep should also affect the fragments generated by clast cracking through insolation weathering.

Bimodal a axes patterns might be inherited from clast alignment during the very initial phase of stone pavement formation on lava flows, prior to trapping of any aeolian dust and subsequent accretionary profile development. Williams & Zimbelman (1994) report small (1 m²) sheetflow-derived stone mosaics on bare bedrock. However, whether such orientation patterns may be preserved during the entire period of accretionary rise remains speculative. Pattern inheritance may even be excluded if a profile or surface shows any evidence of disturbance or lateral displacement such as fossil stone pavements, truncated soil horizons (McFadden et al. 1986), tilted carbonate collars around pavement clasts (McFadden et al., 1998) or turned-around stones (Helms et al., 2003).

For asymmetrical regimes, the mean deviation angle of 21±10 ° is close to the calculated minimum friction angle due to unconcentrated overland flow. Orientation patterns from debris-covered hill slopes in the Mojave Desert (Abrahams et al., 1990) argue for no other than a hydraulic formation process. Abrahams et al. (1990) term the mechanism runoff creep. This phrase, initially used by De Ploey & Moeyersons (1975), describes downslope transport of clasts due to local fluvial erosion triggered by the clast itself. To what extent such "non-collision" or "obstacle-free" processes play a role remains speculative.

The second angle mode of asymmetric regimes which is oblique towards slope aspect cannot be explained by any of the aforementioned processes, as these would always result in symmetrical patterns because the direction of gravity-controlled processes is bound to slope aspect. Similarly, the causes of the close spatial proximity of different modality and symmetry types remain unresolved. One reason for this pitfall may be inadequate measurements of slope aspect in the field at these sites. However, given the overall good agreement of results for symmetrical regimes, such a stochastic explanation is unsatisfying. Results by Adelsberger & Smith (2009) and a few plots of our study (e.g. LSM-14, NTC-228) show that there are stone pavements without preferred axes orientation. These may be the result of formation processes other than lateral ones, whose influence should decline with increasing catchment size where channel runoff dominates. The negligible influence of slope gradient on stone pavement properties (via flow velocity control) may result from the superimposed effects of slope curvature and slope length which control water discharge distribution.

3.5.3 Recovery experiments

Results of our recovery plot experiments, as modern analogues, give further arguments for the proposed formation processes. First of all, it is obvious that stones have moved into the cleared plots from outside within only ten months. Exhumation and relative concentration of coarse material is unlikely, given the virtually stone-free aeolian sub-surface. Animal burrowing may move stones to a certain degree (Haff & Werner, 1996). However, given the large area of our cleared plots the observed amount and distance of recovery due just to animals appears unlikely. Second, stones from inside the plots are better sorted than the surrounding objects and they are overall smaller. As overland flow is generated by vigorous rain events, only extreme ones may generate flows sufficient to drag large clasts. Thus, the size of relocated stones is a function of event frequency and intensity and, thus, a function of time. Our measurements of re-migrated stones show a successive increase in larger stones with time (histograms in fig. 3.3).

Perhaps the most convincing argument for lateral transport as a stone pavement formation process comes from orientation patterns of the stones inside the plots. These exhibit ubiquitous bimodal patterns, both with symmetrical and asymmetrical regimes. Mean angle deviations from

slope aspect are almost identical to those from intact stone pavement plots, clearly indicating similar process-response systems. Animal-related stone displacement would not result in such clear orientation patterns.

Pattern formation which is associated with lateral displacement does not require long transportation distances. Less than one clast a axis length would suffice to rotate the stone as a result of collision with an obstacle. However, the recovery experiments show that stones were moved into the cleared area over several decimetres.

Orientation patterns of stones are independent of polygonal patterns of the vesicular layer. Doming of soil peds due to swell and shrink processes could be able to align stone a axes parallel to ped boundaries, thus creating a trimodal pattern of clasts with angles around 60 °. However, except for two plots in the Laguna Salada study area, trimodality was not observed – especially not where we measured orientation of both, clasts and ped faces. Furthermore, there is no difference in resulting clast patterns between intact soil structures and mechanically destroyed ones. Therefore, we suggest doming of soil peds plays a minor role in creating the observed orientation patterns.

3.5.4 Fossil stone pavements

Results from four soil profiles show that bimodal orientation patterns were formed in the past, and they are preserved through fossilization. Moreover, absolute angles and mean separating angles are almost identical to the modern analogues. This suggests that even slope aspects triggering of formation processes were similar.

Disturbance or even exhumation of these buried stones by swelling and shrinking of the clay-rich soil matrix is unlikely, given the narrow intervals of stone concentration. There must have been at least two prominent periods of enhanced dust accumulation and negligible surface runoff leading to burial of older stone pavements in the Cima Volcanic Field.

Dominant bimodal orientation patterns, similar to their modern analogues, also appear in the two soil profiles with weak pedogenetic overprint and high clast content. It seems to be confusing to find both mature soils with stone lines and immature, clast-rich soils only 30 m apart. But given their proximity to shallow drainage channels the latter may be regarded as sites of preferred accumulation of laterally transported stones. Delivery of fresh clasts with respective axes orientations and subsequent infilling of suspension load (mobilised aeolian fines) would lead to the described soil texture and the juvenile character.

3.6 Conclusions

Quantitative description of circular data has been taken forward with our proposed algorithm. We suggest further calibration of the model with artificially created data with known “degrees of

modality type" and subsequent appliance to diverse types of circular earth data (e.g. mineralogical, sedimentological, tectonic, climatic data) in order to provide quantitative measures for further geoscientific disciplines.

Remarkably, stone pavements with preferred azimuthal orientation patterns of their length axes are frequent in a wide variety of arid environments. This calls for lateral geomorphologic processes, especially to explain slope aspect-symmetrical bimodal orientations. Even in cold deserts with negligible surficial runoff, preferred orientation patterns evolve and form closed pavements above vesicular layers of aeolian dust. These findings provoke several implications regarding models of stone pavement formation and their utilisation as tools for landscape research.

3.6.1 Implications for stone pavement genesis

Once a fine grained (vesicular) layer has formed, the processes of bimodal alignment during deposition of clasts may become initiated. Formation of a vesicular layer may be very rapid, provided there is an active dust source and sufficient surface roughness. At the eastern margin of Laguna Salada, a 2 cm-thick vesicular layer with overlying stone pavement has formed on a gravely feeder road which is abandoned since the 1990s. Therefore, the age of formation or abandonment of a now pavement-covered landform does not play a significant role for clast patterns. We suggest, as most other authors have done recently (cf. introduction section), that stone lifting by dust accretion is important. However, this cannot be the only mechanism involved in stone pavement formation because buried clasts cannot act as sediment traps. We suggest that during moister climates denser vegetation adopts this trapping role, as the modern analogue (Black Rock Desert) indicates. After a switch back to drier conditions, new stones establish another stone pavement while their precursors rest under a dust cover. Since this cover contains virtually no stones, these stones must be transported from elsewhere, possibly from local delivery centres such as erosion patches or bedrock outcrops upslope. Almost identical orientation angles of buried and modern clasts imply persistent formation processes over large time-scales. Consequently, the accretionary model of stone pavement formation should be complemented by this lateral component.

3.6.2 Implications for stone pavements and buried sediments as an environmental archive

The presented mobile nature of stone pavements contrasts with findings that imply their stability. However, potential of mobility does not necessarily imply continuous rearrangement of clasts. A closed stone pavement is barely susceptible to lateral clast rearrangement. However, if a site becomes disturbed, e.g. by artificial clearing or by shifts in climatic conditions, the process of recovery starts again. Sun-path controlled crack patterns in clasts (Eppes et al., 2010), micro-lamin-

ation stratigraphies of rock varnish (Liu & Broecker, 2007), clast rubification (Helms et al., 2003) and further chronofunctions (e.g. Al-Farraj & Harvey, 2000) are consistent with this dual nature of stone pavements. An important implication arises from the observed orientation patterns on alluvial fan sites. Stones on active alluvial fans are often aligned perpendicular to slope aspect due to their alluvial origin (Bridge & Demicco, 2008). The different orientation pattern of a modern stone pavement shows that after abandonment of a fan section the geomorphologic process regime has shifted. With ongoing trapping of aeolian material and subsequent development of a smooth vesicular layer, the surficial stones become detached and begin to form an orientation pattern no longer controlled by the initial processes which formed the alluvial fan. Concluding, the general role of stone pavement as age indicator should be treated with care (also cf. Dietze et al., 2011).

In contrast, the pedogenetically overprinted aeolian sediments below stone pavements may represent a valuable, undisturbed environmental archive. In mature soil profiles we found no indicators of truncation. We suggest that either an intact stone pavement together with a vesicular layer of mostly hard to very hard dry consistence or a denser vegetation cover may have protected the sediment column from erosion. Successions of fossil stone pavements and vesicular horizons (Dietze et al., 2011) also indicate intact stratigraphy. Such a system records episodes of preferred dust accumulation (which is related to periods of environmental instability, e.g. McFadden et al., 1986), pedogenetic overprint (which allows reconstruction of environmental conditions; Birkeland, 1990; Chadwick & Davis, 1990; Kleber, 2000), periods of stone pavement formation (which are, as our results from Black Rock Desert indicate, restricted to specific moisture conditions) and formation of vesicular layers (which may also be related to certain environmental conditions). Therefore, further study of these archives, often aided by the linkage to lake histories (Oviatt, 1991; Wells, 2003; Contreras et al., 2005), will be a next step towards a broad understanding of landscape evolution in modern desert regions. For Black Rock Desert, Schmidt (2008) and Schmidt et al. (2008) have already demonstrated the feasibility of this approach.

Acknowledgements

We would like to thank the Mojave National Preserve Administration, Brian Cooperider and Manuel Uribe for supporting field work in the US and Manfred Buchroithner for providing access to the Nevado Tres Cruces area. We kindly thank Elisabeth Dietze, Dominik Faust and Kai Hartmann for their essential comments on an earlier draft of the manuscript. We also thank the two anonymous reviewers as well as Andrew Plater for invaluable ideas and comments.

References

Abrahams, A.D., Soltyka, N., Parsons, A.J., Hirsch, P.J., 1990. Fabric analysis of a desert debris slope: Bell Mountain, California. Journal of Geology 98, 264-272.

Adelsberger, K.A., Smith, J.R., 2009. Desert pavement development and landscape stability on the Eastern Libyan Plateau, Egypt. Geomorphology 107, 178-194.

Al-Farraj, A., Harvey, A.M., 2000. Desert pavement characteristics on Wadi terrace and alluvial fan surfaces: Wadi Al-Bih, U.A.E. and Oman. Geomorphology 35, 279–297.

Allen, J.R.L., 1982. Sedimentary structures. Their character and physical basis. Volume I. – Developments in Sedimentology 30A. Elsevier, Amsterdam.

Anderson, K.C., Wells, S.G., Graham, R.C., 2002. Pedogenesis of vesicular horizons, Cima volcanic field, Mojave Desert, California. Soil Science Society of America Journal 66, 878-887.

Birkeland, P.W., 1990. Soil-geomorphic research - a selective overview. Geomorphology 3, 207-224.

Birkeland, P.W., 1999. Soils and geomorphology. Oxford University Press, Oxford.

Borradaile, G., 2003. Statistics of Earth Science Data. Springer, Berlin.

Bridge, J.S., Demicco, R.V., 2008. Earth surface processes, landforms and sediment deposits. Cambridge University Press, Cambridge.

Buchalter, B.J., Bradley, R.M., 1992. Orientation order in random packings of ellipses. Physical Review 46, 3046-3056.

Chadwick, O.A., Davis, J.O., 1990. Soil forming intervals caused by eolian sediment pulses in the Lahontan Basin, northwestern Nevada. Geology 18, 243-246.

Collinson, J.D., Thompson, D.B., 1989. Sedimentary structures. Unwin Hyman, London.

Contreras, J., Martín-Barajas, A., Herguera, J.C., 2005. Subsidence of the Laguna Salada Basin, northeastern Baja California, Mexico, inferred from Milankovitch climatic changes. Geofísica Internacional 44, 103-111.

Cooke, R.U., 1970. Stone pavements in deserts. Annals of the Association of American Geographers 60, 560-577.

Cooke, R.U., Warren, A., Goudie, A.S., 1993. Desert Geomorphology. UCL Press, London.

De Ploey, J., Moeyersons, J., 1975. Runoff creep of coarse debris: experimental data and some field observations. Catena 2, 275-288.

Dietze, M., Muhs, S., Dietze, E., 2011. Ambiguities of relative age indicators on abandoned surfaces of arid environments. Zeitschrift für Geomorphologie N.F. 55, 49-75.

Dunkerley, D.L., 1995. Surface stone cover on desert hillslopes: parameterizing characteristics relevant to infiltration and surface runoff. Earth Surface Processes and Landforms 20, 207-218.

Eppes, M.C., McFadden, L.D., Wegmann, K.W., Scuderi, L.A., 2010. Cracks in desert pavement rocks: Further insights into mechanical weathering by directional insolation. Geomorphology 123, 97-108.

Fujioka, T., Chappell, J., Honda, M., Yatsevich, I., Fifield, K., Fabel, D., 2005. Global cooling initiated stoney deserts in central Australia 2-4 Ma, dated by cosmogenic ^{21}Ne-^{10}Be. Geology 33, 993-996.

Garreaud, R., Vuille, M., Clement, A.C., 2003. The climate of the Altiplano: observed current conditions and mechanisms of past changes. Palaeogeography, Palaeoclimatology, Palaeoecology 194, 5-22.

Haff, P.K., Werner, B.T., 1996. Dynamical Processes on Desert Pavements and the Healing of Surficial Disturbances. Quaternary Research 45, 38-46.

Helms, J.G., McGill, S.F., Rockwell, T.K., 2003. Calibrated, late Quaternary age indices using clast rubification and soil development on alluvial surfaces in Pilot Knob Valley, Mojave Desert, southeastern California. Quaternary Research 60, 377-393.

Higgitt, D.L., Allison, R.J., 1999. Characteristics of stone covers on the surface of basalt flows in arid, northeast Jordan. Geomorphology 28, 263-280.

Kleber, A., 2000. Compound soil horizons with mixed calcic and argillic properties - examples from the northern Great Basin, USA. Catena 41, 111-131.

Kohlbeck, F., Mojica, J., Scheidegger, A.E., 1994. Clast orientations of the 1985 lahars of the Nevado del Ruiz, Colombia and implications for depositional processes. Sedimentary Geology 88, 175-183.

Leeder, M.R., 1982. Sedimentology. Allen & Unwin, London.

Legates, D.R., Willmott, C.J., 1990. Mean Seasonal and Spatial Variability in Gauge-Corrected, Global Precipitation. International Journal of Climatology 10, 111-127.

Liu, T., Broecker, W.S., 2007. Holocene rock varnish microstratigraphy and its chronometric application in the drylands of western USA. Geomorphology 84, 1-21.

Mabbutt, J.A., 1977. Desert Landforms. MIT Press, Cambridge.

Major, J.J., 1998. Pebble orientation on large, experimental debris-flow deposits. Sedimentary Geology 117, 151-164.

Marchetti, D.W., Cerling, T.E., 2005. Cosmogenic ^{3}He exposure ages of Pleistocene debris flows and desert pavements in Capitol Reef National Park , Utah. Geomorphology 67, 423-435.

Mardia, K.V., Jupp, P.E., 2000. Directional Statistics. John Wiley & Sons, Chichester.

Martín-Barajas, A., Vásquez-Hernández, S., Carreno, A.L., Helenes, J., Suárez-Vidal, F., Alvarez-Rosales, J., 2001. Late Neogene stratigraphy and tectonic control on facies evolution in the Laguna Salada Basin, northern Baja California, Mexico. Sedimentary Geology 144, 5-35.

Matmon, A., Simhai, O., Amit, R., Haviv, I., Porat, N., McDonald, E.V., Benedetti, L., Finkel, R., 2009. Desert pavement-coated surfaces in extreme deserts present the longest-lived landforms on Earth. Geological Society of America Bulletin 121, 688-697.

McFadden, L.D., Wells, S.G., Dohrenwend, J.C., 1986. Influences of quaternary climatic changes on processes of soil development on desert loess deposits of the Cima volcanic field, California. Catena 13, 361-389.

McFadden, L.D., Ritter, J.B., Wells, S.G., 1989. Use of multiparameter relative-age methods for age estimation and correlation of alluvial fan surfaces on a desert piedmont Eastern Mojave Desert, California. Quaternary Research 32, 276-290.

McFadden, L.D., McDonald, E.V., Wells, S.G., Anderson, K., Quade, J., Forman, S.L., 1998. The vesicular layer and carbonate collars of desert soils and pavements: formation, age and relation to climate change. Geomorphology 24, 101-145.

Meadows, D.G., Young, M.H., McDonald, E.V., 2008. Influence of relative surface age on hydraulic properties and infiltration on soils associated with desert pavements. Catena 72, 169-178.

Moores, J.E., Pelletier, J.D., Smith, P.H., 2008. Crack propagation by differential insolation on desert surface clasts. Geomorphology 102, 472-481.

NCDC, 2010. National Climatic Data Center. http://www.ncdc.noaa.gov/oa/ncdc.html [22.06.2011].

NGDC, 2010. National Geophysical Data Center. http://www.ngdc.noaa.gov [22.06.2011].

Nichols, K.K., Bierman, P.R., Eppes, M.C., Caffee, M., Finkel, R., Larsen, J., 2007: Timing and surficial process changes down a Mojave Desert piedmont. Quaternary Research 68, 151-161.

Oviatt, C.G., 1991. Quaternary geology of the Black Rock Desert, Millard County, Utah. Utah Geological and Mineral Survey, Special Studies 73.

Parsons, A.J., Abrahams, A.D., Howard, A.D., 2009. Rock-Mantled Slopes. In: Parsons, A.J., Abrahams, A.D., Eds. Geomorphology of Desert Environments. Springer, Berlin.

Pelletier, J.D., Cline, M., DeLong, S.B., 2007. Desert pavement dynamics: numerical modeling and field-based calibration. Earth Surface Processes and Landforms 32, 1913-1927.

Pettijohn, F.J., 1975. Sedimentary rocks. Harper & Row, New York.

Poesen, J. W., van Wesemael, B., Bunte, K., Solé Benet, A., 1998. Variation of rock fragment cover and size along semiarid hillslopes: a case-study from southeast Spain. Geomorphology 23, 323-335.

Quade, J., 2001. Desert pavements and associated rock varnish in the Mojave Desert: ho old can they be?. Geology 29, 855-858.

Rao Jammalamadaka, S., 2001. Topics in Circular Statistics. World Scientific Press, Singapore.

Schmidt, J.-U., 2008. Bodenevolution während der letzten 30.000 Jahre in der Black Rock Desert, W Utah, SW USA. Unpublished Diploma Thesis, Technische Universität Dresden.

Schmidt, J.-U., Kleber, A., Dietze, M., 2008. Soil evolution during the past 30,000 years In the Black Rock Desert, Utah, SW USA. Geological Society of America Abstracts with Programme 40/6, 532.

Sharon, D., 1962. On the nature of hamadas in Israel. Zeitschrift für Geomorphologie N.F. 6, 129-147.

Soil Survey Division Staff, 1993. Soil Survey Manual. Soil Conservation Service. U.S. Department of Agriculture Handbook 18.

Spelz, R.M., Fletcher, J.M., Owen, L.A., Caffee, M.W., 2008. Quaternary alluvial-fan development, climate and morphologic dating of fault scarps in Laguna Salada, Baja California, Mexico. Geomorphology 102, 578-594.

Turrin, B.D., Dohrenwend, J.C., Drake, R.E., Curtis, G.H., 1985. K-Ar ages from Cima volcanic field, eastern Mojave Desert, California. Isochron/ West 44, 9-16.

Valentine, G.A., Harrington, C.D., 2006. Clast size controls and longevity of Pleistocene desert pavements at Lathrop Wells and Red Cone volcanoes, southern Nevada. Geology 34, 533-536.

Wainwright, J., Parsons, A.J., Abrahams, A.D., 1999. Field and computer simulation experiments on the formation of desert pavements. Earth Surface Processes and Landforms 24, 1025-1037.

Wells, N., 2000. Are there better alternatives to standard rose diagrams? Journal of Sedimentary Research 70, 37-46.

Wells, S.G., 2003. Late Quaternary geology and paleohydrology of pluvial Lake Mojave, southern California. Geological Society of America Special Paper 368, 79-114.

Wells, S.G., Dohrenwendt, J.C., McFadden, L.D., Turrin, B.D., Mahrer, K.D., 1985. Late Cenozoic landscape evolution on lava flow surfaces of the Cima Volcanic field, Mojave Desert, California. Geological Society of America Bulletin 96, 1518-1529.

Wells, S.G., McFadden, L.D., Poths, J., Olinger, C.T., 1995. Cosmogenic ^{3}He surface-exposure dating of stone pavements: Implications for landscape evolution in deserts. Geology 23, 613-616.

Williams, S.H., Zimbelman, J.R., 1994. Desert Pavement Evolution: An Example of the Role of Sheetflood. Journal of Geology 102, 243-248.

Appendix

Table 3.A.1. Descriptions of relief and surface properties for surficial clast orientation plots; * estimated mean annual precipitation [mm/a] in brackets. ** Instead of distance to channel the specific catchment [km²] was calculated from DEM drainage analysis.

ID	*coordinates*	*slope inclination*	*slope aspect*	*distance to channel*	*distance to outcrop*	*clast lithology*	*pavement coverage*
	(UTM zone 11N, 19S)	[°]	[°]	[m]	[m]		[%]
Cima Volcanic Field							
CVF-001	608580/3892116	3	279	17	45	basalt	100
CVF-002	608568/3892124	4	286	34	10	basalt	100
CVF-003	608568/3892122	6	283	32	14	basalt	95
CVF-004	608577/3892110	5	287	15	30	basalt	100
CVF-005	608576/3892112	5	286	18	29	basalt	95
CVF-006	608586/3892102	2	281	16	20	basalt	95
CVF-007	608586/3892100	4	289	8	24	basalt	100
CVF-008	608612/3892043	3	307	6	25	basalt	95
CVF-009	608561/3891986	2	269	8	60	basalt	95
CVF-010	608609/3891967	5	276	24	55	basalt	60
CVF-011	608576/3891964	4	275	60	35	basalt	95
CVF-012	608563/3891954	2	271	92	12	basalt	95
CVF-013	608568/3892125	<1	288	20	8	basalt	100
CVF-014	608570/3892126	4	289	13	21	basalt	100
CVF-015	608572/3892125	5	286	7	26	basalt	95
CVF-016	608582/3892115	5	291	8	42	basalt	95
Laguna Salada							
LSM-01	611470/3578899	4	84	10	n.d.	granitic	85
LSM-02	611478/3578901	4	76	14	n.d.	granitic	75
LSM-03	612604/3590026	3	70	7	n.d.	basaltic cinder	90
LSM-04	612582/3590049	4	76	10	n.d.	basaltic cinder	90
LSM-05	612728/3589882	2	44	40	n.d.	basaltic cinder	85
LSM-06	612727/3589880	2	43	40	n.d.	basaltic cinder	80
LSM-07a	612716/3589892	2	34	40	n.d.	basaltic cinder	80
LSM-07b	612716/3589892	2	34	40	n.d.	basaltic cinder	80
LSM-08	610776/3591101	1	118	400	n.d.	basalt, calcrete	100
LSM-09	610753/3591114	1	121	400	n.d.	basalt, calcrete	100
LSM-10	610794/3591154	2	92	400	n.d.	basalt, calcrete	100
LSM-11	679079/3520220	4	254	8	n.d.	rhyolite	100
LSM-12	679083/3520228	4	247	5	n.d.	rhyolite	100
LSM-13	679078/3520235	4	250	8	n.d.	rhyolite	100
LSM-14	678994/3520495	2	327	10	n.d.	rhyolite	100
LSM-15	623744/3601807	1	227	3	n.d.	basalt	90
Black Rock Desert							
BRD-001	885312/4340075	1	84	8	300	basaltic cinder	95 (276*)
BRD-002	871684/4301857	<1	64	23	125	rhyolite, calcrete	80 (293*)
BRD-003	865317/4339538	2	212	35	25	basalt	90 (229*)
BRD-004	887898/4318131	1	309	15	15	basalt	40 (329*)
BRD-005	864422/4303977	< 1	155	80	200	rhyolite	80 (270*)
BRD-006	876397/4298982	3	268	95	10	basalt	90 (310*)
BRD-008	889944/4321843	< 1	148	18	5	basalt	80 (339*)
BRD-009	892206/4305124	2	108	65	20	basalt	40 (363*)
Nevado Tres Cruces							
NTC-220	550602/7025428	4	199	0.69**	166	basalt	90
NTC-221	550582/7025395	5	199	0.66**	186	basalt	90
NTC-222	550572/7025372	7	199	0.65**	206	basalt	95
NTC-223	550557/7025337	9	199	0.63**	212	basalt	85
NTC-224	550554/7025324	11	199	0.62**	244	basalt	80
NTC-225	550543/7025294	15	199	0.61**	277	basalt	75
NTC-226	550535/7025283	19	199	0.55**	299	basalt	70
NTC-227	550516/7025248	21	199	0.49**	321	basalt	70
NTC-228	550496/7025221	20	199	0.43**	241	basalt	75
NTC-229	550491/7025216	20	199	0.30**	370	basalt	70
NTC-230	550487/7025201	20	199	0.19**	405	basalt	70
NTC-231	550486/7025175	21	199	0.18**	437	basalt	70

Table 3.A.2. Descriptions of clast geometry and orientation properties for surficial plots. Measured clasts: number of digitised stones with objects passing analysis preconditions in brackets. Stone axes measures are given as geometric means with 1standard deviation. Mean anisotropy resembles ratio of a and b axes. Degrees of modality type are calculated according to equations 2 to 4 with the bold one indicating the dominating type. Angle description data are only appropriate for bimodal patterns (bold values).

ID	*measured clasts*	*mean a axis* [mm]	*mean b axis* [mm]	*mean an-isotropy*	*degree of uniformity (Iuf)*	*degree of unimodality (Ium)*	*degree of bimodality (Ibm)*	*mean angles* [°]	*angle 1* [°]	*angle 2* [°]	*equili-brium*
Cima Volcanic Field											
CVF-001	105 (100)	48 ± 28	25 ± 14	2.0 ± 0.5	0.26	0.15	**0.59**	**82/98**	**125**	**27**	**0.43**
CVF-002	101 (101)	61 ± 26	33 ± 17	1.9 ± 0.4	**0.46**	0.38	0.16	84/96	317	221	0.39
CVF-003	111 (108)	59 ± 26	35 ± 17	1.8 ± 0.4	0.23	0.19	**0.58**	**68/112**	**335**	**223**	**0.45**
CVF-004	104 (96)	61 ± 25	34 ± 15	1.9 ± 0.6	0.35	**0.43**	0.22	79/101	334	253	0.29
CVF-005	103 (102)	67 ± 36	36 ± 20	1.9 ± 0.4	**0.41**	0.30	0.29	72/108	335	263	0.42
CVF-006	148 (145)	60 ± 32	33 ± 18	1.8 ± 0.4	0.27	0.13	**0.60**	**83/97**	**295**	**356**	**0.41**
CVF-007	104 (101)	79 ± 41	43 ± 22	1.9 ± 0.5	0.20	0.14	**0.66**	**60/120**	**206**	**265**	**0.50**
CVF-008	100 (86)	117 ± 38	70 ± 26	1.8 ± 0.5	0.21	0.19	**0.6**	**65/115**	**347**	**281**	**0.46**
CVF-009	104 (98)	57 ± 31	31 ± 19	1.9 ± 0.4	0.25	0.24	**0.51**	**79/101**	**336**	**252**	**0.32**
CVF-010	103 (93)	106 ± 40	68 ± 26	1.6 ± 0.3	0.23	0.18	**0.59**	**73/107**	**323**	**251**	**0.44**
CVF-011	106 (100)	63 ± 32	34 ± 22	2.0 ± 0.5	0.26	0.16	**0.58**	**86/94**	**238**	**326**	**0.43**
CVF-012	100 (97)	79 ± 40	42 ± 21	2.0 ± 0.4	0.24	0.22	**0.54**	**89/91**	**288**	**200**	**0.40**
CVF-013	101 (91)	62 ± 35	37 ± 24	1.8 ± 0.4	0.21	0.19	**0.60**	**85/95**	**197**	**284**	**0.49**
CVF-014	103 (98)	53 ± 24	30 ± 16	1.9 ± 0.5	0.24	0.19	**0.57**	**73/107**	**312**	**240**	**0.43**
CVF-015	104 (99)	65 ± 35	37 ± 20	1.8 ± 0.5	0.26	0.21	**0.53**	**89/91**	**55**	**145**	**0.38**
CVF-016	104 (99)	58 ± 30	33 ± 21	1.9 ± 0.5	0.24	0.24	**0.52**	**90/90**	**163**	**70**	**0.35**
Laguna Salada											
LSM-01	104 (99)	63 ± 29	38 ± 18	1.7 ± 0.4	0.28	0.15	**0.57**	**79/101**	**136**	**35**	**0.41**
LSM-02	105 (101)	41 ± 15	26 ± 12	1.6 ± 0.3	0.20	0.13	**0.67**	**62/118**	**88**	**27**	**0.55**
LSM-03	500 (465)	38 ± 14	22 ± 10	1.8 ± 0.5	0.26	0.04	**0.70**	**66/114**	**132**	**18**	**0.63**
LSM-04	105 (100)	56 ± 22	32 ± 13	1.9 ± 0.6	0.20	0.07	**0.73**	**67/113**	**173**	**117**	**0.59**
LSM-05	105 (99)	50 ± 16	28 ± 9	1.9 ± 0.4	0.27	0.14	**0.59**	**82/98**	**27**	**122**	**0.56**
LSM-06	105 (101)	49 ± 18	28 ± 12	1.9 ± 0.5	0.28	0.09	**0.62**	**78/102**	**144**	**70**	**0.59**
LSM-07a	105 (100)	39 ± 13	23 ± 9	1.8 ± 0.5	0.21	0.08	**0.71**	**70/110**	**113**	**43**	**0.56**
LSM-07b	105 (96)	36 ± 14	21 ± 9	1.8 ± 0.4	**0.53**	0.40	0.07	65/115	104	38	0.47
LSM-08	105 (97)	28 ± 6	14 ± 4	2.1 ± 0.5	0.28	0.09	**0.62**	**69/111**	**77**	**170**	**0.57**
LSM-09	105 (99)	61 ± 37	33 ± 17	1.9 ± 0.5	**0.57**	0.30	0.13	73/107	65	172	0.50
LSM-10	105 (104)	39 ± 34	22 ± 18	1.8 ± 0.3	0.25	0.19	**0.57**	**80/100**	**118**	**19**	**0.43**
LSM-11	105 (104)	40 ± 18	19 ± 10	2.2 ± 0.7	**0.52**	0.34	0.14	73/107	355	282	0.42
LSM-12	105 (101)	72 ± 28	38 ± 17	2.0 ± 0.5	0.28	0.15	**0.57**	**75/105**	**295**	**224**	**0.47**
LSM-13	105 (105)	35 ± 9	17 ± 5	2.1 ± 0.5	0.25	0.19	**0.56**	**72/108**	**204**	**312**	**0.46**
LSM-14	105 (97)	53 ± 20	30 ± 11	1.9 ± 0.5	**0.56**	0.20	0.24	70/110	195	265	0.54
LSM-15	105 (100)	65 ± 21	39 ± 14	1.7 ± 0.4	0.27	0.13	**0.61**	**63/117**	**285**	**352**	**0.53**
Black Rock Desert											
BRD-001	104 (100)	32 ± 9	20 ± 7	1.7 ± 0.3	**0.42**	0.27	0.31	65/115	98	33	0.51
BRD-002	101 (96)	43 ± 10	26 ± 6	1.7 ± 0.4	0.25	0.14	**0.61**	**75/105**	**87**	**162**	**0.49**
BRD-003	105 (98)	62 ± 34	34 ± 21	1.9 ± 0.5	0.18	0.10	**0.72**	**69/111**	**56**	**167**	**0.53**
BRD-004	91 (61)	46 ± 36	29 ± 26	1.7 ± 0.4	0.34	**0.41**	0.25	80/100	62	150	0.58
BRD-005	113 (79)	25 ± 9	14 ± 5	1.9 ± 0.5	0.19	0.19	**0.62**	**62/118**	**33**	**95**	**0.73**
BRD-006	113 (102)	52 ± 16	29 ± 13	1.9 ± 0.5	0.25	0.15	**0.60**	**85/95**	**28**	**111**	**0.54**
BRD-008	87 (80)	32 ± 11	18 ± 8	2.0 ± 0.5	0.21	0.12	**0.67**	**59/121**	**27**	**86**	**0.79**
BRD-009	100 (93)	35 ± 12	21 ± 8	1.7 ± 0.4	0.24	0.13	**0.63**	**73/107**	**75**	**182**	**0.66**
Nevado Tres Cruces											
NTC-220	100 (83)	35 ± 14	19 ± 9	1.9 ± 0.6	0.21	0.26	**0.53**	**67/113**	**144**	**76**	**0.50**
NTC-221	105 (78)	38 ± 21	21 ± 12	1.9 ± 0.5	**0.64**	0.21	0.15	78/102	65	142	0.58
NTC-222	121 (106)	31 ± 12	17 ± 8	2.0 ± 0.6	0.21	0.15	**0.63**	**70/110**	**154**	**85**	**0.63**
NTC-223	109 (98)	49 ± 25	27 ± 16	2.0 ± 0.6	0.22	0.11	**0.67**	**70/110**	**45**	**113**	**0.62**
NTC-224	120 (119)	57 ± 27	26 ± 14	2.3 ± 0.6	0.21	0.11	**0.68**	**63/117**	**85**	**150**	**0.67**
NTC-225	112 (104)	53 ± 36	28 ± 19	2.0 ± 0.6	0.23	0.11	**0.66**	**60/120**	**113**	**173**	**0.75**
NTC-226	105 (94)	40 ± 29	21 ± 16	2.0 ± 0.5	0.20	0.16	**0.64**	**66/114**	**74**	**144**	**0.58**
NTC-227	109 (97)	40 ± 19	21 ± 11	2.1 ± 0.7	0.23	0.09	**0.68**	**67/113**	**153**	**86**	**0.66**
NTC-228	111 (100)	41 ± 22	23 ± 14	1.9 ± 0.5	0.35	0.19	**0.46**	**68/112**	**94**	**162**	**0.64**
NTC-229	108 (104)	38 ± 18	21 ± 10	1.9 ± 0.6	0.19	0.14	**0.67**	**65/115**	**66**	**131**	**0.57**
NTC-230	108 (100)	52 ± 32	27 ± 16	2.0 ± 0.6	**0.49**	0.37	0.14	72/108	54	130	0.55
NTC-231	108 (107)	57 ± 29	28 ± 15	2.1 ± 0.7	**0.59**	0.41	0.01	67/113	76	140	0.65

Table 3.A.3. Statistics of clast geometry and orientation parameters for stone pavement recovery plots and buried stone lines. See appendix 1 and 2 for explanations. Further, orientation parameters of polygonal soil structures are presented for selective plots (…_polygons). Also, stone pavement orientation patterns of the mature stone pavement surrounding the cleared plots are given for comparison (…_outside). Orientation parameters were not calculated for plots with insufficient sample numbers.n.d. – not determined due to scarce data amount.

ID	*number of clasts/ objects*	*mean a axis* [mm]	*mean b axis* [mm]	*mean aniso-tropy*	*degree of uniformity*	*degree of unimodality*	*degree of bimodality*	*mean angles* [°]	*angle 1* [°]	*angle 2* [°]	*equilibrium*
Stone pavement recovery plots											
A1a_polygons	110	n.d.	n.d.	n.d.	**0.65**	0.23	0.12	77/103	115	39	0.64
A3a_polygons	70	n.d.	n.d.	n.d.	**0.48**	0.35	0.17	70/110	22	96	0.68
M2a_polygons	30	n.d.	n.d.	n.d.	n.d.	n.d.	n.d.	n.d.	n.d.	n.d.	n.d.
LSM_07_polygons	100	n.d.	n.d.	n.d.	**0.62**	0.24	0.15	71/109	136	64	0.63
A1a_2008_03	121 (20)	15 ± 6	4 ± 1.7	1.7 ± 0.5	n.d.	n.d.	n.d.	n.d.	n.d.	n.d.	n.d.
A1a_2008_09	200 (63)	18 ± 9	5 ± 1.8	1.8 ± 0.6	0.24	0.23	**0.53**	**88/92**	**45**	**132**	**0.51**
A1a_2009_07	314 (89)	19 ± 9	6 ± 1.5	1.5 ± 0.4	0.25	0.19	**0.56**	**86/94**	**145**	**50**	**0.54**
A1a_outside	121 (77)	32 ± 21	13 ± 1.8	1.8 ± 0.5	0.27	0.14	**0.59**	**87/93**	**44**	**133**	**0.55**
A2a_2008_03	279 (27)	12 ± 6	3 ± 1.7	1.7 ± 0.5	n.d.	n.d.	n.d.	n.d.	n.d.	n.d.	n.d.
A2a_2008_09	297 (44)	15 ± 7	4 ± 1.7	1.7 ± 0.5	0.20	0.22	**0.58**	**65/115**	**88**	**158**	**0.31**
A2a_2009_07	255 (49)	16 ± 6	4 ± 1.7	1.7 ± 0.5	**0.47**	0.47	0.06	65/115	33	95	0.37
A2a_outside	102 (95)	44 ± 25	12 ± 2.0	2.0 ± 0.5	0.17	0.18	**0.65**	**76/104**	**175**	**100**	**0.63**
A3a_2008_03	111 (16)	14 ± 5	3 ± 1.7	1.7 ± 0.4	n.d.	n.d.	n.d.	n.d.	n.d.	n.d.	n.d.
A3a_2008_09	132 (19)	14 ± 5	3 ± 1.7	1.7 ± 0.6	n.d.	n.d.	n.d.	n.d.	n.d.	n.d.	n.d.
A3a_2009_07	127 (36)	17 ± 6	4 ± 1.8	1.8 ± 0.6	0.24	0.34	**0.42**	**82/98**	**134**	**38**	**0.36**
A3a_outside	58 (52)	66 ± 43	24 ± 1.9	1.9 ± 0.5	0.23	0.23	**0.54**	**72/108**	**113**	**40**	**0.64**
M1a_2008_03	542 (50)	13 ± 5	4 ± 1.6	1.6 ± 0.5	0.19	0.31	**0.50**	**73/107**	**45**	**156**	**0.54**
M1a_2008_09	643 (51)	13 ± 5	3 ± 1.6	1.6 ± 0.5	0.25	0.24	**0.51**	**83/97**	**65**	**162**	**0.55**
M1a_2009_07	228 (66)	18 ± 7	4 ± 1.6	1.6 ± 0.5	0.27	0.14	**0.60**	**83/97**	**174**	**77**	**0.57**
M1a_outside	100 (86)	41 ± 26	17 ± 1.8	1.8 ± 0.4	0.20	0.31	**0.49**	**84/96**	**56**	**139**	**0.59**
M2a_2008_03	287 (79)	17 ± 7	4 ± 1.8	1.8 ± 0.5	0.25	0.18	**0.57**	**85/95**	**14**	**100**	**0.54**
M2a_2008_09	315 (85)	17 ± 6	4 ± 1.8	1.8 ± 0.5	0.26	0.13	**0.61**	**85/95**	**4**	**118**	**0.56**
M2a_2009_07	293 (86)	18 ± 7	4 ± 1.7	1.7 ± 0.5	0.23	0.21	**0.56**	**88/92**	**135**	**48**	**0.55**
M2a_outside	77 (73)	41 ± 27	17 ± 1.9	1.9 ± 0.4	0.25	0.20	**0.55**	**86/94**	**155**	**69**	**0.53**
Buried stone lines											
CVF07-101	127 (85)	49 ± 21	32 ± 14	1.6 ± 0.4	0.29	0.18	**0.53**	**72/108**	**56**	**163**	**0.52**
CVF07-102	66 (57)	48 ± 34	30 ± 18	1.7 ± 0.4	0.25	0.17	**0.58**	**76/104**	**38**	**144**	**0.56**
CVF07-104	66 (42)	53 ± 20	32 ± 11	1.7 ± 0.3	0.33	0.17	**0.51**	**91/89**	**81**	**172**	**0.59**
CVF07-105	30 (28)	49 ± 18	28 ± 9	1.8 ± 0.4	0.24	0.12	**0.64**	**57/123**	**52**	**167**	**0.62**

4 Alignment of stone-pavement clasts by unconcentrated overland flow

Chapter 4 is submitted to the peer-reviewed journal Earth Surface Processes and Landforms (ISSN 0196-9837) as:

Alignment of stone-pavement clasts by unconcentrated overland flow – implications of numerical and physical modelling

Authors: Michael Dietze[1], Juliane Groth[2], Arno Kleber[1]

[1] Institute of Geography, Technische Universität Dresden

[2] Institute of Geography, Leopold-Franzens-Universität Innsbruck

Publication history: submitted: February 2012

Full reference: Dietze M, Groth J, Kleber A. (submitted). Alignment of stone-pavement clasts by unconcentrated overland flow – implications of numerical and physical modelling. Earth Surface Processes and Landforms.

Internet link: not available

Abstract: The crucial role of stone pavements in arid environments for aeolian or alluvial processes and as numerical dating tools is increasingly acknowledged. This role is based on the assumption that stone pavements are stable landforms, formed gradually over time and predominantly by vertical processes. However, this is challenged by evidence of stone pavement clast reworking or burial. Bimodal, mostly slope aspect-symmetrical clast orientation is a frequent phenomenon in various study areas. It implies that stone pavements may be influenced by unidirectional lateral processes besides vertical ones.

Here, the finding of lateral processes contributing to pavement evolution is supported by numerical modelling and physical experiments. These unequivocally show that unconcentrated overland flow can transport clasts to form a closely packed stone mosaic with characteristics similar to those of natural stone pavements. The commonly observed length-axes orientation angle of 40±14 ° for natural stone pavement clasts is consistently reproduced by angle-dependent force equilibrium. Monte Carlo runs confirm the natural scatter and allow characterisation of the control parameters of clast orientation. The model explains up to 70 % of the natural variance. It is further validated by flume experiments, which confirm model predictions of single object orientation angles. Experiments with multiple objects yield artificial stone pavements with properties similar to those found in the field.

The unidirectional lateral process acting on natural stone pavements requires the presence of a vesicular horizon. This underlines the tight genetic coupling of this common epipedon feature and the clast cover. The presented findings highlight the role of stone pavements as process and environment proxies. However, stone pavements represent information since the last surface disturbance only. This has to be considered when using them as an age indicators.

Keywords: Stone pavement; Desert pavement; Overland flow; Numerical model; Flume experiment

4.1 Introduction

Stone pavements are widespread, prominent surface features of arid environments. They cover extensive areas, predominantly with gently inclined relief. Mature stone pavements form a closely packed mosaic of coarse particles resting upon or being partly embedded in finer sediment. Such clast monolayers may occur as patches of a few square metres but may also cover huge areas (Cooke et al., 1993). Individual clasts are typically several centimetres in length. However, properties of stone pavements may vary considerably, depending on factors such as lithological composition, previous clast transport processes, disaggregation processes and the palaeo-environmental history of a site. Clast cover density, exposure of intervening silty materials, clast size, degree of sorting, fracturing, desert varnish cover and rounding may further depend on both, surface age and genesis of the landform they cover: alluvial fans, fluvial terraces, lava flows, beach ridges etc. (Wells et al., 1985; McFadden et al., 1989; Al-Farraj and Harvey, 2000; Spelz et al., 2008). Stone pavements are typically associated with underlying fine, i.e. silty to loamy sediment, which has a distinctive foamy structure with isolated, spherical to oval pores up to several millimetres in diameter, which is often covered by a few millimetres of loose but slightly coarser sediment (McFadden et al., 1998). It is referred to as vesicular horizon (Springer, 1958). The combination of stone pavement and vesicular horizon has a key function in controlling infiltration capacity (Young et al., 2004) and hence surface runoff, one of the major geomorphological processes in arid landscapes. Furthermore, stone pavement-covered sites are crucial components of ecological systems (Wood et al., 2005).

The abundance, spatial extent, barrenness, low topographic heterogeneity and presumed stable nature of stone pavement-covered areas make them increasingly interesting for human demands. Military manoeuvres, facility building and recreational activities such as off-road driving are common land-uses on these sensitive landforms despite poor understanding of their impact, the longevity of effects and the secondary processes they may trigger (Lovich and Bainbridge, 1999; Prose and Wilshire, 2000; Yonovitz and Drohan, 2009). Intact stone pavements are regarded as sinks for aeolian dust by many authors. Aeolian mantles up to two metres thick (Wells et al., 1985) or the loess content of the vesicular horizons (Spelz et al., 2008; McFadden et al., 1998; Matmon et al., 2009) underline this sink function. However, once disturbed, stone pavements may become a remarkable source of dust (cf. Cooke et al., 1993) directly impacting facilities built upon them, e.g. solar-thermal power plants. Furthermore, stone pavement-covered surfaces are frequently used for relative (McFadden et al., 1989; Al-Farraj and Harvey, 2000) and absolute age estimations (Matmon et al., 2009). All age-related approaches rely on the assumption that stone pavements result from time-transgressive evolution and represent stable surfaces as long as they exist, thus fulfilling major preconditions for chronofunctions.

4.1.1 Stone pavement formation and stability

Stone pavement formation is explained by a variety of processes, often in combination, succession and superposition (Cooke, 1970; Amit and Gerson, 1986). Classical ideas favoured stone pavements as denudation residues (Blake, 1858; Sharon, 1962). Mabutt (1977) suggested they may be the result of different weathering regimes with physical fragmentation limited to the surface and predominantly chemical weathering in the epipedon. However, virtually clast-free subsurface sediments are more typically explained by clast exhumation through freeze-thaw or swell-shrink processes (Springer, 1958; Cooke, 1970). Another formation model evolved from observations that fine sediments below the clast cover are often allochthonous (Mabutt, 1977; Wells et al., 1985; McFadden et al., 1986). According to this "growth hypothesis", clasts always remain on the surface. They act as dust trap due to their roughness. Fractions of the aeolian sediments, which are trapped by the clast layer, can be effectively incorporated into the vesicular horizon. Aggregates of the vesicular horizon shrink upon desiccation to form cracks. During rainfall, the trapped sediment is translocated into these cracks and then into the aggregates via horizontal channels and matric suction. Subsequent soil wetting and aggregate swell closes the cracks (McFadden et al., 1986, Anderson et al., 2002). Thus, swell-shrinking of the vesicular-horizon incorporates the trapped aeolian matter, prevents the clasts from being buried and leads to accretionary sediment profiles. Hence, the stone pavement and vesicular horizon form a genetically coupled system.

There are reports of further, lateral processes that may play an initial or minor role in stone pavement evolution: incipient colluviation of rock fragments from topographic highs to lows (Wells et al., 1985), clast entrainment on bare bedrock by flowing water (Williams and Zimbelman, 1994), random lateral motion that leads to clast packing (Pelletier et al., 2007), rain drop impact on small stones (Haff and Werner, 1996), unsystematic dislodgement of single clasts by animals (Haff and Werner, 1996) and "recovery" of disturbed stone pavements by fine material erosion (Wainwright et al., 1999).

Furthermore, there is evidence that stone-pavement surfaces may become unstable (cf. Dietze and Kleber, 2012): e.g. clasts that lie upside down even at locations remote to human impact (Haff, 2001; Helms et al., 2003), stone pavements buried by several decimetres of accretionary aeolian deposits (Wells et al., 1985), deviating cosmogenic radionuclide-based ages of clasts lying at the surface and boulders partly embedded in it (Marchetti and Cerling, 2005) as well as heterogeneous soil-sediment complexes under stone pavements of similar maturity (Dietze et al., 2011). Dietze et al. (2011) further demonstrate how relative age estimation based on stone pavement clast and soil morphological properties may fail and conclude that the chronofunction of pavement-covered surfaces is not a prior, universal characteristic.

4.1.2 Surface disturbance and recovery

Stone pavements evolve from initial surfaces – either virtually free of clasts, covered by a disturbed stone pavement or covered by clasts that were deposited by a different process regime (e.g. river terraces, alluvial fans) – to tightly packed clast mosaics. The transition from initial to established stages of stone pavement evolution is at time scales of 10^2 to 10^5 years (for a review cf. Dietze and Kleber, 2012). Furthermore, surface modification appears to be episodic and non-linear (Haff and Werner, 1996; Dietze and Kleber, 2012).

Small-scale disturbed stone pavements or patches cleared from their clast cover, both representing an initial stage of pavement evolution, may occur i) at sites that suffered from civil and military off-roading (Lovich and Bainbridge, 1999), ii) at sites that experienced unusual intense animal activity (Haff, 2001), iii) at plant scars, i.e. remnants of deceased, large perennial plants (McAuliffe & McDonald, 2006) and iv) at plots that were artificially prepared (Wainwright et al., 1999; Dietze and Kleber, 2012;). In any event, if there are too few clasts present to recover the entire disturbed area by selective removal of fines, potentially accompanied by small-scale lateral transport of clasts (Wainwright et al., 1999), lateral contribution of fresh rock fragments is crucial to restore the paved surface (e.g. Haff and Werner, 1996). Plant scar evolution is an example of such systematic removal of coarser clasts by burrowing rodents which results in a net loss of clasts at the affected site (McAuliffe and McDonald, 2006) and consequently insufficient material to re-form a closed stone pavement by in-situ material redistribution.

Large-scale clast-free surfaces occur at degrading young lava flows and surfaces stripped to bedrock or to petrocalcic horizons (Wells et al., 1985; McFadden et al., 1986; Williams & Zimbelman, 1994). Respective stone pavement evolution models for such surfaces are presented by McFadden et al. (1986) and Anderson et al. (2002). Another type of large-scale, clast-free surfaces is present at sites where an existing stone pavement was buried by clast-free, fresh sediment (Wells et al., 1985; Dietze et al., 2011), caused by increased vegetation cover (Quade, 2001), which adopted the role as dust trap (Dietze and Kleber, 2012). At such sites, lateral contribution of fresh rock fragments is essential to restore the paved surface, too.

4.1.3 Clast orientation patterns

Dietze and Kleber (2012) present orientation measurements of stone pavement clasts. Their study areas are located in different environmental settings. Cima volcanic field, eastern Mojave Desert, California, USA, is a warm desert in which abundant aeolian material is trapped on basalt flows below well-developed stone pavements. Laguna Salada, northern Baja California, Mexico, is a hot desert where extensive stone pavements cover alluvial fan surfaces of basaltic and rhyolitic rock. Black Rock Desert, southern Sevier Basin, Utah, USA, is a semi-arid environment. It is as-

sumed to be near the modern limit of stone pavement occurrence as clast cover percentage decreases from nearly 100 % in the west to less than 40 % towards the moister eastern basin margin (Dietze & Kleber, 2012). Stone pavements are developed on dissected basaltic an rhyolitic lava flows and relict shore-line features. The Nevado Tres Cruces area, high Atacama Desert, Copiapó province, Chile, is a cold and hyper-arid desert. Several decimetres of aeolian material are deposited below well-developed stone pavements which cover extensive alluvial landforms with clasts derived from basaltic rock.

Throughout these climatically and geomorphologically different areas stone pavements show prevailing bimodal, slope aspect-symmetrical orientation patterns of clast length axes (cf. idealised rose diagram in figure 4.2B). A mean angle of 40±14 ° separates two modes of axes angles from the azimuth of slope aspect. This angle was found in intact surficial stone pavements as well as in those which were buried by several decimetres of aeolian material. Furthermore, artificially cleared and currently recovering plots show the very same orientation pattern of the newly introduced rock fragments. The pattern was observed in more than 50 % of all investigated plots, regardless of study area and relief position. Another 25 % exhibited a similar bimodal pattern but not symmetrical to slope aspect. Therefore, preferred clast orientation is assumed to be a very common characteristic of stone pavements, at least in the areas under study. Dietze & Kleber (2012) concluded that unidirectional lateral processes contribute significantly to the recovery and maintenance of those stone pavements.

None of the aforementioned lateral processes is suitable to explain bimodal, slope aspect-symmetrical orientation angles. The dominant role of slope aspect points at unidirectional gravity-related lateral processes in general. In particular, creep has been mentioned by McFadden et al. (1998) to result in tilted clasts. De Ploey and Moeyersons (1975) introduce a process termed runoff creep which describes small-scale lateral dislocation of coarse particles by scouring of fine material due to surface runoff. However, Dietze and Kleber (2012) documented rock fragments dislocated over several decimetres upon a cleared plot within a few months. One may doubt, whether creep processes are sufficient for such transport (cf. movement rates in Bateman et al., 2012). Wainwright et al. (1999) were able to restore an in-situ disturbed stone pavement by surface runoff in field experiments. In their experiments fine material was removed to leave behind a clast lag. Whether the resulting lag deposit featured any clast orientation patterns was not measured. Unconcentrated overland flow on not yet completely closed stone pavement surfaces may also contribute to clast movement and rotation upon collision. However, when running over such a rough surface water flow velocity should be reduced fundamentally along with water drag force upon such a rough surface (cf. log relationship in equation 1). If clasts are already partly embedded in the vesicular horizon, their mobilisation may be further limited.

On initially bare or almost clast-free surfaces, unconcentrated overland flow may be a hitherto poorly discussed mechanism of surficial clast transport and stone pavement formation. It is a pro-

cess which is very effective in transporting clasts (e.g. Ballance, 1984; North and Davidson, 2012). In some cases, missing clast cover behind large objects provides insight into the effects of water flowing on stone pavement surfaces (figure 4.1C), may it be due to missing deposition or scouring of clasts. Flow events are highly episodic; recurrence intervals of sediment-delivering flows in catchments up to 1 km² are at the order of 3 to 7 years, e.g. in the Mojave Desert (Griffiths et al., 2006). Process parameters such as flow depth and mean flow velocity may be measured on site with appropriate equipment (e.g. Smith et al., 2011). For "monitoring" non-linear, event-based stone pavement modification this is not adequate. However, a combination of numerical modelling and physical experiments may offer an appropriate approach to elucidate the efficiency of unconcentrated overland flow to create a stone pavement cover with slope aspect-symmetrical clast orientations.

This paper presents an approach to explain the frequent bimodal slope aspect-symmetrical orientation patterns in stone pavements by unconcentrated overland flow. The approach can explain two important phenomena observed in stone pavements, i) how clasts are transported laterally, which is necessary at least where an older generation of stone pavement is buried below aeolian deposits and covered by a modern generation of clasts and where a stone pavement has recovered despite of insufficient in-situ clast abundance, and ii) how the orientation pattern is generated. Therefore, a conceptual model is presented which elucidates boundary conditions and the surficial processes that act on an initially clast-free surface and result in a closed stone pavement. This conceptual model is then transferred into a numerical one whose relevant parameters result from field or laboratory measurements. Physical experiments are conducted to independently test the validity of this model.

Figure 4.1. Stone pavement surfaces on a basalt flow in Cima volcanic field, USA. A: disturbed stone pavement in its recovering stage, i.e. 1 by 1 meter plot cleared from all clasts, photographed after 16 months (cf. Dietze and Kleber, 2012). B: mature, closely packed and well-varnished stone pavement. C: gap in clast cover downslope of a boulder.

4.2 Materials and methods

4.2.1 Conceptual model

The following assumptions about boundary conditions were derived from the stone pavements studied by Dietze & Kleber (2012) and form the basis of an idealised conceptual model of unidirectional lateral clast transport that leads to preferred clast alignment patterns on initially virtually clast-free surfaces. The resulting stone pavement consists of a mono layer of clasts with coarse particles resting upon the fine-grained, smooth but yet very firm vesicular horizon. Some clasts may be partly embedded in this horizon (McFadden et al., 1998). These stone pavements are found on landforms with evidence of episodic unconcentrated overland flow (Dietze and Kleber, 2012). The formation of a new generation of stone pavement would rely on two preconditions: i) the availability of clasts mainly from upslope, for instance from bedrock or clast outcrops, and ii) the existence of fixed obstacles on the initially clast-free surface (e.g. dispersed boulders, deeply embedded rock fragments, plants and plant remnants).

Torrential rainfall events may generate intense runoff which results in unconcentrated overland flow, capable of dragging rock fragments. According to e.g. Allen (1982), deposition of an anisotropic object would result in length-axis orientation perpendicular to water flow direction (figure 4.2A). This is a yet unobserved pattern in stone pavements (Adelsberger and Smith, 2009; Dietze and Kleber, 2012). However, as depicted in figure 4.2B, collision with another object results in a surface-normal turning moment. This leads to alignment of the transported object at an angle off the slope-aspect normal (Allen, 1982). This alignment angle depends on several primary factors: i) point of collision (maximum rotation upon collision at the corners versus no rotation upon collision at the projection point of the objects mass centre); ii) ratio of a and b axis (the larger the ratio, the larger the angle); iii) strength of the activating force (i.e. water drag force) and iv) strength of the retarding force (i.e. friction force).

During the initial stages of stone pavement recovery stones of arbitrary size (within realistic limits) may be transported by unconcentrated overland flow and be deposited without collision due to decreasing flow velocity. However, they may be remobilised during the next heavy runoff event until collision eventually fixes them. Once an object has collided with one or more other objects, potential for further mobilisation is reduced significantly because the ratio of water drag force to friction force declines due to overlapping of clast length axes and respective reduction of the total area susceptible to water drag.

Collision, however, requires the presence of obstacles. In the case of recovery of small patches (e.g. plant scars) the intact stone pavement downslope of the disturbed site represents these obstacles. In the case of recovery of large areas (i.e. the case of buried stone pavements) obstacles must be delivered first. Vegetation or rock fragments larger than average are plausible obstacles to clasts in transport (cf. figure 4.1 and 4.6B for examples and the large standard deviations of clast dimensions in table 4.1). For the latter obstacle type, the following hypothesis may provide a plausible solution. Episodic overland flow events may transport clasts of different sizes over the

initially bare surface to the next drainage channel. Larger clasts are more likely to become deposited compared to smaller ones at that time. They may either be re-mobilised during this or a subsequent runoff event or become an obstacle for succeeding objects, further reducing the potential of re-mobilisation (again, due to clast length axes overlapping and respective relative reduction of water drag force). Thus, formation of a closed surface cover would commence at dispersed collision spots to migrate upslope from there while broadening.

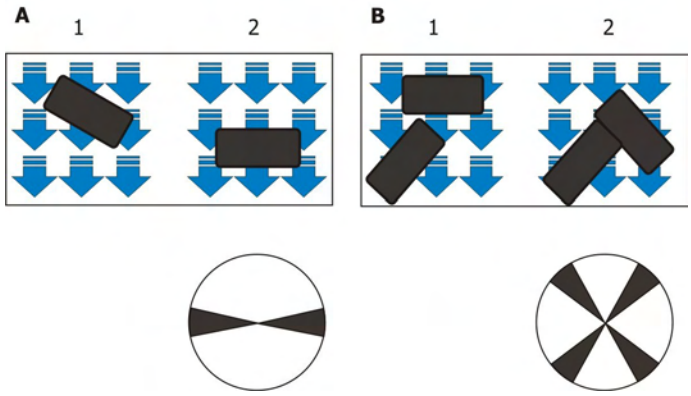

Figure 4.2. Conceptual model of preferred clast-axes orientation by unconcentrated overland flow. A: free lateral clast transport, i.e. during transport a clast is rotated until its a axis is oriented normal to flow direction (e.g. Allen, 1982). B: lateral transport with object collision, i.e. a flow-transported object with its a axis normal to flow direction is subject to a different alignment angle because of collision with another, fixed object. Simplified bidirectional rose diagrams illustrate the idealised statistical distribution of a-axes orientation angles according to this concept if many such depositions are considered. Blue arrows indicate water flow direction, i.e. slope aspect. Numbers 1 and 2 indicate successive stages of transport and orientation.

4.2.2 Numerical model

This conceptual model may be translated into a set of physical equations. Figure 4.3A illustrates important variables and parameters of the modelling approach. The transported object is characterised by its *a*, *b* and *c axes* and a mean specific density ρ_o. Dislocation may take place by unconcentrated overland flow of a fluid with the specific density ρ_f. According to the commonly applied logarithmic relationship (Carstensen, 2008), mean flow velocity can be calculated for arbitrary depth integrals z after equation 1:

$$v(z) = (g\ d\ \gamma)^{0.5} / \kappa log\ [(7.5\ z) / D_{50}]. \qquad (1)$$

There, g is the gravitational acceleration, d the flow depth, γ the slope inclination, κ the Kármán constant (after Schlichting and Gersten, 2006) and D_{50} the mean grain diameter of the surface material. Integration over and division by the c axis or, if $d < c$, the flow depth yields v, the mean flow velocity affecting the object. The model assumes an angle-dependent equilibrium of an activating force (F_A) and a retarding force (F_R). Movement is realised as dragging over a smooth, fine-grained surface formed by the vesicular horizon, which results in a friction force. The activat-

ing force is described by the drag equation (e.g. Allen, 1982):

$$F_A = 1 / 2\, \rho_f\, v^2\, c_d\, A_o. \quad (2)$$

There, c_d is the drag coefficient and A_o the object area perpendicular to the flow direction. The angle-dependent drag coefficient was approximated after Hölzer (2007). Sensitivity tests revealed that the complete range of possible c_d values resulted in minor orientation angle differences of 3.2 °. Therefore the mean drag coefficient of 1.27 was used as constant. Hence, F_A is only angle-dependent via the area of the object perpendicular to flow direction A_o, which is calculated after equation 3 and illustrated in figure 4.3B.

$$A_o = k\, c\, (a^2 + b^2)^{0.5}\, cos\, [\phi' + arctan\, (b / a)]. \quad (3)$$

There k is a geometry correction factor which accounts for deviations of the object from the ideal cuboid shape. Further, ϕ' is the rotation angle. It is defined as the angle between a axis and slope aspect-normal (figure 4.3B), whereas the orientation angle ϕ is the angle between a axis and slope aspect, i.e. $\phi = 90\ ° - \phi'$.

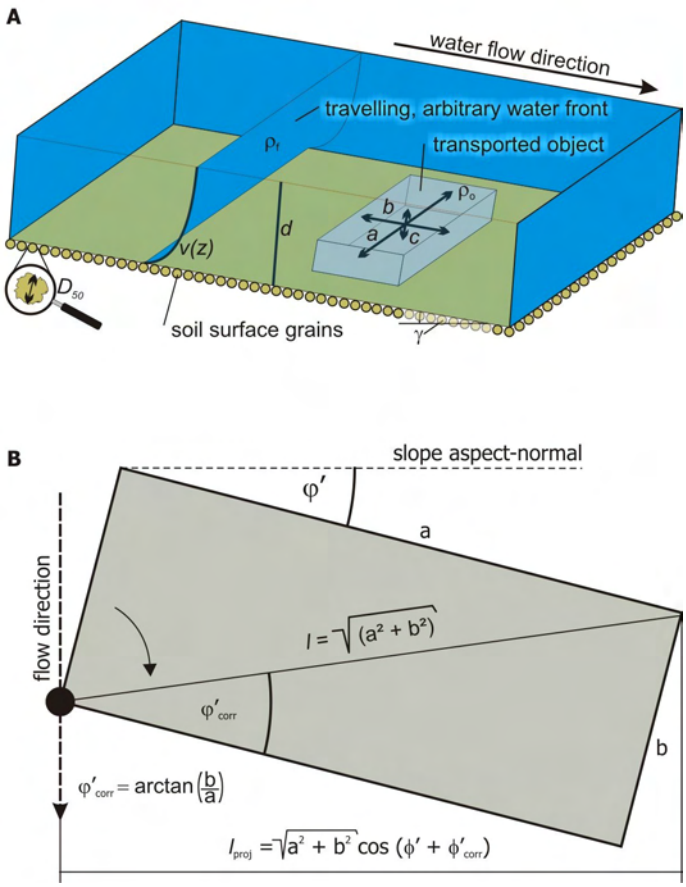

Figure 4.3. Illustration of important model parameters. A: sketch in perspective view to illustrate definitions of object and fluid properties. B: sketch in plan view of a geometric object to illustrate definition and calculation of the object area perpendicular to flow direction. The c axis is not shown but used for multiplication with object length perpendicular to flow direction l_{proj}. The latter results from the longest possible length l multiplied by the cosine of the rotation angle ϕ' and the correction angle ϕ'_{corr} due to object geometry.

The retarding force on the other side results from the product of buoyancy-corrected gravitational force and slope angle-related kinetic friction. It is described by equation 4:

$$F_R = V_o\, g\, (\rho_o - \rho_f)\, cos\, (\gamma)\, \mu. \qquad (4)$$

There, V_o is the object volume, $\rho_o - \rho_f$ is the difference between the specific densities of object and fluid and μ is the coefficient of kinetic friction. A step closer to reality allows collision not only at the corners of the dragged object but at an arbitrary location (P) along its a axis. This is considered by calculating the collision correction factor f_c after equation 5:

$$f_c = \left| (a / 2 - P) / (a / 2) \right|. \qquad (5)$$

Introducing f_c into equation 2, inserting equations 1 and 3 in 2, identifying equations 2 and 4 and solving for ϕ allows calculating orientation angles of colliding objects. Equation 6 provides a shortened version of these steps. Table 4.1 gives a summary of the necessary parameter values for the angle calculation.

$$\phi = 90 - \arccos [2 F_R / (f_c\, k\, \rho_f\, v^2\, c_d\, c\, (a^2 + b^2)^{0.5})] - arctan\, [b / a] \qquad (6)$$

The input model parameters (table 1) are based on field data. These were derived from one of the areas studied by Dietze and Kleber (2012): Cima volcanic field, eastern Mojave Desert, USA. This area was chosen for its well-developed stone pavements and vesicular horizons as well as for clear indications of unconcentrated overland flow events. Furthermore, this area has a long history of stone pavement-related research (e.g. Wells et al., 1985; Anderson et al., 2002; Wood et al., 2005), making it a key site for comparing the results of our study with established concepts. The climate of the area is semi-arid with occasional torrential summer precipitation events (cf. McFadden et al., 1986). On a 560±80 ka old basaltic lava flow stone pavements are underlain by several decimetres of aeolian dust (McFadden et al., 1986). The lava flow is geomorphologically decoupled from the surrounding alluvial landscape and is dissected by small drainage lines that eventually coalesce to channels and valleys. Mean slope inclination at the investigated plots is 4±1 °, specific catchments are 1440±210 m² based on DEM analysis (1 arc second NED, courtesy of the U.S. Geological Survey). A detailed description of site and stone pavement properties (e.g. stone axes lengths and surface grain diameter) is presented by Dietze et al. (2011) and Dietze and Kleber (2012). Object densities were determined by weight and volume measurements. The coefficient of kinetic friction on the wetted surface results from field measurements with a force level.

A test of the model was performed by comparing model results (random collision points) with 100 measured orientation angles from a surficial stone pavement plot (plot CVF-15 in Dietze and Kleber, 2012). Comparison is based on correlation analysis (r and R^2 after Pearson) of the relative angle contributions to the bins (18 equally wide classes from zero to 180 °) of the two respective rose diagrams. To estimate the contribution of each parameter as well as the entire parameter ensemble to the resulting angle uncertainty and scatter, Monte Carlo runs were performed, based on

the data in table 4.1. Random samples of each model parameter, according to their distribution functions, were used and the orientation angle was calculated 10^4 times for each target value. Gaussian uncertainty propagation was calculated as a further statistical estimator of scatter.

Table 4.1. Parameters for angle calculations of stone pavement clasts. Measured values are given as mean ± one standard deviation. $\Delta\,\phi$ indicates the sensitivity of a parameter according to Monte Carlo runs.

Symbol	***Definition***	***Value***	***Δ ϕ [°]***
g	gravitational acceleration	9.81 m s^{-2}	n.d.
κ	Kármán constant	0.41	n.d.
a	a axis of the object	68±19 mm	11.2
b	b axis of the object	39±13 mm	7.1
c	c axis of the object	18±7 mm	2.8
k	object geometry correction factor	0.6±0.1	2.1
ρ_o	specific density of the object	2.53±0.16 g cm^{-3}	1.3
ρ_ϕ	specific density of the fluid	1.0 g cm^{-3}	1.4
d	overland flow depth	17 mm	n.d.
D_{50}	mean surface grain radius	105±17 µm	0.7
γ	slope inclination	4±1 °	4.3
μ	coefficient of kinetic friction	1.14±0.16	1.8
c_d	drag coefficient	1.27	n.d.

4.2.3 Flume experiments

To perform independent tests of the numerical model, a flume was used to study the impact of unconcentrated overland flows on different objects and object ensembles. It may be emphasised that the flume experiments did not intend to simulate natural conditions as closely as possible. Rather, they were conducted to investigate the principal robustness of the assumptions and to infer the influence of basic model parameters. Rigorous testing of all parameters would in principle have required preparing a fine-grained sediment bed, probably with vesicular structure, and using a much more powerful pump.Rainfall simulation and runoff generation experiments in the field would have been suitable as well.

The device (width 27 cm, length 130 cm) was tilted by 2 °. This value is lower than the slope gradient at the study site at Cima volcanic field but is within the range of other stone pavement-covered sites (e.g. Dietze and Kleber, 2012). The flume was operated with a constant runoff of 0.72±0.04 l/s. In a first experiment five sample cuboids of different geometry were used (figure 4.5A). The cuboids were made of gypsum. This material was chosen for its low specific density, which made it possible to perform tests with different sample cuboid shapes under the precondition of $F_A \geq F_R$. The material was poured into casting moulds of respective geometry and painted with a waterproof varnish after hardening. The cuboids were equipped with a small wire loop at one edge (1.6 mm in diameter, formed by bending a piece of metal wire around a small rod and at-

tached to the object with cyanoacrylate adhesive). This allowed us to fix them in the flume without preventing lateral rotation (figure 4.5A). The specific density and coefficient of kinetic friction (wet flume surface) were measured for each cuboid separately (mean ρ_o = 1.14±0.02 g cm^{-3} and mean μ = 0.62±0.13). All cuboids were mounted in succession, rotated by hand to their largest possible area perpendicular to flow direction and then released to allow free rotation around the small pin until F_A was overwhelmed by F_R. Orientation angles of ten to fifteen measurements were noted. The aim of this experiment was to test the validity of the numeric model to predict orientation angles for single objects.

In a second experiment 30 fabricated gypsum cuboids (30 mm by 10 mm by 10 mm) as well as 18 natural clasts were used to form an artificial stone pavement. For this, seven artificial obstacles (cf. figure 4.5C) were fixed in the lower section of the flume. Subsequently the sample objects were released in succession at random starting points at the upper end of the flume. Images were taken of the resulting patterns. From the images orientation angles were calculated according to Dietze and Kleber (2012). The main aim of this latter experiment was to check whether bimodal, slope aspect-symmetrical clast orientation patterns do evolve.

A third experiment was conducted to simply test whether individual object deposition without collision is a temporary phenomenon or not. Therefore, single objects of different shape (cf. figure 4.5B) were set into motion by runoff (0.72±0.04 l/s). Then runoff was reduced until – depending on the shape of the respective sample cuboid – the object was deposited on the flume floor without any collision. Subsequently, runoff was increased again to the initial value to observe whether the cuboids were re-mobilised. Another simple test was made to infer the reaction of a freely resting object (30 mm by 10 mm by 10 mm) to collision with another, dragged object of the same shape. Therefore, runoff was set to a value sufficiently low to prevent object mobilisation but sufficiently high to allow continuous drag of objects already in motion (i.e. $F_{kinetic\ friction} < F_{drag} < F_{static\ friction}$). An object was set in motion by hand in the middle part of the flume to allow collision with another object, resting in the lower part of the flume. In these two tests runoff adjustments were made by hand to fit the mentioned criteria. Flow depth however was not measured because the main goal of these two tests was to check object reactions in a descriptive way.

4.3 Results

The numerical model reproduces the angle of 40±14 °, commonly found in natural environments (Dietze and Kleber, 2012), with the mean parameters depicted in table 4.1. Model input consists of measured site and clast parameters. Collision at the object corner was assumed. Figure 4.4A shows the influence of flow depth on orientation angle. According to the modelled force equilibrium, for the common orientation angle of 40 °, a flow depth of 17 mm is necessary. Below a flow depth of 5 mm, stones may be transported but do not experience any alignment after collision with

another clast. Hence, for the mean environmental parameters in table 4.1, this flow depth represents the critical value where $F_A = F_R$. On the other end, stones cannot reach an orientation angle smaller than 32 ° regardless of flow depth.

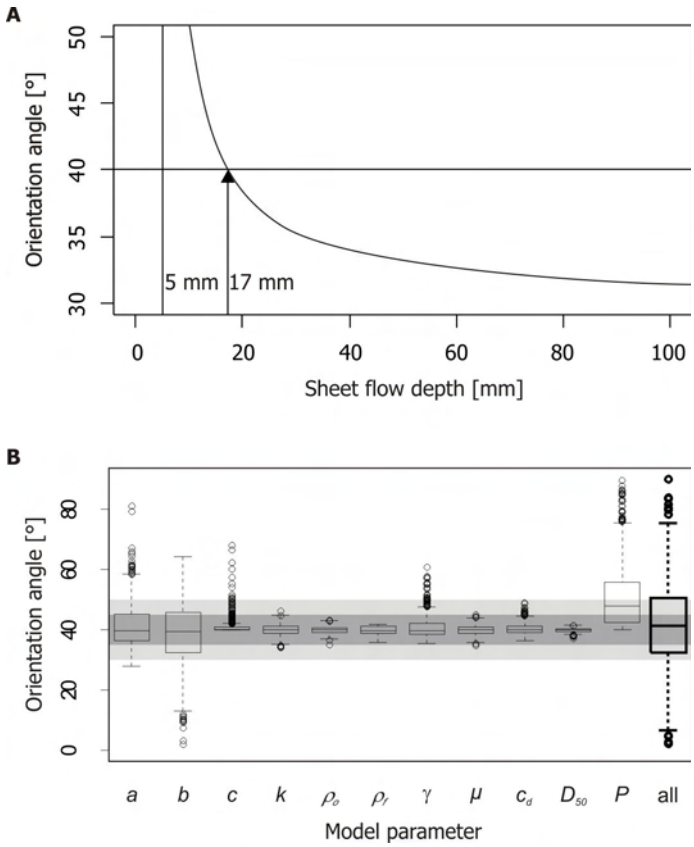

Figure 4.4. Results of the modelling approach. A: relationship between flow depth and orientation angle for the mean parameters from table 4.1. An angle of 40 ° is reached at a flow depth of 17 mm. The stone is not subject to alignment after collision for flow depths below 5 mm whereas the alignment angle cannot reach values below 32 °, no matter how deep the flow gets. B: contribution of individual and amalgamated model parameter uncertainty to the scatter of orientation angles. For the full parameter test a flow depth of 37 mm was used. Light grey polygon delimits 10 ° scatter, dark grey polygon highlights 5 ° scatter.

Results of the sensitivity tests based on the values in table 4.1 are shown in column four of this table as well as in figure 4.4B. Differences in a and b axes have the greatest individual impact on orientation angles: 7 and 11 ° within the 1σ range. However, note the non-normal distribution of values as illustrated by the two box plots. All other parameters account for not more than 4.3 ° of angle variation. The highly skewed data distribution for the c axis length test is caused by lengths that are larger than the flow depth. Such objects do not contribute to the F_A term but only to the F_R term. The influence of collision points (P) not only at the object corners but everywhere along the a axis is also depicted in figure 4.4B. Monte Carlo runs with modifications of all parameters and a flow depth of 37 mm returned an orientation angle of 40±13 °. Calculation of Gaussian uncertainty propagation yielded 40±26 °. Correlation of modelled with measured natural orientation angles

shows that the presented model is able to explain almost 70 % of the total variance in the real pattern (i.e. $R^2 = 0.69$).

Flume experiments (figure 4.5B) with single rotatable gypsum cuboids yielded a mean angle scatter of 3 ° around the average orientation angles. Although the experiments confirm the numerical modelling result in general, comparison of experimental with modelled angles shows some unsystematic deviations (root mean square error = 6.4 °). These may be attributed to the fact that the metal loops on the cuboids were not perfectly round. This resulted in some irregular movement of the cuboids. Figure 4.5C and D show the resulting alignment patterns for the multi object experiments. In both cases a bimodal axes orientation pattern, symmetrical to slope aspect, has evolved in a closed layer of laterally transported objects. If an object was deposited along its way due to decreased runoff, it was remobilised by re-increased water flux or by the pulse which was introduced by another transported and colliding object. Final fixation did not occur before an object collided with an assemblage of other objects.

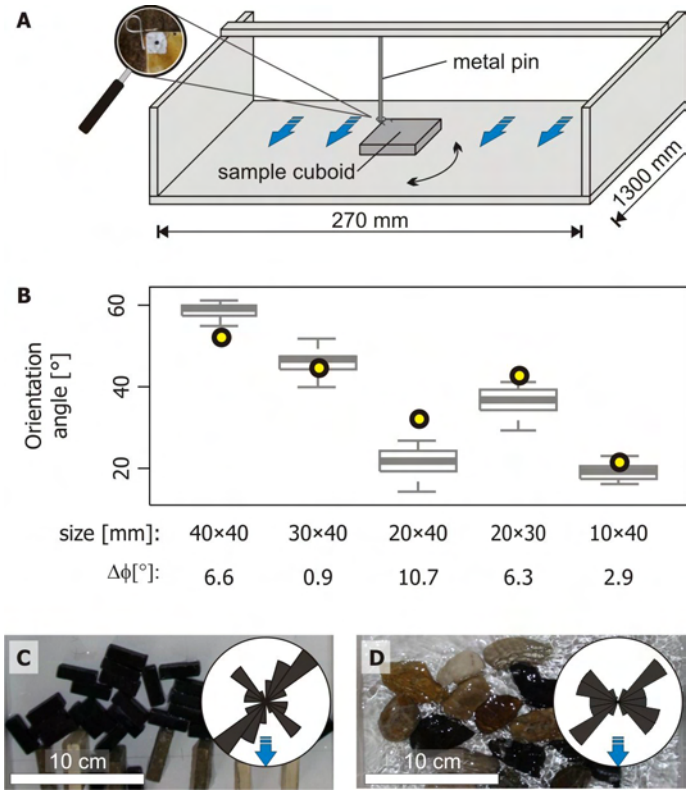

Figure 4.5. Setup and results of the flume experiments. A: sketch of the flume with single sample mounting device. B: box plots show measured orientation angles of single objects (sizes in mm, height 10 mm) versus modelled angles (yellow circles). $\Delta\phi$ quantifies deviation of the model from measurements. C and D: artificial mosaic of 30 gypsum cuboids (30 mm by 10 mm by 10 mm) and 18 clasts, deposited in front of obstacles, along with rose diagrams of a-axis orientation angles. Blue arrows indicate water flow direction.

4.4 Discussion

Field data revealed persistent clast orientation patterns for different stone pavement-covered landforms in different environmental settings (Dietze and Kleber, 2012). These patterns occur in accretionary stone pavements as well as in stone pavements with only a few centimetres thick vesicular horizon derived from aeolian deposition. They appear to be a common feature in warm and cold desert environments, under hyper-arid to semi-arid climatic conditions. Hence, stone pavements from a variety of different landscapes are similar in two aspects: the presence of a vesicular horizon and a bimodal, slope aspect-symmetrical clast orientation pattern.

4.4.1 Model and experiments

The remarkably systematic axes orientation patterns may be described by an angle-dependent force equilibrium. Most model parameters are natural constants or directly measured values. The only factor applied for correction (k) accounts just for minor changes of the orientation angle (less than 2.1 °). This indicates robustness and causal plausibility of the presented model. Further support comes from the well-predicted orientation angles of a real stone pavement plot even though only random collision points were used. It may be emphasised that 17 mm flow depth are sufficient to reproduce an orientation angle of 40 ° for clasts with the mean properties from table 4.1 at the corners only. For random collision locations deeper flows (approximately 37 mm) and, accordingly, higher flow velocities that act on the clast area perpendicular to flow direction are needed. Although neither measured nor modelled it may be argued that unconcentrated overland flows also transport suspension load, e.g. mobilised from the loose, fine-grained material on top of many vesicular horizons (McFadden et al., 1998). This increases specific density of the flow and in turn reduces the depth, necessary to create the orientation angle of 40 °. Applying the model to stone pavement properties other than described in table 4.1 requires respective parameter adjustments.

Independent confirmation of the numerical modelling results comes from flume experiments. Although parameters such as object density, coefficient of kinetic friction and flow depth differ from natural conditions, model results for single objects are in good agreement with empirical data. The flume experiments with multiple objects show that it is indeed possible to create bimodal orientation patterns within a closely packed, clast-covered surface. Flow-transported sample cuboids as well as natural objects show such a bimodal alignment.

4.4.2 Natural boundary conditions

There are three basic issues that may challenge the application of the proposed model to the natural system of stone pavements: i) Can formation of a vesicular horizon predate formation of a clast cover? ii) Is the vesicular horizon resistive enough to prevent erosion? iii) Are unconcentrated overland flow depths of 17 mm and beyond possible or even frequent?

Formation of a vesicular horizon is usually described in relation with a covering stone pavement. Indeed, the clast cover can be responsible for trapping aeolian dust, the material the vesicular horizon consists of (McFadden et al., 1986; Anderson et al., 2002). Furthermore, formation of vesicular voids in fine-grained material is usually explained by elevation of air pressure within the soil matrix due to infiltrating water and air retention within the matrix (e.g. Springer, 1958; Evenari et al., 1974). However, vesicles and vesicular horizons are not necessarily bound to stone pavements. They are also reported from bare surfaces in laboratory experiments as well as from disturbed and intact, clast-free or clast-poor natural environments (e.g. Volk and Geyger, 1970; Evenari et al., 1974; Prose & Wilshire, 2000; Ries and Hirt, 2008). Actually, many experiment-based results show that vesicles are typically better developed where no clast cover is present (e.g. Springer, 1958; Figueira and Stoops, 1983; Sullivan and Koppi, 1991). These experiments also show that artificially created vesicular horizons reach properties similar to natural vesicular horizons after not more than 20 to 30 cycles of wetting and drying (Figueira & Stoops, 1983). Therefore, vesicular structure may reform within some months or a few years and is not bound to the pre-existence of a stone pavement. Accordingly, formation of a vesicular horizon may predate formation of a stone pavement.

Grabowski et al. (2011) highlight several parameters that decrease the erodibility of cohesive sediment, such as clay content, dissolved ions, bioturbation and crusts. Vesicular horizons are in accordance with these parameters: they show the highest clay content throughout the entire Holocene sediment column, are depleted in soluble ions but enriched in calcium carbonate, and bioturbation is negligible (McFadden et al., 1998; McAuliffe and McDonald, 2006). Accordingly, although the vesicular horizon is composed of aeolian dust, it often develops remarkable firmness (Anderson et al., 2002). Excavated aggregates which had been left abandoned at the surface for more than two years, were not yet disintegrated (figure 4.6). Similarly, plots which were cleared from their covering stone pavement show no traces of erosion except for a few, very shallow drainage lines (Dietze and Kleber, 2012). Therefore, a well-developed vesicular horizon (figure 4.6A) appears to be resistant enough to withstand marked erosion by unconcentrated overland flow.

Unconcentrated overland flow depths of a few centimetres are described in field experiments (Sidorchuk et al., 2008; Smith et al., 2011) and in rainfall calculations at clast-covered areas (Williams and Zimbelman, 1994). The vesicular horizon supports runoff because of low infiltration capacity due to its isolated pore system and high clay content (e.g. Young et al., 2004). Given the upslope contribution areas of the plots at Cima volcanic field and the generally low hydraulic conductivities of mature vesicular horizons (less than $1.5 \cdot 10^{-6}$ m/s, Young et al., 2004), site conditions are assumed to provide sufficient surface runoff, following the estimations of Williams and Zimbelman (1994). Griffiths et al. (2006) present mean recurrence intervals for sediment-delivering runoff events of 4.1±1.1 years for small catchments (i.e. less than 14 ha) throughout the Mojave

Desert. However, recurrence intervals of surface runoff may be remarkably shorter: the catchments described in Griffiths et al. (2006) were several hectares in size and therefore suffer from recording only larger events due to catchment-internal sediment storage.

Figure 4.6. Aggregates of a vesicular horizon at Cima volcanic field, USA.: A: adhering aggregates with vesicular structure form a smooth but consolidated surface; B: isolated aggregates left abandoned in 2007; C: two of the isolated aggregates in 2009.

4.4.3 Further implications

It is likely that there are stone pavements which are not predominantly related to unconcentrated overland flow processes. This is especially relevant for hyper-arid regions such as the high Atacama desert, Chile, where stone pavements frequently cover steep slopes (Dietze and Kleber, 2012), or if the specific catchment of a site is too small to support sufficiently deep flows. The study of such sites will presumably provide another possibility to test and possibly improve the proposed model. Creeping processes (de Ploey and Moeyersons, 1975; McFadden et al., 1998) may be a further option to create the commonly observed clast orientation pattern due to lateral clast transport.

If the occurrence of plant scars (McAuliffe and McDonald, 2006) is a systematic feature on stone pavement surfaces at large time scales, then recovery of such patches by overland flow-transported clasts may provide an explanation for frequent bimodal clast orientation patterns also at sites not comprising a buried generation of stone pavements. However, investigation of this idea would at least require axes orientation measurements at such scar features.

It may be emphasised that the described model is not primarily designed to account for initial stone pavement formation on bare bedrock. Deposition of aeolian dust is an obvious feature in all studied areas. It underlines the important role of accretionary processes to form the system of vesicular horizon and stone pavement (Mabutt, 1977, McFadden et al., 1986). However, in the case of buried stone pavements below modern, intact ones (Wells et al., 1985; Dietze et al., 2011), the process of lateral clast transport and alignment must have affected considerable areas, not only small patches. Accordingly, in such cases the term re-formation may be more appropriate than recovery.

Alteration of existing clast orientation patterns by creep or unconcentrated overland flow might be expected once a stone pavement has developed. However, collision of clasts with one or more clasts downslope and subsequent collision contacts with clasts from upslope will eventually build a resistive fabric. It appears unlikely that such a structure is modified by running water, especially when considering the high hydraulic roughness of a clast-covered surface which results in remarkable decrease of mean runoff velocity (cf. log function in equation 1). The stable location of clasts in intact stone pavements is independently highlighted by findings of ubiquitous, sun path-controlled crack orientation patterns in clasts (McFadden et al., 2005; Eppes et al., 2010). Such systematic patterns would not be possible, if an established stone pavement is continuously affected by clast re-orientation.

Although very common, bimodal patterns are not present in all instances of stone pavements (Adelsberger and Smith, 2009). If stone pavements lack bimodal clast orientation, they may have formed by other than slope-related processes, have been reworked, or may have remained essentially in situ during their accretionary rise above the self-trapped aeolian mantle. However, bimodal clast orientation patterns are a powerful proxy to deduce evolution processes of stone pavements. This is especially relevant for landforms which exhibited different orientation patterns due to their primary formation (e.g. alluvial fans with slope-normal clast orientations; Bridge and Demicco, 2008) and whose surfaces are now prone to being modified by other geomorphological processes. Furthermore, buried oriented stone pavements may serve as environmental proxies in sediment archives since they integrate information about past runoff characteristics.

4.5 Conclusions

The phenomena of burial and lateral recovery or re-formation of stone pavements, which may affect sites due to severe environmental change, raise doubt on whether stone pavements form continuously over time by vertical processes only and hence indicate surface stability. Rather, stone pavements do not necessarily represent the age of landform formation or decoupling from the processes that created them, but the time since the last recovery from perturbation of the system. Buried stone pavement strata in several profiles of the Cima volcanic field (Dietze et al., 2011), one of them in the Holocene section (McFadden et al., 1986), suggest that such perturbation actually took place.

In such settings, in addition to vertical ones, unidirectional lateral processes should be taken into account, especially on sites affected by unconcentrated overland flow. The mechanism described in this article is able to re-form disturbed stone pavement covers that in turn control ecological and hydrological site characteristics.

The common notion on the relationship between stone pavement and vesicular horizon is that the stone pavement allows formation of the vesicular horizon by trapping dust, whereas the vesi-

cular horizon allows maintenance of the stone pavement by swell-shrink cycles. The presented results imply that there is a further genetic connection: formation of a vesicular horizon may allow reformation of a stone pavement by lateral processes such as unconcentrated overland flow. Although the formation of vesicular horizons is not necessarily based on a pre-existing stone pavement (e.g. Ries and Hirt, 2008), there appears to be a tight co-evolution of a stone pavement and its underlying vesicular horizon. This results in a unique earth surface system.

Acknowledgements

We kindly thank Dirk Carstensen, Elisabeth Dietze as well as Susi & Lance Solly for frequent contributions to the different stages of the manuscript. We also warmly thank the anonymous reviewers and the editor for constructive comments and raised ideas.

References

Adelsberger, KA, Smith, JR. 2009. Desert pavement development and landscape stability on the Eastern Libyan Plateau, Egypt. Geomorphology **107**: 178-194. DOI: 10.1016/j.geomorph.2008.12.005

Al-Farraj, A, Harvey, AM. 2000. Desert pavement characteristics on Wadi terrace and alluvial fan surfaces: Wadi Al-Bih, U.A.E. and Oman. Geomorphology **35**: 279-297. DOI: 10.1016/S0169-555X(00)00049-0

Allen, JRL. 1982. Sedimentary structures. Their character and physical basis: Developments in Sedimentology 30A. Elsevier: Amsterdam.

Amit, R, Gerson, R. 1986. The evolution of holocene reg (gravelly) soils in deserts: An example from the dead sea region. Catena **13**: 59-79. DOI: 10.1016/S0341-8162(86)80005-4

Anderson, KC, Wells, SG, Graham, RC. 2002. Pedogenesis of vesicular horizons, Cima volcanic field, Mojave Desert, California. Soil Science Society of America Journal **66**: 878-887. DOI: 10.2136/sssaj2002.8780

Ballance, PF. 1984. Sheet-flow-dominated gravel fans of the non-marine middle Cenozoic Simmler Formation, central California. Sedimentary Geology **38**: 337-359. DOI: 10.1016/0037-0738(84)90085-X

Bateman, MD, Bryant, RG, Foster, IDL, Livingstone, I, Parsons, AJ. 2012. On the formation of sand ramps: A case study from the Mojave Desert. Geomorphology **161-162**: 93-109. DOI: 10.1016/j.geomorph.2012.04.004

Blake, WP. 1858. Report of a Geological Reconnaissance in California. New York.

Bridge, JS, Demicco, RV. 2008. Earth surface processes, landforms and sediment deposits. Cambridge University Press: Cambridge.

Carstensen, D. 2008. Schubspannungen. In Martin, H, Pohl, R (eds). Technische Hydromechanik 4 – Hydraulische und numerische Modelle. Verlag für Bauwesen: Berlin, München.

Cooke, RU. 1970. Stone pavements in deserts. Annals of the Association of American Geographers **60**: 560-577.

Cooke, RU, Warren, A, Goudie, AS. 1993. Desert Geomorphology. UCL Press, London.

De Ploey J, Moeyersons J. 1975. Runoff creep of coarse debris: experimental data and some field observations. Catena **2**: 275-288. DOI: 10.1016/S0341-8162(75)80017-8

Dietze, M, Kleber, A. 2012. Contribution of lateral processes to stone pavement formation in deserts inferred from clast orientation patterns. Geomorphology **139-140**: 172-187. DOI: 10.1016/j.geomorph.2011.10.015

Dietze, M, Muhs, S, Dietze, E. 2011. Ambiguities of relative age indicators on abandoned surfaces of arid environments. Zeitschrift für Geomorphologie N.F. **55** Supplementary Issue 3: 49-75. DOI: 10.1127/0372-8854/2011/0055S3-0051

Eppes, MC, McFadden, LD, Wegmann, KW, Scuderi, LA. 2010. Cracks in desert pavement rocks: further insights into mechanical weathering by directional insolation. Geomorphology **123**: 97-108. DOI: 10.1016/j.geomorph.2011.10.015

Evenari, M, Yaalon, D, Gutterman, Y. 1974. Note on soils with vesicular structure in deserts. Zeitschrift für Geomorphologie **18**: 162-172.

Figueira, H, Stoops, G. 1983. Application of micromorphometric techniques to the experimental study of vesicular layer formation. Pédologie **33**: 77-89.

Grabowski, RC, Droppo, IG, Wharton, G. 2011. Erodibility of cohesive sediment: The importance of sediment properties. Earth-Science Reviews **105**: 101-120. DOI: 10.1016/j.earscirev.2011.01.008

Griffiths, PG, Hereford, R, Webb, RH. 2006. Sediment yield and runoff frequency of small drainage basins in the Mojave Desert, U.S.A. Geomorphology **74**: 232-244. DOI: 10.1016/j.geomorph.2005.07.017

Haff, PK. 2001. Desert Pavement: An Environmental Canary? The Journal of Geology **109**: 661-668. DOI: 10.1086/321960

Haff, PK, Werner, BT. 1996. Dynamical Processes on Desert Pavements and the Healing of Surficial Disturbances. Quaternary Research **45**: 38-46. DOI: 10.1006/qres.1996.0004

Helms, JG, McGill, SF, Rockwell, TK. 2003. Calibrated, late Quaternary age indices using clast rubi-

fication and soil development on alluvial surfaces in Pilot Knob Valley, Mojave Desert, southeastern California. Quaternary Research **60**: 377-393. DOI: 10.1016/j.yqres.2003.08.002

Hölzer, A. 2007. Bestimmung des Widerstandes, Auftriebs und Drehmoments und Simulation der Bewegung nichtsphärischer Partikel in laminaren und turbulenten Strömungen mit dem Lattice-Boltzmann-Verfahren [Ph.D. Thesis]: Martin-Luther-University Halle-Wittenberg.

Lovich, JE, Bainbridge, D. 1999. Anthropogenic degradation of the southern California desert ecosystem and prospects for natural recovery and restoration. Environmental Management, v. 24, p. 309-326. DOI: 10.1007/s002679900235

Mabutt, JA. 1977. Desert Landforms. MIT Press: Cambridge.

Marchetti, DW, Cerling, TE. 2005. Cosmogenic ^{3}He exposure ages of Pleistocene debris flows and desert pavements in Capitol Reef National Park, Utah. Geomorphology **67**: 423-435. DOI: 10.1016/j.geomorph.2004.11.004

Matmon, A, Simhai, O, Amit, R, Haviv, I, Porat, N, McDonald, EV, Benedetti, L, Finkel, R. 2009. Desert pavement-coated surfaces in extreme deserts present the longest-lived landforms on Earth: Geological Society of America Bulletin **121**: 688-697. DOI: 10.1130/B26422.1

McAuliffe, JR, McDonald, EV. 2006. Holocene environmental change and vegetation contraction in the Sonoran Desert. Quaternary Research **65**: 204-215. DOI: 10.1016/j.yqres.2005.11.006

McFadden, LD, Wells, SG, Dohrenwend, JC. 1986. Influences of quaternary climatic changes on processes of soil development on desert loess deposits of the Cima volcanic field, California. Catena **13**: 361-389. DOI: 10.1016/0341-8162(86)90010-X

McFadden, LD, Ritter, JB, Wells, SG. 1989. Use of multiparameter relative-age methods for age estimation and correlation of alluvial fan surfaces on a desert piedmont Eastern Mojave Desert, California. Quaternary Research **32**: 276-290. DOI: 10.1016/0033-5894(89)90094-X

McFadden, LD, McDonald, EV, Wells, SG, Anderson, K, Quade, J, Forman, SL. 1998. The vesicular layer and carbonate collars of desert soils and pavements: formation, age and relation to climate change. Geomorphology **24**: 101-145. DOI: 10.1016/S0169-555X(97)00095-0

McFadden, LD, Eppes, MC, Gillespie, AR, Hallett, B. 2005. Physical weathering in arid landscapes due to diurnal variation in the direction of solar heating GSA Bulletin **117**: 161-173. DOI: 10.1130/B25508.1

North, CP, Davidson, SK. 2012. Unconfined alluvial flow processes: Recognition and interpretation of their deposits, and the significance for palaeogeographic reconstruction. Earth-Science Reviews **111**: 199-223. DOI: 1910.1016/j.earscirev.2011.11.0089

Pelletier, JD, Cline, M, DeLong, SB. 2007. Desert pavement dynamics: numerical modeling and field-based calibration. Earth Surface Processes and Landforms **32**: 1913-1927. DOI:

10.1002/esp.1500

Prose, DV, Wilshire, HG. 2000. The lasting effects of tank maneuvers on desert soils and intershrub flora. USGS open file report OF 00-512.

Quade J. 2001. Desert pavements and associated rock varnish in the Mojave Desert: how old can they be? Geology **29**: 855-858. DOI: 10.1130/0091-7613.

Ries, JB, Hirt, U. 2008. Permanence of soil surface crusts on abandoned farmland in the Central Ebro Basin/Spain. Catena **72**: 282-296. DOI: 10.1016/j.catena.2007.06.001

Schlichting, H, Gersten, K. 2006. Grenzschicht-Theorie. Springer: Heidelberg.

Sharon, D. 1962. On the nature of hamadas in Israel: Zeitschrift für Geomorphologie N.F. **6**: 129-147.

Sidorchuk, A, Schmidt, J, Cooper, G. 2008. Variability of shallow overland flow velocity and soil aggregate transport observed with digital videography. Hydrological processes **22**: 4035-4048. DOI: 10.1002/hyp.7006

Smith, MW, Cox, NJ, Bracken, LJ. 2011. Modeling depth distributions of overland flows. Geomorphology **125**: 402-413. DOI: 10.1016/j.geomorph.2010.10.017

Spelz, RM, Fletcher, JM, Owen, LA, Caffee, MW. 2008. Quaternary alluvial-fan development, climate and morphologic dating of fault scarps in Laguna Salada, Baja California, Mexico. Geomorphology **102**: 578-594. DOI: 10.1016/j.geomorph.2008.06.001

Springer, ME. 1958. Desert pavement and vesicular layer of some soils of the desert of the Lahontan Basin, Nevada. Soil Science Society of America Proceedings **22**: 63-66.

Sullivan, LA, Koppi, AJ. 1991. Morphology and genesis of silt and clay coatings in the vesicular layer of a desert loam soil. Australian Journal of Soil Research **29**: 579-586. DOI: 10.1071/SR9910579

Volk, OH, Geyger, E. 1970. "Schaumböden" als Ursache der Vegetationslosigkeit in ariden Gebieten. Zeitschrift für Geomorphologie N.F. **14**: 79-95.

Wainwright, J, Parsons, AJ, Abrahams, AD. 1999. Field and computer simulation experiments on the formation of desert pavement. Earth Surface Processes and Landforms **24**: 1025-1037. DOI: 10.1002/(SICI)1096-9837(199910)24:11

Wells, SG, Dohrenwend, JC, McFadden, LD, Turrin, BD, Mahrer, KD. 1985. Late Cenozoic landscape evolution on lava flow surfaces of the Cima Volcanic field, Mojave Desert, California. Geological Society of America Bulletin **96**: 1518-1529. DOI: 10.1130/0016-7606(1985)96

Williams, SH, Zimbelman, JR. 1994. Desert Pavement Evolution: An Example of the Role of Sheetflood. Journal of Geology **102**: 243-248.

Wood, YA, Graham, RC, Wells, SG. 2005. Surface control of desert pavement pedologic process

and landscape function, Cima Volcanic field, Mojave Desert, California. Catena **59**: 205-230. DOI: 10.1016/j.catena.2004.06.001

Yonovitz, M, Drohan, J. 2009. Pore morphology characteristics of vesicular horizons in undisturbed and disturbed arid soils; implications for arid land management. Soil Use and Management **25**: 293-302. DOI: 10.1111/j.1475-2743.2009.00225.x

Young, MH, McDonald, EV, Caldwell, TG, Benner, SG, Meadows, DG. 2004. Hydraulic Properties of a Desert Soil Chronosequence in the Mojave Desert, USA. Vadose Zone Journal **3**: 956-963. DOI: 10.2113/3.3.956

5 Formation mechanisms and control factors of vesicular soil structure

Chapter 5 is accepted by the peer-reviewed journal Catena (ISSN 0341-8162) as:

Formation mechanisms and control factors of vesicular soil structure

Authors: Michael Dietze[1], Sebastian Bartel[1], Martin Lindner[2], Arno Kleber[1]

[1] Institute of Geography, Technische Universität Dresden

[2] Institute of Geography, Leopold-Franzens-Universität Innsbruck

Publication history: submitted: February 2012, accepted: June 2012

Full reference: Dietze M, Bartel S, Lindner M, Kleber A. (accepted): Formation mechanisms and control factors of vesicular soil structure. Catena.

Internet link: not available

Abstract: vesicular structure is a widespread feature of soils in arid environments. Typically associated with stone pavements, it has a major control function for dust and water fluxes and, hence, for site ecology. Previous models of vesicular structure formation and stability are inconsistent and mostly focused on the investigation of isolated control parameters. To test existing models, to infer plausible mechanisms of vesicular structure formation and to unveil controlling environmental and sedimentological parameters, we present quantitative data of vesicle properties of artificial and natural vesicles.

Vesicles are not unstable but their changes in size are non-linear with time. They form due to surface sealing by puddling and by a wetting front, which advances downward, thereby elevating gas pressure within the sediment matrix. Translocation of clay or precipitation of calcium carbonate support vesicle stabilisation. Vesicular structure forms within a wide range of environmental and sedimentological settings: at least 6.3-15.7 mm of water per wetting cycle, 0-70 % sand content, 0.8-5.6 mS/cm electric conductivity and 1-28 % calcium carbonate content. High sand contents favour larger and rounder vesicles, whereas increasing calcium carbonate content has the opposite effect. The concentration of dissolved ions does not considerably influence vesicle formation. Under an artificial cover stone vesicles could not be created at all, whereas they were concentrated around stone margins. The main limiting factor for vesicle formation in natural environments is root activity. The type and density of surface cover determines fine material fluxes into the aggregates of vesicular horizons. The shape of vesicles may be related to dust influx intensity. Accordingly, horizons with spherical vesicles may indicate constant low dust influx on poorly vegetated surfaces and be, therefore, used as proxies of environmental conditions.

Keywords: Desert soils; Vesicular horizon; Experiment; Soil formation

5.1 Introduction

Soils and sediments with vesicular structure are widespread in semi-arid and arid environments. They comprise spherical to oval, isolated pores, several hundred micrometres to a few millimetres in diameter, which may be interconnected by channel pores. This structure develops in fine-grained materials and reaches a thickness between a few millimetres and some centimetres. It is referred to as vesicular horizon, abbreviated as Av (Springer, 1958). Mature vesicular horizons show a prismatic to columnar structure and a secondary platy structure. Their basal parts are typically clay-enriched, the pores become elongated and interconnected (Miller, 1971; Anderson et al., 2002). Many vesicular horizons are associated with a stone pavement, together forming genetically coupled systems (McFadden et al., 1998).

Horizons with vesicular structure have a crucial ecological control function. Due to the isolated pore system they determine infiltration rate, soil moisture, surface runoff, ecological site characteristics and especially the reaction of a surface to land use (Pierson et al., 1994; Young et al., 2004; Wood et al., 2005; Meadows et al., 2008). Lovich & Bainbridge (1999) demonstrated the degradation of desert ecosystems as the result of human activity such as off-road driving, over-grazing, urbanisation or military exercises. Prose & Wilshire (2000) drew special attention to vesicular horizons under military use. Furthermore, together with the stone pavement, the vesicular horizon influences processes such as trapping and emission of dust, surface recovery from disturbance and surface stability (McFadden et al., 1986; Yonovitz & Drohan, 2009; Sweeney et al., 2011; Dietze et al., 2011; Dietze & Kleber, 2012).

Despite of the considerable environmental significance of vesicular structure the actual formation processes of vesicles have received limited attention. There are several experiment-based models of the formation of vesicular structure. However, their conclusions are contradictory, which fact has been poorly discussed, yet. Most models assume that vesicles originate from a temporal increase of soil air pressure. However, the mechanisms invoked for this differ greatly among the models: gas production by algae photosynthesis (Bazilevich et al., 1953), CO_2 release due to hydrogen carbonate crystallisation (Paletskaya et al., 1958), matrix contraction during soil drying (Rozanov cited in Paletskaya et al., 1958), soil air displacement by an advancing wetting front (Springer, 1958) and solar heating of the soil (Evenari et al., 1974; Brown & Dunkerley, 1996). According to these models, a necessary precondition for gas pressure increase is sealing of the soil surface due to e.g. biological, mineralogical or mechanical crusts as well as puddling of the surface during rain events. The model of Hugie & Passey (1964) differs from the others by suggesting that vesicles form as gas bubbles migrate upwards through a supersaturated soil matrix and eventually get stuck as the matrix looses fluidity. Volk & Geyger (1970) explain vesicles as a combination of upward migration and thermal expansion of air bubbles. Further discrepancy arises from suggestions about stability and longevity of vesicular structure. Springer (1958) and Hugie & Passey

(1964) argue for destruction and reformation of vesicles with each rain event whereas Sullivan & Koppi (1991) attest vesicles a lifetime of many wetting-drying events, based on laminated clay and silt coatings on vesicle walls. Another discrepancy is whether a surface cover aids or prevents vesicle formation. There is one source that found vesicles formed beneath an object, which covered the surface (Evenari et al., 1974). The vast majority of other researchers (e.g. Springer, 1958; Hugie and Passey, 1964; Miller, 1971; Figueira and Stoops, 1983; Sullivan and Koppi, 1991) were able to produce vesicles without such objects and even mention the absence of vesicles beneath clasts.

Part of this uncertainty and contradiction regarding formation and longevity of vesicular structure may originate from the lack of standardised experimental methods, e.g. used materials, sample container sizes, wetting and drying techniques and objects covering the sediment. Besides differing treatment strategies, serious ambiguity results from trying to compare the quality of vesicle formation. Contributing quantitative descriptors of vesicular structure may be a step beyond just conceptual descriptions of controlling factors.

So far, no systematic investigation has been reported focussing on the environmental conditions that limit formation and maintenance of vesicular structure. However, these may be relevant to estimate the impact of future climate change on soil conditions and the role of vesicular soils for dust emission versus dust trapping (Sweeney et al., 2011). Furthermore, if controlling conditions are known, these may be transferred to the past, rendering buried vesicular horizons (e.g. McFadden et al., 1986; Dietze et al., 2011) a proxy of environmental archives.

Here, existing models of vesicular structure formation are evaluated, based on multi-parameter laboratory experiments. A holistic setup is introduced to overcome current ambiguities of inhomogeneous experiment approaches. Artificial vesicular structure is created in sediments with systematically modified material properties and environmental conditions. Parameters which modify and limit vesicle formation will be discussed based on artificial and natural vesicular structure. An approach is introduced to derive quantitative vesicle properties from both types of vesicular structure. This allows comprehensive and unbiased evaluation of formation models and modifying parameters. Based on the results, the most likely mechanisms of vesicle formation, the role of vesicular structure in modern environments and their value as proxies in palaeo-environmental archives will be discussed.

5.2 Materials and methods

5.2.1 Study areas

Natural vesicular horizons were investigated in several study areas throughout the semi-arid to arid south-western North America. Depending mainly on humidity, stone pavement coverage ranges from nearly 100 % to 20 %. Vegetation coverage shows the opposite trend (Dietze & Kleber,

2012). The ubiquitous vesicular horizon is composed of aeolian fine material and is usually overlain by a few millimetres of slightly coarser, loose matter filling the voids between pavement stones (McFadden et al., 1998; Dietze et al., 2011).

The Black Rock Desert, south-western Sevier Basin, Utah, USA, is in the focus of this study because this basin, located at elevations around 1500 m a.s.l., appears to be the modern limit of vesicle formation. The playa environment in the Basin and Range province hosts several geomorphologically isolated, stone pavement-covered landforms, i.e. Neogene to Quaternary lava flows and shore lines of Pleistocene Lake Bonneville (Oviatt, 1991). However, since the last period of enhanced dust deposition was closely linked to the lake desiccation (11.9 and 9.5 ^{14}C ka BP, cf. Oviatt, 1988; Godsey et al., 2005), the constructional ages of the landforms are irrelevant for the properties of vesicular horizons developed on them (cf. McFadden et al., 1986; Yonovitz & Drohan, 2009). The Basin is further characterised by a humidity gradient due to the rain shielding effect of the Cricket Mountains along its western margin. Vegetation grades from dense grass (e.g. *Bromus tectorum*) and the saltbush-greasewood association around playa margins in the western basin part, via Great Basin Sagebrush (*Artemisia tridentata*) in combination with various steppe grasses, towards grass-rich pinyon-juniper forests along the slopes of the Pavant Range in the east (West & Young, 2000). Mean annual precipitation (MAP) is less than 150 mm in the west and surpasses 350 mm along the foot slopes of the Pavant Range in the east (NCDC, 2012). MAP at the studied plots was interpolated as described by Dietze & Kleber (2012).

The basalt flows of Cima volcanic field in the eastern Mojave Desert, California, USA, have well-developed stone pavements above several decimetres of aeolian dust. The surfaces virtually free of vegetation exhibit strongly developed vesicular horizons and have been thoroughly investigated in earlier studies (e.g. McFadden et al., 1986; 1998; Anderson et al., 2002; Young et al., 2004; Wood et al., 2005), making this a key site for connecting and comparing data. Climate is arid to semi-arid with mean annual precipitation around 160 mm (interpolated values from NCDC, 2012; cf. Dietze & Kleber, 2012). Laguna Salada, Baja California, Mexico, is the driest study area. Mean annual precipitation is supposed to be less than 80 mm (Spelz et al., 2008). Three more sites cover the climatic gradient from the hyper-arid Laguna Salada to the semi-arid Black Rock Desert and provide supplementary information to support trends from the previous two study sites. Samples were taken from the Virgin River Canyon site, Rye Patch Dam and Stockton Bar, Utah, USA. All sites are located on geomorphologically isolated landforms, i.e. local culmination, with clear indication of aeolian deposition.

Table 5.1. General characteristics of study sites. Coordinates are given in UTM system, zone 12N. MAP: mean annual precipitation. Precipitation data source: NCDC (2012). Precipitation values of the Black Rock Desert sites were interpolated from 11 weather stations according to Dietze & Kleber (2012).

ID	*Study area*	*Location name*	*Coordinates*	*MAP [mm]*	*Landform type*	*Landform age*	*Relief properties*	*Land cover*
PM-01	Black Rock Desert	Pot Mountain	4339538/865317	229	Basalt volcano with shoreline apron (Provo phase)	14 ^{14}C ka BP , Oviatt et al. (1992)	Gently inclined ancient shore platform, margin dissected	Unused, grass with stone pavement patches
PM-02	Black Rock Desert	Pot Mountain	4339536/865314	229	Basalt volcano with shoreline apron (Provo phase)	14 ^{14}C ka BP, Oviatt et al. (1992)	Gently inclined ancient shore platform, margin dissected	Unused, grass with stone pavement patches
PB-01	Black Rock Desert	Pavant Butte	4340075/885312	276	Basalt volcano with shoreline apron (Bonneville phase)	15.5 ^{14}C ka BP, Oviatt (1991)	Gently inclined ancient shore platform, dissected by channels	Virtually unused, dispersed vegetation and large stone pavement patches
TH-01	Black Rock Desert	Tabernacle Hill	4318131/887898	329	Basalt volcano with lava field, above the ancient lake level (Provo phase)	14.3 ^{14}C ka BP, Oviatt & Nash (1989)	Flat areas between structural relief (spines, ravines, domes)	Extensive cattle grazing where vegetation present, severe stone pavement patches
NT-01	Black Rock Desert	North Twin Peak	4301857/871684	293	Rhyolite plateau, above the highest lake level (Bonneville phase)	2400 ka, Evans et al. (1980)	Virtually flat plateau with very shallow drainage system	Unused, dispersed vegetation and large stone pavement patches
LR-01	Black Rock Desert	Lava Ridge	4298982/876397	310	Basalt plateau, above the highest lake level (Bonneville phase)	2500 ka, Best et al. (1980)	Flat plateau with incision scarps towards the plateau margin	Extensive cattle grazing, stone pavement very sparsely, with grasses and bushes
LS-01	Laguna Salada	Feeder Road	3524100/673405	80	Feeder road to quarry, abandoned since road building in 1985	0.025 ka, road construction	Track 1 m above surrounding alluvial fans, cut from main road	Unused, no vegetation present, stone pavement closed and beginning to be separated by aeolian layer
LS-02	Laguna Salada	Alluvial Fan, NE	3601807/623751	80	Alluvial fan, dissected and abandoned	age unknown	Diminishing bar and swale relief, shallow drainage network	Unused, vegetation concentrated to drainage channels
CF-01	Cima Volcanic Field	560 ka basalt flow	3891967/608609	161	Basaltic lava flow above alluvial plain	560 ka, Turrin et al. (1985)	Stepped plateaus with local bedrock outcrops and smooth topography	Unused, extensive stone pavement patches, vegetation in drainage channels
CF-02	Cima Volcanic Field	560 ka basalt flow	3891964/608576	161	Basaltic lava flow above alluvial plain	560 ka, Turrin et al. (1985)	Stepped plateaus with local bedrock outcrops and smooth topography	Unused, extensive stone pavement patches, vegetation in drainage channels
RP-01	Rye Patch Dam	Rye Patch Dam	4480582/389439	200	Disscected ancient lake bottom	13.5 ^{14}C ka BP, Benson et al. (1997)	Elongated ridge, approximately 10 m wide, gently inclined	Unused, virutally free of vegetation, well covered by stones
VR-01	Virgin River Canyon	Virgin River Canyon	4113169/281065	219	Sandstone plateau	age unknown	Gently undulating, broadly dissected plateau	Extensive cattle grazing, dispersed shrubs, bare ground with dispersed stone
SB-01	Stockton Bar	Stockton Bar	4480925/385397	330	Lacustrine bar	15.3 to 14.5 ^{14}C ka BP, Burr & Currey (1988)	Gently inclined ridge of the lacustrine bar	Unused, dense grass stock, very few stones present

5.2.2 Field methods

The studied plots showed no indication of disturbance or erosion (table 1). In the Black Rock Desert, all plots were located on landforms as similar in bedrock type as possible, with slopes inclined by 0 to 5 °. In the Cima volcanic field, two plots on a 560±80 ka old, approximately 4 ° inclined lava flow (Turrin et al., 1985) were studied to focus on intra-site variability. Plots in the Laguna Salada were located on an alluvial fan section inclined by approximately 3 ° and on a level gravely quarry feeder road, which has been abandoned since the mid 1980s.

Description of site characteristics included the parameters land cover, preservation of primary relief, percentage of stone pavement and vegetation coverage, development of rock varnish and clast weathering (cf. Dietze et al., 2011). Small profiles were dug and described according to Soil Survey Division Staff (1993) and Birkeland (1999).

The thickness of loose material, which covers the vesicular horizon, was noted and a sample was taken with a spatula. Mean vesicular horizon consistence was determined from 10 aggregates. Furthermore, the horizon was described by separating individual aggregates and splitting them horizontally and vertically. Av aggregates were subdivided into two macroscopic domains (domains 3 and 4 after Anderson et al., 2002): domain 1, forming the upper part of the aggregate is dominated by well-rounded vesicles and has a similar colour as the overlying loose material. Domain 2 forms the lower part. It typically shows platy structure, fewer and smaller vesicles as well as clay-enrichment, which results in a more reddish colour. Thickness, boundary shape and boundary distinctiveness were noted prior to sampling each domain separately. Sub-samples from several aggregates were amalgamated to gain sufficient material for sedimentological analyses.

Samples for mineralogical analysis were taken from three selected Av plots (CF-01, PM-01, LR-01). Further, profile CF-01, which exhibited a buried vesicular horizon, was chosen for detailed mineralogical analysis (cf. figure 5.4). Dietze et al. (2011) described this profile in detail (CVF07-001 therein). Furthermore, a surface sample was taken from the Soda Lake playa, a probable source area of the aeolian material which constitutes the vesicular horizon in this area (Wells et al., 1985).

5.2.3 Laboratory analyses

Laboratory analyses after Schlichting et al. (1995) involved grain size measurements (sieve-pipette method). From material < 2 mm, pH value was determined in KCl solution (20 g material in 50 ml solution). Electrical conductivity (EC, 10 g sample in 50 ml deionised water) was measured with an Inolab pH/Cond Level 1 device. Calcium carbonate content was determined with a Scheibler apparatus. For clay mineral analysis the fraction < 2 µm was separated (mechanical dispersion and separation by sedimentation). Oriented aliquots were measured with a Seifert XRD C 3000 TT diffractometer (CuKα radiation, 40 kV, 30 mA, 2.5-30.01 ° 2θ, step scan 15.0 s, step size

0.03°) three times after the following preparation steps: air drying, solvating with ethylene glycol (48 hours) and heat treatment (2 h at 550 °C). XRD of unoriented powder samples was conducted using a SIEMENS D 5000 diffractometer (CoKα, 40 kV, 30 mA, 5-80 ° 2θ, step scan 4 s, step size 0.03 °). The software Siemens Diffracplus BASIC 4.0#1 was used for evaluation.

5.2.4 Laboratory experiments

In accordance with other approaches (e.g. Springer, 1958; Figueira & Stoops, 1983), artificial vesicular structure was created in fine-grained material which was filled into plastic containers and subjected to wetting-drying cycles. Based on published Av horizon properties, wetting, drying and material parameters were modified to evaluate their influence on vesicle formation. Loess-like sediment from Zaschendorf, Saxony (UTM zone 33 N, 4348392/424781) was used as reference material because of its low values of sand content, EC and calcium carbonate content (table 2). In this material vesicles form fast and become abundant as previous experiments demonstrated (Schlapa, 2009). XRD analysis confirmed that the mineralogical composition of the reference material and of selected natural Av horizons (CF-01, PM-01, LR-01) was similar. Another sample consisted of Tabernacle Hill vesicular horizon material. It was included to compare artificial with natural vesicular structure. Table 5.2 summarises the parameters of all prepared samples. Figure 5.1 shows texture, EC and calcium carbonate content data of vesicular structure from previous publications together with prepared materials of the present study. It demonstrates that the experiment setup covers nearly the entire range of known individual Av horizon properties. To account for contingent biogenic gas production as mechanism of vesicle formation (Bazilevich et al., 1953) one sample of the reference material was sterilised at 120 °C and 2 $\cdot 10^5$ Pa.

All experiments were conducted with similar starting conditions. Figure 5.2 provides a sketch of the main preparation and experiment steps. 200 g of air-dried and sieved (< 2 mm) material was put into a plastic container (12 cm height, 10 cm diameter) and packed by vibration. Infiltration time after raining (approximately 1 mm drop diameter) with 60 ml deionised water for 15±3 s from a height of 20 cm was noted. Afterwards, the material was oven-dried at 50 ° C. Ten wetting-drying cycles were conducted. Vesicles begin to form after not more than five cycles and may reach a saturation level after 20 to 30 cycles. Thereafter, vesicle size does no longer increase systematically (Miller, 1971; Figueira & Stoops, 1983). As we wanted to study the effects of different parameters on vesicle quality, the cycle number was kept well below this saturation level. A vertical section was prepared from each aggregate by mechanical cracking and subsequent grinding to receive a smooth surface. Digital images were taken under a ZEISS stereo microscope.

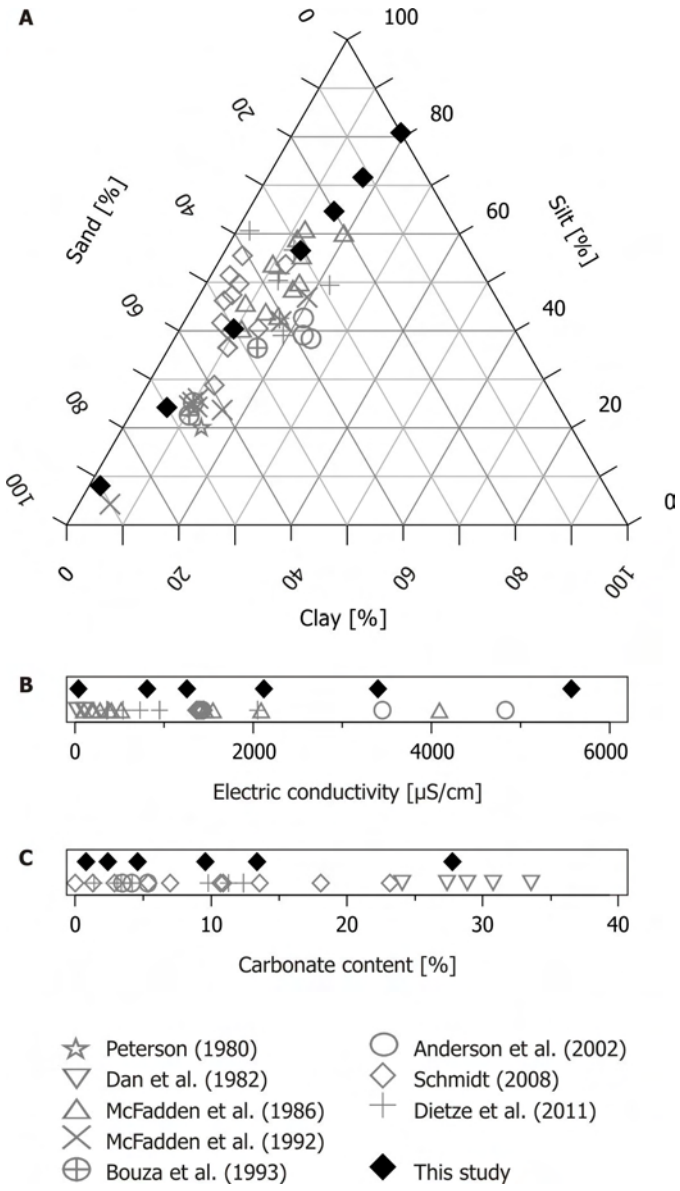

Figure 5.1. Data of vesicular horizons. A: Grain size data, B: Electrical conductivity, C: Calcium carbonate content of published samples as indicated in the legend from several study sites plotted in grey. The material from Zaschendorf with modified physical and chemical properties is plotted in black.

The method of water application may influence vesicle formation in several ways. If a downward migrating wetting front is the driving force of air compression and, hence, probably vesicle formation, application from the bottom of the sediment body should yield no vesicular structure at all. To test this, water was injected to the bottom with a small pipe (3 mm diameter) pierced through the sediment column. Wetting from above was performed with two further techniques: gentle flooding and fine spray. These methods were chosen to study effects of splash processes and drop impact vibrations. The standard amount of water, 60 ml (9.4 mm), was chosen to ensure complete surficial wetting of the material. However, effects of raining with 40, 80 and 100 ml (i.e. 6.3, 12.6 and 15.7 mm) water were tested as well.

The drying temperature may influence gas pressure within the sealed matrix. Brown & Dunkerley (1996) suggested a considerable contribution of solar heating to this mechanism. Evenari et al. (1974) argued similarly, although they dried their material on a window sill. We dried the reference material at two temperatures: 50 ° C as a typical environmental value and 105 ° C as an extreme scenario, unlikely to be reached under natural conditions.

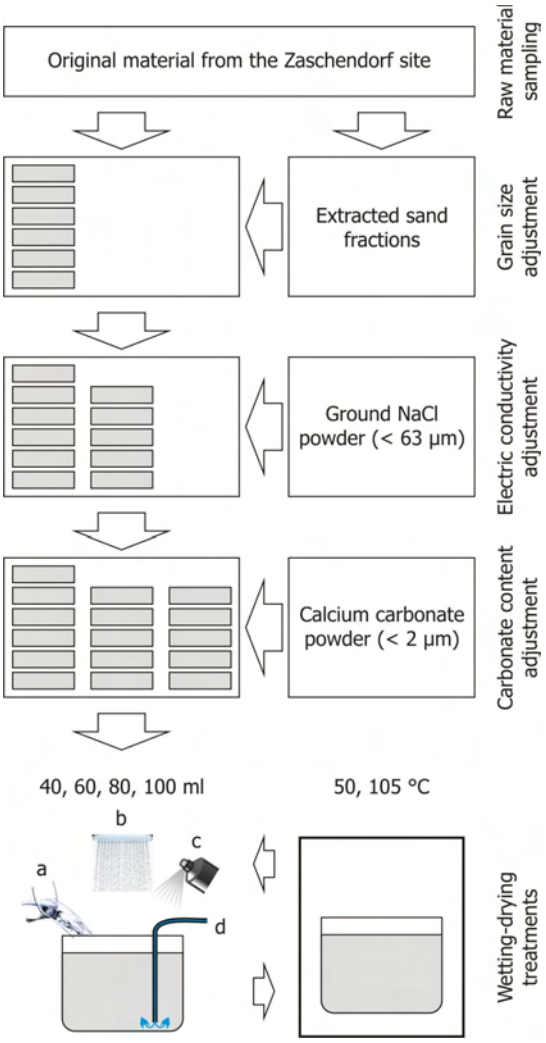

Figure 5.2. Flow chart of the main preparation and experiment steps for artificial creation of vesicular structure.

In natural environments, vesicular horizons are often related to stone pavements. However, there is disagreement whether vesicles form with or without surface cover (see introduction). Accordingly, experiments were performed with a bare sediment surface and a cover of basalt fragments of different sizes (1-2, 2-4, 5-8 cm a-axes lengths).

Grain size composition controls infiltration capacity, establishment of a closed wetting front as well as the abundance of material which could be detached by puddling. From the Zaschendorf

reference material percentage of sand (and as a result silt and clay) was modified by adding sand (fraction > 63 µm) sieved from the original material to the reference material until the following sand contents were reached: 0, 11, 20, 30, 50, 70 and 90 %.

Soluble salts, especially sodium chloride (Peterson, 1980), within the soil matrix may influence vesicle formation due to clay mineral dispersion (Das & Datta, 1987) and alteration of water tension (Miller, 1971). Accordingly, halite was ground in a corundum mortar and sieved to a grain size < 63 µm (cf. Das & Datta, 1987). The reference material had an EC of 38.9 µS/cm. Salt powder was added to adjust to the following salt contents and respective EC values: 0.25, 0.5, 1.0, 2.0 and 5.0 % (810, 1260, 2120, 3400 and 5570 µS/cm).

Calcium carbonate may play a role in developing vesicles (i.e. CO_2 release during crystallisation, Paletskaya et al., 1958). The reference material has a calcium carbonate content of 0.8 %. Calcium carbonate powder (grain size < 2 µm) was added until the following carbonate contents were reached: 1, 2.4, 4.6, 9.6, 13.4 and 27.8 %.

Table 5.2. Parameters of samples used for artificial vesicle formation. Modified values are in italics. Preparation steps see text. All samples were made of material from Zaschendorf except sample TH-01 which consists of sediment from the Tabernacle Hill site.

ID	*Sand [%]*	*Silt [%]*	*Clay [%]*	*$CaCO_3$ [%]*	*EC [µS/cm]*	*Water [ml]*
TH-01	26.7	65.4	7.9	4.8	128	60
Z_W_II	11.11	71.86	17.03	0.8	38.9	60 *(flooding)*
Z_W_III	11.11	71.86	17.03	0.8	38.9	60 *(bottom)*
Z_W_IV	11.11	71.86	17.03	0.8	38.9	60 *(spray)*
Z_W40	11.11	71.86	17.03	0.8	38.9	*40*
Z_W60	11.11	71.86	17.03	0.8	38.9	*60*
Z_W80	11.11	71.86	17.03	0.8	38.9	*80*
Z_W100	11.11	71.86	17.03	0.8	38.9	*100*
Z_T50	11.11	71.86	17.03	0.8	38.9	60 (T = 50 °C)
Z_T105	11.11	71.86	17.03	0.8	38.9	60 (T = 105 °C)
Z_S00	*0*	*80.8*	*19.2*	0.8	38.9	60
Z_S20	*20*	*64.64*	*15.36*	0.8	38.9	60
Z_S30	*30*	*56.56*	*13.44*	0.8	38.9	60
Z_S50	*50*	*40.41*	*9.59*	0.8	38.9	60
Z_S70	*70*	*24.24*	*5.76*	0.8	38.9	60
Z_S90	*90*	*8.28*	*1.72*	0.8	38.9	60
Z_E08	11.11	71.86	17.03	0.8	*809*	60
Z_E13	11.11	71.86	17.03	0.8	*1257*	60
Z_E21	11.11	71.86	17.03	0.8	*2120*	60
Z_E34	11.11	71.86	17.03	0.8	*3400*	60
Z_E56	11.11	71.86	17.03	0.8	*5570*	60
Z_C02	11.11	71.86	17.03	*2.4*	38.9	60
Z_C05	11.11	71.86	17.03	*4.6*	38.9	60
Z_C10	11.11	71.86	17.03	*9.6*	38.9	60
Z_C15	11.11	71.86	17.03	*13.4*	38.9	60
Z_C30	11.11	71.86	17.03	*27.8*	38.9	60

5.2.5 Quantification of vesicular structure properties

To distinguish vesicle boundaries from matrix material properly, appropriate light conditions were established. In the field all sections were positioned so that sunlight fell onto the surface at a low angle, thus casting shadows inside vesicular hollows. Alternatively, the sections were placed in the shadow, which also resulted in considerably darker voids compared to the bright matrix. Under the stereo microscope appropriate illumination conditions (i.e. low illumination angles) may be set much easier. Figure 5.3 shows examples of both field and laboratory sections, used for further analysis.

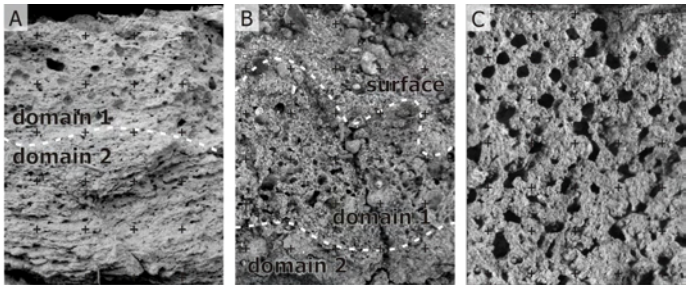

Figure 5.3. Examples of sections through aggregates with vesicular structure. A, B: Natural vesicular structure with two zones, i.e. zone of preferred vesicle occurrence (domain 1) and zone of dominant platy structure (domain 2). C: Artificial vesicular structure prior to digitising respective objects. Crosshair distance is 10 mm.

All vertical section images were imported to ArcGIS 9.3, rescaled and geometrically corrected. Subsequently, images were digitised after adjusting histograms iteratively for small analysis areas to ensure high intensity contrast. The following objects were digitised: aggregate surface line, boundaries of vesicles as well as a and b axes of the objects. The following parameters were subsequently derived: centroids and respective coordinates, their distance to the aggregate surface (depth), vesicle area (A), vesicle perimeter (Pe), length and angle (ϕ) against the horizontal for a and b axes. Based on these data, further parameters were derived: lobation ratio (LR, Beckmann, 1962), A-Pe^2 ratio (Bisdom & Schoonderbeek, 1983) and the a-b-axes product. All parameters were tested for correlation among each other (correlation coefficients after Pearson and coefficients of determination R^2). To compare a-axes angles with other parameters, these circular values were transformed into a measure of axes-angle deviation from the horizontal line ($\Delta\phi$) by the equation: $\Delta\phi = 1 - |\sin\phi|$.

Objects which could easily be designated as non-vesicular were omitted, i.e. vughs and voids due to experiments and preparation. However, the strict definition for vesicles after Stoops (2003) as smooth and spherical pores was not applied. According to Volk & Geyger (1970), Anderson et al. (2002) and own observations in the field, not all vesicles are well-rounded. They may frequently exhibit elongated, interconnected and contorted boundaries. Accordingly, such objects were digitised as well.

Digitising objects from raster data is problematic if objects become smaller than the pixel size. The images of this study had pixel sizes of 28±13 µm (natural samples) and 3±1 µm (artificial samples). Hence, the smallest resolvable object diameter is around 100 µm (10 µm respectively). This is in accordance with reported vesicle diameters, which are in the range of 100 µm to some 1000 µm (Peterson, 1980; Collins et al., 1986; Blank et al., 1996). However, this approach may encompass very small natural objects incorrectly. Furthermore, tests revealed that object size parameters (i.e. perimeter, area and axes lengths) were skewed towards small values (skewness 2.2±1.0). In order to suppress the influence of both too small (digitising uncertainties) and too large (extreme values) objects, only data between quantile $_{0.2}$ and quantile $_{0.8}$ was included to further analysis. This reduced skewness towards a log-normal data distribution type.

5.3 Results

5.3.1 Natural vesicular horizons

5.3.1.1 Soil morphological and sedimentary properties

Table 3 provides surface, soil morphological and sedimentological characteristics for all investigated natural vesicular horizons. The last two columns illustrate the relationship between mean annual precipitation at a site and respective site properties. The relationships are described by the Kendall rank correlation coefficient τ. Due to the small number of samples (n = 5) the coefficients may be interpreted just as illustrative for general trends Furthermore, the Tabernacle Hill site (TH-01) was omitted because of systematic deviation from general trends. This could be related to its location adjacent to a gypsum playa (Oviatt, 1991) with respective changes in aeolian sediment composition.

In the Black Rock Desert, with increasing humidity, stone pavement coverage decreases whereas vegetation coverage increases systematically. Along with decreasing stone pavement cover, properties that are typically associated with a vesicular horizon diminish gradually: the covering loose aeolian material (designated as C horizon since it represents the youngest deposited material) as well as the total Av horizons become thinner and less consolidated. In the vesicular horizon, clay content decreases from dryer sites towards moister sites, whereas sand shows the opposite trend. The covering C horizon is always different in texture from the material of the Av and exhibits decreasing sand but increasing clay content with increasing humidity. EC does not show any distinct pattern. Calcium carbonate content shows a weak trend to increase in the surficial C horizon but to decrease in the basal Av horizon with increasing humidity.

Including vesicular horizons from the other investigated sites exhibits similar trends, although often less dominant. At Cima Volcanic Field, intra-site variability of texture is moderate, i.e. 15 % on average, except for the extraordinary differences in calcium carbonate content of one Av

sample. This equals the range described by other investigators (McFadden et al., 1986; Anderson et al., 2002). The exceptionally young feeder road site in the Laguna Salada (LS-01) exhibits a stone pavement on top of recently deposited aeolian material. This 2 cm thick layer shows prominent vesicular structure (figure 5.3B) and its properties follow the general trends described above.

Table 5.3. Field descriptions, sedimentologic parameters and correlation results of natural samples. Sites are sorted by humidity. Grey shading indicates samples from the Black Rock Desert. Soil firmness is described according to Birkeland (1999): 1 – loose, 2 – soft, 3 – slightly hard, 4 – medium hard, 5 – hard, 6 – very hard, 7 – extremely hard. Kendall's τ is calculated for the Black Rock Desert (without the Tabernacle Hill site, cf. text for explanation) and for all sites. Correlation coefficients which explain more than 25 % and 50 % of total variance are in italics and bold, respectively.

Site	*LS-01*	*LS-02*	*CF-01*	*CF-02*	*RP-01*	*VR-01*	*PM-01*	*PM-02*	*PB-01*	*NT-01*	*LR-01*	*TH-01*	*SB-01*	*τ (BRD)*	*τ (all sites)*
Mean annual precipitation [mm]	80	80	161	161	200	219	229	229	276	293	310	329	330	n.d.	n.d.
DP coverage [%]	95	95	85	85	80	30	90	90	95	60	30	70	20	*-0.56*	-0.44
Vegetation coverage [%]	0	0	0	0	5	60	5	5	2	10	80	5	80	*0.56*	*0.68*
Mean Av ped size [cm]	n.d.	5	n.d.	n.d.	4.5	4	9	8	6	5	7	11	0	-0.32	0.37
Av ped firmness	1.5	3,5	3.5	4.5	1.5	3	7	6	5	1	1.5	5	1	**-0.74**	-0.1
C horizon, thickness [mm]	3	2	4	3	1	0	3	3	2.5	0	0	2	0	**-0.89**	-0.28
Av, thickness [cm]	1.3	2	7	7	4	3.1	10	9	5	2.5	0.6	5	0.7	**-0.74**	0.06
Av domain 1, thickness [cm]	1.3	0.7	1.2	1.1	1.5	1.1	1.5	1.5	1	0.3	0.6	2	0.7	*-0.53*	0.06
Av domain 2, thickness [cm]	0	1.3	5.8	5.9	2.5	2.0	8.5	7.5	4	2.2	0	3	0	**-0.95**	0.02
C horizon, sand [%]	86.64	68.28	48.01	46.21	27.24	n.d.	68.13	n.d.	64.44	63.34	n.d.	32.27	n.d.	*-0.55*	-0.41
C horizon, silt [%]	13.14	31.20	46.28	51.08	68.72	n.d.	29.17	n.d.	32.67	31.70	n.d.	63.67	n.d.	0.18	0.23
C horizon, clay [%]	0.21	0.52	5.71	2.71	4.03	n.d.	2.71	n.d.	2.88	4.96	n.d.	4.06	n.d.	*0.55*	0.49
Av domain 1, sand [%]	55.89	17.72	31.36	30.25	15.49	n.d.	24.96	n.d.	51.16	48.61	71.51	26.70	n.d.	**0.74**	0.22
Av domain 1, silt [%]	22.88	60.42	47.04	46.17	72.37	n.d.	57.71	n.d.	37.23	40.99	27.94	65.37	n.d.	*-0.53*	-0.07
Av domain 1, clay [%]	8.54	21.85	21.60	23.58	12.13	n.d.	17.33	n.d.	11.60	10.40	0.55	7.92	n.d.	**-0.74**	*-0.52*
Av domain 2, sand [%]	n.d.	59.54	32.70	40.07	10.74	n.d.	38.07	n.d.	47.89	53.22	n.d.	30.14	n.d.	0.11	0.02
Av domain 2, silt [%]	n.d.	32.24	42.34	35.49	80.62	n.d.	41.18	n.d.	31.82	41.55	n.d.	57.78	n.d.	0.32	0.21
Av domain 2, clay [%]	n.d.	8.21	24.96	24.44	8.65	n.d.	20.75	n.d.	20.30	5.23	n.d.	12.08	n.d.	**-0.74**	-0.17
C horizon, EC [µS/cm]	136	156	260	350	373	n.d.	119	n.d.	387	111	126	126	n.d.	-0.11	-0.04
Av domain 1, EC [µS/cm]	141	172	211	235	562	n.d.	136	n.d.	422	72	97	128	n.d.	-0.32	-0.15
Av domain 2, EC [µS/cm]	n.d.	1403	218	348	3290	n.d.	127	n.d.	304	83	n.d.	135	n.d.	*-0.53*	-0.21
C horizon, $CaCO_3$ [%]	1.4	3.8	1.0	1.2	7.2	n.d.	5.5	n.d.	4.4	21.4	10.2	3.8	n.d.	*0.53*	0.4
Av domain 1, $CaCO_3$ [%]	1.4	4.6	10.2	11.0	15.0	n.d.	17.0	n.d.	5.0	17.6	14.8	4.8	n.d.	0.11	0.26
Av domain 2, $CaCO_3$ [%]	n.d.	4.0	8.4	1.4	6.4	n.d.	11.6	n.d.	6.0	11.3	n.d.	3.8	n.d.	*-0.53*	0.13

5.3.1.2 Vesicle parameters

Comprehensive descriptive statistics are provided in table 5.A.1. Only vesicle area is discussed here as main size parameter and *LR* as main shape parameter, because parameters of size (i.e. area, perimeter, axes lengths, axes product) and shape (i.e. *LR* and $A\text{-}Pe^2$ ratio) showed consistent correlation among each other with R^2 values mostly above 0.7 (table A.2). Figure 5.4 illustrates the parameter distributions for all study areas sorted by humidity. Individual vesicle areas range between 11 and 394 $\cdot 10^{-7}$ m² with an average relative quartile range of 76±27 %. *LR* ranges between 1.13 and 2.45 with an average relative quartile range of 29±12 %. The parameter range of the Black Rock Desert area is similar to the range of all studied sites. In contrast to the surface properties (table 2), there is no unique trend in vesicle parameters that may be attributed to humidity alone. There is no robust relationship of any vesicle parameter with depth. R^2 of all tested variables remain below 0.1, both for natural and artificial vesicles. In a similar way, the a-axes angles of vesicles are independent from any other vesicle parameter.

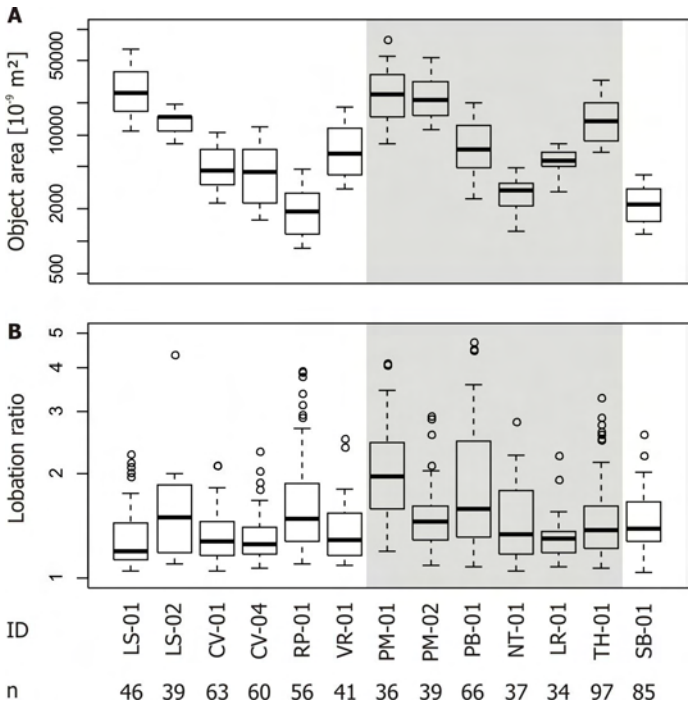

Figure 5.4. Box plots of properties of natural vesicular structure. Data is sorted by increasing site humidity. Numbers of included objects are given at the bottom as n. Grey shading indicates plots from the Black Rock Desert.

5.3.1.3 Mineralogical results

Diffraction patterns (both, bulk material and the clay mineral fraction) of Av horizon material from the Black Rock Desert, Cima Volcanic Field and from Zaschendorf show an overall similar mineralogical composition. Quartz, albite, illite/muscovite and kaolinite are ubiquitous. Mixed-

layer phyllosilicates were also identified in all samples, although they were less abundant in the two samples from the Black Rock Desert. The samples from Cima volcanic field further comprise actinolite and anorthoclase in addition. The material from Zaschendorf differs from the other sites by the absence of calcite.

Clay mineral analysis of profile CF-01 from Cima volcanic field is illustrated in figure 5.5. All samples contain kaolinite and illite/muscovite. However, expandable mixed-layer phases occur only in the two vesicular horizons and the deeper, strongly pedogenetically overprinted part of the profile. A similar mineralogical composition is also present in the material from Soda Lake playa. In sample 3AvbBt chlorite was detected. The peak in the air-dried sample 2C around 15 Å does not correspond to any realistic mineral phase and is assumed to be an artefact.

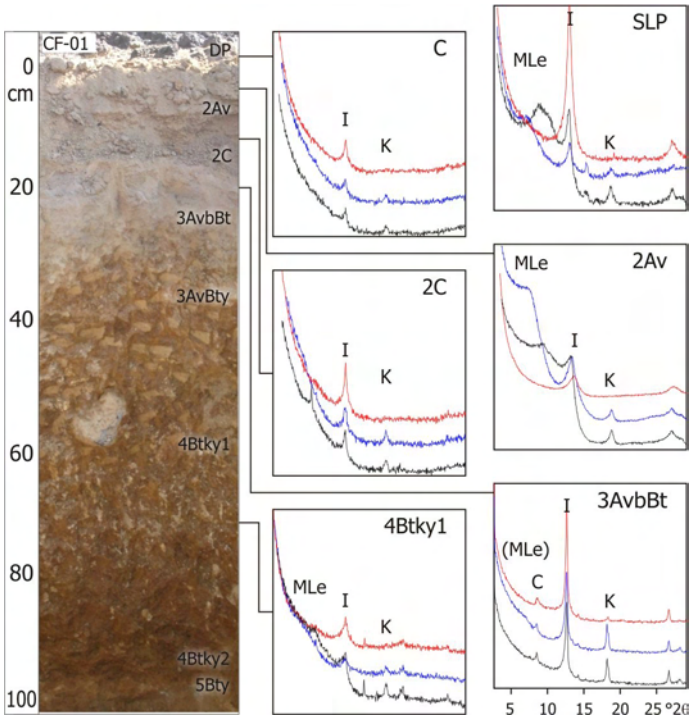

Figure 5.5. X-ray diffractograms of the fraction < 2 µm for selected samples from profile CF-01 and Soda Lake playa (SLP). Horizon designation after Soil Survey Division Staff (1993) and Birkeland (1999). For a detailed site and profile description see Dietze et al. (2011). The graphs inside the plots show diffractograms after respective treatments: black – air dried, blue – ethylene glycol-solvated, red – thermal treatment. All curves are normalised for illustrative reasons. Clay mineral types: K – kaolinite, I – illite/muscovite, C – chlorite, MLe – expandable mixed-layer mineral.

5.3.2 Artificial vesicular structure

5.3.2.1 General experiment results

All wetting techniques from above led to puddling of the surface and subsequent formation of water film of a few millimetres. After establishment of the water film air bubbles escaped from the surface. At such locations little craters remained, 2 to 7 millimetres in diameter.

After a small number of cycles a polygonal crack system began to develop. The cracks formed during drying and were filled with sediment again during wetting. Cracks were not spatially stable. Rather they re-formed at different locations with time. Cracks typically originate at the centres of cover stones where the sediment underneath remained dry and no crust formed.

A peculiar phenomenon, which occurred during experiment setups with rapid wetting and flooding, was the lifting of stones by escaping air, regardless of stone size. Soon after infiltration had begun several air bubbles escaped along the stone margin and thereby lifted one edge repeatedly. Lift height was hardly quantifiable due to the rapidity of the lifting process (less than three seconds) but was in the range of a few mm at the lifted edge.

Vesicles formed under nearly all experiment setups. However, abundance and size of the artificial cavities scattered broadly. Vesicles did not form under the central parts of cover stones. Rather, the outer rims of any cover object was a preferred location for vesicle formation, indicated by enhanced abundance, size and depth (figure 5.6 A). Also, vesicles formed along the container side walls. Vesicles formed explicitly in the sterilised material with no obvious difference in any vesicle parameter compared to the reference material.

Diameters of artificial vesicles are in general one order of magnitude smaller than those of natural ones (cf. table 5.A.1) but within the range of values reported from other experiments (e.g. Figueira & Stoops, 1983). This holds true for artificial vesicles formed in material derived from Tabernacle Hill. Vesicle areas range between 2 and 177 $\cdot 10^{-9}$ m^2 with an average relative quartile range of 95±52 %. *LR* ranges between 1.10 and 1.81 with an average relative quartile range of 27±6 %.

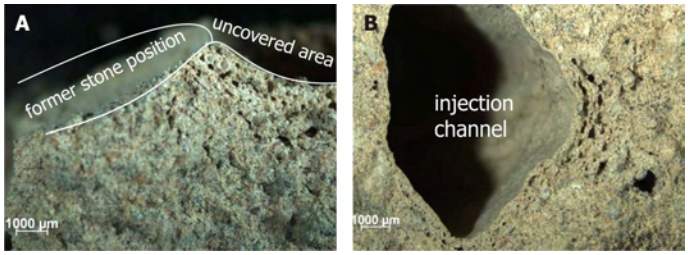

Figure 5.6. Microscope images of artificial vesicular structure. A: Whereas the uncovered area shows a zone with abundant development of vesicles, there are no such objects below the area covered by a stone during the experiment. B: Vesicles formed only along the channel of an injection pipe where water ascended during wetting.

5.3.2.2 Changes in infiltration time

With ongoing vesicle-formation cycles, infiltration time increased exponentially by one order of magnitude (figure 5.7), in accordance with the finding of Young et al. (2004) of logarithmically decreasing hydraulic conductivities. Results of wetting with 100 ml are not plotted because infiltration always lasted longer than two hours. Infiltration time was further modulated by several parameters. Water amount played a fundamental role, whereas water application method had only sec-

ondary influence (figure 5.7A). Texture showed an unexpected pattern: coarser material resulted in longer infiltration times towards the end of the experiments (figure 5.7B). One would expect higher rates for better-draining material. Similarly, increasing calcium carbonate content resulted in more rapid infiltration (figure 5.7D).

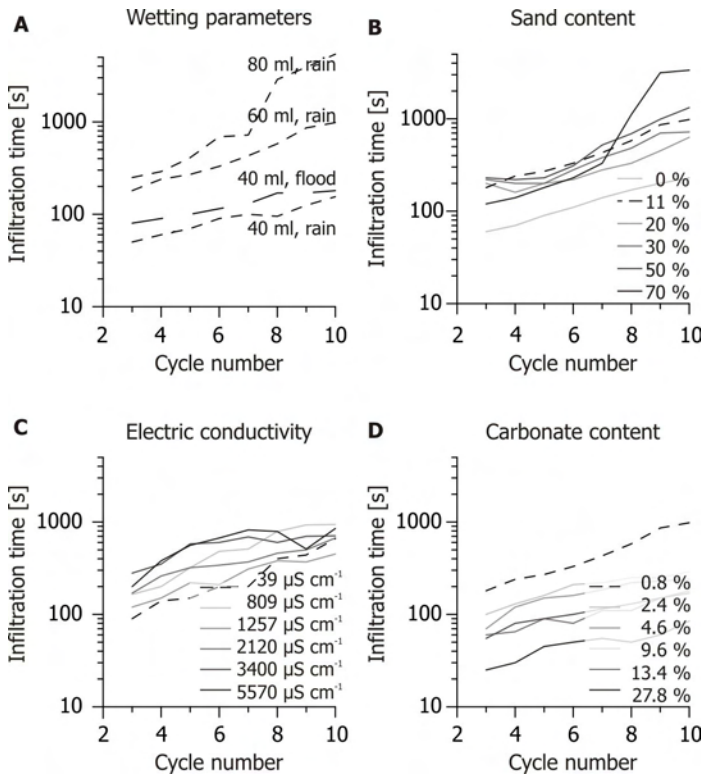

Figure 5.7. Infiltration times (logarithmic scale) during 10 vesicle-formation cycles for different sample series. A: modified amounts of applied water and wetting technique. B: Modified sand content. C: Modified salt content (i.e. EC). D: Modified calcium carbonate content.

5.3.2.3 Influence of wetting and drying parameters

The main results of the different experiment setups are summarised in figure 5.8. Details are provided in table 5.A.1. The presentation of parameter values will refer to the medians in this table. Vesicle depth below the surface is not presented here to avoid potential bias due to that the images sometimes did not cover the entire depth interval of vesicle formation.

From the performed wetting techniques all but wetting from the bottom produced surficial vesicular structure. However, vesicles also formed by the latter technique, once water ascended along the injection channel and penetrated the material. Vesicles formed along the channel, perpendicular to its side wall (figure 5.6B). This may be regarded as a wetting front, too, which propagates laterally towards the dry sediment interior.

Figure 5.8A presents a summary of vesicle parameters for the different wetting types. Water

application technique (flooding, spraying and raining) as well as water amount show one consistent influence: the higher the wetting rate, the larger and more spherical are the resulting vesicles. From the different techniques, spraying resulted in the smallest vesicles whereas flooding created the largest ones. Figure 5.8B shows that the influence of drying temperature on vesicle area is marginal except for an overall larger scatter after drying at 105 °C. However, *LR* from experiments at this higher temperature was systematically smaller.

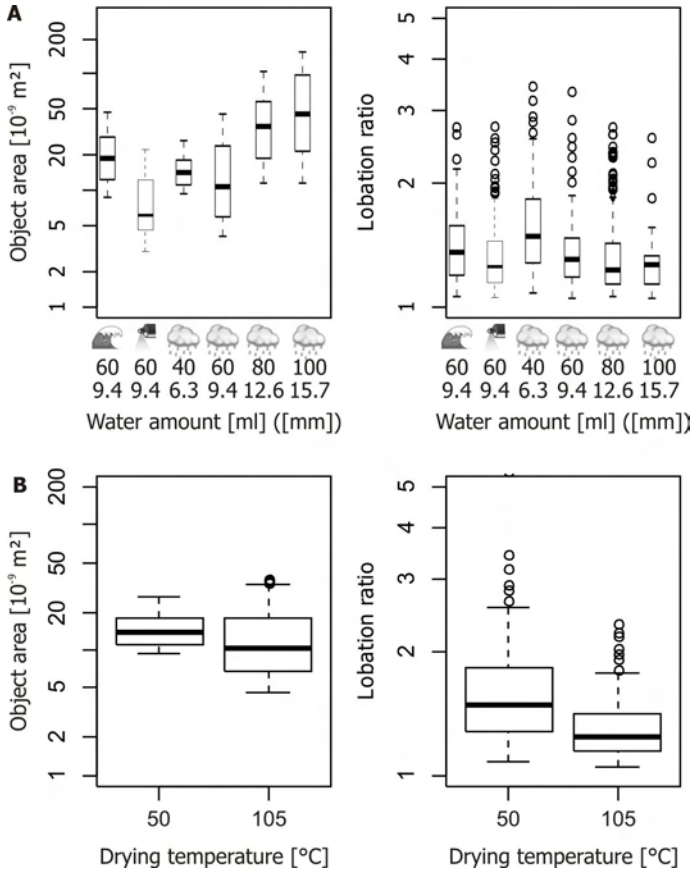

Figure 5.8. Vesicle parameters for different environmental properties. The parameters modified according to table 5.2 are plotted below each box plot. The box plots are separated linearly according to these modified parameters. The ordinate is in logarithmic scale. The left panel shows vesicle area data, the right panel shows lobation ratio data. A: Changes in wetting technique (flooding, spraying, raining, each with 60 ml water) and amount (40, 60, 80 and 100 ml water, each with raining). B: Changes in drying temperature.

5.3.2.4 Influence of sediment properties

Texture has a fundamental control function for all vesicle parameters (figure 5.9A). The sample with 90 % sand content could not be preserved because of its loose consistence, but all other samples yielded valid results. Changes from zero to 70 % sand content result in systematic object area increase and *LR* decrease. Vesicle size increases exponentially except for the sample with 70 % sand content. *LR* decreases logarithmically but only for objects larger than quantile $_{0.75}$. Figure 5.9A also includes material from Tabernacle Hill (grey box plots), which followed the general be-

haviour of the artificial formations despite of different EC and calcium carbonate values. The range of changes due to texture was in the order of changes caused by different wetting amounts (figure 5.8A).

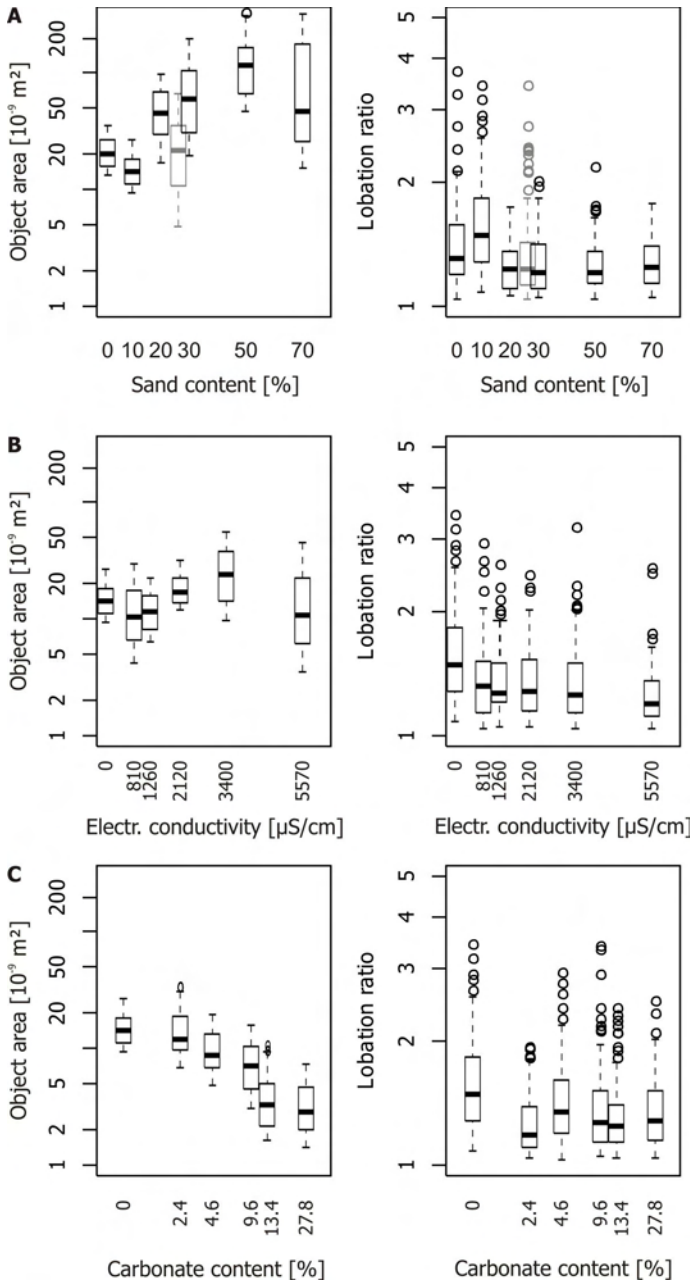

Figure 5.9. Vesicle parameters for different sediment properties. The modified parameters according to table 5.2 are plotted below each box plot. The box plots are separated linearly according to the modified parameters. The ordinate is in logarithmic scale. The left panel shows vesicle area data, the right panel shows lobation ratio data. A: Changes in sand content. The grey plots indicate material from Tabernacle Hill. B: Changes in EC due to added salt. C: Changes in calcium carbonate content.

The materials with modified EC showed precipitated salt crusts on the surface after each drying, dissolved again after subsequent wetting. Effects of differences in salt content are irrelevant in

comparison to the other investigated parameters (cf. data ranges in figure 5.9B). However, added salts apparently led to larger vesicles up to an EC value of 3400 µS/cm. Calcium carbonate content has a systematic negative effect on vesicle size. Object area decreases from 14.1 to 2.9 $\cdot 10^{-9}$ m² on average. *LR* is not influenced by this parameter.

The admixed calcium carbonate also modified texture due to its grain size below 2 µm. Attributing calcium carbonate to the clay fraction and recalculating the respective grain size classes corrects texture for this parameter. Figure 5.10 shows vesicle areas for the formations with sand content changes together with the carbonate-corrected formations, both following a systematic pattern. Apparently, calcium carbonate content controls vesicle size in these experiments indirectly via texture alteration.

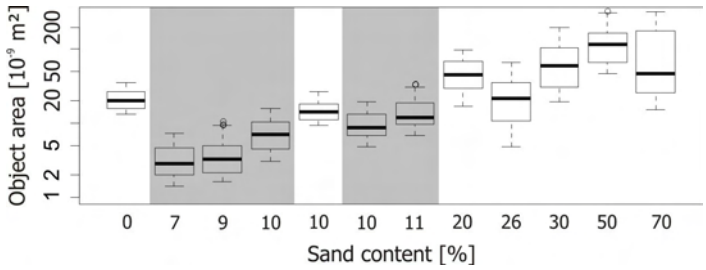

Figure 5.10. Vesicle area for different sand contents. Texture was corrected for calcium carbonate content for formations with grey shading.

5.4 Discussion

5.4.1 Models of vesicle formation

Based on the experiment results, the current vesicle formation models may be evaluated. The suggested mechanism of Bazilevich et al. (1953) that algae produce gas via photosynthesis cannot play a major role because vesicles also formed in sterilised material. In contrast, no vesicles were produced if the material was wet only once and then left abandoned. Algae crusts in general were not necessary (and not present) to form vesicles in the experiments. This does not negate contribution of algae to vesicle formation but illustrates that they do not play a decisive role. The model of Paletskaya et al. (1958), i.e. gas production by hydrogen carbonate crystallisation during drying generates vesicles, appears unlikely because i) vesicles also formed in material with as little as 0.8 % calcium carbonate content and ii) increased calcium carbonate content had a negative effect on vesicle size (figure 5.9C). Rozanov (in Paletskaya et al., 1958) speculated that gas pressure increases due to contraction of a crust-sealed matrix during drying. If so, then higher sand contents should result in i) weaker crusting and ii) less contraction during drying because of lower cohesiveness. However, vesicles become larger and better-rounded with increasing sand content. Therefore, experiment results contradict this model, too. Brown & Dunkerley (1996) and Evenari et al. (1974) argue for solar heating of a surface-sealed sediment body to increase gas pressure and form vesicles.

In contrast, figure 5.8C shows no influence of drying temperature on vesicle size. Similarly, Miller (1971) reported vesicles formed in completely shaded material not affected to solar heating at all. Consequently, we found no support for the role of solar heating for vesicle formation except for the phenomenon that it may result in better-rounded objects. Hugie & Passey (1964) explain vesicles as remaining cavities of air bubbles that moved through a water-saturated matrix and eventually got stuck. Apart from the fact that laminated clay and carbonate coatings on vesicle walls (Sullivan & Koppi, 1991) argue against this hypothesis, experiment results of exponentially increasing infiltration times with cycle number along with the finding of systematically increasing bulk density (Miller, 1971) imply that vesicles are enduring.

Our results are in broad agreement only with the model of Springer (1958). Three mechanisms in combination lead to a rising gas pressure within the matrix: i) a downward migrating wetting front, ii) a sealed surface due to fine material puddling and iii) a water table on top of the puddled surface. The water front further leads to reduced negative pore pressure which results in declining particle cohesion and shear strength. Surfaces allow formation of vesicles only where a closed water film is able to spread out. Consequently, areas which were covered by stones did not host vesicles (figure 5.6A). There, air can escape from the matrix along the stone margin. Brown & Dunkerley (1996) found a strong negative correlation ($R^2 = 0.93$) between cover stone size and vesicle abundance in natural systems. This finding of a stone cover preventing vesicle formation appears to contradict reports of enhanced vesicle formation under glass Petri dishes used as artificial cover (Evenari et al., 1974). Apparently, a smooth glass surface together with the level rim of such an item allows sufficient sealing of the surface. However, glass slides are not adequate to serve as proxy for natural objects such as stones with irregular, rough boundaries and non-prefect cuboid shapes.

Although Springer (1958) reports formation of vesicles by infiltration and surface sealing, he also suggests vesicles are transitory, unstable formations, being destroyed and re-formed at different locations with every wetting event. This latter perception stands in contrast to the results derived by systematically increasing infiltration times, apart from puddling effects. Further arguments for long-term stability of vesicular structure were discussed before with respect to the model of Hugie & Passey (1964). Vesicular structure partially shows interconnected and coalesced vesicles which results in increased *LR* (Miller, 1971; figure 5.4B). This would unlikely come to pass, if the cavities were destroyed with every wetting event.

5.4.2 Control parameters of vesicle formation

Vesicles and vesicular horizons were found in the studied natural environments only where mean annual precipitation was below 350 mm. There is a strong statistical relationship between humidity and macroscopic/morphological soil properties, such as firmness of the Av horizon,

thickness of the covering C horizon, thickness of the Av domain 1 and clay contents of both Av domains. Across the Black Rock Desert moister sites allow only thin and weakly consolidated Av horizon aggregates. Figure 5.11 illustrates this trend.

The figure also highlights the major factor which limits formation and/or maintenance of vesicular structure: root penetration of the upper centimetres of the soil. Roots may disturb the formation of vesicles by i) supporting preferential water flow paths, ii) acting as pathways for gas escape during wetting front propagation and iii) actively destroying vesicles during growth. Root abundance is in turn related to vegetation type and vegetation dispersion, land-use and, hence, to humidity in general. The persistent relationship depicted in table 5.3 (τ = 0.68 for mean annual precipitation and vegetation cover) supports this finding.

In contrast to macroscopic and soil-morphological properties, natural samples showed no relationship between humidity and any measured vesicle size and shape parameter. Accordingly, there presumably are further factors (apart from humidity and root abundance) that contribute to vesicle morphology. The main difference between artificial and natural vesicles is object size which differs by one order of magnitude. In the experiments of Miller (1971) remarkable increase of vesicle area did not start before 8 or 14 cycles, which is when the experiments presented here stopped. According to Miller (1971), the dominant vesicle size class changed from 0.25-0.50 mm after the initial cycles to larger than 1 mm after 25 cycles, which resulted in an decrease of bulk density of up to 60 %, and was predominantly due to the merging of small vesicles into larger ones. Figueira & Stoops (1983) report similar values from micromorphometrical data. Therefore, natural vesicular structure, which forms over many years and, thus, over several tens to hundreds of wetting-drying cycles, may be expected to consist of much larger vesicles.

Sediment and wetting parameters which favour rapid infiltration and percolation led to systematically larger and more spherical vesicles (figures 5.8A and 5.9A). This may be interpreted as more rapid rise of gas pressure and better separation of a coherent matrix. The amount of water provided per unit time, sand content and calcium carbonate content (with negative sign) all have remarkable but non-linear impact on vesicle size parameters (cf. table 5.A.1). *LR* declines only in the extreme values, but with increasing wetting rate vesicles become rounder with a logarithmic trend.

The amount of provided water, 6.3 to 15.7 mm per cycle, may be an overestimation of natural rain events in arid and semi-arid landscapes. However, surface runoff (e.g. due to Hortonian overland flow) may easily contribute to additional water per unit area, with similar consequences as initially high rainfall. This behaviour is also supported by the finding of Brown & Dunkerley (1996) that vesicular horizons are much better developed at foot slopes that receive more runoff compared to top slopes. The higher the water column above the puddled surface, the higher is static pressure and consequently infiltration rate, which in turn results in higher gas pressure and larger vesicles. The extremely long „infiltration“ times for wetting with 100 ml water are inter-

preted to be the result of a higher water volume than pore volume of the material.

Texture coarsening leads to more rapid percolation, to a better connected water body due to less preferential flow paths and thus to a higher gas pressure if the surface remains sealed. Furthermore, in coarse material cohesion between individual grains is low compared to clay-rich sediment. Consequently, vesicular structure formation in the upper millimetres of coarse-grained material is much more efficient compared to fine-grained material and leads to a remarkable increase in total infiltration time for the entire sediment body (figure 5.7B). Vesicle areas vary by one order of magnitude, depending on sand content (figure 5.9A). Smaller vesicles in the formation with 70 % sand content may indicate a threshold due to limited surface sealing because of insufficient puddling. However, based on just one measurement this finding remains tentative.

The negative effect of calcium carbonate content on vesicle size underlines the physical nature of vesicle formation. Figure 5.10 illustrates that the effect is adequately described by assuming that the artificially added powder shifts texture towards higher clay content, with consequences for infiltration time and particle cohesion. Precipitated calcium carbonate might as well contribute to matrix cementation and consequently reduce vesicle expansion during subsequent wetting-drying cycles. Although calcium carbonate plays a limiting role in vesicle formation it may help to stabilise vesicular structure by forming laminae on vesicle walls (Sullivan & Koppi, 1991). However, our experiments could not pursue this long-term process due to their duration.

Admixture of salt has no relevant influence on vesicle size but tends to create better-rounded objects. This is in accordance with Miller (1971) who suggested contribution of capillary pressure to the creation of the spherical geometry of vesicles which in turn is controlled by water tension. However, periodic translocation of chlorides with each wetting-drying cycle hinders direct attribution of this parameter to vesicle properties.

The frequent positive outliers in nearly all *LR* box plots indicate the presence of some vesicles with an unusually large deviation from spherical shape. This may be the result of coalescence of initially isolated vesicles during the growth process. With increasingly coarser texture this effect declines (figure 5.9A).

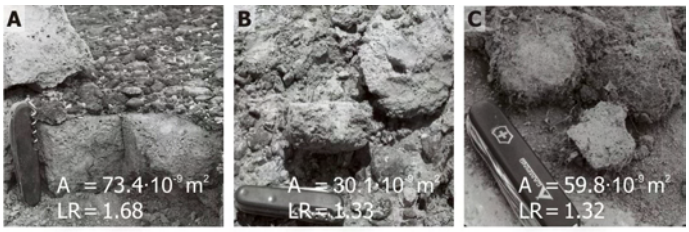

Figure 5.11. Av horizon aggregates of different quality from the Black Rock Desert. A: Pavant Butte site (PB-01), B: North Twin Peak site (NT-01), C: Lava Ridge site (LR-01). The three sites are sorted by mean annual precipitation (cf. table 5.3). They show systematic change in stone cover density, aggregate size, aggregate firmness, boundary distinctiveness and root penetration. Vesicle area (*A*) and lobation ratio (*LR*) are given as medians according to table 5.A.1.

5.4.3 Implications for natural vesicular horizons

The loose material on top of many Av horizons plays an important role in fine material fluxes. During rain events dispersed clay and soluble components are removed from this material and translocated into the vesicular horizon (cf. discussion by McFadden et al., 1986). The coarse remnants of this C horizon may be, in turn, subject to splash erosion and lateral transport (e.g. by unconcentrated overland flow) towards drainage channels and subsequent fluvial removal. The resulting relative increase of fine components in the vesicular horizon is supported by several lines of evidence: i) the presence of mixed-layer clay minerals in the Soda Lake playa material and both, the modern and the buried Av horizon (figure 5.5) but not in the loose material on top of both horizons, and ii) vesicular horizons become successively finer with time, i.e. their silt and clay contents increase systematically (Young et al., 2004). However, removal of coarse C horizon components due to splash erosion and overland flow appears to be restricted to vegetation-free, stone-covered surfaces (cf. discussion by Volk & Geyger, 1970). The strong negative correlations between humidity and C horizon thickness (τ = -0.89) and humidity and clay content of the Av horizon (τ = -0.74) imply that the winnowing effect is replaced by admixture of C horizon material to the surficial horizon under more humid conditions because with a dense grass cover the removal of accumulated C horizon material by runoff is limited. Studies by Griffiths et al. (2006) highlighted that even stone pavement-covered sites deliver sediment after rain events with average recurrence intervals of 4.9 years. A likely source of this sediment is the loose surficial C horizon. Although the sediment budget of stone pavement-covered sites e.g. at Cima volcanic field is positive in total (accumulation of several decimetres of aeolian material; Wells et al., 1985), the individual flux components may have different contributions with time. Under modern conditions dust flux into the system is 11.0±0.7 g/m² a (Reheis, 2003) and out-flux due to surface runoff is 24±10 g/m² a (Griffiths et al., 2006) which results in net erosion of fine material. However, this net erosion appears to be still buffered by the reservoir of the surficial C horizon because the vesicular horizon is very resistive to erosion (Dietze & Kleber, 2012; cf. Grabowski et al., 2011, for a review of erosion-limiting soil properties). This may predominantly be due to medium hard to hard consistence (e.g. Anderson et al., 2002), negligible potential for bioturbation (McAuliffe & McDonald, 2006) and relatively low EC but high calcium carbonate content (McFadden et al., 1998).

The dominance of well-rounded vesicles in many natural systems (figure 5.4) argues for a constant but moderate in-flux of aeolian material. If the input is too high, Av horizon and stone pavement become buried (Wells et al., 1985; Dietze et al., 2011). If the input is too low, vesicular structure develops and continues to grow until bulk density cannot be reduced anymore and the vesicles start to coalesce (Miller, 1971; Figueira & Stoops, 1983). Their walls become laminated with clay and carbonates and they eventually collapse (Sullivan & Koppi, 1991). According to Anderson et al. (2002) translocation takes place along the vertical aggregate boundaries and then into the aggregate by matrix suction and along horizontal channel pores. Therefore, in accordance with Sulli-

van & Koppi (1991), the translocated clay is not "illuvial" *sensu stricto*. Gradual transformation of an active vesicle formation zone to a zone of dominantly prolonged objects, parallel to the surface (e.g. McFadden et al., 1998; Anderson et al., 2002) might be a consequence of continuous and moderate dust influx. However, neither natural nor artificial vesicular structure from this study showed any robust correlation between object depth below surface and shape parameters or a-axes angle deviation from the horizontal plane.

The relationship between stone pavements and underlying vesicular horizons has been discussed by several authors (Springer, 1958; McFadden et al., 1986, 1998; Anderson et al., 2002; Dietze & Kleber, 2012). Maintenance of a stone pavement at the surface is usually attributed to doming of the Av horizon aggregates. However, the lifting of stones by escaping gas bubbles after rapid wetting may be a further mechanism which prevents stones from burial. This process may be especially relevant to further close a stone pavement which can no longer be modified by any externally forced, lateral process (cf. Dietze & Kleber, 2012).

Vesicular horizons, if buried in accretionary profiles, may serve as proxies for palaeo-environmental conditions. The presented field data and experiment results showed that vesicular horizons may form under a wide variety of environmental factors. However, their limitation to sites with only marginal plant-root density may be used to qualitatively describe (palaeo-)environments of their formation. Furthermore, vesicle morphology (i.e. *LR*) may further be used to descriptively characterise the dust flux intensity during vesicle formation.

5.5 Conclusions

Quantitative examination of natural and artificial vesicular structure provides new insight into major processes of vesicle formation. Vesicles are persistent soil properties and form primarily by repeatedly advancing wetting fronts that lead to surface sealing, gas pressure increase, reduced inter-grain connection and, thus, growing of isolated spherical voids. Accordingly, high wetting rates, high sand and low calcium carbonate contents lead to larger and more spherical vesicles, whereas wetting type, drying temperature and electric conductivity have minor influence. A surface cover, which protects the underlying material from wetting and subsequent sealing, prevents vesicle formation. However, root activity is the most likely reason for limited occurrence of vesicular horizons in nature.

Vesicular structure may be the most obvious feature of vesicular horizons. Beyond vesicle formation further mechanisms affect the properties of this unique formation of semi-arid and arid environments: i) the incorporation of fine material together with lateral removal of coarse fractions of overlying loose material on stone-covered surfaces and ii) complete admixture of the loose material under a grass cover. Besides their restriction to regions with mean annual precipitation below 350 mm, well-rounded vesicles indicate moderate and continuous in-flux of aeolian material.

The genetic relationship between stone pavements and vesicular horizons may be complemented by another mechanism: air escaping from the soil lifts rock fragments repeatedly and may contribute to stone pavement maintenance.

Acknowledgements

We kindly thank Bernd Ullrich for providing access to XRD facilities and Heiner Siedel for microscopy time. Sebastian Schlapa is warmly thanked for his amazing experiment constructions. We especially acknowledge Elisabeth Dietze, Dominik Faust and Daniela Sauer for their input throughout the different stages of the manuscript. We further thank the editor and two reviewers for their invaluable comments and suggestions.

References

Anderson, K., Wells, S.G., Graham, R.C., 2002. Pedogenesis of vesicular horizons, Cima Volcanic Field, Mojave Desert, California. Soil Sci. Soc. Am. J. 66, 878-887.

Bazilevich, N.I., Gollerbakh, M.M., Litvinov, M.A., Rodin, L.E., Shteinberg, D.M., 1953. O roli biologicheskih faktorov v obrazovanii takyrov trasse Glavnogo Turkmenskogo kanala (The role of biological factors in the formation of takyrs along the course of the Main Turkmenistan Canal). Botan. Zhur. 38.

Beckmann, W., 1962. Zur Mikromorphometrie von Hohlräumen und Aggregaten im Boden. Z. Pflanz. Bodenkunde 99, 129-139.

Benson, L.V., Smoot, J.P., Kashgarian, M., Sarna-Wojcicky, A., Burdett, J.W., 1997. Radiocarbon ages and environments of deposition of the Wono and Trego Hot Springs Tephra Layers in the Pyramid Lake Subbasin, Nevada. Quat. Res. 47, 251-260.

Best, M.G., McKee, E.H., Damon, P.E., 1980. Space-time-composition pattern of late Cenozoic mafic volcanism, southwestern Utah and adjoining areas. Am. J. Sci. 280, 1035-1050.

Birkeland, P.W., 1999. Soils and Geomorphology. 3rd ed., Oxford University Press, New York, Oxford.

Bisdom, E.B.A., Schoonderbeek, D., 1983. The characterization of the shape of mineral grains in thin sections of soils by quantimet and besi. Geoderma 30, 303-322.

Blank, R.R., Young, J.A., Lugaski, T., 1996. Pedogenesis on talus slopes, the Buckskin range, Nevada, USA. Geoderma 71, 121-142.

Bouza, P., Del Valle, H.F., Imbellone, P.A., 1993. Micromorphological, physical, and chemical characteristics of soil crust types of the central Patagonia region, Argentina. Arid Soil Res. Rehab. 7, 355-368.

Brown, K.J., Dunkerley, D.L., 1996. The influence of hillslope gradient, regolith texture, stone size and stone position on the presence of a vesicular layer and related aspects of hillslope hydrologic processes: a case study from the Australian arid zone. Catena 26, 71-84.

Burr, T.N., Currey, D.R., 1988. The Stockton Bar. Utah Geol. Mineral. Survey Misc. Pub. 88-1, 66-73.

Collins, J.F., Smillie, G.W., Hussain, S.M., 1986. Laboratory studies of crust development in Irish and Iraqi soils. III. Micromorphological observations of artificially-formed crusts. Soil Till. Res. 6, 337-350.

Dan, J., Yaalon, D.H., Moshe, R., Nissim, S., 1982. Evolution of reg soils in Southern Israel and Sinai. Geoderma 28, 173-202.

Das, A., Datta, B., 1987. Effect of electrolyte solution on saturated hydraulic conductivity of soils varying in clay type and content, and iron oxides. Z. Pflanz. Bodenkunde 150, 187-192.

Dietze, M., Kleber, A., 2012. Contribution of lateral processes to stone pavement formation in deserts inferred from clast orientation patterns. Geomorphology 139-140, 172-187.

Dietze, M., Muhs, S., Dietze, E., 2011. Ambiguities of relative age indicators on abandoned surfaces of arid environments. Z. Geomorphol. 55, Suppl. issue 3, 49-75.

Evans, S.H., Jr., Crecraft, H.R., Nash, W.P., 1980. K/Ar ages of silicic volcanism in the Twin Peaks/Cove Creek dome area. Isochron/West 28, 21-24.

Evenari, M., Yaalon, D., Gutterman, Y., 1974. Note on soils with vesicular structure in deserts. Z. Geomorphol. 18, 162-172.

Figueira, H., Stoops, G., 1983. Application of micromorphometric techniques to the experimental study of vesicular layer formation. Pédologie 33, 77-89.

Godsey, H.S., Currey, D.R., Chan, M.A., 2005. New evidence for an extended occupation of the Provo shoreline and implications for regional climate change, Pleistocene Lake Bonneville, Utah, USA. Quat. Res. 63, 212-223.

Grabowski, R.C., Droppo, I.G., Wharton, G., 2011. Erodibility of cohesive sediment: The importance of sediment properties. Earth-Science Reviews 105, 101-120.

Griffiths, P.G., Hereford, R., Webb, R.H., 2006. Sediment yield and runoff frequency of small drainage basins in the Mojave Desert, U.S.A. Geomorphology 74, 232-244.

Hugie, V.K., Passey, H.B., 1964. Soil Surface Patterns of some Semiarid Soils in Northern Utah, Southern Idaho, and Northeastern Nevada. Soil Sci. Soc. Am. J. 28, 786-792.

Lovich, J.E., Bainbridge, D., 1999. Anthropogenic degradation of the southern California desert ecosystem and prospects for natural recovery and restoration. Environ. Manage. 24, 309-326.

McAuliffe, J.R., McDonald, E.V., 2006. Holocene environmental change and vegetation contraction

in the Sonoran Desert. Quat. Res. 65, 204-215.

McFadden, L.D., Wells, S.G., Dohrenwend, J.C., 1986. Influences of quaternary climatic changes on processes of soil development on desert loess deposits of the Cima volcanic field, California. Catena 13, 361-389.

McFadden, L.D., Wells, S.G., Brown, W.J., Enzel, Y., 1992. Soil Genesis on Beach Ridges of Pluvial Lake Mojave: Implications for Holocene Lacustrine and Eolian Events in the Mojave Desert, Southern California. Catena 19, 77-97.

McFadden, L.D., McDonald, E.V., Wells, S.G., Anderson, K., Quade, J., Forman, S.L., 1998. The vesicular layer and carbonate collars of desert soils and pavements: formation, age and relation to climate change. Geomorphology 24, 101-145.

Meadows, D.G., Young, M.H., McDonald, E.V., 2008. Influence of relative surface age on hydraulic properties and infiltration on soils associated with desert pavements. Catena 72, 169-178.

Miller, D.E., 1971. Formation of Vesicular Structure in Soil. Soil Sci. Soc. Am. J. 35, 635-637.

NCDC, 2012. National Climatic Data Center. http://www.ncdc.noaa.gov/oa/ncdc.html [27.05.2012].

Oviatt, C.G., 1988. Late Pleistocene and Holocene lake fluctuations in the Sevier Lake Basin, Utah, USA. J. Paleolimnol. 1, 9-21.

Oviatt, C.G., 1991. Quaternary Geology of the Black Rock Desert, Millard County, Utah. Utah Geological and Mineral Survey, Special Studies 73.

Oviatt, C.G., Nash, W.P., 1989. Late Pleistocene basaltic ash and volcanic eruptions in the Bonneville basin, Utah. Geol. Soc. Amer. Bull. 101, 292-303.

Oviatt, C.G., Currey, D.R., Sack, D., 1992. Radiocarbon chronology of Lake Bonneville, Eastern Great Basin, USA. Palaeogeogr. Palaeocl. Palaeoecol. 99, 225-241.

Paletskaya, L., Lavrov, A., Kogan, S., 1958. Pore formation in takyr crust. Sov. Soil Sci. 3, 245-250.

Peterson, F.F., 1980. Holocene desert soil formation under sodium salt influence in a playa- margin environment. Quat. Res. 13, 172-186.

Pierson, F.B., Blackburn, W.H., Van Vactor, S.S., Wood, J.C., 1994. Partitioning small scale spatial variability of runoff and erosion on sagebrush rangeland. Water Ressour. Bull. 30, 1081-1089.

Prose, D.V., Wilshire, H.G., 2000. The lasting effects of tank manouvers on desert soils and inter-shrub flora. USGS open file report OF 00-512.

Reheis, M.C., 2003. Dust deposition in Nevada, California, and Utah, 1984-2002. USGS open file report OF 03-138, 66.

Schlapa, S., 2009. Experimentelle Untersuchungen zur Formation von Wüstenpflastern und Vesikularhorizonten. Unpublished Diploma Thesis, Technische Universität Dresden.

Schlichting, E., Blume, H.P., Stahr, K., 1995. Bodenkundliches Praktikum. Pareys Studientexte 81. 2nd ed., Blackwell, Berlin.

Schmidt, J.-U., 2008. Bodenevolution während der letzten 30.000 Jahre in der Black Rock Desert, W Utah, SW USA. Unpublished Diploma Thesis, Technische Universität Dresden.

Soil Survey Division Staff, 1993. Soil Survey Manual. Soil Conservation Service. U.S. Department of Agriculture Handbook 18.

Spelz, R.M., Fletcher, J.M., Owen, L.A., Caffee, M.W., 2008. Quaternary alluvial-fan development, climate and morphologic dating of fault scarps in Laguna Salada, Baja California, Mexico. Geomorphology 102, 578-594.

Springer, M.E., 1958. Desert Pavement and Vesicular Layer of Some Soils of the Desert of the Lahontan Basin, Nevada. Soil Sci. Soc. Am. J. 22, 63-66.

Stoops, G., 2003. Guidelines for Analysis and Description of Soil and Regolith Thin Sections. Madison, Wisconsin, Soil Science Society of America.

Sullivan, L.A., Koppi, A.J., 1991. Morphology and genesis of silt and clay coatings in the vesicular layer of a desert loam soil. Aust. J. Soil Res. 29, 579-586.

Sweeney, M.R., McDonald, E.V., Etyemezian, V., 2011. Quantifying dust emissions from desert landforms, eastern Mojave Desert, USA. Geomorphology 135, 21-34.

Turrin, B.D., Dohrenwend, J.C., Drake, R.E., Curtis, G.H., 1985. K-Ar ages from Cima volcanic field, eastern Mojave Desert, California. Isochron/West 44, 9-16.

Volk, O.H., Geyger, E., 1970. "Schaumböden" als Ursache der Vegetationslosigkeit in ariden Gebieten. Zeitschrift für Geomorphologie N.F. 14, 79-95.

Wells, S.G., Dohrenwendt, J.C., McFadden, L.D., Turrin, B.D., Mahrer, K.D., 1985. Late Cenozoic landscape evolution on lava flow surfaces of the Cima Volcanic field, Mojave Desert, California. Geol. Soc. Amer. Bull. 96, 1518-1529.

West, N.E., Young, J.A., 2000. Intermountain Valleys and Lower Mountain Slopes, in: Barbour, M.G., Billings, W.D. (Eds.), North American Terrestrial Vegetation. 2 ed., Cambridge University Press, Cambridge, pp. 255-284.

Wood, Y.A., Graham, R.C., Wells, S.G., 2005. Surface control of desert pavement pedologic process and landscape function, Cima Volcanic field, Mojave Desert, California. Catena 59, 205-230.

Yonovitz, M., Drohan, J., 2009. Pore morphology characteristics of vesicular horizons in undisturbed and disturbed arid soils; implications for arid land management. Soil Use and Management 25, 293-302.

Young, M.H., McDonald, E.V., Caldwell, T.G., Benner, S.G., Meadows, D.G., 2004. Hydraulic Properties of a Desert Soil Chronosequence in the Mojave Desert, USA. Vadose Zone J. 3, 956-963.

Appendix

Table 5.A.1. Descriptive statistics of natural and artificial samples. Values for each sample and parameter are quantile $_{0.25}$ - quantile $_{0.50}$ - quantile $_{0.75}$. Note the different units for natural (upper section) and artificial (lower section) samples. The second column comprises the main differing sample properties. Number of samples (n) refers to the total number of digitised objects. Lobation ratio is calculated after Beckmann (1962), *A-Pe²* ratio after Bisdom & Schoonderbeek (1983), i.e. the initial ratio is multiplied by 10^3.

ID (natural)	***MAP [mm]***	***n***	***Area [10^{-7} m²]***	***Perimeter [10^{-3} m]***
LS-01	80	79	166.53 - 250.6 - 393.6	5.00 - 6.50 - 7.70
LS-02	80	55	110.1 - 146.31 - 149.9	4.50 - 4.86 - 5.90
CF-01	161	108	33.62 - 45.33 - 69.40	2.33 - 2.93 - 3.35
CF-04	161	101	22.92 - 44.34 - 69.98	1.95 - 2.64 - 3.40
RP-01	200	95	11.72 - 19.42 - 28.98	1.46 - 1.87 - 2.51
VR-01	219	70	42.77 - 65.92 - 117.33	2.82 - 3.48 - 4.40
PM-01	229	50	146.8 - 238.6 - 340.5	5.56 - 8.19 - 10.86
PM-02	229	101	61.81- 100.5- 143.4	3.61 - 5.31 - 7.05
PB-01	276	111	47.90 - 73.39 - 119.85	3.05 - 3.91 - 5.22
NT-01	293	58	22.29 - 30.07 - 34.87	1.90 - 2.21 - 2.76
LR-01	310	52	50.16 - 59.81 - 69.68	2.78 - 3.22 - 3.53
TH-01	329	161	87.7 - 135.3 - 199.5	3.99 - 4.90 - 6.18
SB-01	330	141	15.33 - 22.49 - 30.98	1.65 - 1.97 - 2.48
ID (artificial)	***characteristic property***	***n***	***Area [10^{-9} m²]***	***Perimeter [10^{-4} m]***
Z_W_II	60 ml, flooding	237	12.37 - 19.04 - 28.94	4.62 - 5.73 - 7.46
Z_W_IV	60 ml, spraying	229	4.50 - 6.05 - 12.15	2.65 - 3.29 - 4.54
Z_W40	40 ml, raining	417	11.05 - 14.07 - 18.21	4.47 - 5.12 - 6.27
Z_W60	60 ml, raining	206	6.00 - 10.83 - 24.13	3.24 - 4.36 - 6.54
Z_W80	80 ml, raining	435	18.84 - 35.63 - 58.23	5.45 - 7.44 - 10.22
Z_W100	100 ml, raining	134	21.53 - 45.99 - 97.78	5.79 - 8.46 - 12.25
Z_T100	105 °C temperature	218	3.52 - 5.39 - 8.04	2.33 - 2.98 - 3.82
Z_S00	0 % sand	628	15.61 - 20.35 - 26.75	5.25 - 5.81 - 6.87
Z_S10	10 % sand	417	11.05 - 14.07 - 18.21	4.47 - 5.12 - 6.27
Z_S20	20 % sand	117	30.18 - 45.38 - 69.72	6.74 - 8.14 - 10.08
TH_01	26 % sand	359	10.87 - 21.43 - 35.93	4.03 - 5.84 - 7.69
Z_S30	30 % sand	141	31.16 - 60.85 - 106.94	6.91 - 9.60 - 13.34
Z_S50	50 % sand	91	67.6 - 118.6 - 166.1	11.01 - 13.25 - 16.43
Z_S70	70 % sand	60	25.60 - 47.36 - 176.85	6.23 - 8.43 - 16.30
Z_E00	0 µS/cm	417	11.05 - 14.07 - 18.21	4.47 - 5.12 - 6.27
Z_E08	810 µS/cm	294	6.71 - 10.33 - 17.32	3.28 - 4.16 - 5.43
Z_E13	1260 µS/cm	296	8.22 - 11.44 - 15.99	3.62 - 4.50 - 5.27
Z_E21	2120 µS/cm	428	13.65 - 17.00 - 22.16	4.74 - 5.37 - 6.30
Z_E34	3400 µS/cm	231	14.39 - 23.69 - 37.59	4.81 - 6.18 - 7.88
Z_E56	5570 µS/cm	177	6.17 - 10.84 - 22.21	3.00 - 4.15 - 5.91
Z_C01	0.8 % carbonate	417	11.05 - 14.07 - 18.21	4.47 - 5.12 - 6.27
Z_C02	2.4 % carbonate	264	9.70 - 12.11 - 18.73	3.87 - 4.50 - 5.43
Z_C05	4.6 % carbonate	341	6.87 - 8.73 - 12.98	3.34 - 4.02 - 5.01
Z_C10	9.6 % carbonate	232	4.50 - 6.98 - 10.48	2.71 - 3.49 - 4.23
Z_C15	13.4 % carbonate	204	2.11 - 3.26 - 5.03	1.91 - 2.27 - 2.90
Z_C30	27.8 % carbonate	272	2.03 - 2.86 - 4.57	1.83 - 2.16 - 2.73

Table 5.A.1., continued

a axes length [10^{-4} m]	*b axes length [10^{-4} m]*	*a-b-axes product [10^{-7} m²]*	*Lobation ratio*	*A/Pe² ratio*
15.72 - 23.19 - 31.63	9.67 - 13.44 - 20.95	15.72 - 31.01 - 70.91	1.13 - 1.20 - 1.38	57.66 - 66.47 - 70.35
15.52 - 16.91 - 22.55	7.77 - 11.29 - 13.08	11.21 - 19.54 - 23.59	1.19 - 1.45 - 1.84	43.35 - 54.90 - 67.00
7.52 - 10.96 - 14.79	4.28 - 6.05 - 9.29	3.05 - 6.05 - 11.44	1.16 - 1.29 - 1.45	54.90 - 61.91 - 68.42
7.01 - 10.63 - 15.23	4.03 - 6.57 - 9.48	2.52 - 6.94 - 13.49	1.18 - 1.25 - 1.40	56.72 - 63.43 - 67.70
4.13 - 6.27 - 10.65	2.30 - 3.51 - 5.39	1.09 - 2.34 - 5.72	1.27 - 1.47 - 1.87	42.57 - 54.11 - 62.46
8.47 - 12.45 - 18.78	5.02 - 6.77 - 11.54	4.81 - 7.23 - 19.76	1.17 - 1.29 - 1.52	52.23 - 61.77 - 68.28
13.12 - 20.94 - 30.82	7.89 - 10.66 - 15.15	10.24 - 19.22 - 46.68	1.58 - 1.96 - 2.45	32.48 - 40.56 - 50.33
8.51 - 13.59 - 20.00	5.12 - 6.92 - 9.83	4.31 - 8.09 - 19.66	1.29 - 1.46 - 1.61	49.41 - 54.56 - 61.86
8.91 - 13.46 - 18.44	4.43 - 6.99 - 11.03	3.68 - 9.28 - 17.24	1.31 - 1.58 - 2.41	33.00 - 50.45 - 60.66
4.81 - 7.67 - 9.63	3.18 - 4.49 - 5.93	1.61 - 3.72 - 5.39	1.17 - 1.33 - 1.79	44.57 - 60.01 - 67.90
7.07 - 9.08 - 11.24	4.44 - 5.90 - 7.36	3.59 - 5.34 - 7.21	1.19 - 1.32 - 1.35	58.84 - 60.40 - 67.05
11.87 - 16.70 - 24.65	7.46 - 9.56 - 14.07	9.23 - 15.83 - 33.21	1.22 - 1.38 - 1.61	49.47 - 57.74 - 65.47
4.93 - 7.04 - 9.26	3.07 - 3.85 - 4.80	1.59 - 2.47 - 4.44	1.28 - 1.39 - 1.66	47.99 - 57.37 - 62.41
a axes length [10^{-5} m]	***b axes length [10^{-5} m]***	***a-b-axes product [10^{-9} m²]***	***Lobation ratio***	***A/Pe² ratio***
14.13 - 19.73 - 28.47	8.87 - 11.04 - 15.46	12.53 - 21.78 - 44.01	1.19 - 1.36 - 1.57	50.73 - 58.52 - 66.98
9.17 - 12.08 - 16.44	5.71 - 6.69 - 8.90	5.51 - 8.06 - 14.34	1.14 - 1.25 - 1.44	55.38 - 63.84 - 69.91
15.27 - 19.11 - 25.88	7.43 - 9.09 - 11.70	11.35 - 17.37 - 30.28	1.27 - 1.48 - 1.81	43.96 - 53.66 - 62.51
9.34 - 14.68 - 27.75	5.53 - 8.62 - 15.26	5.17 - 12.65 - 42.35	1.18 - 1.30 - 1.47	54.22 - 61.17 - 67.52
16.74 - 28.45 - 42.65	9.51 - 15.50 - 24.39	15.92 - 44.10 - 104.02	1.14 - 1.23 - 1.42	55.84 - 64.79 - 70.11
8.20 - 12.45 - 28.50	5.41 - 8.02 - 21.23	4.44 - 9.98 - 60.51	1.14 - 1.26 - 1.33	59.90 - 63.25 - 70.03
8.66 - 10.63 - 14.47	5.22 - 6.08 - 7.99	4.35 - 6.76 - 10.51	1.12 - 1.30 - 1.49	53.59 - 61.30 - 69.17
18.07 - 21.57 - 28.31	9.75 - 11.82 - 15.23	17.62 - 25.50 - 43.12	1.19 - 1.30 - 1.56	50.90 - 61.35 - 66.63
15.27 - 19.11 - 25.88	7.43 - 9.09 - 11.70	11.35 - 17.37 - 30.28	1.27 - 1.48 - 1.81	43.96 - 53.66 - 62.51
21.65 - 29.33 - 37.78	11.81 - 18.36 - 26.63	25.57 - 53.85 - 100.61	1.10 - 1.22 - 1.36	58.60 - 65.07 - 72.31
11.66 - 20.26 - 32.92	7.19 - 12.03 - 18.98	8.38 - 24.37 - 62.48	1.12 - 1.22 - 1.42	56.18 - 65.12 - 71.01
22.00 - 35.55 - 56.00	13.42 - 23.30 - 38.94	29.52 - 82.83 - 218.06	1.10 - 1.20 - 1.40	56.66 - 66.18 - 72.67
33.80 - 49.62 - 67.85	20.82 - 30.90 - 44.97	70.4 - 153.3 - 305.1	1.13 - 1.20 - 1.36	58.72 - 66.11 - 70.53
20.33 - 24.96 - 64.84	12.03 - 18.86 - 44.73	24.46 - 47.07 - 290.03	1.14 - 1.24 - 1.40	56.87 - 64.05 - 70.10
15.27 - 19.11 - 25.88	7.43 - 9.09 - 11.70	11.35 - 17.37 - 30.28	1.27 - 1.48 - 1.81	43.96 - 53.66 - 62.51
10.14 - 15.07 - 22.14	6.45 - 9.13 - 13.28	6.54 - 13.76 - 29.40	1.13 - 1.31 - 1.50	52.95 - 60.70 - 70.31
12.33 - 15.45 - 21.71	6.88 - 8.63 - 11.64	8.48 - 13.33 - 25.27	1.20 - 1.27 - 1.49	53.32 - 62.85 - 66.28
16.28 - 20.12 - 26.62	9.87 - 11.43 - 14.56	16.07 - 23.00 - 38.76	1.15 - 1.28 - 1.53	52.00 - 62.16 - 69.46
14.43 - 21.90 - 31.26	8.76 - 13.09 - 18.09	12.64 - 28.67 - 56.55	1.13 - 1.25 - 1.49	53.52 - 63.56 - 70.16
9.49 - 15.99 - 28.05	5.90 - 10.44 - 16.89	5.60 - 16.69 - 47.38	1.11 - 1.20 - 1.35	58.77 - 66.58 - 71.46
15.27 - 19.11 - 25.88	7.43 - 9.09 - 11.70	11.35 - 17.37 - 30.28	1.27 - 1.48 - 1.81	43.96 - 53.66 - 62.51
12.15 - 15.44 - 19.62	7.46 - 9.44 - 13.47	9.06 - 14.58 - 26.43	1.10 - 1.18 - 1.38	57.53 - 67.27 - 72.56
10.67 - 13.99 - 20.85	6.37 - 8.24 - 10.44	6.80 - 11.53 - 21.77	1.19 - 1.34 - 1.60	49.87 - 59.43 - 66.75
7.72 - 11.14 - 16.30	5.01 - 6.88 - 10.74	3.87 - 7.66 - 17.51	1.13 - 1.26 - 1.50	52.99 - 63.01 - 70.14
6.25 - 8.12 - 13.94	3.82 - 4.85 - 8.21	2.39 - 3.94 - 11.44	1.14 - 1.24 - 1.39	57.09 - 64.04 - 70.01
5.74 - 7.54 - 10.72	3.47 - 4.62 - 6.52	1.99 - 3.48 - 6.99	1.15 - 1.28 - 1.51	52.68 - 62.14 - 69.22

Table 5.A.2. Mean coefficients of determination (R^2 after Pearson) for natural (n = 13) and artificial (n = 24) samples. σ R^2 represents one sigma scatter. R^2 greater than 0.5 are in bold. P1 and P2 indicate correlated vesicle parameters: *A* – area, *Pe* – perimeter, *a* – a axis length, *b* – b axis length, *LR* – lobation ration after Beckmann (1962), *A-Pe²* ratio – ratio after Bisdom & Schoonderbeek (1983), *Δ φ* – deviation of a axis angle from the horizontal line.

Parameters		***Natural samples***	***Artificial samples***
P1	***P2***	***R^2±σR^2***	***R^2±σR^2***
A	Pe	0.70±0.20	0.83±0.10
A	a	0.54±0.19	0.69±0.14
A	b	0.47±0.21	0.68±0.17
A	axes product	0.72±0.25	0.90±0.07
a	b	0.15±0.16	0.33±0.23
LR	A-Pe² ratio	0.88±0.11	0.92±0.04
depth	A	0.03±0.05	0.01±0.02
depth	Pe	0.05±0.06	0.01±0.01
depth	a	0.06±0.06	0.02±0.01
depth	b	0.04±0.06	0.02±0.02
depth	axes product	0.03±0.03	0.01±0.01
depth	LR	0.07±0.11	0.05±0.04
depth	A-Pe² ratio	0.07±0.11	0.05±0.05
Δ ϕ	A	0.04±0.06	0.02±0.02
Δ ϕ	Pe	0.01±0.01	0.02±0.02
Δ ϕ	a	0.04±0.03	0.01±0.01
Δ ϕ	b	0.04±0.03	0.01±0.01
Δ ϕ	axes product	0.03±0.03	0.01±0.01
Δ ϕ	D	0.05±0.07	0.02±0.02
Δ ϕ	LR	0.03±0.05	0.01±0.01
Δ ϕ	A-Pe² ratio	0.03±0.04	0.01±0.02

6 Environmental history recorded in stone pavement-covered soil-sediment complexes

Chapter 6 is submitted to the peer-reviewed journal Journal of Quaternary Research (ISSN 1099-1417) as:

Environmental history recorded in stone pavement-covered soil-sediment complexes, Cima volcanic field, USA.

Authors: Michael Dietze[1], Elisabeth Dietze[2], Arno Kleber[1]

[1] Institute of Geography, Technische Universität Dresden

[2] Institute of Geographical Sciences (EDCA)

Publication history: submitted: 29.06.2012

Full reference: Dietze M, Dietze E, Kleber A. (submitted). Environmental history recorded in stone pavement-covered soil-sediment complexes, Cima volcanic field, USA. Journal of Quaternary Science.

Internet link: not available

Abstract: Palaeo-environmental information of arid landscapes is typically recorded in terminal basins which hosted lakes during pluvial periods but which may suffer from desiccation-caused record hiatuses. Accretionary soil-sediment-successions may serve as corresponding archives. A special type of accretionary system is coupled to stone pavements. On a basalt flow in California, six stone pavement-covered soil profiles are used for correlation and development of a profile evolution model. Soil morphological, texture, physical and chemical data is used to quantify genetic processes through end-member modelling analysis (EMMA).

The accumulated sequence consists of a rubble zone, a transition zone and three separate units of predominantly aeolian origin. Each unit is covered by an individual generation of stone pavement. The modelled end-members (local detritus, proximal sand, proximal dust, remote dust, pedogenesis) allow quantifying palaeo-environmental processes that formed the archive. There is a substantial temporal offset between lava flow emplacement and accumulation of the aeolian mantle. The latter comprises three phases of enhanced sediment flux caused by an unstable level of Lake Mojave. Vegetation is suggested as the key driver of sediment accretion and stone pavement burial. Only during periods of environmental instability stone pavements are able to recover or to form a new generation.

Keywords

Palaeosol; Terrestrial archive; Landscape evolution; End-member modelling; Mojave Desert

6.1 Introduction

Palaeo-environmental studies typically base on the evaluation of archives, which have recorded signals by a variety of proxies. However, in arid environments such archives are sparse. Arid landscapes may certainly preserve the geomorphologic history of individual landforms (Laity, 2008), but do not support well continuous archives. Exceptions are closed terminal lake basins (e.g. Mensing, 2001; Wells et al., 2003), which may have hosted fresh water bodies during pluvial periods of the Quaternary. Therefore, they may continuously record environmental signals. However, they may also suffer from temporal desiccation and thus from interrupted deposition, reworking or even erosion of previously deposited material. Accordingly, there is a need to include further environmental archives that essentially resolve these sedimentation hiatuses, such as sand ramps (Lancaster & Tchakerian, 1996), rock varnish micro-laminations (Liu & Broecker, 2008), packrat midden remnants (Betancourt et al., 1990), speleothems (Winograd et al., 1992) and soil-sediment successions (Chadwick & Davis, 1990; Kleber, 2000; Suchodoletz et al., 2009; Meszner et al., 2011). However, most of these archive types are often either discontinuous, cover only small time windows or are prone to reworking and erosion of their upper parts.

Accretionary systems may contain hiatuses to a lesser degree. A special type of accretionary soil development is related to a prominent surface type in arid environments: stone pavements. These are monolayers of varnish-coated clasts, ideally tightly packed. They are widespread on various landforms, although most often they are associated with alluvial fans. If there is a nearby dust source, they are underlain by several centimetres to a few metres of virtually stone-free aeolian dust (Wells et al., 1985; Dietze & Kleber, 2012).

According to a now generally accepted model (McFadden et al., 1986), the rough clast-covered surface traps aeolian material, which is deposited upon and between the stones. With subsequent rainfall events the fine materials become washed below the surface. There, they form a soil horizon, featuring isolated vesicular pores, which may measure up to a few millimetres: the vesicular horizon, Av, which is further characterised by coarse prismatic structure (Springer, 1958). Swell-shrink dynamics (i.e. ped doming) of the vesicular horizon maintain the clasts at the surface (McFadden et al., 1998; Anderson et al., 2002). Hence, stone pavement and vesicular horizon may act together to form a sediment column which thickens with time (McFadden et al., 1986). Accordingly, stone pavement-covered soil profiles may be valuable archives because they record periods of dust deposition and are least susceptible to profile truncation due to erosion.

The described model of dust accretion and stone pavement formation was developed based on field work in the eastern Mojave Desert, California, USA. This area has been in the focus of palaeo-environmental research for many decades. One of the latest comprehensive works is presented by Enzel et al. (2003). Special attention to accretionary, stone pavement-covered soils on lava flows is given by Wells et al. (1985) and McFadden et al. (1986). Dietze et al. (2011) compared age indicators on two of the lava flows and concluded that surface and soil profiles imply different histories. While the surface shows overall similar properties, soil properties may vary significantly within small spatial distance.

Such small-scale heterogeneity is difficult to interpret in terms of a generalised picture and calls for studying various closely spaced profiles, trying to correlate persistent properties, identifying extreme or exceptional features and developing a conclusive conceptual model of sediment and soil evolution. Based on a robust standard profile the extraction of quantitative environmental and geomorphological information may become possible. Properties of stone pavement-covered soil-sediment profiles may be attributed to environmental conditions that led to their formation as well as to thresholds that led to their fossilisation (Dietze & Kleber, 2012; Dietze et al., accpeted). Decomposition of multi-dimensional environmental data, such as grain size distributions, allows deciphering and quantifying process-related end-members (Weltje & Prins, 2007), which can be used to further characterise the formation history of the archives.

The scope of this paper is a detailed picture of the spatial heterogeneity of accretionary soil-sediment complexes on a basaltic lava flow of the Cima volcanic field. Correlation of profiles and composition of a standard profile serve as base for retrieving descriptive and quantitative environmental proxies. A profile evolution concept is developed which is consistent with published information derived from other archives of the wider study area.

6.2 Study area

Cima volcanic field is situated in the eastern Mojave Desert, USA (Figure 6.1). More than 40 cinder cones and associated lava flows rest at an elevation around 900 m a.s.l. on an alluvial plain. Climate is currently arid with mean annual precipitation of 69 to 160 mm and mean annual temperatures from 21 to 15 °C (climate stations in Baker, 320 m a.s.l., and Yucca Grove, 1204 m a.s.l.; NCDC, 2012). The surface of the investigated 560± 80 ka old lava flow (McFadden et al., 1986) is predominantly flat, dissected by shallow drainage channels or valleys, and shows some bedrock outcrops. Vegetation is restricted to drainage channels. The stone pavement at the investigated sites is well-varnished, tightly packed and composed of clasts with mean diameters of 53±11 mm (1σ, cf. Dietze & Kleber, 2012).

Landscape evolution of the wider area, especially the timing of enhanced dust activity, is closely related to the history of the Mojave River. During the Quaternary this stream fed at least four separate lake basins (Tchakerian & Lancaster, 2002). Lake Mojave, the most important one for this study area, covered the present Soda Lake and Silver Lake playas and was formed by the overspill of Manix Basin near the current location of Afton Canyon between 22.6 (Wells et al., 2003) or 18.1k (Meek, 2004) ^{14}C a BP. Wells et al. (2003) present a detailed history of Lake Mojave. Incipient (22.6k ^{14}C a BP) and intermittent (21.2k ^{14}C a BP) conditions lead to two stable lake phases (18.4 to 16.6 and 13.7 to 11.4k ^{14}C a BP). These were separated by drying events and intermittent conditions. Between 11.4 and 8.7k ^{14}C a BP an intermittent lake dominated. From 8.7k ^{14}C a BP the basin graded to the present day playa environment.

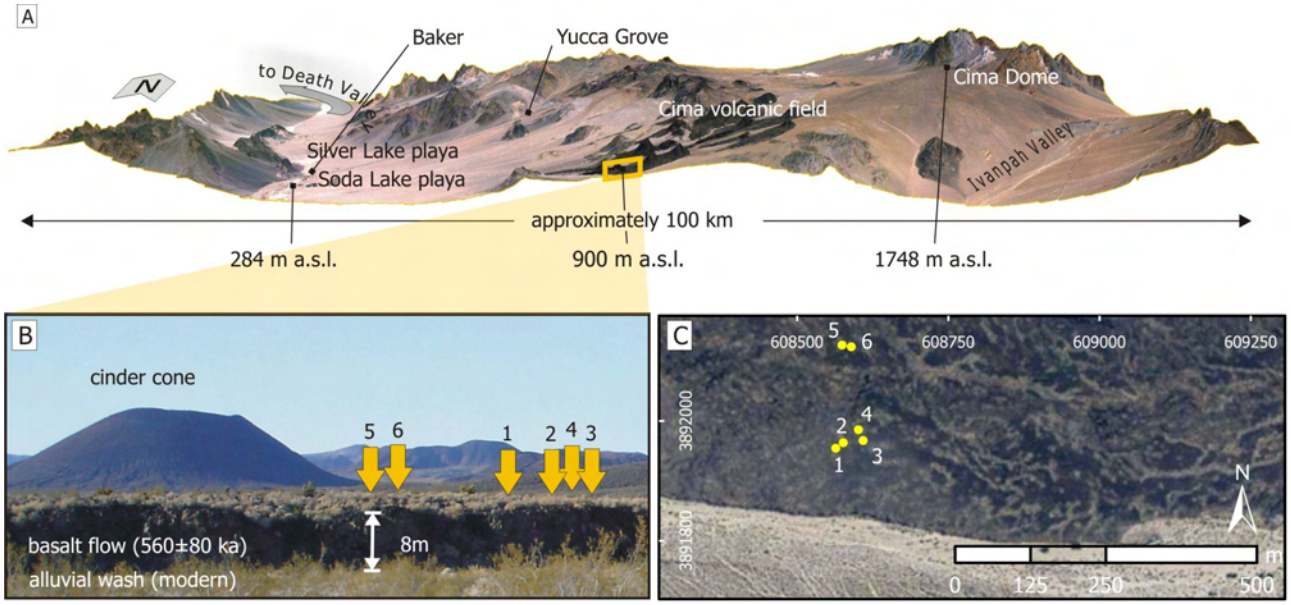

Figure 6.1. Environmental setting of the studied site. A: Perspective view (satellite image draped over a DEM) of the eastern Mojave Desert with the central Cima volcanic field resting on an alluvial plain, gently sloping from Cima Dome westwards to Soda Lake playa. Climate stations are located near Baker and Yucca Grove. B: View over the alluvial plain that is covered by the studied lava flow. The flow forms step of 8 m. A cinder cone is visible in the background. Yellow arrows indicate locations of studied soil profiles. C: Aerial image of the investigated lava flow. Yellow dots indicate studied soil profiles. Coordinates in UTM system zone 12N. Data source: Cal-Atlas (2009).

The first intermittent lake period is certainly related to the establishment of Lake Mojave after Lake Manix overspill. The latest intermittent period may represent the climatic transition from the latest Pleistocene to the Holocene. However, the intermittent period between 16.6 and 13.7k ^{14}C a BP may be explained either by a climatic shift towards drier conditions (Wells et al., 2003) or a spatial shift in the Mojave River course; according to Meek (2004), the river filled Coyote Basin and therefore caused a lake level drop in the Soda Lake and Silver Lake basins. Prior to the onset of Lake Mojave, alluvial fans and delta sediments were shed into the playas of Soda Lake and Silver Lake Basin. The playa area was smaller than today, and alluvial fan sediments consisted of gravel- to sand-sized particles. Pedogenetic calcium carbonate morphology up to stage VI indicates significant soil formation on these surfaces (Wells et al., 2003). Hence, material exposed to aeolian transport may have been limited.

6.3 Materials and Methods

6.3.1 Field and laboratory work

Detailed profile descriptions are already presented by Dietze et al. (2011). In the present paper the focus is on common properties of the profiles and on stratigraphic relationships with only a brief presentation of morphological features. The profiles were described in hand-dug pits in close

proximity to each other. Pedogenetic properties, including carbonate and gypsum morphology were described according to Harden et al. (1991), Soil Survey Division Staff (1993) and Birkeland (1999). Samples (vertical thickness 2 cm) were collected based on field descriptions.

Air-dried sub-samples (< 2000 µm) were used for measurements of calcium carbonate content, pH value (in KCl solution) and electric conductivity (10 g sample and 50 ml deionised water) as described in Schlichting et al. (1995). Grain size measurements (sieve-pipette method, no calcium carbonate removed) were conducted with the following class boudaries: 2, 5, 6.3, 10, 20, 50, 63, 80, 100, 125, 200, 250, 500, 630, 1000 and 2000 µm.

6.3.2 Statistical analysis and correlation work

Dietze et al. (2012) developed a MATLAB-based end-member modelling analysis (EMMA) algorithm for grain size composition data which uses the principals of factor analysis and different scaling procedures. End-member (EM) modelling goes beyond classical dimension reduction approaches for compositional data (cf. Weltje, 1997). It is assumed that single grain size distributions are composed of discrete EMs that may be interpreted as typical sedimentation processes (Dietze et al., 2012). EMMA unmixes the EM distributions (i.e. grain size loadings), keeps their original scale and quantifies their contribution to each sample (i.e. scores). This is especially reasonable for multi-modal grain size distributions, where standard univariate measures (e.g. mean, skewness, and kurtosis) fail.

A total of 60 samples (m) with 16 grain size classes (n) was used. The two main parameters that determine the modelling results are the range limits for the weight transformation (l_w) and the number of EM (q). These two parameters were systematically changed from $l_w = 0$ to $l_w = 0.2$ and from $q = 2$ to $q = 15$ to determine the optimal parameter configuration with respect to model robustness and reliability. Evaluation of the modelling results bases on mean absolute deviation of modelled from original data as well as on mean row-wise and mean column-wise R^2 between original and modelled data. However, the main aim is to find genetically meaningful EMs. Hence, as few EMs as possible were used according to the principal of parsimony (Weltje & Prins, 2007; Dietze et al., 2012).

Correlation of the profiles and construction of a standard profile based on consideration of morphological, sedimentological and chemical profile properties as well as on EM scores. Major stratigraphic units were delimited whenever features could not be exclusively attributed to pedogenetic origin but required a sedimentologic unconformity.

6.4 Results

6.4.1 Properties of soil-sediment complexes

Figure 6.2 shows sketches of the studied profiles. Horizon designations do not include layer boundaries at this stage. Profiles 1 to 3 are located along a very shallow slope hollow and lie 30 m apart from each other on a barren patch of the lava flow (figure 6.6A). Profile 4 is situated perpendicular to this sequence on the vegetation-covered margin of the slope hollow. Only 2 metres west of profile 1 large, angular blocks indicate a local bedrock outcrop. Profiles 5 and 6 are located 200 m north of the first topo-sequence. Profile 5 marks the central part of a barren stone pavement patch, approximately 80 m downslope of a 2 m high step, formed by a lava outcrop. Profile 6 is located in similar proximity to the lava outcrop but only a few metres from a vegetation-covered drainage channel.

Loose sediment directly underlying the stone pavement is interpreted as the most recently deposited material. It is very similar in grain size composition to the modern dust samples collected in this area by Reheis (2003). Directly below, a vesicular horizon is always present. Separated by a sharp boundary, a lower horizon of single grain or weakly to moderately developed, medium subangular blocky structure follows.

Many profiles show a complex pattern of grain size composition with depth. Calcium carbonate contents change considerably from profile to profile, from less than 1 to 17 %. However, there is no systematic pattern such as a common depth of leaching. Rather, abrupt changes are related to changes in grain size composition as also described by McFadden et al. (1986). A similar picture can be drawn from the EC values. Despite of commonly low values in the upper few decimetres, no systematic changes are visible that control the location of the maximum values (approximately 5.5 mS/cm). Soil pH ranges between 7.2 and 8.4 with no clear pattern.

Fossilised vesicular horizons and stone lines occur in some profiles. Stone lines were found at two typical depths: 12±4 and 55±8 cm. Dietze & Kleber (2012) measured clast length axes orientation and found preferred bimodal alignment patterns (rose diagrams in figure 6.2). The clasts are juvenile, virtually unweathered (figure 6.5C). In contrast, clasts at the bottom of the profiles are strongly weathered or nearly disintegrated, with abundant altered minerals (figure 6.5B). Furthermore, in the basal part of profile 2 a pocket is exposed, which is filled with virtually dust-free (no visible quartz grains) sand and gravel derived from basalt.

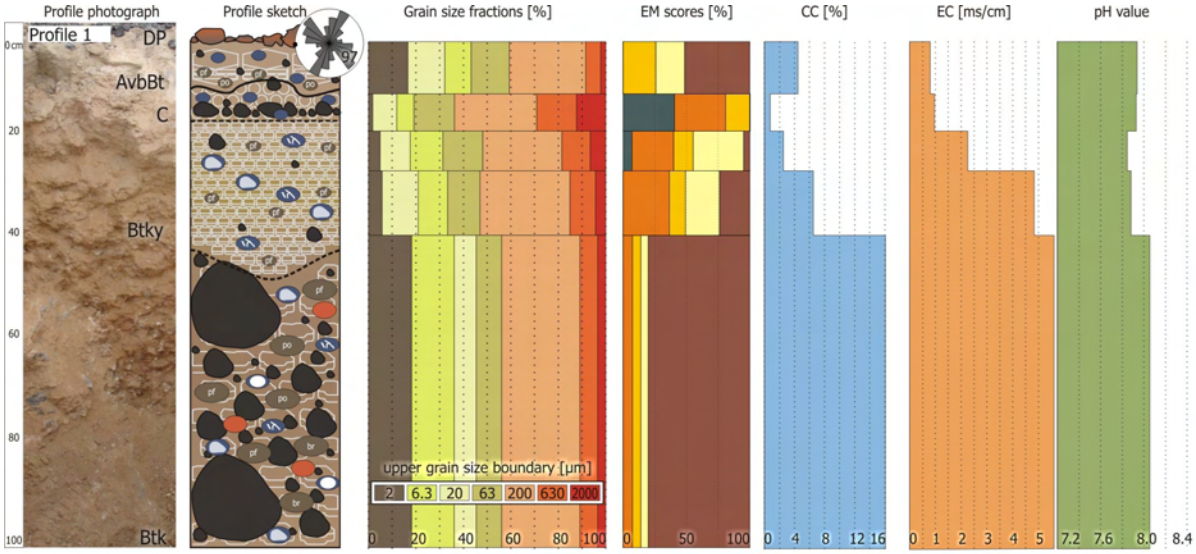
Profile photograph
Profile sketch
Grain size fractions [%]
EM scores [%]
CC [%]
EC [ms/cm]
pH value
Profile 1
DP
AvbBt
C
Btky
Btk
upper grain size boundary [µm]
2
6.3
20
63
200
630
2000
97

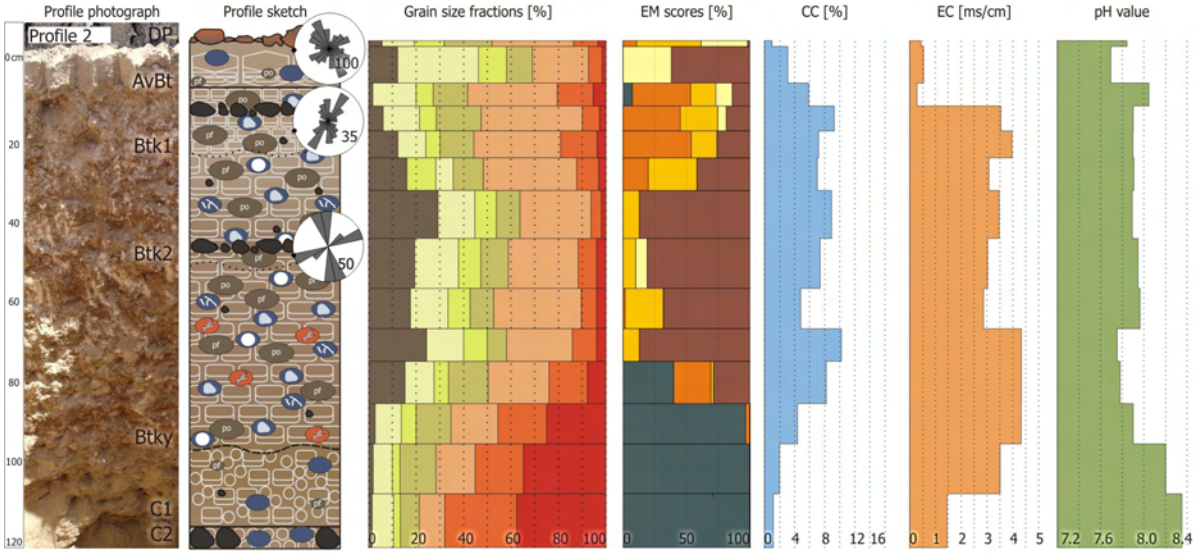
Profile photograph
Profile sketch
Grain size fractions [%]
EM scores [%]
CC [%]
EC [ms/cm]
pH value
Profile 2
DP
AvBt
Btk1
Btk2
Btky
C1
C2
100
35
50

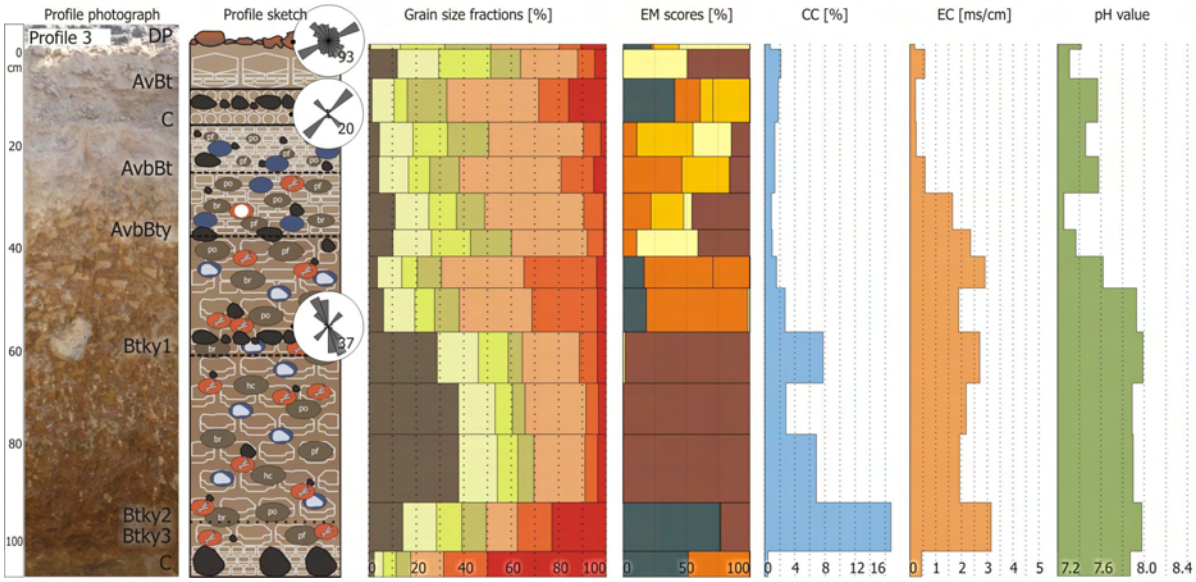
Profile photograph
Profile sketch
Grain size fractions [%]
EM scores [%]
CC [%]
EC [ms/cm]
pH value
Profile 3
DP
AvBt
C
AvbBt
AvbBty
Btky1
Btky2
Btky3
C
93
20
37

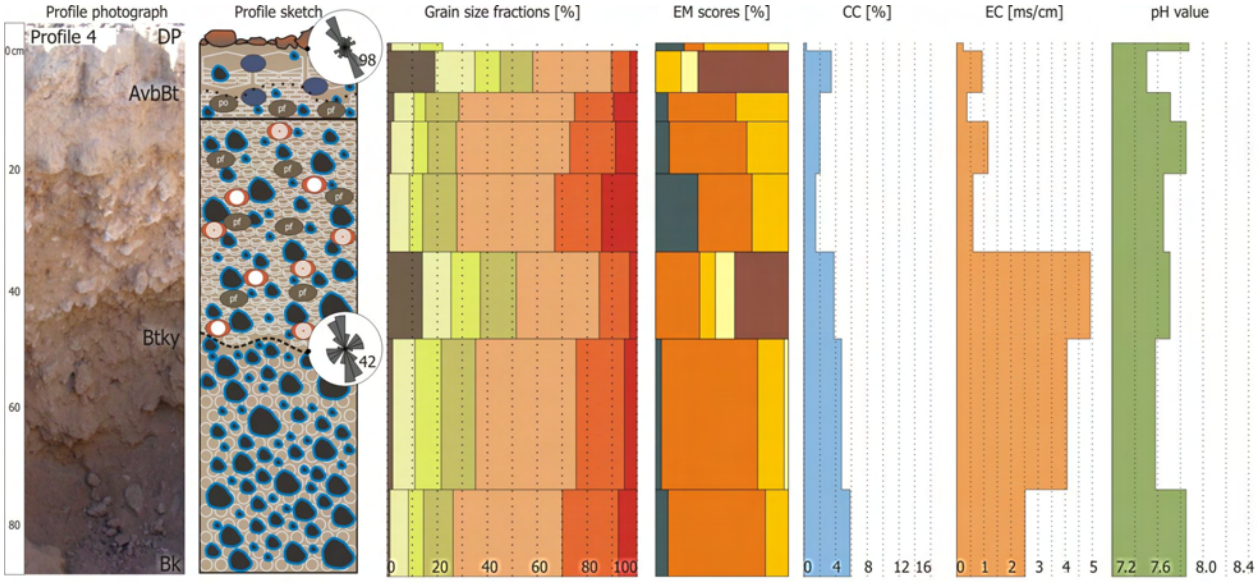
Profile photograph
Profile sketch
Grain size fractions [%]
EM scores [%]
CC [%]
EC [ms/cm]
pH value
Profile 4
DP
AvbBt
Btky
Bk
0cm
20
40
60
80
98
42
0 20 40 60 80 100
0 4 8 12 16
0 1 2 3 4 5
7.2 7.6 8.0 8.4

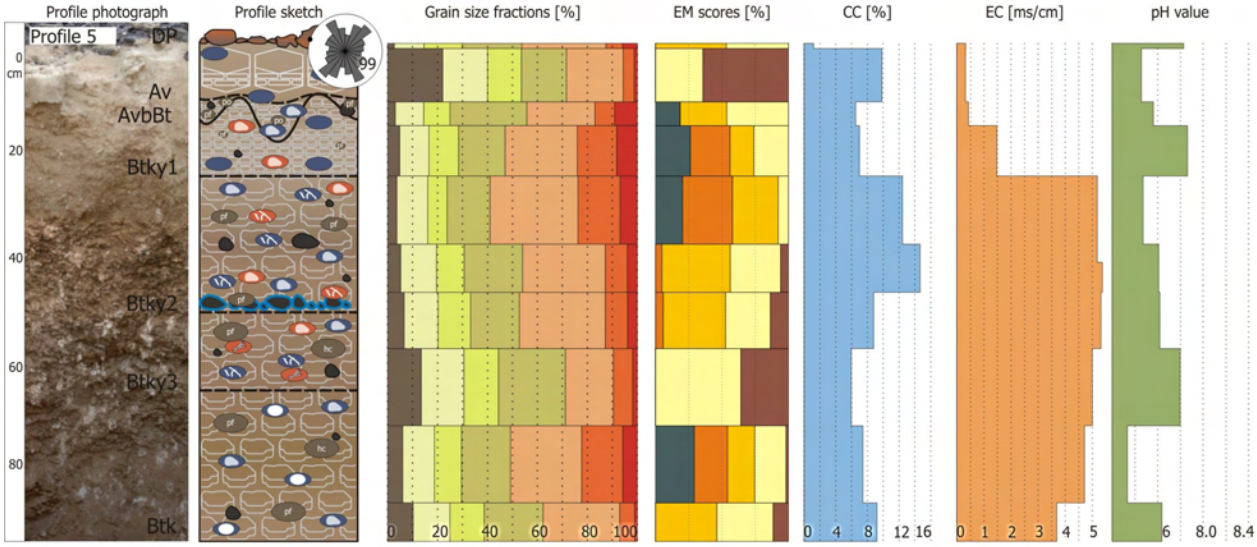
Profile photograph
Profile sketch
Grain size fractions [%]
EM scores [%]
CC [%]
EC [ms/cm]
pH value
Profile 5
DP
Av
AvbBt
Btky1
Btky2
Btky3
Btk
0
cm
20
40
60
80
99
0 20 40 60 80 100
0 4 8 12 16
0 1 2 3 4 5
6 8.0 8.4

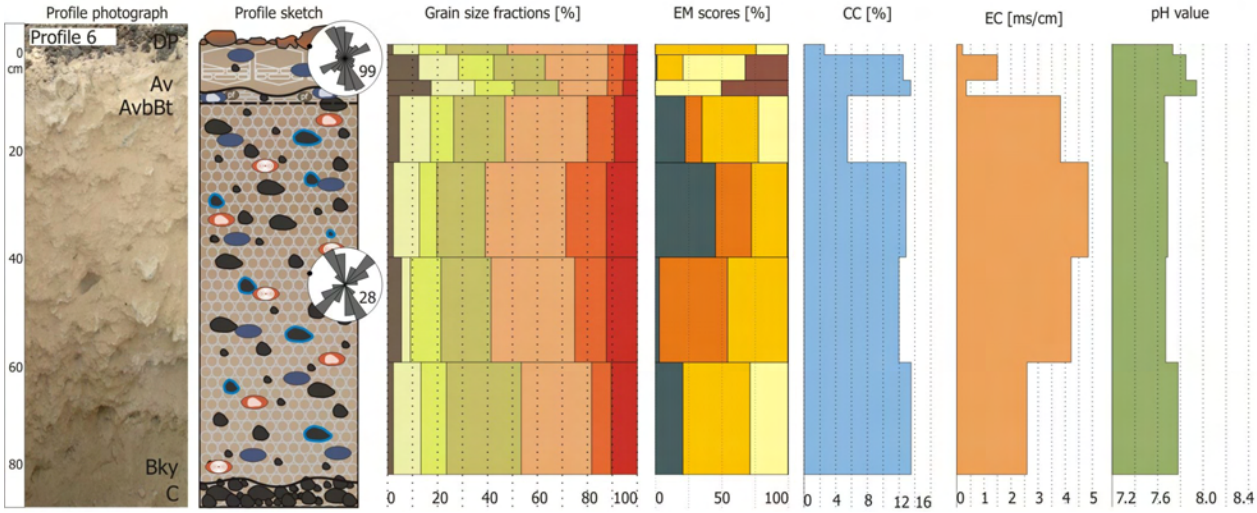
Profile photograph
Profile sketch
Grain size fractions [%]
EM scores [%]
CC [%]
EC [ms/cm]
pH value
Profile 6
DP
Av
AvbBt
Bky
C
0
cm
20
40
60
80
99
28
0 20 40 60 80 100
0 50 100
0 4 8 12 16
0 1 2 3 4 5
7.2 7.6 8.0 8.4

Figure 6.2. Morphology, texture, statistics and chemical properties of individual profiles. Rose diagrams show clast length axes orientations for modern and fossil stone pavements and for clast-rich profiles (number of samples provided in rose diagrams, data and treatment according to Dietze & Kleber, 2012). Grain size class legend see profile 1. EM scores: end-member scores, CC: calcium carbonate content, EC: electric conductivity. Legend of sketch elements in figure 6.3.

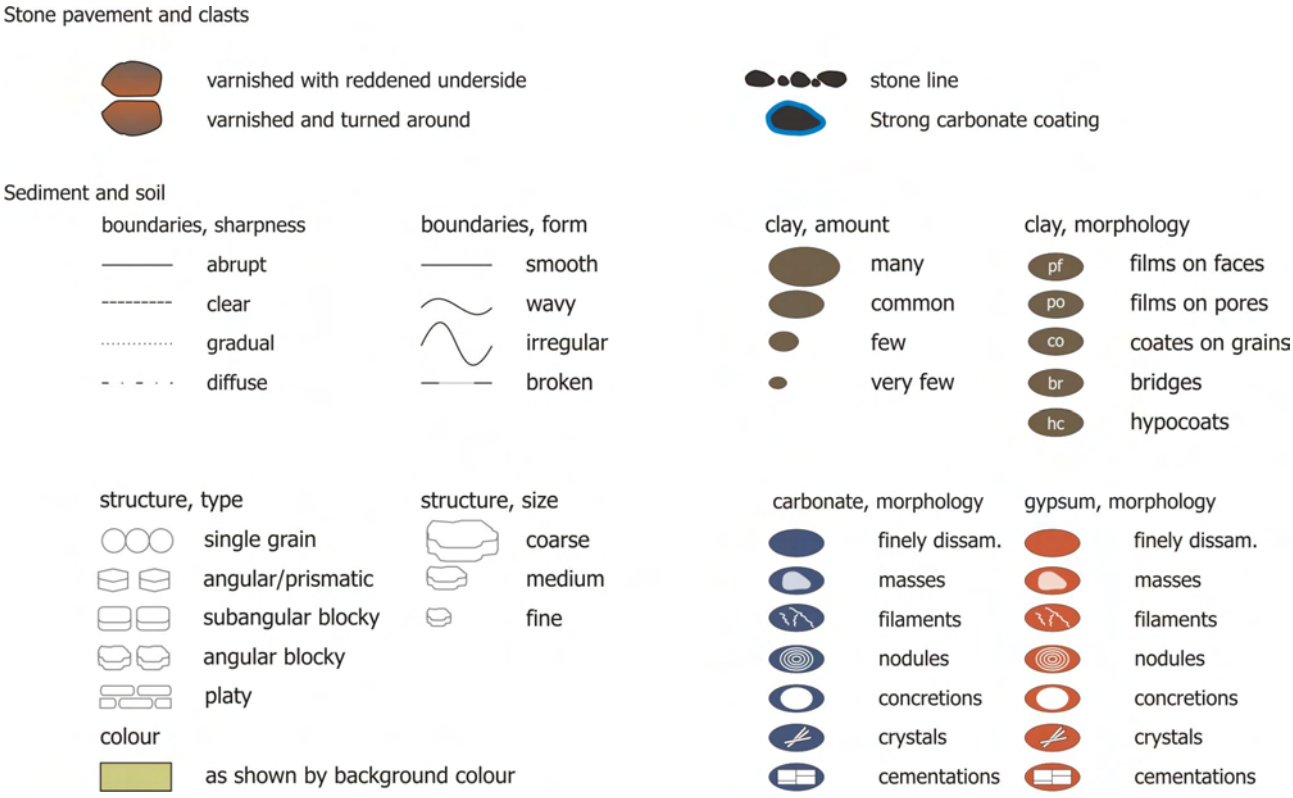

Figure 6.3. Legend to soil-sediment profile sketches (figure 6.2). Morphology descriptions after Harden et al. (1991), Soil Science Society Staff (1993), Birkeland (1999).

6.4.2 End-member modelling approach

The systematic parameter tests revealed an optimum EM number of q = 5, also in accordance with the Kaiser criterion (R^2 = 0.96 prior to rotation), and a weight transformation limit of l_w = 0.09. This resulted in a mean absolute model deviation of 3.13 % and a total mean explained variance of R^2 = 0.68. Mean row-wise and column-wise explained variance is 0.63 and 0.72 for all samples and grain size classes, respectively. Modifications of lw did not change their peak positions within grain size classes and changed row-wise and column-wise explained variance of the model only slightly. Bar plots in figure 6.2 show EM scores for all profiles, i.e. the contribution of each EM to the sample composition.

The five loading distributions (figure 6.4), sorted after their mode position, have distinct individual modes. EM 1 has a broad mode in the coarse particle classes (2000-250 µm) and some minor contribution of the silt and clay fraction. EM 2 has a clear double-mode between 500 and 125 µm.

EM 3 has a broad mode between 125 and 25 µm but rises again in the clay fraction. EM 4 has a clear mode in the coarse silt fraction (50 to 20 µm) and a minor mode in the fine silt fraction (5 to 2 µm). EM 5 is dominated by the clay fraction.

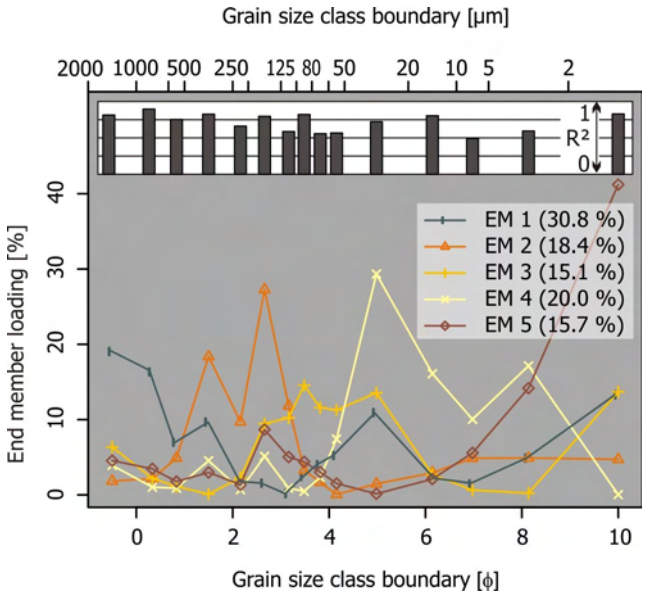

Figure 6.4. End-member (EM) loadings after modelling with q = 5 and l_w = 0.09. Portion of explained variance by each EM in brackets. The inset bar chart visualises the explained variance (0 to 1) per grain size class.

6.4.3 Profile correlation and standard profile

In general, there are two distinct types of profiles. Type I (profiles 1, 2, 3, 5) mainly consists of aeolian material and is very poor in clasts. It shows mature pedogenetic alteration and complex stratigraphic subdivisions (Dietze et al., 2011). Type II (profiles 4, 6) is composed of a stone-rich matrix filled with aeolian material. Pedogenetic alteration is marginal. Stratigraphic subunits are sparse. This profile type is found in the proximity of local drainage channels. Figure 6.6 shows the correlated soil profiles and the inferred stratigraphic units. The basal rubble zone (RZ; cf. Wells et al., 1985) with strongly weathered clasts and sandy to gravely detritus is exposed in several profiles. Upwards, a transition zone (TZ) grades into the layers dominated by aeolian deposits. On top of the TZ the profiles basically exhibit three units of accretionary development and pedogenetic sediment alteration.

Unit S I is characterised by strong pedogenetic alteration of the aeolian parent material. Strongly developed coarse subangular blocky to angular blocky structure and prominent clay-morphological features of various types indicate mature pedogenesis. The soil matrix is engulfed with masses, filaments, crystals and concretions of calcium carbonate and gypsum. There is a tendency to high clay content in this unit. Coarse and medium sand contents decline remarkably compared to the RZ and TZ. Clast content is very low except for profile 1, which is located close to a bedrock outcrop. EMs 2 to 5 are dominant. The unit may end abruptly with a stone line at a mean depth of 55±8 cm (figure 6.5A).

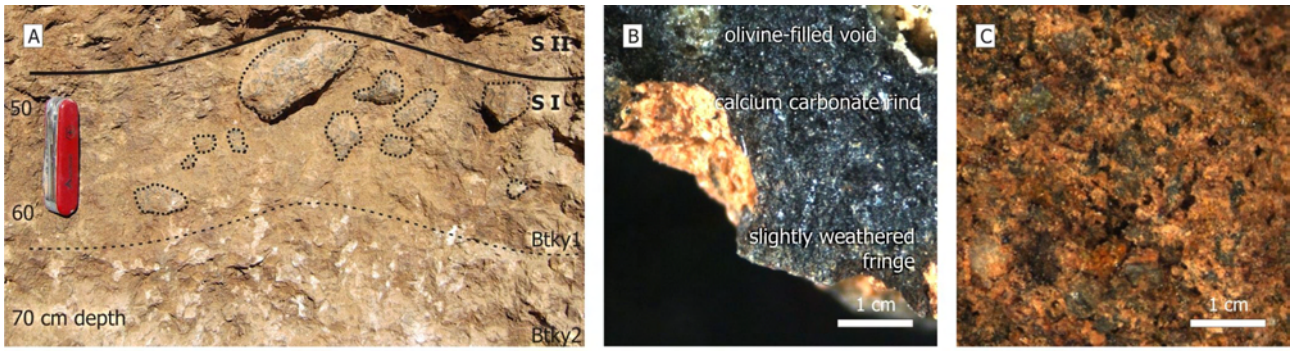

Figure 6.5. Pedogenetic and clast weathering features in soil profiles of type I. A: Section of profile 3 at the boundary between two Btky horizons. Abundant clasts between 45 and 60 cm depth are highlighted by dotted lines around objects (i.e. lower stone line as depicted in figure 6.2). The lower Btky horizon shows compound properties: clay enrichment and calcium carbonate features. B: Juvenile clast buried at a depth around 50 cm with preserved olivine-filled caverns, slightly weathered surface and calcium carbonate rind. C: Strongly weathered clast remnant from a depth of approximately 110 cm, i.e. the basal rubble zone (Wells et al., 1985).

Although soil structure of unit S II is still moderately to strongly developed subangular blocky to angular blocky or partly platy (profile 3), clay contents are typically lower compared to S I. Few to common clay films are developed on ped faces and on pores. Calcium carbonate occurs predominantly as masses and filaments. Gypsum morphology is diverse; there may be filaments, nodules or crystals, but visible gypsum may also be entirely absent. Clast content in this unit is low, too. EM 4 dominates the scores. Another stone line at a depth of 14±5 cm and a fossilised vesicular horizon may be present at the upper boundary. The unit may be separated into a lower unit S II a with a lower sand content and more strongly developed soil structure and an upper unit S II b with more contribution of coarse material and an overall weaker soil structure.

Unit S III has – apart from the vesicular horizon – a single grain to weakly developed subangular blocky soil structure. Calcium carbonate and gypsum morphologies are generally very weakly developed and show finely disseminated features to masses. Clay morphology is also marginal and reduced to films on pores. The vesicular horizon is developed equally well in all profiles with a strong and coarse prismatic structure and medium hard to hard consistence (Dietze et al., 2011). This unit is completed by the modern stone pavement.

The two profiles of type II are entirely composed of unit S III, although this unit has a remarkable thickness there. In the topo-sequence of figure 6.6A, the form of the shallow slope hollow is resembled by the profile characters. Profile 4 at the slope hollow margin contrasts sharply with the other three profiles.

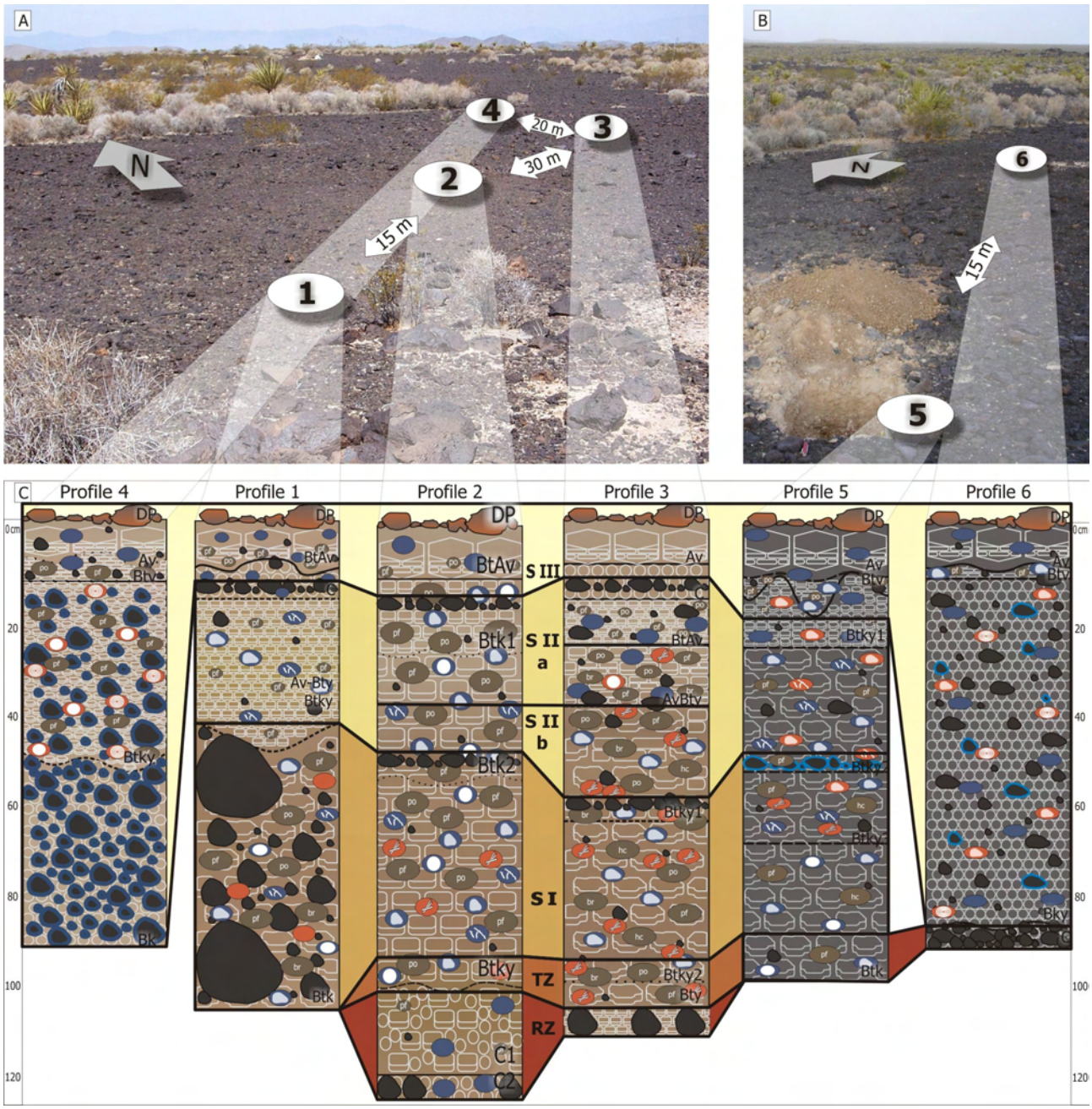

Figure 6.6. Correlation of soil profiles. A: Position of the four profiles of topo-sequence A along a shallow slope hollow flanked by vegetation. B: Position of the two profiles of topo-sequence B. C: Correlated profiles with inferred stratigraphic units. Detailed profile descriptions see figure 6.2.

6.5 Discussion

6.5.1 End-member modelling interpretation

EM loadings (figure 6.4) may be interpreted as process proxies. The coarse sand-dominated EM 1 is regarded to represent local detritus which is predominantly transported by surface runoff. However, it may as well include particles of physical clast weathering. The secondary mode in the

coarse silt and clay fraction may be interpreted as reworked dust and pedogenetically altered material. EM 2 is regarded as aeolian sand from a proximal source. Its grain size modes are close to the mean grain sizes of sand ramps throughout the eastern Mojave Desert: 1.67 to 2.23 ϕ (213 to 314 µm) with a mean standard deviation of 0.75 to 1.09 ϕ (Lancaster & Tchakerian, 1996). EM 3 with a broad mode in the fine sand and coarse silt fractions is interpreted as proximal dust, as indicated by the coarse grain size and poor sorting. EM 4 has a dominant and sharp peak in the coarse silt fraction and a minor peak in the fine silt fraction. It is interpreted as remote dust. The secondary mode would be expected to occur in the clay fraction but was also observed in another EM model (Bokhorst et al., 2011). EM 5 covers the clay fraction. Since there is no geomorphologic process that enriches the finest grain size fractions in such a system, enrichment of translocated clay (regarded as pedogenesis further on) is the most likely explanation for the composition of this EM.

With a picture of the geomorphologic and pedogenetic proxy function of each EM loading one can focus on their contribution to sample composition of the studied profiles (EM scores in figure 6.2). Table 6.1 provides a summary of the relative contributions of each EM (normalised by sample interval thickness) to stratigraphic units and profile types. Apart from the rubble zone contribution of local detritus to the grain size fraction < 2000 µm ranges between 9 and 20 % throughout all stratigraphic units. Local sand decreases upwards in the profiles. Contribution of dust does not show consistent patterns. Contribution of the pedogenesis EM does not follow field results of soil-morphological characteristics. This is attributed to the clay-enriched lower parts of vesicular horizons, also of fossil ones, which obscures other trends. The boundary between unit S I and S II is strikingly revealed by EM scores in profile 3 although soil-morphologic features alone do not change significantly. Profiles of type I are clearly distinct from those of type II with respect to the pedogenesis EM and both, the proximal sand and proximal dust EM.

Table 6.1. Relative contributions of end-members to the stratigraphic units and soil profile types.

Stratigraphic unit/ profile type	***Detritus [%]***	***Proximal sand [%]***	***Proximal dust [%]***	***Remote dust [%]***	***Pedogenesis [%]***
S III (n = 20)	9.0	17.7	36.7	20.7	15.9
S II (n = 19)	19.9	18.8	6.0	33.3	22.0
S I (n = 12)	10.4	25.7	24.1	19.8	20.0
TZ (n = 4)	17.5	24.3	32.7	9.6	15.9
RZ (n = 2)	27.0	36.3	27.4	7.9	1.4
Type I (n = 45)	16.5	16.5	18.4	18.8	29.8
Type II (n = 15)	12.0	29.0	31.8	14.5	12.7

In all profiles the surficial vesicular horizons take an outstanding position. They always show a sharp increase of pedogenetic alteration (EM 5 scores between 30 and 70 %) compared to samples from directly above and below. The remaining vesicular horizon composition is described by proximal and remote dust EMs. This finding is completely in line with the suggested genesis of vesicu-

lar horizons: aeolian dust is trapped on the surface and with rainfall the fine fractions of this material are translocated along aggregate boundaries to the interior whereas coarse remnants may be removed laterally by runoff (McFadden et al., 1998; Anderson et al., 2002, Dietze et al., accepted).

Interpretation of the basal part of profile 1 as S I rather than as RZ is supported by the high score of the pedogenesis EM. Vice versa, profiles 4 and 6 only show marginal contribution of the pedogenesis EM throughout the entire outcrops, except for the vesicular horizon. Rather they are composed of clasts, local detritus and proximal to remote aeolian sediment, which supports their stratigraphic designation and their rapid formation by fluvially transported clasts and subsequent infilling of aeolian material (Dietze et al., 2011).

6.5.2 Correlated profiles as environmental archive

The studied profiles are far from being a complex system. All profiles have comparably small catchments (1440±210 m² based on analysis of 1 arc second NED, courtesy of the U.S. Geological Survey). Only three major geomorphologic processes influence them: i) accretion of aeolian material from local and supra-local sources, ii) admixture of coarse material, delivered by lateral translocation and iii) pedogenetic alteration. These processes are well resembled by the grain size composition and can therefore be quantified by EMMA. Low scatter in burial depths of fossilised stone pavements (75 and 151 % of the mean clast diameter, respectively) and their still intact preferred clast orientation patterns indicates minimum post-depositional profile disturbances. Especially clast exhumation by turbation or swell-shrink processes (Springer, 1958; Cooke et al., 1993) may be excluded. Features of profile erosion are missing as well.

A virtually dust-free, detritus-filled pocket in the upper part of the RZ in profile 2 implies a substantial temporal offset between RZ formation and the period of aeolian activity. Nearly disintegrated clasts of the RZ reflect long exposure close to the surface under a moist climate rather than rapid burial by an aeolian blanket. Pedogenesis did not significantly affect the detritus-filled pocket within the strongly weathered clast deposit. The matrix still has a single grain structure with calcium carbonate masses. Pedogenesis EM score is zero. Furthermore, since the loose pocket filling is very susceptible to erosion, its presence indicates that profile 2 is a local depot centre.

The transition to aeolian-dominated deposition is gradual from a sedimentologic perspective but not from a temporal point of view. Throughout the wider study area the oldest aeolian accumulations have depositional ages younger than 34.8 ka and the majority of onset dates cluster between 25 and 20 ka (Rendell & Sheffer, 1996; Tchakerian & Lancaster, 2002; Bateman et al., 2012). The onset of massive aeolian deposition coincided with the incipient conditions of Lake Mojave (Rendell & Sheffer, 1996; Wells et al., 2003). Therefore, we suggest that the aeolian sediments of the investigated profiles may be correlated to this phase of increased aeolian activity. The different weathering intensities of clasts (figure 6.5) support the idea of a large age offset between the RZ and its overlying aeolian layers.

Accretionary sediment units S I to S III show consistent patterns. Local detritus occurs at the unit boundaries. Pedogenesis gets increasingly immature the closer to the surface the respective unit is located. Compound horizon properties are the result of polygenetic soil formation. After parent material deposition and leaching of soluble salts and calcium carbonate, clay translocation created argillic properties. With a second cycle of sediment deposition and decalcification the now buried argillic horizon became engulfed with secondary carbonate (Kleber, 2000). We exclude the possibility of sodium-supported clay dislocation because of the distance of our sites to possible sodium sources and the lack of pedogenic properties typical for natric horizons. Furthermore, we assume that at least the lowermost argillic horizon was formed during Pleistocene times when soil moisture was greater than in nowadays (cf. McFadden et al., 1986). Vesicular horizons are ubiquitous in the upper section of unit S III. However, one fossilised vesicular horizon in unit S II just below a fossil stone pavement highlights the systematic coupling of this feature to a profile position close to an (ancient) surface.

Surficial and fossilised stone pavements may be interpreted as environmental proxies as well. Studies from the Black Rock Desert, southern Sevier Basin, Utah, show that stone pavements and associated vesicular horizons may exist up to a mean annual precipitation (MAP) of approximately 300 mm only (Dietze et al., accepted). Quade (2001) reports an even lower maximum MAP for the Mojave Desert. With increasing moisture, vegetation cover increases systematically. Since clasts are assumed to be maintained at the surface by doming of the vesicular horizon (e.g. McFadden et al., 1986), and the latter becomes destroyed by plant roots (Dietze et al., accepted), dense vegetation cover prevents stone pavement maintenance. Therefore, stone pavements may indicate MAP lower than approximately 300 mm along with sparse vegetation cover. Stone pavements further indicate moderate dust deposition rates as they become fossilised upon oversupply of dust. However, quantification of a threshold is difficult. Modern conditions, i.e. dust in-flux of 11.0±0.7 g/m² a (Reheis, 2003), allow their maintenance, at least.

If a stone pavement is buried below aeolian material, some other agent must take over its function to trap further aeolian sediment. During glacial times vegetation zones of the Mojave Desert shifted to lower elevations. According to Spaulding (1990) and Quade (2001), in this area elevations as low as some 400 m a.s.l. were covered by vegetation during the Last Glacial Maximum (LGM). Plants, especially grass and shrub communities, are indeed an alternative, very effective agent for dust trapping and would tolerate even higher dust fluxes. A vegetation cover would thus allow accretionary profile growth without a maintained stone pavement. However, it requires climatic conditions that favour sufficient vegetation cover, i.e. higher effective moisture during the cold episodes of the Quaternary. The supposed 1000 m downward migration of vegetation zones during the LGM (Quade, 2001) renders the study area at approximately 900 m a.s.l. a highly variable transition zone. Therefore, even short changes of effective moisture may have significant impact on vegetation cover. Seven short periods of dune sand deposition in the Cronese basin and

the Kelso Dunes area indicate that vegetation cover in the Mojave Desert suffered from such episodic pulses of instability (Tchakerian & Lancaster, 2002). Mensing (2001) and Liu & Broecker (2008) also discuss several of such short switches in the regional climate of the wider area during the latest Pleistocene and Holocene. Similar short time intervals in which "stone horizons" formed on a sand ramp in the Mojave Desert are also discussed by Bateman et al. (2012).

Systematic bimodal and slope aspect-symmetrical clast orientation patterns in stone pavements are another environmental proxy. Dietze et al. (2012) argued that such orientation patterns may be created by lateral clast transport over the fine-grained and firm vesicular horizon by unconcentrated overland flow. Lateral delivery of fresh clasts is essential to form a new generation of stone pavement after the fossilisation of an older one. Accordingly, stone pavements with bimodal clast orientation patterns may indicate a period of i) frequent unconcentrated overland flow together with climatic conditions that support ii) prior formation of a firm but fine-grained surface (i.e. the vesicular horizon) and iii) a considerably decreased vegetation cover. These three preconditions were presumably fulfilled during the aforementioned short periods of environmental instability.

The stone pavement-covered profiles record environmental information present in no other known type of archive. Playas and playa margins may be well-suited for studying lake histories (Wells et al., 2003), but periods of advanced dust mobilisation during lake desiccation are not recorded. Dune and sand ramp sediments in turn are excellent recorders of aeolian activity phases in the eastern Mojave Desert, given that there is mobile material present (Lancaster & Tchakerian, 1996; Tchakerian & Lancaster, 2002). However, they do not primarily reflect phases of lake level instability but rather short-term relations between event-based sediment delivery, storage and mobilisation. Such events have taken place regardless of the lake level in the study area (Tchakerian & Lancaster, 2002).

6.5.3 Scenario of profile evolution

In the following, we attempt to decipher the sequence of processes to form our profiles and to tentatively correlate these to known phases in the palaeo-environmental history of the region. Soon after lava flow emplacement the landform started to degrade by weathering and colluviation of clasts into topographic lows, forming the RZ (figure 6.7A). In one of the local depot centres fine-grained volcanoclastic material is deposited in a small pocket (figure 6.7B). Aeolian material deposition is marginal at that time. The RZ deposits are exposed for a long time and suffer from intense weathering.

With the entering of Mojave River water to the Soda Lake and Silver Lake basins Lake Mojave comes into being. During its incipient and intermittent stages, between 22.6 and 18.4k ^{14}C a BP, it delivers abundant sediment for downwind transport. The regional climate supports dense vegetation on the lava flow. Aeolian material is deposited on the lava flow surface. Aeolian deposits cover clasts

of the RZ and gradually form the TZ. Thickening of the allochthonous mantle detaches site characteristics from bedrock-determined conditions. Sediments of unit S I are deposited (figure 6.7C).

Between 18.4 and 16.6k ^{14}C a BP the lake stabilises and Lake Mojave I becomes persistent. The shore-related dust flux declines. Still under moist climate, pedogenesis within the aeolian mantle involves decalcification of the soil matrix and subsequent formation of argillic properties (figure 6.7D).

During a presumably short period of increased aridity, vegetation cover declines remarkably. Formation of a surficial vesicular horizon is no longer limited by plant root activity. A firm vesicular structure evolves. The isolated pore system prevents rapid infiltration (Dietze et al., accepted). As the result of torrential rainfall events unconcentrated overland flows can create a surficial clast mosaic (figure 6.7E). Clasts from local delivery centres (e.g. bedrock or rubble zone outcrops) are transported to form a first stone pavement.

Then, the lake level begins to fluctuate and dust flux increases. An intermittent lake forms between 16.6 and 13.7k ^{14}C a BP. Around 15.5k ^{14}C a BP the lake falls completely dry (Wells et al., 2003), which could however have been independent from climate. The increasing dust flux may lead to enhanced aeolian accretion and burial of the stone pavement. However, without assisting vegetation cover, burial may stop eventually due to decreased surface roughness and give way to erosion of the deposited aeolian material. With recovery of the vegetation cover, dust accretion can continue and unit S II forms (figure 6.7F).

The lake level stabilises and Lake Mojave II comes into being between 13.7 and 11.8k ^{14}C a BP. Dust flux is at a minimum again. Pedogenesis causes decalcification of S II and contemporaneous carbonate precipitation in S I. The compound horizon of this lower unit evolves (figure 6.7G). After decalcification, S II is affected by clay illuviation.

During another short climatic switch towards drier conditions vegetation cover declines and the second stone pavement forms by lateral clast transport over an undisturbed vesicular horizon (figure 6.7H). This stone pavement generation is not present in the profiles of the topo-sequence from figure 6.6B, which may be the result of a spatially non-uniform vegetation retreat.

During the transition to the Holocene, Lake Mojave grades into the modern playa environment via a third intermittent phase. Vegetation traps abundant aeolian material and the second stone pavement generation becomes fossilised (figure 6.7I). Decalcification and carbonate precipitation create compound soil horizons in the lower units.

With establishment of the playa conditions and migration of the dense grass and bush cover to higher elevations, the modern stone pavement can develop. Holocene periods of enhanced dust mobilisation may partly bury this pavement but without vegetation as a replacement agent, deposition declines as soon as the rough surface becomes levelled (figure 6.7J). Deposited fine material may even be removed if not protected by a covering stone pavement.

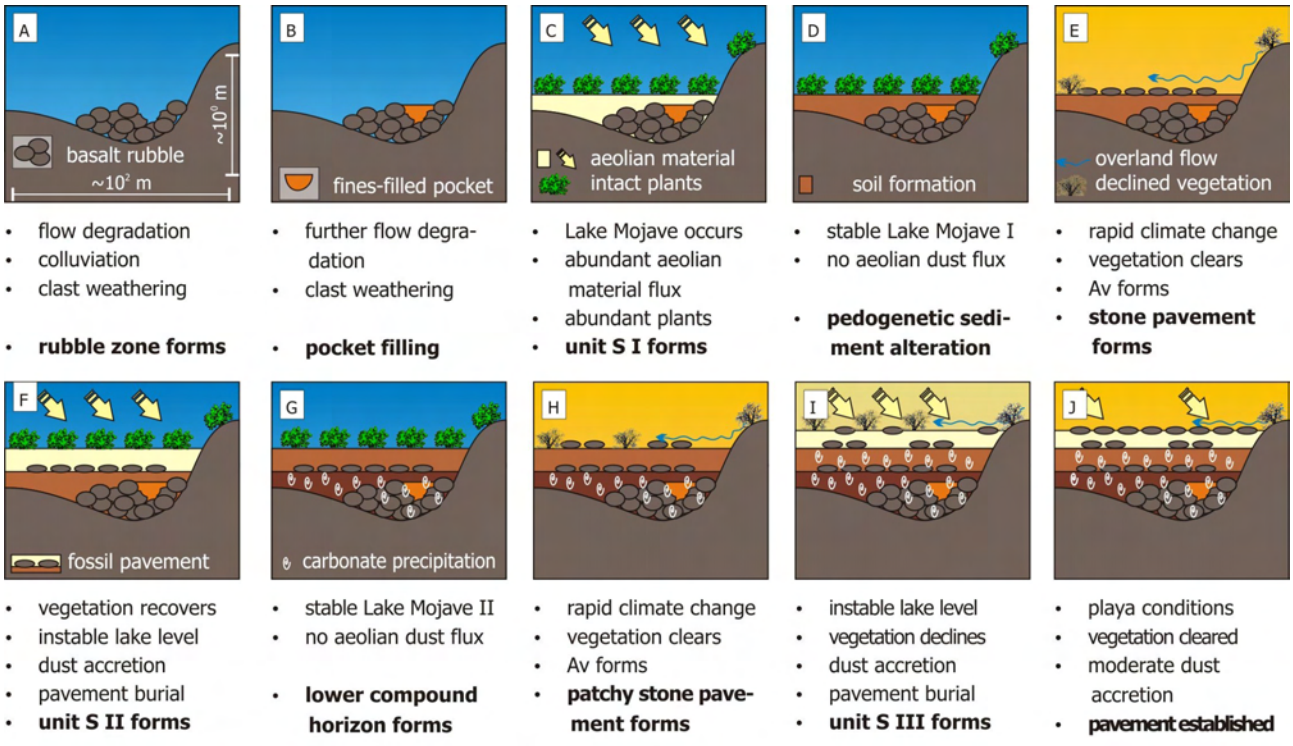

Figure 6.7. Scenario of standard profile evolution. Descriptions see text. The stages A to J correspond to changing environmental conditions of the lake/playa basin, dust flux, vegetation cover and pedogenesis.

6.6 Conclusions

The surface evolution of the investigated middle Pleistocene lava flow at Cima volcanic field is far from representing temporally and spatially homogeneous interaction of geomorphologic and pedogenetic processes. Prominent small-scale differences in subsurface properties may only be resolved by interpreting a series of environmental archives rather than only a single soil pit. Correlated soil-sediment complexes reveal three distinct periods of aeolian sediment deposition, soil formation and stone pavement development. The documented aeolian history may be as young as approximately 25 ka and, thus, indicates a significant age hiatus in the documented history on the lava flow. Colluviation and weathering of the lava flow surface may have dominated for several hundreds of thousand years without remarkable contribution of any accretionary processes. However, during presumably the last 25 ka aeolian dust accretion was the overwhelming process contributing to surface modification on the lava flow. Due to missing deposits, there is no information preserved about previous dynamics.

The onset of major dust activity may have been impossible without a key impulse: the entering of the Mojave River to the process catchment and subsequent formation of a Lake system. However, from the three periods of enhanced dust activity only the youngest one is clearly linked to climatic forcing. The two other periods were presumably controlled by the singular event of incision at Afton Canyon and either a switch of the Mojave River course or a climatic signal.

All three aeolian sediment units are covered by a stone pavement that persistently indicates formation by lateral processes. Formation of this clast-dominated surface cover type requires a barren surface, especially free of vegetation. However, fossil stone pavements argue for a dust-trapping mechanism other than clasts: a rather dense vegetation cover. Therefore, stone pavement formation may be best explained to take place during periods of increased aridity. In the case of the Cima volcanic field, these aridity pulses may have forced vegetation to temporally migrate to higher elevations than usual during mean pluvial conditions. This barrenness allowed formation of the vesicular horizon, lateral transport of reworked clasts by unconcentrated overland flow and clast alignment upon collision to form a new generation of stone pavement. Accordingly, stone pavement formation is an episodic phenomenon rather than a systematic and time-transgressive one, which has implications for its interpretation as palaeo-environmental and as surface age indicator.

Acknowledgements

We kindly thank Dominik Faust for his invaluable contributions to the mansucript. Arno Kleber could discuss Profile 3 of this paper with Eric McDonald in the field; we also thank him for first sedimentological analyses of that profile performed in the DRI laboratory in Las Vegas.

References

Anderson KC, Wells SG, Graham RC. 2002. Pedogenesis of vesicular horizons, Cima volcanic field, Mojave Desert, California. *Soil Science Society of America Journal* **66**: 878-887. DOI: 10.2136/sssaj2002.8780.

Bateman MD, Bryant RG, Foster IDL, Livingstone I, Parsons AJ. 2012. On the formation of sand ramps: A case study from the Mojave Desert. *Geomorphology* **161-162**: 93-109. DOI: 10.1016/j.geomorph.2012.04.004

Betancourt JL, Devender TRV, Martin PS, (eds). 1990. *Packrat middens: The last 40,000 years of biotic change*. University of Arizona Press, Tucson.

Birkeland PW. 1999. *Soils and geomorphology*. 3rd edition, Oxford University Press: New York, Oxford.

Bokhorst MP, Vandenberghe, J, Sümegi, P, Łanczont, M, Gerasimenko, NP, Matviishina, ZN, Marković SB, Frechen, M. 2011. Atmospheric circulation patterns in central and eastern Europe during the Weichselian Pleniglacial inferred from loess grain-size records. *Quaternary International* **234**: 62-74.

Cal-Atlas. 2009. Cal-Atlas Geospatial Clearinghouse. http://atlas.ca.gov/ [29.06.2012]

Chadwick OA, Davis JO. 1990. Soil-forming intervals caused by eolian sediment pulses in the Lahontan Basin, northwestern Nevada. *Geology* **18**: 243-246. DOI: 10.1130/0091-7613

Cooke RU, Warren A, Goudie AS. 1993. *Desert Geomorphology*. UCL Press: London.

Dietze E, Hartmann K, Diekmann B, IJmker J, Lehmkuhl F, Opitz S, Stauch G, Wünnemann B, Borchers A. 2012. An end-member algorithm for deciphering modern detrital processes from lake sediments of Lake Donggi Cona, NE Tibetan Plateau, China. *Sedimentary Geology* **243-244**: 169-180. DOI: 10.1016/j.sedgeo.2011.09.014.

Dietze M, Kleber A. 2012. Contribution of lateral processes to stone pavement formation in deserts inferred from clast orientation patterns. *Geomorphology* **139-140**: 172-187. DOI: 10.1016/j.geomorph.2011.10.015.

Dietze M, Muhs S, Dietze E. 2011. Ambiguities of relative age indicators on abandoned surfaces of arid environments. *Zeitschrift für Geomorphologie N.F.* **55** Supplementary Issue 3: 49-75. DOI: 10.1127/0372-8854/2011/005553-0051.

Dietze M, Bartel S, Lindner M, Kleber A. (accepted). Formation mechanisms and control factors of vesicular soil structure. Catena.

Enzel J, Wells SG, Lancaster N. (eds). 2003. Paleoenvironments and Paleohydrology of the Mojave and Southern Great Basin Deserts. *Geological Society of America Special Paper* **368**.

Harden JW, Taylor EM, Hill C, Mark RK, McFadden LD, Reheis MC, Sowers JM, Wells SG. 1991. Rates of soil development from four soil chronosequences in the Southern Great Basin. *Quaternary Research* **35**: 383-399. DOI: 10.1016/0033-5894(91)90052-7.

Kleber A. 2000. Compound soil horizons with mixed calcic and argillic properties - examples from the northern Great Basin, USA. *Catena* **41**: 111-131. DOI: 10.1016/S0341-8162(00)00111-9.

Laity J. 2008. *Deserts and Desert Environments*. 1st edition, Wiley-Blackwell.

Lancaster N, Tchakerian VP. 1996. Geomorphology and sediments of sand ramps in the Mojave Desert. *Geomorphology* **17**: 151-165. DOI: 10.1016/0169-555X(95)00101-A.

Liu T, Broecker WS. 2008. Rock varnish evidence for latest Pleistocene millennial-scale wet events in the drylands of western United States. *Geology* **36**: 403-406. DOI: 10.1130/G24573A.1.

McFadden LD, Wells SG, Dohrenwend JC. 1986. Influences of quaternary climatic changes on processes of soil development on desert loess deposits of the Cima volcanic field, California. *Catena* **13**: 361-389. DOI: 10.1016/0341-8162(86)90010-X.

McFadden LD, McDonald EV, Wells SG, Anderson K, Quade J, Forman SL. 1998. The vesicular layer and carbonate collars of desert soils and pavements: formation, age and relation to climate change. *Geomorphology* **24**: 101-145. DOI: 10.1016/S0169-555X(97)00095-0.

Meek N. 2004. Mojave River history from an upstream perspective. In *Breaking up: The 2004 Desert Symposium Field Trip and Abstracts*. Reynolds RE. (ed).University of Fullerton, Desert Studies Consortium, Fullerton: 41-49.

Mensing SA. 2001. Late-Glacial and Early Holocene Vegetation and Climate Change near Owens Lake, Eastern California. *Quaternary Research* **55**: 57-65. DOI: 10.1006/qres.2000.2196.

Meszner S, Fuchs M, Faust D. 2011. Loess-Palaeosol-Sequences from the loess area of Saxony (Germany). *Eiszeitalter und Gegenwart, Quarternary Science Journal* **60**: 47-65. DOI: 10.3285/eg.60.1.03.

NCDC, 2012. http://www.ncdc.noaa.gov/oa/ncdc.htmI [29.06.2012].

Quade J. 2001. Desert pavements and associated rock varnish in the Mojave Desert: how old can they be? *Geology* **29**: 855-858. DOI: 10.1130/0091-7613.

Reheis MC, 2003. *Dust deposition in Nevada, California, and Utah, 1984-2002*. USGS open file report OF 03-138, 66.

Rendell HM, Sheffer NL. 1996. Luminescence dating of sand ramps in the Eastern Mojave Desert. *Geomorphology* **17**: 187-197. DOI: 10.1016/0169-555X(95)00102-B.

Schlichting E, Blume H-P, Stahr K. 1995. *Bodenkundliches Praktikum*. 2nd edition, Blackwell: Berlin, Oxford.

Soil Survey Division Staff. 1993. Soil Survey Manual. *Soil Conservation Service. U.S. Department of Agriculture Handbook* **18**.

Spaulding WG. 1990. Vegetation dynamics during the last deglaciation, southeastern Great Basin, U.S.A. *Quaternary Research* **33**:188-203. DOI: 10.1016/0033-5894(90)90018-G.

Springer ME. 1958. Desert pavement and vesicular layer of some soils of the desert of the Lahontan Basin, Nevada. *Soil Science Society of America Proceedings* **22**: 63-66.

Suchodoletz H von, Kühn P, Hambach U, Dietze M, Zöller L, Faust D. 2009. Loess-like and palaeosol sediments from Lanzarote (Canary Islands/Spain) - indicators of palaeoenvironmental change during the Late Quaternary. *Palaeogeography, Palaeoclimatology, Palaeoecology* **278**, *71-87. DOI: 10.1016/j.palaeo.2009.03.019.*

Tchakerian VP, Lancaster N. 2002. Late Quaternary arid/humid cycles in the Mojave Desert and western Great Basin of North America. *Quaternary Science Reviews* **21**: 799-810. DOI: 10.1016/S0277-3791(O1)00128-7.

Wells SG, Dohrenwend JC, McFadden LD, Turrin BD, Mahrer KD. 1985. Late Cenozoic landscape evolution on lava flow surfaces of the Cima Volcanic field, Mojave Desert, California. *Geological Society of America Bulletin* **96**: 1518-1529. DOI: 10.1130/0016-7606(1985)96.

Wells SG, Brown WJ, Enzel J, Anderson RY, McFadden LD. 2003. Late Quaternary geology and paleohydrology of pluvial Lake Mojave, southern California. In *Paleoenvironments and Paleohydrology of the Mojave and Southern Great Basin Deserts.* Enzel J, Wells SG, Lancaster N. (eds). Geological Society of America Special Paper **368**; 79-114.

Weltje GJ. 1997. End-member modeling of compositional data: numerical–statistical algorithms for solving the explicit mixing problem. *Mathematical Geology* **29**: 503-549. DOI: 10.1007/BF02775085.

Weltje GJ, Prins MA. 2007. Genetically meaningful decomposition of grain-size distributions. *Sedimentary Geology* **202**: 409-424. DOI: 10.1016/j.sedgeo.2007.03.007.

Winograd IJ, Coplen TB, Landwehr JM, Riggs AC, Ludwig KR, Szabo BJ, Kolesar PT, Revesz KM. 1992. Continuous 500,000-Year Climate Record from Vein Calcite in Devils Hole, Nevada. *Science* **258**: 255-260.

7 Synthesis

7.1 Formation of stone pavements and vesicular horizons

The findings of stone pavement, vesicular horizon and stratified soil-sediment properties – from semi-arid to hyper-arid, from hot to cold regions and throughout different landform types – stand in contrast with many established formation models of gravel-covered surfaces (cf. chapter 1.2.). Particularly, thin strata of fossilised stone pavements, even in sequences with more than 30 % clay content (containing expandable mixed-layer clay minerals; chapter 5.3.1.3) argue against clast exhumation through swell-shrink cycles of the soil matrix as a major process of coarse particle concentration at the surface (e.g. Cooke, 1970). The strong aeolian component in vesicular horizons renders an interpretation of stone pavements as the result of deflation unlikely (e.g. Blake, 1858) for all studied sites. Different weathering regimes (e.g. Mabutt, 1977; Bockheim, 2010) can also not account for this strong aeolian imprint. Disturbed sites, healing by deposition of fresh clasts argue against a pure vertical formation and maintenance of stone pavements (e.g. McFadden et al., 1986).

Certainly, stone pavement evolution is not the result of just one process (cf. Cooke, 1970; Amit & Gerson, 1986) and is obviously subject to equifinality (e.g. Cooke et al., 1993). However, some processes can be deciphered without much doubt. Accretion of aeolian material is an essential feature at all investigated sites. Although this process is intimately related to stone pavements, the latter are not necessarily the only agents that allow dust accretion. Selective removal of fine material by deflation or fluvial processes (Griffiths et al., 2006; Sweeney et al., 2012) may take place, but is limited to discrete events and affects a narrow grain size fraction (i.e. the fraction of the loose aeolian material on top of the vesicular horizon which is not translocated to the aggregate interior). Another process component which may be deciphered from preferred clast orientation patterns is lateral clast transport (chapter 3). This component is necessary to explain recovery of a disturbed site with not enough clasts present at the surface to restore the stone pavement just by fine material erosion (chapter 4.1.2). Lateral clast transport is also necessary to form a new generation of stone pavement above a fossilised one. Accordingly, a lateral process component is essential to fully explain the observed properties of stone pavements throughout many different landscapes.

Apart from evolving continuously over time spans up to several million years (e.g. Matmon et al., 2009; Fujioka & Chappell, 2011), stone pavements may as well form rapidly, probably within a few centuries (chapter 6.5) or millennia (Bateman et al., 2012). Rapid formation may be bound to discrete event-based processes. Upon heavy rainfall, unconcentrated overland flows of a few centimetres height may be able to drag clasts over an initially bare surface with a few fixed obstacles (such as perennial plants, plant remnants or large rock fragments). The dragged clasts may become aligned upon collision to form a slope aspect-symmetrical orientation pattern. Accordingly, a large area may be covered with time. Recovery may start at isolated obstacle locations and subsequent

collisions form upslope broadening cones of oriented clast agglomerations (chapter 4.4). However, not all site properties are suitable to allow unconcentrated overland flow of sufficient power to drag clasts. Accordingly, a further mechanism of unidirectional lateral clast transport is required. The gas escaping from vesicular horizons upon wetting is able to lift clasts a few millimetres normal to the surface, which results in a net downslope displacement on any inclined surface due to the clast falling back parallel to the gravitation vector (chapter 5.4.3). For either of the proposed mechanisms of lateral clast transport the vesicular horizon plays a fundamental role.

Formation of vesicular structure is principally possible in a wide range of environmental and sedimentologic properties but limited by plant root activity. Thereby, macroscopic vesicular horizon properties show a tight relation to site humidity, in contrast to nearly humidity-independent parameters of vesicle size and shape (chaper 5.3). Vesicle formation can be explained, according to the proposed experimental evaluations, by just one conceptual model (Springer, 1958) with secondary contributions of further processes: upon wetting and infiltration i) the surface begins to seal by puddling and ii) soil air is replaced by water, which results in an increase of gas pressure. This pressure within the wet soil matrix may lead either to gas bubbles escaping from the soil (and thereby lifting clasts or forming small craters) or to formation and expansion of isolated spherical voids, the vesicles. However, with respect to the model of Springer (1958) there is one major modification, revealed by the experiments: vesicles are no transitory feature, destroyed and recreated with each wetting-drying cycle, but are rather stable formations, expanding and stabilising with time (chapter 5.4).

Since in the laboratory vesicles form exclusively on bare surfaces and adjacent to the margins of covering clasts but not under such surface-sealing objects, whereas at natural sites vesicles are abundant, also under stone pavement clasts, syngenetic formation of these two features appears questionable. Lateral migration of clasts subsequent to vesicle formation may be a more appropriate interpretation, also in accordance with the frequently observed clast orientation patterns.

Formation of vesicles may be a rapid process (a few wetting-drying cycles are sufficient to create spherical pores) whereas formation of a vesicular horizon is not. This pedogenetic horizon may include further distinct properties such as multiple morphological domains, laminae of calcite, silt and clay on vesicle walls, primary prismatic and secondary platy structure along with interconnected and elongated pores that control material fluxes into and within this horizon (Figueira & Stoops, 1983; Anderson et al., 2002; chapter 5). Accordingly, the vesicular horizon is the result of an interplay of dust influx and dust re-distribution (into the aggregates but also off-site by lateral water flow), primarily controlled by surface cover type.

7.2 Relationships among stone pavements, vesicular horizons and environmental conditions

Stone pavements and vesicular horizons are typically described to form a genetically coupled system: The rough stony surface acts as trap for aeolian material, which actually allows formation of the vesicular horizon. In turn, doming of vesicular horizon aggregates is suggested to maintain the clast cover at the surface (e.g. McFadden et al., 1986; Anderson et al., 2002). Apart from these established relationships there are new aspects, deciphered by the analyses and experiments presented in this dissertation (chapters 3, 4, 5). A clast cover is not essential to form a vesicular horizon. This surface feature forms on bare ground as well, both in the field and under laboratory conditions. However, the vesicular horizon in turn appears to be vital to form a new generation of stone pavement and to maintain it, predominantly by i) decreasing infiltration capacity and supporting overland flow, ii) providing a smooth but resistive surface for clast dragging by water and iii) allowing small-scale clast rearrangement (chapter 4). Apart from the described aggregate doming (McFadden et al., 1986), soil air release from the vesicular horizon upon rainfall contributes another mechanism of active clast lifting – along with a lateral component on inclined surfaces – which may keep a stone pavemenent intact (chapter 5).

Stone pavement-covered landforms appear to be least susceptible to sediment loss by surface runoff events (Griffiths et al., 2006) or deflation (Sweeney et al., 2011). This renders them a potentially valuable archive of environmental information, stored in the accretionary system, provided the presence of a proximal active dust source such as fluctuating lakes, playas and large ephemeral streams (chapter 6). However, although material out-flux is small, there still is a net loss in fine sediment from stone pavement-covered surfaces (chapter 5.4.3). This negative budget component appears to be currently derived from the loose material on top of the vesicular horizon (chapter 5).

The surface cover composition, i.e. proportion of clasts versus grass-dominated vegetation, has a crucial control function for the fine sediment flux of the loose surficial material into the vesicular horizon. Under a clast cover, only the silt and clay fraction is incorporated to the vesicular horizon, whereas the sand component is removed from the site. Under a grass cover, all fine material fractions are incorporated to the vesicular horizon. This flux controls several morphological properties of this horizon (e.g. firmness, thickness and texture). In turn, these properties control infiltration efficiency, soil moisture and surface runoff susceptibility of a site. Accordingly, the vesicular horizon triggers but is also affected by a series of processes and plays a key role in landscape evolution and site ecology.

Both, stone pavements and vesicular horizons were only found at study sites with mean annual precipitation below 350 mm. Since the integrity of the clast cover relies on an intact vesicular horizon the latter may be the key feature that determines the presence of both formations. Furthermore, under increased moisture, vegetation may take over the role of clasts to trap aeolian material and lead to the burial of the stone pavement by ongoing sediment accretion.

7.3 Value of stone pavement-covered soil-sediment sequences as environmental archive

Stone pavements are no "hallmarks of stability" (cf. Haff & Werner, 1996). They are no final stage of landscape evolution. Rather, they are an example of potential dynamic equilibrium, controlled by dust flux, moisture-related vegetation cover, non-linear runoff events, systematic small-scale disturbance (plant scars, animal activity) and subsequent recovery. Stone pavements may be stable features over millions of years (Matmon et al., 2009), if environmental conditions support this, or they may be dynamic features that form within a few centuries, if environmental conditions support different modes of vegetation cover and dust flux (chapter 6). This dual nature of stone pavements provides a universal explanation for the hitherto contradictory findings of indicators of both, stability and instability (3.1).

Stone pavements as surface feature and the underlying soil-sediment sequences do not act as co-genetic archives of environmental change. They are decoupled landscape elements with soil being able to change properties considerably even over small spatial distances as the result of different geomorphologic processes that accumulate and erode sediments (chapter 2.6). Stone pavements can become buried, even during short events of enhanced dust accretion. Lateral processes play a fundamental role i) even before the initial stone pavement formation stage (i.e. rubble zone formation, Wells et al., 1985), ii) presumably during the maintenance of stone pavements, but certainly iii) during formation of a new generation of stone pavement.

The dual nature of stone pavements along with the decoupled genesis of accretionary soil-sediment sequences and surface cover has fundamental consequences for a series of related interpretations. Using stone pavement or soil properties as isolated relative age indicators is questionable. Studies from Cima volcanic field show that many stone pavement properties on 10^4 versus 10^5 year old lava flows are very similar, apart from clast-related age indicators (e.g. varnish cover and edge rounding). This implies that stone pavement properties are sensitive on small time scales (10^2-10^4 years) rather than necessarily the entire period since the last surface disturbance (in the case of the Cima volcanic field this was probably the transition from late Pleistocene to modern arid conditions, chapter 6). Likewise, the formation age of a landform may become irrelevant for the stone pavement and vesicular horizon age. Spatial soil-sediment heterogeneity at the metre scale may become as high as a temporal offset of more than 530 ka.

Stone pavements and the associated aeolian mantles provide a palaeo-environmental proxy-function. Bimodal, slope aspect-symmetrical clast orientation patterns on stone pavement-covered alluvial fans, fluvial terraces or shorelines imply that stone pavement formation represents a different geomorphologic regime (slope processes and/or unconcentrated overland flow), which can be inferred from these clast orientation patterns (chapter 3.6). Likewise, the spherical form of vesicles is related to a constant dust influx to the system as without fresh dust accretion the vesicles would become interconnected and loose sphericity. Besides these two surface-related properties, there are further, more classical proxies of terrestrial archives which may be investigated in such

accretionary sequences (e.g. grain size composition and pedogenetic sediment overprint, especially compound horizon properties).

Accordingly, stone pavement-covered profiles are a unique type of terrestrial environmental archive. They may allow reconstruction of landscape evolution by providing information no other archive does. For example at the Cima volcanic field, amalgamation of six profiles on a 540 ka old lava flow allows to decipher a rather young aeolian history (less than 30 ka) along with a large age offset to the lava flow emplacement. This aeolian history consisted of three distinct phases of dust accretion, vesicular horizon genesis, stone pavement formation and overall pedogenetic overprint. However, it the studied area only one of these phases could be clearly linked to climate-controlled changes in geomorphologic process interactions.

7.4 Value of quantification, experiment and modelling approaches

Developing and integrating approaches to quantify field and laboratory data, inferring measurement and model uncertainties, providing numerical models and experiments and transforming measured sample parameters (e.g. grain size composition) into process-controlled proxies is one overarching background goal of this dissertation. The attempts primarily helped to solve the following challenges: i) providing independent approaches to a given research question, ii) avoid subjective interpretations of data already at an early stage, iii) reduce natural complexity to a few – if possible – independent parameters, and iv) infer local and global uncertainty as well as parameter sensitivities.

To deliver quantitative clast-length-axes orientation data (directions, modality types and modality proportions), a new approach needed to be developed (chapter 3). This step was necessary to avoid inappropriate and partly misleading interpretations of classic rose diagram plots (cf. Wells, 2000) and provided a major precondition to decipher the systematic control of bimodal clast axes orientation by slope aspect. Furthermore, it formed the base for the numerical model of lateral clast transport by unconcentrated overland flow (chapter 4). Development of another quantification approach (chapter 5) was necessary to provide a systematic evaluation of experiment-based models of vesicular structure formation. Accordingly, it was possible to extract functional relationships between environmental and sedimentologic control factors and respective changes in vesicle parameters.

An essential, typically ignored task is to deliver not only expected values of target variables (e.g. median or mean of a measured clast transport parameter) but also to provide an estimation of the uncertainties, related to this expected value. In this dissertation uncertainty estimation was included ubiquitously: Field work typically based on a series rather than on single entities (multiple correlated soil profiles, stone pavement orientation plots with more than 100 samples each, parallel stone pavement recovery plots). Vesicle experiment evaluation based on 279±132 objects per sample. Clast alignment angles in flume experiments and physical clast parameters for numeric modelling were also measured repeatedly. Based on the uncertainties or scatters of these individu-

al parameters, global uncertainties (i.e. overall scatter in orientation angles) were calculated independently by Gaussian uncertainty propagation and Monte Carlo runs. The latter approach further yielded information about the sensitivity of individual parameters regarding the orientation angle of clasts transported by water drag force.

Many of the introduced approaches may be readily used for further investigations in related fields, such as river network orientation analysis (e.g. Dietze & Kleber, 2011) and end-member modelling of grain-size data from different types of archives (e.g. Dietze et al., 2012).

7.5 Outlook

During the nearly six years of research, key answers and solutions to the stated objectives (chapter 1.4) were found. Likewise, a series of subsequent objectives arose. Regarding clast orientation patterns, implementation of a numerical model of multi-object ensembles with specific physical parameters for single objects is currently in progress and aims to establish a better approximation of kinetics, discrete parameter sensitivity and control functions of the resulting object mosaic. With the help of such a model it may be possible to infer palaeo-overland flow characteristics from natural clast alignment measurements by solving equation 6 in chapter 4.2.2 for the overland flow velocity, given that the potential contribution of creep or other post-depositional processes to clast alignment alteration can be isolated.

The effect of clast lifting due to soil air escape upon wetting and its potential contribution to lateral clast transport is currently under systematic investigation. The primary objectives concern i) if lifting and downslope transport are systematic and reproducible phenomena, ii) what the main control parameters are (e.g. clast weight, clast surface area, slope inclination, rainfall intensity, air pressure within the sediment, clast lift height), iii) if and how clasts become rotated upon collision with other objects to form a bimodal orientation pattern, iv) which mean displacement lengths are reached and v) if the assumed processes may be transferred into a physically-based, numerical model of pressure equilibria.

From the present results of environmental and sedimentologic control parameters of vesicle formation, transfer functions should be developed. These may allow to infer vesicle properties from more readily and spatially available data about e.g. rainfall characteristics, grain size distribution and calcium carbonate contents.

Both, numerical and statistical approximations of stone pavement and vesicular horizon formation and maintenance limits would be valuable base information to describe the relevant processes and their efficiency not only at the plot scale but also in a spatial model of a landscape. With such quantitative data one might create a spatial prediction of stone pavement occurrence to provide a profound base for e.g. dust emission models (e.g. Shao et al., 2007). In addition, spatial stone pavement distribution is already under investigation, using remote sensing approaches.

Acknowledgements

I am thankful for having had the opportunity to work on this dissertation throughout the last years. Accordingly, I would like to thank Arno Kleber for offering this research subject to me, for all his patience with me and the freedom he afforded to let me grow into my current state. I would also like to thank the many students who worked with me, may it be during field trips, seminar projects, bachelor or diploma theses. I would further like to encourage Sieglinde Gerstenhauer and Beate Winkler to keep on beeing just the way they are in handling monotonic work and excessive (PhD) students. I would like to warmly thank Bernd Ullrich for his enduring support and tolerance of my sometimes extraordinary ideas and discomposure throughout the last decade. Furthermore, I would like to thank my many colleagues and friends for encouraging me and for the enduring hours of rich discussions and advice.

I would like to thank my wife and my son for so many things, not to be noted here.

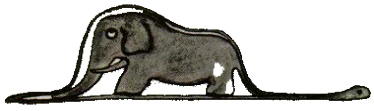

References

Al-Farraj A, Harvey AM. 2000. Desert pavement characteristics on Wadi terrace and alluvial fan surfaces: Wadi Al-Bih, U.A.E. and Oman. Geomorphology 35: 279-297.

Amit R, Gerson R. 1986. The evolution of holocene reg (gravelly) soils in deserts: An example from the dead sea region. Catena 13: 59-79.

Amit R, Gerson R, Yaalon DH. 1993. Stages and rate of the gravel shattering process by salts in desert Reg soils. Geoderma 53: 295-324.

Amundson RG, Chadwick OA, Sowers JM, Doner HE. 1989. Soil evolution along an altitudinal transect in the Eastern Mojave Desert of Nevada, U.S.A. Geoderma 43: 349-371 .

Anderson K, Wells SG, Graham RC. 2002. Pedogenesis of vesicular horizons, Cima Volcanic Field, Mojave Desert, California. Soil Science Society of America Journal 66: 878-887.

Arnalds O, Gisladottir FO, Sigurjonsson H. 2001. Sandy deserts of Iceland: an overview. Journal of Arid Environments 47: 359-371.

Bachmann GO, Machette MN. 1977. Calcic soils and calcretes in the southwestern United States. US Geological Survey Open-File Report 77-794: 1-163.

Bateman MD, Bryant RG, Foster IDL, Livingstone I, Parsons AJ. 2012. On the formation of sand ramps: A case study from the Mojave Desert. Geomorphology 161-162: 93-109.

Bazilevich NI, Gollerbakh MM, Litvinov MA, Rodin LE, Shteinberg DM. 1953. O roli biologicheskih faktorov v obrazovanii takyrov trasse Glavnogo Turkmenskogo kanala (The role of biological factors in the formation of takyrs along the course of the Main Turkmenistan Canal). Botanicheskii zhurnal 38: 1.

Betancourt JL, Devender TRV, Martin PS, (eds). 1990. Packrat middens: The last 40,000 years of biotic change. University of Arizona Press, Tucson.

Blake WP. 1858. Report of a Geological Reconnaissance in California. H. Ballière, New York.

Bockheim JG. 2010. Evolution of desert pavements and the vesicular layer in soils of the Transantarctic Mountains. Geomorphology 118: 433-443.

Bouza P, Del Valle HF, Imbellone PA. 1993. Micromorphological, physical, and chemical characteristics of soil crust types of the central Patagonia region, Argentina. Arid Soil Research and Rehabilitation 7: 355-368.

Brown KJ, Dunkerley DL. 1996. The influence of hillslope gradient, regolith texture, stone size and stone position on the presence of a vesicular layer and related aspects of hillslope hydrologic processes: a case study from the Australian arid zone. Catena 26: 71-84.

Cooke RU. 1970. Stone pavements in deserts. Annals of the Association of American Geographers 60: 560-577.

Cooke RU, Warren A, Goudie AS. 1993. Desert Geomorphology. UCL Press, London.

Dietze E, Hartmann K, Diekmann B, IJmker J, Lehmkuhl F, Opitz S, Stauch G, Wünnemann B, Borchers A. 2012. An end-member algorithm for deciphering modern detrital processes from lake sediments of Lake Donggi Cona, NE Tibetan Plateau, China. Sedimentary Geology 243-244: 169-180.

Dietze M, Kleber A. 2011. A new algorithm for investigating circular data in earth science. XVIII INQUA-Congress, Bern, 21.-27.07.2011. http://www.inqua2011.ch/?a=programme&subnavi=abstract&id=264 [10.07.2012].

Dong Z, Liu X, Wang X. 2002. Aerodynamic roughness of gravel surfaces. Geomorphology 43: 17-31.

Dorn RI. 2009. Desert rock coatings. In Parsons AJ, Abrahams AD, (eds). Geomorphology of Desert Environments. Springer, Heidelberg, New York: 153-186.

Evenari M, Yaalon D, Gutterman Y. 1974. Note on soils with vesicular structure in deserts. Zeitschrift für Geomorphologie N.F. 18: 162-172.

Figueira H, Stoops G. 1983. Application of micromorphometric techniques to the experimental study of vesicular layer formation. Pédologie 33: 77-89.

Fox S-J, Mills A, Poch R. 2009. Micromorphology of surface crusts in the Knersvlakte, South Africa. Journal of Mountain Science 6: 189-196.

Free EE. 1911. Desert Pavements and Analogous Phenomena. Science 53: 355.

Fujioka T, Chappell J. 2011. Desert landscape processes on a timescale of millions of years, probed by cosmogenic nuclides. Aeolian Research 3: 157-164.

Fürst M. 1965. Hammada – Serir – Erg. Zeitschrift für Geomorphologie 9: 385-421.

GLCF (2008): Global Landcover Facility. – http://glcf.umiacs.umd.edu/ index.shtml [10.12.2008]

Goossens D. 2005. Effect of rock fragment embedding on the aeolian deposition of dust on stone-covered surfaces. Earth Surface Processes and Landforms 30: 443-460.

Griffiths PG, Hereford R, Webb RH. 2006. Sediment yield and runoff frequency of small drainage basins in the Mojave Desert, U.S.A. Geomorphology 74: 232-244.

Haff PK. 2001. Desert Pavement: An Environmental Canary? Journal of Geology 109: 661-668.

Haff PK, Werner BT. 1996. Dynamical Processes on Desert Pavements and the Healing of Surficial Disturbances. Quaternary Research 45: 38-46.

Harden JW, Taylor EM. 1983. A quantitative comparison of soil development in four climatic regimes. Quaternary Research 20: 342-359.

Harden JW, Taylor EM, Hill C, Mark RK, McFadden LD, Reheis MC, Sowers JM, Wells SG. 1991. Rates of soil development from four soil chronosequences in the Southern Great Basin. Quaternary Research 35: 383-399.

Helms JG, McGill SF, Rockwell TK. 2003. Calibrated, late Quaternary age indices using clast rubification and soil development on alluvial surfaces in Pilot Knob Valley, Mojave Desert, southeastern California. Quaternary Research 60: 377-393.

Hugie VK, Passey HB. 1964. Soil Surface Patterns of some Semiarid Soils in Northern Utah, Southern Idaho, and Northeastern Nevada. Soil Science Society of America Journal 28: 786-792.

Inglis DR. 1965. Particle Sorting and Stone Migration by Freezing and Thawing. Science 148: 1616-1617.

Jessup RW. 1960. The stony tableland soils of the southeastern portion of the australian arid zone and their evolutionary history. Journal of Soil Science 11: 188-196.

Kleber A. 2000. Compound soil horizons with mixed calcic and argillic properties - examples from the northern Great Basin, USA. Catena 41: 111-131.

Kröpelin S, Verschuren D, Lézine AM, Eggermont H, Cocquyt C, Francus P, Cazet JP, Fagot M, Rumes B, Russell JM, Darius F, Conley DJ, Schuster M, Suchodoletz H von, Engstrom DR. 2008. Climate-driven ecosystem succession in the Sahara: the last 6000 years. Science 320: 765-768.

Laity J. 2008. Deserts and Desert Environments. Wiley-Blackwell, Chichester.

Lebedeva M, Golovanov D, Inozemtsev S. 2009. Microfabrics of desert soils of Mongolia. Eurasian Soil Science 42: 1204-1217.

Legates DR, Willmott CJ, 1990. Mean Seasonal and Spatial Variability in Gauge-Corrected, Global Precipitation. International Journal of Climatology 10: 111-127.

Liu T, Broecker WS. 2007. Holocene rock varnish microstratigraphy and its chronometric application in the drylands of western USA. Geomorphology 84: 1-21.

Lovich JE, Bainbridge D. 1999. Anthropogenic degradation of the southern California desert ecosystem and prospects for natural recovery and restoration. Environmental Management 24: 309-326.

Lowdermilk WC, Sundling HL. 1950. Erosion Pavement, Its Formation and Significance. Transactions of the American Geophysical Union 31: 96-100.

Mabutt JA. 1977. Desert Landforms. MIT Press, Cambridge, Massachusettes.

Mächtle B. 2007. Geomorphologisch-bodenkundlicheUntersuchungen zur Rekonstruktion der holozänen Umweltgeschichte in der nördlichen Atacama im Raum Palpa/Südperu. Heidelberger Geographische Arbeiten 123.

Marchetti DW, Cerling TE. 2005. Cosmogenic ^{3}He exposure ages of Pleistocene debris flows and desert pavements in Capitol Reef National Park, Utah. Geomorphology 67: 423-435.

Matmon A, Simhai O, Amit R, Haviv I, Porat N, McDonald EV, Benedetti L, Finkel R. 2009. Desert pavement-coated surfaces in extreme deserts present the longest-lived landforms on Earth. Geological Society of America Bulletin 121: 688-697.

McFadden LD, Tinsley JC. 1985. The rate and depth of accumulation of pedogenic carbonate accumulation in soils: Formulation and testing of a compartment model. In Weide DL (ed). Soils and Quaternary geology of the south-western United states. Geological Society of America Special Paper 203: 23-42.

McFadden LD, Kuepfer PL. 1990. Soil geomorphology: the linkage of pedology and surficial processes. Geomorphology 3: 197-205.

McFadden LD, Wells SG, Dohrenwend JC. 1986. Influences of quaternary climatic changes on processes of soil development on desert loess deposits of the Cima volcanic field, California. Catena 13: 361-389.

McFadden LD, Ritter JB, Wells SG. 1989. Use of multiparameter relative-age methods for age estimation and correlation of alluvial fan surfaces on a desert piedmont Eastern Mojave Desert, California. Quaternary Research 32: 276-290.

McFadden LD, McDonald EV, Wells SG, Anderson K, Quade J, Forman SL. 1998. The vesicular layer and carbonate collars of desert soils and pavements: formation, age and relation to climate change. Geomorphology 24: 101-145.

Meckelein W. 1959. Forschungen in der Zentralen Sahara. Westermann, Braunschweig.

Meszner S, Fuchs M, Faust D. 2011. Loess-Palaeosol-Sequences from the loess area of Saxony (Germany). Eiszeitalter und Gegenwart, Quarternary Science Journal 60: 47-65.

Miller DE. 1971. Formation of Vesicular Structure in Soil. Soil Science Society of America Journal 35: 635-637.

NCDC. 2012. National Climatic Data Center. http://www.ncdc.noaa.gov/oa/ncdc.html [05.07.2012].

Oviatt CG. 1988. Late Pleistocene and Holocene lake fluctuations in the Sevier Lake Basin, Utah, USA. Journal of Paleolimnology 1: 9-21.

Oviatt CG. 1991. Quaternary Geology of the Black Rock Desert, Millard County, Utah. Utah Geological and Mineral Survey, Special Studies 73.

Paletskaya L, Lavrov A, Kogan S. 1958. Pore formation in takyr crust. Soviet Soil Science 3: 245-250.

Parsons AJ, Abrahams AD, (eds). 2009. Geomorphology of Desert Environments. Second edition. Springer, Heidelberg, New York.

Pelletier JD, Cook JP. 2005. Deposition of playa windblown dust over geologic time scales. Geology 33: 909-912.

Pelletier JD, Cline M, DeLong SB. 2007. Desert pavement dynamics: numerical modeling and field-based calibration. Earth Surface Processes and Landforms 32: 1913-1927.

Pierson FB, Blackburn WH, Van Vactor SS, Wood JC. 1994. Partitioning small scale spatial variability of runoff and erosion on sagebrush rangeland. Water Ressources Bulletin 30: 1081-1089.

Press F, Siever R. 2000. Understanding Earth. Third edition. Freeman, New York.

Press F, Siever R, Grotzinger J, Jordan T. 2003. Understanding Earth. Fourth edition. Freeman, New York.

Prose DV, Wilshire HG. 2000. The lasting effects of tank manouvers on desert soils and intershrub flora. USGS open file report OF 00-512.

Quade J. 2001. Desert pavements and associated rock varnish in the Mojave Desert: how old can they be? Geology 29: 855-858.

Ries JB, Hirt U. 2008. Permanence of soil surface crusts on abandoned farmland in the Central Ebro Basin/Spain. Catena 72: 282-296.

Schmidt J-U. 2008. Bodenevolution während der letzten 30.000 Jahre in der Black Rock Desert, W Utah, SW USA. Unpublished diploma thesis, Technische Universität Dresden.

Schultz J. 2008. Die Ökozonen der Erde. Ulmer, Stuttgart.

Shao Y, Leys JF, McTainsh GH, Tews K. 2007. Numerical simulation of the October 2002 dust event in Australia. Journal of Geophysical Research 112: D08207-1-D08207-13.

Sharon D. 1962. On the nature of hamadas in Israel. Zeitschrift für Geomorphologie N.F. 6: 129-147.

Shum M, Lavkulich LM. 1999. Use of sample color to estimate oxidized Fe content in mine waste rock. Environmental Geology 37: 281-289.

Spelz RM, Fletcher JM, Owen LA, Caffee MW. 2008. Quaternary alluvial-fan development, climate and morphologic dating of fault scarps in Laguna Salada, Baja California, Mexico. Geomorphology 102: 578-594.

Springer ME. 1958. Desert Pavement and Vesicular Layer of Some Soils of the Desert of the Lahontan Basin, Nevada. Soil Science Society of America Journal 22: 63-66.

Suchodoletz H von, Kühn P, Hambach U, Dietze M, Zöller L, Faust D. 2009. Loess-like and palaeosol sediments from Lanzarote (Canary Islands/Spain) – indicators of palaeoenvironmental change during the Late Quaternary. Palaeogeography, Palaeoclimatology, Palaeoecology 278: 71-87.

Sullivan LA, Koppi AJ. 1991. Morphology and genesis of silt and clay coatings in the vesicular layer of a desert loam soil. Australian Journal of Soil Research 29: 579-586.

Sweeney MR, McDonald EV, Etyemezian V. 2011. Quantifying dust emissions from desert landforms, eastern Mojave Desert, USA. Geomorphology 135: 21-34.

Tchakerian VP, Lancaster N. 2002. Late Quaternary arid/humid cycles in the Mojave Desert and western Great Basin of North America. Quaternary Science Reviews 21: 799-810.

UNEP (United Nations Environment Programme). 1997. World atlas of desertification. Second edition. UNEP, London.

Valentin C. 1994. Surface sealing as affected by various rock fragment covers in West Africa. Catena 23: 87-97.

Valentine GA, Harrington CD. 2006. Clast size controls and longevity of Pleistocene desert pavements at Lathrop Wells and Red Cone volcanoes, southern Nevada. Geology 34: 533-536.

Volk OH, Geyger E. 1970. "Schaumböden" als Ursache der Vegetationslosigkeit in ariden Gebieten. Zeitschrift für Geomorphologie N.F. 14: 79-95.

Wainwright J, Parsons AJ, Abrahams AD. 1999. Field and computer simulation experiments on the formation of desert pavements. Earth Surface Processes and Landforms 24: 1025-1037.

Walker AS. 1986. Eolian Landforms. In Short NM, Blair Jr. RW, (eds). Geomorphology from Space: a Global Overview of Regional Landforms. Special Publication 486. NASA Sientific and Technical Branch, Washington DC: 447-520.

Walther J. 1924. Das Gesetz der Wüstenbildung. Quelle & Meyer, Leipzig.

Wells N. 2000. Are there better alternatives to standard rose diagrams? Journal of Sedimentary Research 70: 37-46.

Wells SG, Dohrenwend JC, McFadden LD, Turrin BD, Mahrer KD. 1985. Late Cenozoic landscape evolution on lava flow surfaces of the Cima Volcanic field, Mojave Desert, California. Geological Society of America Bulletin 96: 1518-1529.

Wells SG, Brown WJ, Enzel J, Anderson RY, McFadden LD. 2003. Late Quaternary geology and paleohydrology of pluvial Lake Mojave, southern California. In Enzel J, Wells SG, Lancaster N, (eds). Paleoenvironments and Paleohydrology of the Mojave and Southern Great Basin Deserts. Geological Society of America Special Paper 368: 79-114.

Williams SH, Zimbelman JR. 1994. Desert Pavement Evolution: An Example of the Role of Sheet-flood. Journal of Geology 102: 243-248.

Wood YA, Graham RC, Wells SG. 2005. Surface control of desert pavement pedologic process and landscape function, Cima Volcanic field, Mojave Desert, California. Catena 59: 205-230.

Yaalon DH, Ganor E. 1973. The Influence of Dust on Soils During the Quaternary. Soil Science 116: 146-155.

Yonovitz M, Drohan J. 2009. Pore morphology characteristics of vesicular horizons in undisturbed and disturbed arid soils; implications for arid land management. Soil Use and Management 25: 293-302.

Young MH, McDonald EV, Caldwell TG, Benner SG, Meadows DG. 2004. Hydraulic Properties of a Desert Soil Chronosequence in the Mojave Desert, USA. Vadose Zone Journal 3: 956-963.

Zech R, Kull C, Kubik PW, Veit H. 2007. LGM and Late Glacial glacier advances in the Cordillera Real and Cochabamba (Bolivia) deduced from ^{10}Be surface exposure dating. Climate of the Past 3: 623-635.

Zomer RJ, Trabucco A, Bossio DA, Straaten O van, Verchot LV, 2008. Climate Change Mitigation: A Spatial Analysis of Global Land Suitability for Clean Development Mechanism Afforestation and Reforestation. Agriculture Ecosystems and the Environment 126: 67-80.

Erklärung

Hiermit versichere ich, dass ich die vorliegende Arbeit ohne unzulässige Hilfe Dritter und ohne Benutzung anderer als der angegebenen Hilfsmittel angefertigt habe; die aus fremden Quellen direkt oder indirekt übernommenen Gedanken sind als diese kenntlich gemacht worden. Bei der Auswahl und Auswertung des Materials sowie bei der Herstellung des Manuskriptes habe ich Unterstützungsleistungen von den Personen erhalten, die als Co-Autoren der Aufsätze erwähnt sind. Als Erstautor aller Aufsätze bin ich verantwortlich für die Struktur der Dokumente, die Anfertigung der Abbildungen, Tabellen und weiterer Listen wie Anhänge. Ich bin ebenso verantwortlich für die Kommunikation während der Einreichung, Begutachtung, Revisionen und Veröffentlichung der Aufsätze. Die folgende Liste fasst die genauen Beiträge zu den Aufsätzen über die Diskussion im Text hinaus zusammen.

1. Dietze M, Muhs S, Dietze E. 2011. Ambiguities of relative age indicators on abandoned surfaces of arid environments. Zeitschrift für Geomorphologie 55 Suppl. 3: 49-75.
   Geländearbeiten (Oberflächen- und Bodenkartierung, Beschreibung und Beprobung), Analysen (Profilentwicklungsindex-Berechnungen, Aufbereitungen und Labormessungen).

2. Dietze M, Kleber A. 2012. Contribution of lateral processes to stone pavement formation in deserts inferred from clast orientation patterns. Geomorphology 139-140: 172-187.
   Geländearbeiten (Oberflächenbeschreibungen, Versuchsflächenpräpartion – z.T. mit A. Kleber, Bodenbeschreibungen, Steineinregelungsmessungen und Visualisierungen), Analysen (GIS-Analysen, Entwicklung des statistischen Ansatzes zur Kennzeichnung der Winkeldaten, statistische Tests und weitere Berechnungen).

3. Dietze M, Bartel S, Lindner M, Kleber A. Formation mechanisms and control factors of vesicular soil structure. Accepeted by Catena, 01.07.2012.
   Geländearbeiten (Oberflächenkartierung, Beschreibungen der natürlichen Vesikularhorizonte, Beprobung und Fotografien), Analysen (Röntgendiffraktometrie und Auswertung, Entwicklung und Anwendung des Quantifizierungsansatzes, Digitalisierung der Vesikelobjekte – z.T. mit S. Bartel), Experimente (Vesikelbildungszyklen – zusammen mit und als Betreuer von S. Bartel und S. Schlapa).

4. Dietze M, Groth J, Kleber A. Alignment of stone-pavement clasts by unconcentrated overland flow – implications of numerical and physical modelling. Submitted to Earth Surface Processes and Landforms, in review since 31.05.2012.
   Geländearbeiten (Steingrößenmessungen, weitere physikalische Parametermessungen), das konzeptionelle und numerische Modell, Experimente (zusammen mit und als Betreuer von J. Gorth).

5. Dietze M, Dietze E, Kleber A. Environmental history recorded in stone pavement-covered soil-sediment complexes, Cima volcanic field, USA. Submitted to Journal of Quaternary Science, 05.07.2012.
   Geländearbeiten (Oberflächen- und Profilbeschreibungen, Beprobung), Analysen (bodenkundliche Parameter, Profilkorrelationen), End-member-Modellierung (Transkription des MATLAB-Quellcodes in R, Auswertung der Daten zusammen mit E. Dietze).

Weitere Personen waren an der geistigen Herstellung der vorliegenden Arbeit nicht beteiligt. Insbesondere habe ich nicht die Hilfe eines oder mehrerer Promotionsberater(s) in Anspruch genommen. Dritte haben von mir weder unmittelbar noch mittelbar geldwerte Leistungen für Arbeiten erhalten, die im Zusammenhang mit dem Inhalt der vorgelegten Dissertation stehen. Die Arbeit wurde bisher weder im Inland noch im Ausland in gleicher oder ähnlicher Form einer anderen Prüfungsbehörde zum Zwecke der Promotion vorgelegt. Ich bestätige, dass ich die Promotionsordnung der Fakultät Forst-, Geo- und Hydrowissenschaften der TU Dresden anerkenne.

_____

Ort, Datum, Unterschrift